Molecular Assembly in the Endocytic Pathway

A Dissertation
Presented to the Faculty of the Graduate School
of
Yale University
in Candidacy for the Degree of
Doctor of Philosophy

by
Neal G. Ravindra

Dissertation Director: Julien Berro, Ph.D.

December 2019

Neal G. Ravindra, M.Phil., Ph.D. Candidate[1,2,3]

Dissertation Committee

Julien Berro, Ph.D.[1,3,4]

Jonathon Howard, Ph.D.[1,5,6]

Megan King, Ph.D.[4]

Lynne Regan, Ph.D.[1,7,8]

External Reviewer

Bruce Goode, Ph.D.[9]

[1]Department of Molecular Biophysics & Biochemistry,

[2]Integrated Graduate Program in Physical & Engineering Biology,

[3]The Nanobiology Institute,

[4]Department of Cell Biology,

[5]Department of Physics,

[6]Quantitative Biology Institute,

Yale University

[7]Center for Synthetic & Systems Biology,

[8]Interdisciplinary Science,

University of Edinburgh

[9]Department of Biology,

Brandeis University

Dedication

I dedicate this dissertation to my parents, Bridget B. Ravindra and Baikadi A. Ravindra, who generously supported me throughout my education with kindness and love, to my sister, Tara R. Ravindra, who lovingly offered advice and helped me persist, and to my dear friends Lea Kiefer, Nandan G. Pandit, Garrett Debs, Martha Braun, and Curran Oi, who supported me and taught me many lessons throughout my time in graduate school.

Abstract
Molecular Assembly in the Endocytic Pathway
Neal G. Ravindra
2019

Proteins assembled into cellular pathways often possess non-catalytic, protein-interaction domains. Src-homology 3 (SH3) domains are protein-interaction domains that spatiotemporally connect molecules through transient binding interactions, recognizing linear peptide motifs and localizing proteins to various sub-cellular structures. In the endocytic pathway, there are many SH3-domain-containing proteins and several endocytic proteins contain multiple SH3 domains. I sought to interrogate the degeneracy in the number of SH3 domains within endocytosis and within endocytic proteins and to clarify the influence of each SH3 domain on the assembly and dynamics of the endocytic molecular machinery.

To this end, in collaboration with Ronan Fernandez, I created a comprehensive library of endogenous, single SH3 domain deletions in the fission yeast *Schizosaccharomyces pombe* and used quantitative fluorescence microscopy to measure the effects of these deletions *in vivo*. I found that endocytic SH3 domains restrict, enhance, or have minor or redundant effects on actin assembly in endocytosis. I also found that some SH3 domains influence the cell's ability to regulate the number of endocytic events. These observations are consistent with simulated perturbations to reaction steps in the Arp2/3 activation pathway, supporting the explanation that SH3 domains are regulators of Arp2/3-mediated actin nucleation in endocytosis.

To investigate the endocytic localization dependence of SH3-domain containing proteins on their SH3 domain(s), in collaboration with Ronan Fernandez, we created a library of single SH3 domain deletions within strains where each SH3 domain's native

protein was also tagged with a fluorescent reporter. Analysis of the localization of these proteins and their fluorescent distribution in live cells reveals that most SH3 domains influence their protein's localization and assembly dynamics into endocytic structures. Furthermore, several SH3 domains are required for robust localization of their protein to endocytic structures while being dispensable for their protein's expression. Thus, endocytic SH3 domains may influence the assembly dynamics of SH3-domain-containing proteins into endocytic structures in addition to playing other assembly and regulatory roles within endocytic structures. Given that SH3 domains participate in a large number of interactions in the endocytic protein-interaction network, relative to other modular domains, a plausible answer to how endocytic proteins are recruited may be through SH3 domain-mediated interactions.

Yet, one challenge to the use of SH3 domains in synthetic biology is that it is poorly understood how distinct sets of SH3 domains interact with distinct sets of proteins, given the potential overlap between SH3 domain-mediated interactions. To address how SH3 domains assemble proteins into distinct pathways, I proposed that SH3 domains achieve binding specificity through *domain-mediated specificity*, where binding preferences emerge from unique biophysical properties, and/or through *contextual specificity*, where binding preferences emerge through unique molecular and cellular environments. I hypothesized that SH3 domains primarily exhibit contextual specificity, which implies that individual SH3 domains are interchangeable. To determine the interchangeability of SH3 domains in a single context, I replaced native endocytic SH3 domains with non-native SH3 domains from other proteins and organisms. Contrary to my suppositions, my findings support the hypothesis that SH3 domains achieve interaction specificity primarily through domain-mediated specificity. However, my results do not entirely rule out contextually-mediated interaction specificity.

Collectively, I describe a range of influences and activities that individual SH3 domains have on molecular assembly during endocytosis. The quantitative measurements of molecular assembly during endocytosis described in this dissertation, especially in the background of single deletions of each SH3 domain in endocytosis, reveal that SH3 domains have a variety of influences on actin assembly, endocytosis and the cell's regulation of the endocytic rate. In particular, SH3 domains appear to play assembly and regulatory roles during endocytosis, perhaps by mediating interactions in the Arp2/3 activation pathway and by influencing the assembly dynamics of SH3 domain-containing proteins and actin accessory factors in the cell. These results add nuance to the purported role of SH3 domains in inducing phase-separated structures that promote local actin assembly in the cell. By providing precise quantitative descriptions into molecular assembly during endocytosis under a variety of perturbations to SH3 domains, this dissertation may inform future synthetic manipulations of endocytosis, especially by deleting or inserting SH3 domains as interchangeable parts in molecular circuits to predictably modulate the activity of the endocytic pathway and govern biological processes relevant to human health.

Contents in brief

List of figures

List of tables

List of frequently used abbreviations

SH3: Src homology-3 domain

WASp or Wsp1p: Wiskott Aldrich Syndrome Protein

Arp 2/3: actin-related protein 2/3 complex

PR: proline-rich region

PRM: proline-rich motif (PXXP), a canonical SH3 domain-interacting peptide sequence

CA: central (C) and acidic (A) domains

F-BAR: Fes/CIP4 homology Bin-Amphiphysin-Rvs domain

N-BAR: N-terminal amphipathic helix-containing BAR domain

fsCC(s): force-sensitive coiled-coil(s)

Acp1p: actin capping protein, subunit 1

Fim1p: fimbrin, an actin cross-linking protein

I. The SH3 domain: a modular protein-interaction domain

Some sections in this chapter are partially adapted from published manuscripts or manuscripts in preparation.

One of the main characters in this dissertation is the SH3 domain. The SH3 domain is a modular protein-interaction domain found within proteins in many different cellular pathways. SH3 domains primarily interact with linear peptide sequences in other proteins, assembling protein complexes with emergent biological activities by interacting with and connecting proteins together throughout the cell. Cells exquisitely structure matter so that each molecule is arranged into its needed place at the right time. In so doing, organisms control energy flows across multiple time and length scales, maintaining order in spite of entropic stagnation. With much smaller and far more specific questions, this dissertation attempts to contribute and deepen understanding of molecular assembly in cellular pathways by focusing on one pathway with a large number of SH3 domains, namely, endocytosis. In studying endocytosis, one cannot ignore the influence of mechanics and force-production on molecular assemblies. In this brief overview, I will describe some of the proteins within endocytosis containing SH3 domains and conceptually connect SH3 domains and mechanical properties of molecular networks to molecular assembly in endocytosis.

A. What are modular protein-interaction domains?

A module usually refers to a standardized component of a larger system that is interchangeable. Applied to molecular biology, a modular domain is considered to be a sub-unit within a protein, though its interchangeability between proteins is not tested, nor necessarily assumed, as the word ‘modular’ does not generally seem to portend a necessary, biological activity or meaning. However, this fluid concept of a modular domain can at least be weaned out into two, perhaps more concrete, concepts, namely, structural modularity and functional modularity. In biology, structural modularity refers to the physical separability of a larger molecule or biological system into structurally independent domains (Bhattacharyya, Reményi, Yeh, & Lim, 2006). For example, a protein can be composed of several sub-domains, which can be physically separated from and function outside the context of the whole protein, folding independently of the whole molecule and possessing biological activity when transformed. Similarly, a protein complex can be separated into multiple, independently folding proteins. Functional modularity refers to the ability of a physically separable unit to possess a function independent of its native context, such that the functional module exhibits the same function in diverse molecular systems (Bhattacharyya et al., 2006). For example, SH3 domains are considered to be both structurally and functionally modular because they independently fold and, across a wide-array of cellular pathways, they interact with linear peptide motifs, connecting proteins through binding interactions.

Today, the foundational conceptualization of a biological system’s or molecule’s functionality is dominated by modular thinking. While one can sequence proteomes, genomes, microbiomes, and so on, the individual sequence does not immediately espouse or reveal biological activity. Instead, these sequences are discretized into modules, aligned and compared with other units so that the purported function of a

system or molecule of interest can be distilled, and thinking about what this system or molecule does crystallizes by building upon information about its structural and/or functional modules (Pawson & Nash, 2003). Modular thinking did not always underlie conceptual frameworks in molecular biology. In the 1960s, in the signaling field, for example, signaling enzymes were considered to be devices that tuned and regulated by conformational shifts induced by another protein, such that conformational shifts, which altered a molecule's activity, propagated signals down the stream (B. J. Mayer, 2015). The spark of modular thinking perhaps ferments with studies, in the late 1970s, of retroviruses that rapidly induce tumors, which led to the identification *src*, a tumor-inducing gene from the *Rous sarcoma* virus and the first identified tyrosine (Tyr) kinase (Eckhart, Hutchinson, & Hunter, 1979; Hunter & Sefton, 1980). Soon after, receptors for growth factors with Tyr kinase activity were identified; amongst these was the epidermal growth factor receptor, EGFR, whose levels were later found to be regulated by endocytic trafficking, perturbations to which are associated with increased incidence of cancer (Downward et al., 1984; Tomas, Futter, & Eden, 2014; Ullrich et al., 1984). Intriguingly, studies isolating catalytic domains of various Tyr kinases (SRC homology region 1) found that these catalytic domain isolates were more active than full-length Tyr kinase proteins and, in particular, a N-terminal region dispensable for kinase activity but important for altering the strength and specificity of kinases, a so called 'modulatory region,' was isolated in 1986 and named, the SRC homology 2 (SH2) domain (Brugge & Darrow, 1984; Levinson, Courtneidge, & Bishop, 1981; B. J. Mayer, 2015; Sadowski, Stone, & Pawson, 1986). Importantly, these studies found that receptor Tyr kinases (RTKs), the first step in a signaling pathway, were the most highly phosphorylated substances in cells, contradictory to the prevailing view that downstream output was amplified by upstream signals, and that rather than simply activating downstream molecules, RTKs physically interacted with and associated with their 'target' molecules

(Margolis et al., 1989). Soon after, ‘modulatory regions’ of oncogenic tyrosine kinases were found to have sequence similarities in several other signaling proteins and a third SRC homology region was isolated in phospholipase C and in Crk, an oncoprotein from a chicken tumor virus, dubbed, the “SH3 domain” (D. Anderson et al., 1990; Bruce J. Mayer, Hamaguchi, & Hanafusa, 1988; Stahl, Ferenz, Kelleher, Kriz, & Knopf, 1988). Coincidently, SH2 domains were found to bind specifically to phosphorylated RTKs and, because these oncogenic, SH2 domain-containing proteins often contained ‘modulatory regions,’ i.e., SH3 domains, activated RTKs induced the assembly of protein complexes by localizing SH2 domain-containing proteins to Tyr-phosphosites (D. Anderson et al., 1990; Moran et al., 1990). This new signaling mechanism transformed thinking as to how signaling works, shifting from a conformational slurry of signal amplification, to a framework in which a signaling pathway was thought to be a system of independent modules of protein-interactions arrayed into a signaling cascade contingent upon macromolecular assembly (B. J. Mayer, 2015).

After SH3 domains were isolated as modular protein-interaction domains, other modular protein-interaction domains were identified, such as PH and PDZ domains in the mid-1990s, which bind phosphoinositol lipids and anchor membrane proteins to the cytoskeleton, respectively (B. J. Mayer, 2015; Pawson & Nash, 2010; Sheng & Sala, 2001; J. W. Yu et al., 2004; A. Zarrinpar, Bhattacharyya, & Lim, 2003). In the early aughts, omics scale data became available with the sequencing of the human genome and along with big data trends, comprehensive characterizations of protein-interactions mediated by modular protein-interaction domains such as the WW domain were reported (Hu et al., 2004). In cell biology, multi-valent, modular protein-interaction domains were recently shown to induce phase-separated, higher-order structures within the cell (Li et al., 2012). In the future, modular protein-interaction domains may be extended for use in

synthetic biology but, for now, their roles in cellular pathways still need to be teased out (B. Mayer & Saksela, 2005).

B. How do SH3 domains connect proteins together in the cell to assemble cellular pathways?

The SH3 domain is a modular protein-interaction domain that interacts with short, linear, proline-rich peptide sequence motifs found within other proteins, allowing the SH3 domain to connect, localize, and assemble proteins into cellular pathways through binding interactions (**Figure 1**). The SH3 domain binding site in SH3 domain-interacting proteins was localized to short, linear peptide sequences in the early 90s (Cicchetti, Mayer, Thiel, & Baltimore, 1992; R. Ren, Mayer, Cicchetti, & Baltimore, 1993). It was also observed that several SH3 domain binding sites were enriched for proline residues, adding SH3 domains to a broader category of modular domains that recognize proline-rich motifs (PRMs), especially prevalent within cytoskeleton and signaling proteins, including the SH3 domain, the WW domain (for conserved tryptophan residues), and the WH1 domain (WASP homology 1 domain) (R. Ren et al., 1993; A. Zarrinpar et al., 2003).

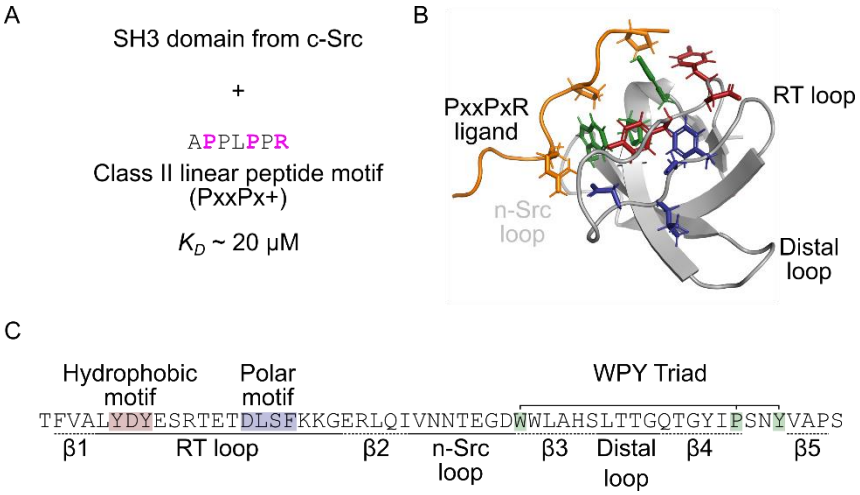

Figure 1. SH3 domains interact with short, proline-rich, linear peptide motifs to localize and concentrate proteins in the cell, contributing to cellular pathway assembly. (A) The affinity of the interaction between the c-Src SH3 domain and a short, linear peptide derived from APP12 (comprising a SH3 domain-binding, class II peptide motif) was measured by fluorescence anisotropy in (S Feng, Kasahara, Rickles, & Schreiber, 1995). The critical residues in the core SH3 domain-interacting motif, PxxP, and the full class II motif, PxxPx+ are highlighted in pink; x = any amino acid residue. (B) The NMR solution structure of the c-Src SH3 domain interacting with the class II motif ligand from APP12 was deposited in the PDB (PDB ID: 1QWE) and reported (S Feng et al., 1995). The structure was annotated in PyMOL to highlight key binding features in the SH3 domain; colors match the binding motifs denoted above the SH3 domain's sequence in (C). The peptide ligand is in orange with the critical residues shown as sticks, as highlighted in pink in (A). Structural features are annotated with the n-Src loop faded to indicate that the structure extents into-the-page. (C) Amino acid sequence of the c-Src SH3 domain with conserved SH3 domain-binding motifs denoted above the sequence and structural features denoted below the sequence.

Why might proline be found in many different proteins to be ‘read’ by modular protein-interaction domains, such as the SH3 domain? One explanation stems from the unique biophysical properties of proline, relative to the other 19 naturally occurring amino acids: proline forms a pyrrolidine ring with an unusual shape that places conformational constraints on its dihedral angle (A. Zarrinpar et al., 2003). As such, proline residues tend to break secondary structure (S. S. C. Li, 2005). Perhaps because of this, rather than being buried in the core, proline-containing sequences are often found on protein surfaces, primed for recognition by modular protein-interaction domains (Holt & Koffer, 2001). With multiple prolines in a linear sequence, PRMs tend to form a left-handed, polyproline type II (PPII) helix, with a pitch of ~3 residues per turn, making it less coiled than an alpha-helix (~3.6 residues per turn) (Kay, Williamson, & Sudol, 2000; S. S. C. Li, 2005; MacArthur & Thornton, 1991). It is hypothesized that the conformational constraints of the PPII helix lower the entropic costs of an interaction, in addition, its backbone residues are prevented from intramolecular hydrogen bonding, freeing them for intermolecular binding, and, furthermore, the backbone and sidechains of amino acid residues in PPII helices are projected outward from the helical axis, additionally priming PRMs for interactions with molecular species (S. S. C. Li, 2005; Petrella, Machesky, Kaiser, & Pollard, 1996; A. Zarrinpar et al., 2003). Lastly, proline is the only amino acid whose N-terminal nitrogen is substituted with carbon from the cyclic side-chain; thus, proteins, and especially SH3 domains, can recognize the proline backbone in a partner protein without extended side-chain contacts, achieving sequence-specific recognition without a high-affinity interaction (Nguyen, Turck, Cohen, Zuckermann, & Lim, 1998).

Domains that recognize PRMs do not have to rely on high-affinity interactions to bind their ligands because they can exploit unique biophysical properties of proline to achieve

selective binding (A. Zarrinpar et al., 2003). In dynamic intracellular signaling environments, weak and transient interactions provide the advantage of allowing rapidly reversible assembly. As a modular protein-interaction domain, the SH3 domain recognizes PRMs in other proteins, binding these short, linear peptide sequences with characteristically poor affinities (~1-200-μM) (Sparks et al., 1996; Sparks, Rider, & Kay, 1998). SH3 domains interact and PRMs interact with an on-rate of ~0.1-$\mu M^{-1}s^{-1}$, implying off-rates on the order of milliseconds to seconds (Demers & Mittermaier, 2009; Hansen, Vallurupalli, Lundstrom, Neudecker, & Kay, 2008; Meneses & Mittermaier, 2014). Thus, SH3 domains connect proteins together in the cell by participating in relatively weak and transient interactions.

The highly conserved WPY triad in SH3 domains binds prolines in PRMs that comprise the core SH3 domain binding motif (PxxP, where x = any amino acid residue) (**Figure 1B-C**) (Fernandez-Ballester, Blanes-Mira, & Serrano, 2004). A motif in the structural RT loop of SH3 domains, namely the hydrophobic binding motif, also forms a groove for binding prolines in the core SH3 domain binding motif (Verschueren et al., 2015). A second binding motif in the RT loop, namely the polar motif, as well as the varying lengths of the RT and n-Src loops in the SH3 domain, contribute additional binding pockets and surfaces that can contribute to the selectivity of a SH3 domain to bind specific PRMs (S. Feng, Chen, Yu, Simon, & Schreiber, 1994; W. A. Lim, Richards, & Fox, 1994; Saksela & Permi, 2012). The SH3 domain itself presents a hydrophobic binding surface that is purportedly adapted to recognize PPII helices selectively, albeit with relatively weak affinity; however, because SH3 domains also display a specificity pocket that can interact with positively charged residues in PRMs, the affinity of a SH3 domain and PRM interaction may be increased through the formation of salt-bridges (W. A. Lim et al., 1994; H. Yu et al., 1994).

SH3 domains can play both assembly and regulatory roles in cells (A. Zarrinpar et al., 2003). For example, the SH3 domain-containing protein, Grb2, is recruited to the membrane upon activation of receptor tyrosine kinases by growth factor stimulation and, once at the membrane, SH3 domains recruit a number of other proteins to trigger a mitogen activated protein kinase (MAPK) signaling cascade in the cell, ultimately leading to proliferation (Buday & Downward, 1993; Rozakis-Adcock, Fernley, Wade, Pawson, & Bowtell, 1993). SH3 domains can also play regulatory roles in the cell. For example, the viral protein, v-Src, lacks a Tyr-527 while the cellular protein, c-Src, is autoinhibited by intramolecular binding of its SH2 to a phosphorylated, C-terminal tyrosine, Tyr-527, preventing its SH3 domain from physically associating with other proteins and stabilizing an intramolecular interaction between c-Src and its SH3 domain (Sefton & Hunter, 1986; Xu, Harrison, & Eck, 1997). Once the Tyr-527 on c-Src is dephosphorylated, an occurrence mimicked by v-Src, the SH3 domain is able to interact with other molecules to recruit and assemble protein complexes and trigger a response; thus the SH3 domain straddles both assembly and regulatory roles, depending on its cellular and molecular context (Moarefi et al., 1997; Nguyen & Lim, 1997).

Elucidating the roles of individual SH3 domains *in vivo* remains a topic of active research and, in an attempt to reduce the range of influences that individual SH3 domains may exert in cells, high-throughput *in vitro* approaches have sought to decode the ligand preferences of SH3 domains and predict their binding partners (Rickles et al., 1994). To connect proteins together through binding interactions, most SH3 domains require a conserved consensus or core peptide motif, PxxP, in their binding partners for recognition (A. Zarrinpar et al., 2003). Owing to the twofold rotational pseudosymmetry of PPII helices and the hydrophobic grooves in SH3 domains that recognize proline backbones, the core PxxP motif is often N- or C-terminally flanked by basic residues,

suggesting that there are specific classes of peptide motifs that can be recognized and bound by SH3 domains: class I (+xxPxxP) and class II motifs (PxxPx+) with another specificity class for non-canonical peptide motifs, class III (Barnett, Bottger, Klein, Tabak, & Distel, 2000; S. Feng et al., 1994; W. A. Lim et al., 1994; Nishida et al., 2001). However, despite some suggestion that the variable RT and n-Src loops may provide specificity pockets that vary in biophysical properties between individual SH3 domains, most SH3 domains display overlap in their ability to bind unique peptide motifs and most SH3 domains have the ability to bind class I and class II peptide motifs (Sparks et al., 1996; Tong et al., 2002).

Thus, despite ongoing and numerous high-throughput efforts, little is known about the binding specificity or underlying modularity of individual SH3 domains *in vivo* (B. J. Mayer, 2015; Saksela & Permi, 2012; Teyra et al., 2017; Verschueren et al., 2015). SH3 domains, as modular protein-interaction domains, have long been of interest in synthetic biology, viewed as a potential molecular interchangeable part, but the question remains: can SH3 domains be inserted into different proteins and pathways to modulate activity (B. J. Mayer, 2015; Pawson & Nash, 2003)? Given that SH3 domains are thought to assemble proteins into cellular pathways and recruit and localize proteins to scaffolds or protein complexes throughout the cell, another question is, how can SH3 domains robustly and reproducibly assemble proteins into a pathway while exhibiting characteristically weak and transient interactions (B. J. Mayer, 2015)? One hint is that degeneracy of SH3 domains, in copy-number within a protein or by abundance within a pathway, may increase the affinity of an interactions between a SH3 domain-containing proteins and their partners through multivalent interactions (Li et al., 2012). These questions and the broader hypothesis that SH3 domains assemble molecules into cellular pathways will be examined in this dissertation.

C. What is endocytosis?

Endocytosis literally means process for insertion into a cell, hailing from Greek (endo- = within, cytos = hollow vessel, namely a cell, and -osis = process) (Shaw, 1969). There are many types of endocytosis: there is clathrin-mediated endocytosis or the oft used synonymous, albeit poorly defined, 'receptor-mediated endocytosis' and clathrin-independent endocytosis, the latter including macropinocytosis (bulk cell drinking), phagocytosis (cell eating), the CLIC/GEEC endocytic pathway, the caveolae/caevolin1-dependent endocytic pathway and others (Doherty & McMahon, 2009). Many of these distinctions are not critical in yeast, especially given that only one linear peptide internalization signal in yeast has been identified, and, even in mammals, most internalization pathways require actin assembly to deform the membrane, involving many overlapping proteins (Doherty & McMahon, 2009; Hinze & Boucrot, 2018; Howard, Hutton, Olson, & Payne, 2002; Tan, Howard, & Payne, 1996). Clathrin-mediated endocytosis is the most well characterized of the endocytic pathways and commonly, this is the pathway referred to by the less jargon-laden term 'endocytosis' (Sandra L. Schmid, 2018).

Endocytosis is a ubiquitous and vital eukaryotic cellular process by which cells control the protein and lipid composition of their membrane and, in so doing, endocytosis regulates how cells interact with their environment (Hinze & Boucrot, 2018). In the process of endocytosis, cells fold their plasma membrane inwards towards the cytoplasm, ingesting substances, lipids, proteins, nutrients, and other molecules. In clathrin-mediated endocytosis, adaptor proteins bridge early coat proteins that mark

sites of endocytosis to clathrin molecules, forming a cage of clathrin triskelia that determines the size and shape of the endocytic vesicle (Roth and Porter, 1964; Pearse, 1976; Gaidarov *et al.*, 1999; Kaksonen *et al.*, 2003; McMahon and Boucrot, 2011; Robinson, 2015).

The core endocytic machinery is well conserved between yeast and mammals, highly reproducible, and has been worked out since Barbara Pearse's discovery of clathrin in 1976 using a combination of microscopy, genetic, and biochemical approaches (**Table 1**) (Crowther, Finch, & Pearse, 1976; B. M. Pearse, 1976; B. M. F. Pearse, 1975; M. J. Taylor, Perrais, & Merrifield, 2011). That is not to say, however, that all of the molecules involved have been elucidated (Goode, Eskin, & Wendland, 2015; Marko Kaksonen & Roux, 2018). Endocytosis remains a challenging cellular pathway to study and collect an inventory of components and parts because it is a complex system, spanning a limited area (ribosome exclusion zone, ~200-nm), and dynamic—key components of the endocytic molecular machinery assemble and disassemble within ~20s (Kukulski, Schorb, Kaksonen, & Briggs, 2012; Sirotkin, Berro, Macmillan, Zhao, & Pollard, 2010).

Table 1. Table of endocytic proteins in yeast and their mammalian orthologs.

Module	Fission yeast	Budding Yeast	Mammals	Description
	SPBC800.10c Ucp8	Ede1p	EPS15, EPS15L1	UB/EH/EF hand domain protein
	Syp1p	Syp1p	FCHO1/2, SGIP1	F-BAR domain protein
	Ubp2p	Ubp2p	-*	Ubiquitin C-terminal hydrolase 2 (fungi only)
	Ubp7p	Ubp7p	-	Ubiquitin C-terminal hydrolase 7 (fungi only)
Early coat	Chc1p	Chc1p	CLTC, CLTCL1	Clathrin heavy chain
	Clc1p	Clc1p	CLTA/B	Clathrin light chain
	Pal1p	Pal1p	-	Membrane associated protein (fungi only)
	Apl1p	Apl1p	AP1B1, AP2B1	AP-2 adaptor complex beta subunit
	Apl3p	Apl3p	AP2A1/2	AP-2 adaptor complex alpha subunit
	Apm4p	Apm4p	AP2M1	AP-2 adaptor complex mu subunit
	Aps2p	Aps2p	AP2S1	AP-2 adaptor complex sigma subunit
	End4p	Sla2p	HIP1, HIP1R	Huntingtin-interacting protein homolog
Intermediate coat	Ent1p	Ent1/2/4p	EPN1/2/3, ENTHD1	Epsin
	Yap18p	Yap1801/2p	CALM, SNAP91, AP180	ENTH, VHS domain protein
	Pan1p	Pan1p	ITSN1/2	Actin cortical patch component with EF hand and WH2 motif (Intersectin complex)
	Shd1p	Sla1p	CIN85	Cytoskeletal protein binding (Intersectin complex)
Late coat	End3p	End3p	EPS15, EPS15L1	Actin cortical patch component (Intersectin complex)
	Lsb4p	Lsb3p, Ysc84	SH3YL1	Actin cortical patch component
	Lsb5p	Lsb5p	TOM1, TOM1L1/2	Actin cortical patch component
	Ucp3p	Gts1p	-	GTPase activating protein (fungi only)
	Wsp1p	Las17p	WAS, WASL	WASp homolog
	Vrp1p	Vrp1p	WIPF1/2, WIP	Verprolin
	Bzz1p	Bzz1p	TRIP10, FNBP1/L	F-BAR domain protein (syndapin-like)
	-	Scd5p	-	(Budding yeast only)
WASp/Myo	Myo1p	Myo3p Myo5p	MYO1E/F	Myosin Type I-e
	Bbc1p	Bbc1p	-	WIP family cytoskeletal protein (fungi only)
	Aim21p	Aim21p	-	Barbed end F-actin assembly inhibitor (fungi only)
	Cdc15p	Hof1p	PSTPIP1/2	Extended Fer/CIP4 (EFC) domain protein
	Cam1p	Cmd1p	CALM1/2/3/4/5	Calmodulin
	Act1p	Act1p	ACTA/B/C/G/L	Actin
	Arc5p	Arc15p	ARPC5, ARPC5L	ARP2/3 actin-organizing complex subunit Arc5
	Arc3p	Arc18p	ARPC3	ARP2/3 actin-organizing complex subunit Arc21
	Arc4p	Arc19p	ARPC4	ARP2/3 actin-organizing complex subunit Arc4
	Arc2p	Arc35p	ARPC2	ARP2/3 actin-organizing complex subunit Arc34
	Arc1p	Arc40p	ARPC1A/B	ARP2/3 actin-organizing complex subunit Sop2
	Arp2p	Arp2p	ACTR2	ARP2/3 actin-organizing complex subunit Arp2
	Arp3p	Arp3p	ACTR3, ACTR3B/C	ARP2/3 actin-organizing complex subunit Arp3
	Dip1p	Ldb17	NCKIPSD	WISH/DIP/SPIN90 ortholog, endocytosis protein
	Abp1p	Abp1p	DBNL	Cofilin/tropomyosin family, debrin ortholog
	Acp1p	Cap1p	CAPZA1/2	F-actin capping protein alpha subunit
	Acp2p	Cap2p	CAPZB	F-actin capping protein beta subunit
Actin	Fim1p	Sac6p	LCP1, PLS1/3	Fimbrin
	Stg1p	Scp1p	TAGLN, TAGLN2/3	Calponin/transgelin-like actin modulating protein
	Twf1p	Twf1p	TWF1/2	Twinfilin
	Crn1p	Crn1p	CORO1A/B/C	Actin binding protein, coronin
	Ppk29, Ppk30, Ppk38	Ark1p, Prk1p, Akl1p	BMP2K, AAK1	Ark1/Prk1 family protein kinase
	Adf1p	Cof1p	DSTN, CFL1, CFL2	Actin depolymerizing factor, cofilin
	Aip1p	Aip1p	WDR1	Actin binding WD repeat protein
	-	Bsp1p	-	(Budding yeast only)
	Cdc3p	Pfy1p	PFN4	Profilin
	Gmf1p	Aim7p	GMFB/G	Cofilin/tropomyosin family Glia Maturation Factor homolog
	Cap1p	Srv2	CAP1/2	Adenylyl cyclase-associated protein
	-	Aim3p	-	Budding yeast only
	Hob3p	Rvs161p	BIN3	BAR adaptor protein (amphiphysin)
	Hob1p	Rvs167p	BIN1/2, AMPH	BAR adaptor protein (amphiphysin/endophilin)
Scission	SPBC29B5.04c	App1p	-	Phosphatase converting phosphatidate to diacylglycerol
	Syj1p	Inp52	SYNJ1/2	Inositol-polyphosphate 5-phosphatase synaptojanin homolog 1
	Vps1p**	Vps1p?	DNM1, DNM1L	Dynamin family GTPase
	Lsb1p	Lsb1p, PIN3	GRAP/2, GRB2	Wiskott-Aldrich syndrome homolog binding protein
Less-well characterized	Mug137p	-	SHGL1/2/3	BAR adaptor protein, involved in endocytosis (predicted)
	Dlc1p	Tda2	TCTEX1D1/2/4, TCTE3, DYNLT1	Dynein light chain

* "-" indicates no known ortholog.

** In fission yeast, Vps1p is not recruited to endocytic patches and its role in budding yeast endocytosis needs to be resolved.

Table modified from (Lacy, Ma, Ravindra, & Berro, 2018).

In endocytosis, over 60 proteins are assembled at a localized site on the membrane to overcome mechanical barriers to internalization such as turgor pressure pushing the membrane outward, membrane bending, and membrane tension (Lacy et al., 2018). Membrane coat proteins mark sites of endocytosis along the membrane, initiating endocytic molecular assembly which results in bending of the plasma membrane into an invaginated, clathrin-coated pit that is elongated and ultimately pinched off from the membrane at scission into a nascent vesicle that is uncoated for transport or diffusion in the cytoplasm (**Figure 2**). In the studies that follow, I focus primarily on the bending, elongation, and scission phases of endocytosis, the stages of which are composed primarily of actin and actin associated proteins (M. Kaksonen, Toret, & Drubin, 2005; Sirotkin et al., 2010). The post-initiation phase of endocytosis exhibits robust, regulated molecular assembly in the model organism *S. pombe*, which has historically been used to study the cytoskeleton, is easily cultured and manipulated genetically, and has a high degree of conservation to higher-order eukaryotes and mammals (Sirotkin et al., 2010).

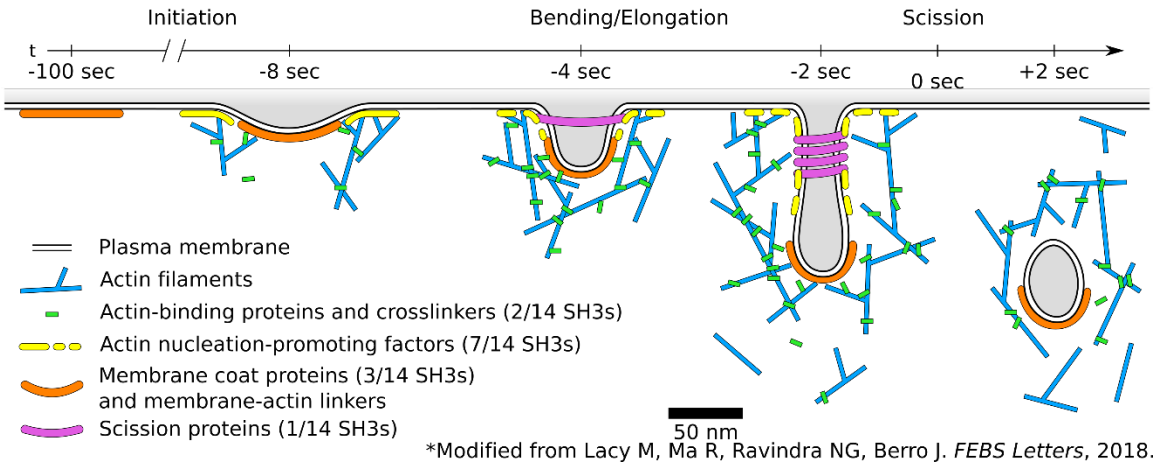

Figure 2. Overview of endocytosis and depiction of significant enrichment of SH3 domains in endocytic proteins compared to proteins involved in other cellular pathways. Overview of endocytosis broken into 3 stages that focus on its mechanical stages, namely membrane deformation and spatial organization. Membrane shapes, actin filaments, and vesicle are drawn to scale, reflecting quantitative microscopy data from yeast. Myosin-I and WASp localizations are represented by dashed lines when the reported localizations in *S. cerevisiae* and *S. pombe* differ. SH3 domains are significantly enriched in the endocytic pathway (14/21 SH3 domains in the cell are involved in endocytosis). SH3 domains are found within various endocytic proteins throughout all stages of endocytosis. It remains unclear whether they are wholly redundant or redundant within an endocytic module. The SH3 domain degeneracy for each endocytic module is indicated in the figure key. Figure was adapted from (Lacy et al., 2018).

D. How are modular protein-interaction domains related to endocytosis?

Of the 61 endocytic proteins, 10 have SH3 domains (14 SH3 domains total), 6 have EF-hand domains, 6 have BAR domains, 4 have ADFH domains, and 4 contain the Eps15 homology (EH) modular protein-interaction domain (7 EH domains total, interacting with the linear peptide motif NPF) (top 5 protein domains found within endocytic proteins by abundance) (Jones et al., 2014; Schultz, Milpetz, Bork, & Ponting, 1998; Szklarczyk et al., 2017). Both SH3 domains and EH domains are modular protein-interaction domains, yet SH3 domains are found in a higher-number of endocytic proteins than EH domains (A. Zarrinpar et al., 2003). In particular, two membrane coat proteins (Ucp8p and End3p) have 5 EH domains and 1 membrane coat protein has 3 SH3 domains (Shd1p) (**Figure 2**). 1 actin-binding protein has 2 SH3 domains (Abp1p). 1 actin nucleation-promoting factor has 2 EH domains (Pan1p) and 6 proteins in the WASp/Myo1p module have 7 SH3 domains (Lsb1p, Lsb4p, Bbc1p, Bzz1p, Myo1p, and Cdc15p). 1 scission protein (Hob1p) has a SH3 domain and an uncharacterized, endophilin A2-like protein, Mug137p, that is purported to be an endocytic protein has 1 SH3 domain (Kjaerulff, Brodin, & Jung, 2011; Carsten Mim et al., 2012).

Modular protein-interaction domains may assemble an over-represented fraction of the molecules assembled in endocytosis. The spatiotemporally coordinated web of the endocytic molecular machinery may, in totem, form a giant component, directional network, i.e., an inter-connected system of protein-interactions (**Figure 3**). Modular protein-interactions may function as hubs in this molecular interaction network, acting as the components primarily responsible for assembly; indeed, SH3 domains are the most inter-connected proteins within the endocytic molecular machinery, and often form a bridge between clusters of proteins, spread out into communities. In addition, several cytoskeletal proteins contain proline-rich motifs or contain domains, such as the SH3

domain, that can bind proline-rich sequences; thus, expectedly, SH3 domains' molecular function is highly associated with cytoskeleton assembly, remodeling, and organization and they are most enriched within proteins associated with the endocytic pathway (**Figure 4**) (Holt & Koffer, 2001). Yet, there are only 21 SH3 domain-containing proteins in yeast, compared to over 200 in mammalian cells. Thus, teasing out the principles of molecular assembly attributable to modular protein-interaction domains may most optimally be done by studying endocytosis in yeast.

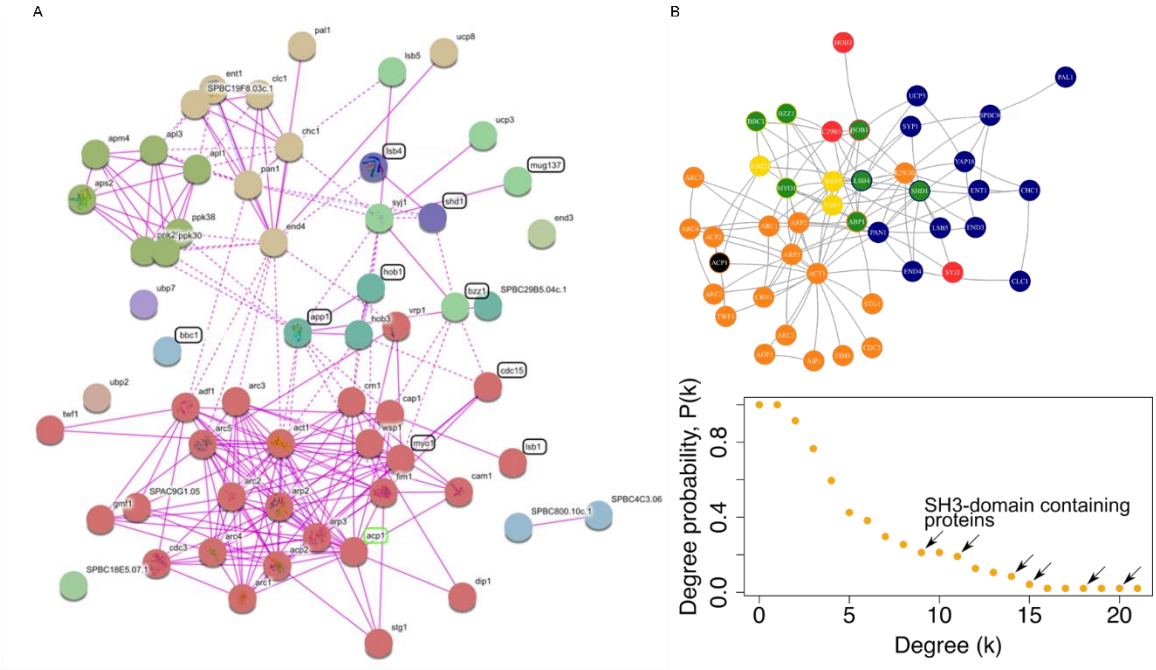

Figure 3. SH3 domains connect many different proteins and communities together within endocytic protein-interaction networks. (A) High-confidence (interaction score > 0.7), physical protein-interactions between endocytic proteins in fission yeast (Szklarczyk et al., 2017). (A) Node colors represent communities determined by hierarchical clustering of a node's edge-betweenness, namely, the number of shortest paths through the node. Dashed lines indicate cross-community interactions between clusters and solid lines represent intra-community interactions. Box around protein name indicates that the protein has at least one SH3 domain. (B, top) Smaller protein-interaction network manually curated based of low-throughput text-mining to confirm interactions between proteins. Node color represents canonical grouping of endocytic proteins into an actin module, a WASP/Myosin I module, a coat protein module, and a scission module (Holland, Shapiro, Xue, & Johnson, 2017; M. Kaksonen et al., 2005). (B, bottom) The degree probability distribution for protein interactions based on the manually curated network above indicating the tendency of SH3 domain-containing proteins to have a higher number of connections (higher degree) relative to other proteins.

E. How are modular protein interaction domains related to molecular force production during endocytosis?

Multi-valent modular protein-interaction domains, and specifically SH3 domains, induce phase-separation and promote local actin polymerization by concentrating actin assembly factors within a higher-order structure (Case, Zhang, Ditlev, & Rosen, 2019; Li et al., 2012). This sort of SH3 domain-mediated, higher-order function may be vital to endocytosis because actin polymerization is essential during endocytosis in order to generate forces and overcome mechanical barriers to internalization (Lacy et al., 2018). A large body of work has focused on how actin polymerization is regulated during endocytosis and SH3 domains, amongst several other factors, have been proposed to contribute to the regulation of actin assembly during endocytosis (Goode et al., 2015; Rodal, Manning, Goode, & Drubin, 2003; Weinberg & Drubin, 2012).

There may be also be a more direct connection between SH3 domains and force production during endocytosis. If SH3 domains form a liquid droplet at sites of endocytosis, then it is estimated that such a droplet will exert a cytoplasmic-facing force on the membrane (L.-P. Bergeron-Sandoval et al., 2017). The droplet will minimize its membrane and cytosolic interfacial energy by minimizing its surface area for a given volume and, thus, by droplet adhesion to the membrane, surface area minimization will pull the clathrin-coated pit inward (towards the cytoplasm) as the droplet pushes to adopt a more spherical shape. If SH3 domains influence the formation of such a droplet, then they may alter the forces produced by the ensemble of endocytic molecules at the membrane.

Even so, direct feedback and coupling between molecular assembly in endocytosis and mechanical properties of the underlying, endocytic molecular structure has not been reported before. Later in this dissertation, I will show that there is good reason to

suppose that a key determinant of molecular assembly during endocytosis is the ability of a higher-order, ensemble of molecules to generate force.

F. Relevance to human health

SH3 domains were first identified in oncogenes (D. Anderson et al., 1990; Bruce J. Mayer et al., 1988; Stahl et al., 1988). For example, the Crk oncoprotein consists only of SH2 and SH3 domains, yet when injected into animals, Crk rapidly induces tumors, suggesting that SH3 domains have powerful biological activities (Trahey et al., 1988). In addition to oncogenic activity, by coordinating molecular assembly during endocytosis, SH3 domains may help cells in tissues maintain homeostasis and balance between different cell types by regulating growth factor levels and growth factor secretion between cells, integrating feedback from various cell circuits through endocytosis (Adler et al., 2018). In addition, SH3 domains may be manipulated and integrated into synthetic circuits to control immune cell response and membrane receptor levels (Esensten, Bluestone, & Lim, 2017; Giron-Perez, Piedra-Quintero, & Santos-Argumedo, 2019; W. A. Lim & June, 2017; Roybal & Lim, 2017).

Annually in the United States, ~610,000 deaths are attributed to heart disease, according to the CDC. At least 13 SH3 domain-containing proteins are associated with cardiovascular disease (**Table 2**). With some of the approaches developed in this dissertation, one can use quantitative microscopy, genetic engineering, and assays for determining the extent of interchangeability of SH3 domains to studying the binding specificity of SH3 domains in different pathways. In the future, these kinds of approaches will help us better understand pathological pathways and identify novel mechanisms by which dysfunctional protein interactions disrupt cellular pathways. More

broadly, by using SH3 domains to manipulate endocytosis or molecular circuits in cardiomyocyte or immune cells, we may be able to predictably control endocytosis to regulate cholesterol levels and control vascular cells' diameter (Goldstein, Anderson, & Brown, 1982; Muro, Koval, & Muzykantov, 2004; D. Wang et al., 2002). Thus, understanding how SH3 domains influence molecular assembly during endocytosis may contribute to our understanding of pathophysiology.

Table 2. Pathway-specific biomedical relevance of studied SH3-domain containing proteins.

SH3 Protein	Description and relevance to cardiovascular health
SPIN90	Adaptor protein that interacts with integrins and is involved with cardiac myocyte differentiation in development (C. S. Lim et al., 2001).
Nck	Integrin protein involved in myofibrillogenesis (C. S. Lim et al., 2001).
SORBS1	Single-nucleotide polymorphisms are tied to ischemic infarction (Hagiwara et al., 2008), hypertension, and blood pressure regulation (Chang et al., 2016).
Endophilin A2	Endocytic protein mediating transport of ion channels and affecting the function & size of vascular smooth muscle cells (C.-Z. Liu et al., 2016).
Cortactin	Connects the actin-cytoskeleton to potassium channels that control blood flow and are associated with disorders that include hypertension (L. Tian et al., 2006).
Nkip1	Mutations cause cardiomyopathy in mice (Herron et al., 2005).
Amphiphysin 2	Endocytic protein whose decreased expression is observed in patients with ventricular arrhythmias (Prokic, Cowling, & Laporte, 2014).
alpha-IIb,beta-3	Involved in platelet signaling that retracts fibrin clots (Haling, Monkley, Critchley, & Petrich, 2011).
p47*phox*	Increases NAD(P)H oxidase enzyme activity in rat basilar arterial endothelial cells, creating reactive oxygen species known to play a critical role in the development of vascular diseases and stroke (Ago et al., 2005; de Mendez, Homayounpour, & Leto, 1997; El-Benna, Dang, Gougerot-Pocidalo, Marie, & Braut-Boucher, 2009; R. M. Taylor et al., 2007).
p67*phox*	(see p47*phox*)
SH3BGR	Critical for sarcomere formation in striated muscle and in cardiac development (Jang et al., 2015).
Nebulette	~20 mutations that either cause or are associated with hypertrophic cardiomyopathy, left ventricular noncompaction cardiomyopathy, and thin-wall dilated cardiomyopathy and endocardial fibroelastosis (Hernandez et al., 2016; Mastrototaro et al., 2015; Purevjav et al., 2010; Ram & Blaxall, 2010).
Dab2	Involved in cholesterol regulation by sorting LDL receptors into endocytic vesicles, linking endocytosis, SH3 domains, and atherosclerosis (Maurer & Cooper, 2006).

G. Do SH3 domains assemble molecules into the endocytic pathway?

In this dissertation, I am interested in a broad hypothesis regarding SH3 domains, namely, that they assemble proteins into cellular pathways by spatiotemporally connecting molecules together through binding interactions. In particular, I am interested in more deeply understanding their role in recruiting endocytic proteins to endocytic structures within the cell and in exploring their role in regulating actin assembly during endocytosis. The studies in this dissertation address the following questions. Why are there so many SH3 domains within endocytic proteins and within endocytic structures? Are SH3 domains important for actin assembly? Or, are they largely dispensable for actin assembly and endocytosis? What is the individual influence of each endocytic SH3 domain on endocytosis and the cell? Are SH3 domains important for the expression and localization of their own protein? Do all single, endocytic SH3 domain deletions exhibit similar phenotypes? Is the process of endocytosis robust to deleting SH3 domains? And, finally, how do SH3 domains assemble distinct sets of proteins into distinct pathways?

II. Diverse influences of SH3 domains on actin assembly and endocytosis

Adapted from submitted work: Ravindra NG (2019). “Comprehensive single-copy deletions of endocytic SH3 domains reveal their diverse influences on actin assembly and endocytosis.” *Molecular Biology of the Cell*

A. Introduction

Molecules in a cellular pathway can be brought together through protein interactions mediated by non-catalytic, protein-interaction domains such as the Src homology-3 (SH3) domain (Bhattacharyya et al., 2006; Pawson & Nash, 2003). SH3 domains interact with proline-rich motifs and are involved in assembling pathways linked to cellular proliferation, signaling, and migration (Bhattacharyya et al., 2006; Kurochkina & Guha, 2013; Saksela & Permi, 2012). In particular, the cellular process of endocytosis is significantly enriched for SH3 domain-containing proteins (Siton-Mendelson & Bernheim-Groswasser, 2017; Xin et al., 2013).

Endocytosis involves the assembly of over 60 proteins at the plasma membrane to bend the membrane into a vesicle and internalize membrane, membrane receptors, and nutrients (Lacy et al., 2018). Actin polymerization is critical to overcome mechanical barriers to membrane bending and internalization and for successful endocytosis (A.E. Carlsson, 2018; Lacy et al., 2018). As such, the timing and activities of components associated with actin polymerization during endocytosis are tightly coordinated (Goode et al., 2015; Marko Kaksonen & Roux, 2018).

At endocytic sites, actin is polymerized into a branched filament network. The Arp2/3 complex creates these branched networks, forming actin patches at sites of endocytosis (T.D. Pollard & Borisy, 2003). Precise understanding of the timing and regulation of Arp2/3 activity in endocytosis remains elusive because it involves the coordination of many dynamic interactions (Rottner, Hanisch, & Campellone, 2010). However, it is understood that a burst of actin polymerization can be initiated by high concentrations of nucleation promoting factors (NPFs) that activate the Arp2/3-complex (Sirotkin et al., 2010). Yet, how Arp2/3 interacts with NPFs and how NPF activity is regulated in a spatiotemporal manner *in vivo* remains an open, yet key, question in understanding the regulation of biochemical assembly in actin networks (Goode et al., 2015). One of the purported roles of SH3 domain-containing proteins in endocytosis is to regulate Arp2/3 activity (Goode et al., 2015; Sun et al., 2017). However, the extent to which SH3 domains influence actin assembly during endocytosis has not yet been comprehensively or quantitatively described.

SH3 domains can form liquid droplets through multivalent interactions that promote actin polymerization and may have a similar role in endocytosis (Li et al., 2012; Sun et al., 2017). However, if multivalent interactions are important, it remains unknown as to whether any single valence unit, namely a specific SH3 domain, is important for the formation of a liquid droplet or required to facilitate a burst of actin polymerization for internalization. In other membrane signaling systems, multivalent interactions increase the dwell time and stoichiometry of the Arp2/3 complex with a NPF but it remains unclear if this or other presumed functionalities of phase-separation are relevant to endocytosis (Case et al., 2019). Rather, a burst of actin polymerization requires high concentrations of NPFs, which can be achieved through numerous, transient, and binary interactions,

which may be more relevant to endocytosis (Pawson & Nash, 2003; E. M. Schmid & McMahon, 2007; Smith, Baker, Halebian, & Smith, 2017).

Another plausible manner in which SH3 domains may affect actin assembly is through influencing the ability of NPFs to interact with Arp2/3, thus modulating the activity of the Arp2/3 complex. Yeast express four NPFs, differentially determining the size and rate of branched actin network assembly: WASp, the strongest, type-I myosin, the second strongest, and the weak activators Pan1p and Abp1p (Sirotkin, Beltzner, Marchand, & Pollard, 2005; Sun, Martin, & Drubin, 2006). In mammals, WASp is auto-inhibited in the cytoplasm but in yeast, WASp is not auto-inhibited; instead, yeast WASp is inhibited from activating Arp2/3 by binding other proteins through multivalent, proline-rich and SH3 domain interactions (Rodal et al., 2003). Stimulation of Arp2/3 nucleation activity by WASp involves both release of WASp inhibition and the additional regulatory control of WASp homodimerization (Padrick et al., 2008). Not much is known about how SH3 domains coordinate binding inhibition and oligomerization states of NPFs *in vivo*. Furthermore, the SH3 domains responsible for facilitating or inhibiting WASp have not been comprehensively documented (Rodal et al., 2003; Sun et al., 2017). The activity of other NPFs in endocytosis may also be regulated by SH3 domain-mediated interactions. For example, myosin-I's SH3 domain and its interaction with verprolin are required for its NPF activity; yet, quantification of myosin-I's SH3 domain's effect on actin assembly in endocytosis is lacking (B. L. Anderson et al., 1998; Evangelista et al., 2000).

Due to degeneracy in the number of SH3 domains in endocytosis and within endocytic proteins, it remains an important challenge to identify the particular domains and interactions that influence actin assembly in endocytosis (Galletta, Chuang, & Cooper, 2008). To figure out the influence of each endocytic SH3 domain on actin assembly and endocytosis, we created *S. pombe* strains containing a reporter for

endocytosis and a single, endogenous SH3 domain deletion. We used a comprehensive library of single endocytic SH3 domain deletions to quantify the influence of each endocytic SH3 domain on endocytosis for the first time. We found that SH3 domains in endocytosis enhance, restrict, or have minor or redundant effects on actin assembly. This variability in activity is consistent with SH3 domain regulation of the localization of NPFs and mediation of WASp interactions in the Arp2/3 activation pathway; specifically, the binding of WASp and G-actin and the formation of a WASp, G-actin, and Arp2/3 ternary complex. Our results demonstrate that most endocytic SH3 domains are not redundant and, as a group, SH3 domains have diverse influences on endocytosis.

B. Results

1. SH3 domains in S. pombe

Endocytosis is the most enriched biological process for SH3 domain-containing proteins in *S. pombe* (**Figure 4**) (D. Huang, B. T. Sherman, & R. A. Lempicki, 2009). There are 26 SH3 domains across 21 proteins in *S. pombe* and 14 of these SH3 domains are found within 10 proteins known to be involved with endocytosis (Letunic & Bork, 2018). Non-endocytic SH3 domains in *S. pombe* are primarily within proteins involved in actin-cytoskeleton organization, for example, in the cytokinetic pathway (**Figure 4**). Of the 14 SH3 domains in endocytic proteins, 2 are within proteins in the actin module, 7 are within the NPF module, 3 are within the membrane coat protein module, and 1 is in the scission module (M. Kaksonen et al., 2005). Among the 61 known *S. pombe* endocytic proteins, 46 contain at least one canonical SH3 domain-binding motif, PXXP (proline, any two amino acids, and another proline residue) (**Figure 4**).

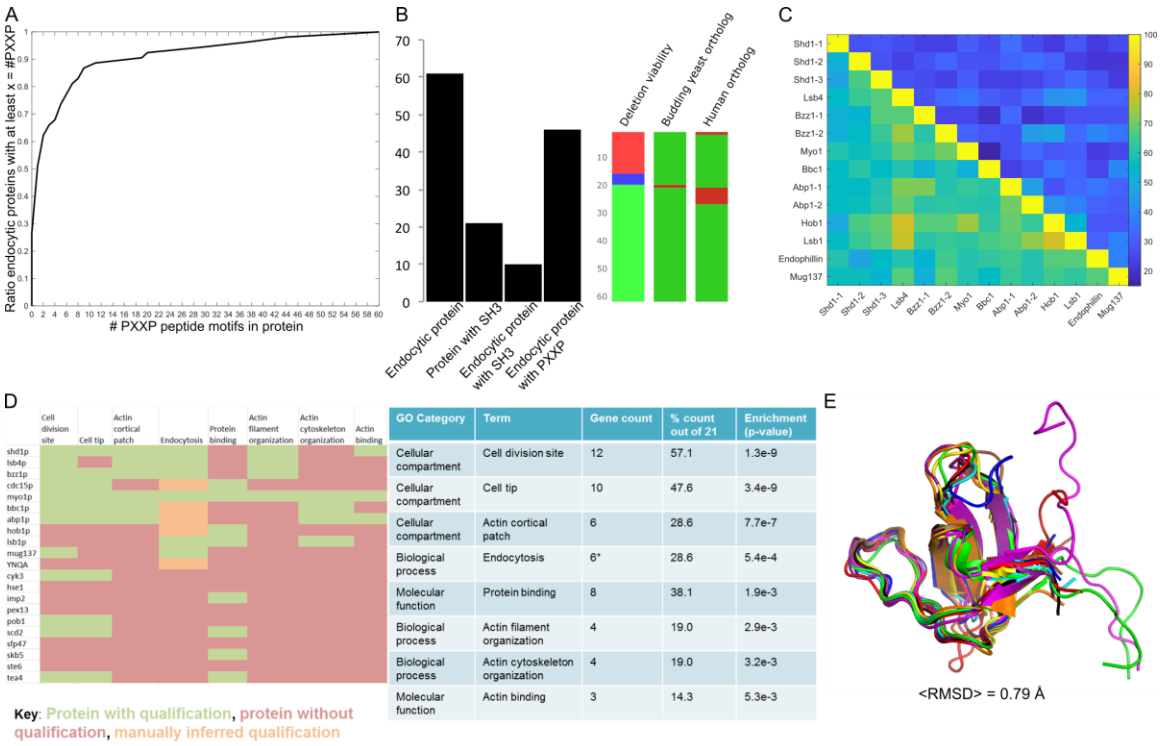

GO Category	Term	Gene count	% count out of 21	Enrichment (p-value)
Cellular compartment	Cell division site	12	57.1	1.3e-9
Cellular compartment	Cell tip	10	47.6	3.4e-9
Cellular compartment	Actin cortical patch	6	28.6	7.7e-7
Biological process	Endocytosis	6*	28.6	5.4e-4
Molecular function	Protein binding	8	38.1	1.9e-3
Biological process	Actin filament organization	4	19.0	2.9e-3
Biological process	Actin cytoskeleton organization	4	19.0	3.2e-3
Molecular function	Actin binding	3	14.3	5.3e-3

Figure 4. Bioinformatic analysis of SH3 domains in *S. pombe*. (A) Cumulative distribution function showing the ratio of endocytic proteins containing a particular number of canonical SH3 domain-binding motifs, PXXP, where P represents proline and X represents any amino acid, within the endocytic proteins peptide sequence. Motif search was performed with PomBase (see methods). (B, left) The number of endocytic proteins, proteins with SH3 domains, and endocytic proteins with SH3 domains or canonical SH3 binding motifs in *S. pombe*. (B, right) Comparison of *S. pombe* endocytic proteins with budding yeast and human proteins. For deletion viability, number of proteins whose deletion is inviable (red), variable (blue), and viable (green). For budding yeast and human orthologs, red indicates that *S. pombe* does not have the budding yeast or human ortholog and green indicates that *S. pombe* has that ortholog. (C) All combinations of pair-wise alignments for endocytic SH3 domains. Lower triangle shows percent similarity and upper triangle shows percent identity. (D) Bioinformatic and gene ontology analysis for endocytic proteins with SH3 domains. Asterisk indicates that 5 genes known to be involved with endocytosis in the literature but not annotated in GO databases were omitted from significance calculations (D. Huang et al., 2009). (E) Structural alignment of endocytic SH3 domains. Representative structures were taken from budding yeast or human orthologs. For complete list of PDB IDs, see "SH3BoundaryDefinition.pdf" on git.yale.edu/ngr4. Structures were aligned to Abp1p's SH3 domain (PDB ID 1JO8) for calculation of the root-mean square deviation in PyMOL.

Integrating data from numerous sources, I created a schematic to show how, in endocytosis, the initial recruitment time of endocytic proteins containing SH3 domains overlaps with the primary driver of actin polymerization, the Arp2/3 complex, and its strongest activator *in vitro*, WASp (**Figure 5**, **Table 3**) (Arasada & Pollard, 2011; Julien Berro & Thomas D. Pollard, 2014; Goode et al., 2015; Kjaerulff et al., 2011; MacQuarrie et al., 2018; Andrea Picco, Mund, Ries, Nédélec, & Kaksonen, 2015; Sirotkin et al., 2010; Urbanek, Chan, & Ayscough, 2015). Throughout endocytosis, other SH3-domain containing proteins arrive such that, ~2s before scission, all SH3 domain-containing proteins have started to be assembled. This excludes the poorly characterized proteins Lsb1p, Lsb4p, and Mug137p, which are known to participate in endocytosis but extensive characterization of their assembly dynamics is lacking (Goode et al., 2015).

Table 3. Recruitment number and timing for endocytic proteins of interest.

Common name	Protein name	Peak (# molecules)	Appears (s)	Peak (s)	Vanishes (s)	Reference
Actin	Act1p	7050	-9	1	10	Sirotkin et al. 2010
Actin binding protein	Abp1p	150	-7	0	8	Sirotkin et al. 2010
Capping protein[(a)]	Acp1p	152	-9	0	11	Berro & Pollard 2014
Actin-related protein (Arp) 2/3 complex	Arp2p[(b)]	320	-13	0	13	Sirotkin et al. 2010
Bni1 synthetic lethal and Bee1 (las17) complex member	Bbc1p	48	~ -6	~ -2	~ 6	MacQuarrie et al. 2018
Syndapin-like	Bzz1p	80	~ -3	~ 2	~ 7	Arasada & Pollard 2011
Extended Fer/CIP4 domain protein	Cdc15p	130	~ -7	~ 1	~ 7	Arasada & Pollard 2011
Amphiphysin/ endophilin	Hob1p	125[(c)]	-3[(c)]	0[(c)]	3[(c)]	Picco et al. 2015
Las17 (WASp) binding protein	Lsb1p	-	-	-	-	Goode et al. 2015
Las17 (WASp) binding protein	Lsb4p	-	-	-	-	Urbanek et al. 2015
Meiotically up-regulated gene (endophilin A-like)	Mug137p	-	-	-	-	Kjaerulff et al. 2011, Wood et al. 2012
Myosin I	Myo1p	400	-9	-2	5	Sirotkin et al. 2010
Intersectin complex member	Shd1p	91[(c)]	-18[(c)]	-4[(c)]	3[(c)]	Picco et al. 2015
WASp	Wsp1p	230	-10	-2	2	Sirotkin et al. 2010

"~" indicates that values were taken from figures within indicated references.

[(a)]Acp1p and Acp2p form a heterodimeric complex to cap actin branched filaments and are referred to as "capping protein." Acp1p is used in this study as a marker for endocytosis..

[(b)]Arp2p chosen as protein to represent Arp2/3 complex since it is the last to appear at endocytic structures *in vivo*

[(c)]Quantitative data is taken from experiments using *S. cerevisiae*, which may differ from *S. pombe*, the organism from which the remainder of the data in the table is drawn from and the organism used in this study.

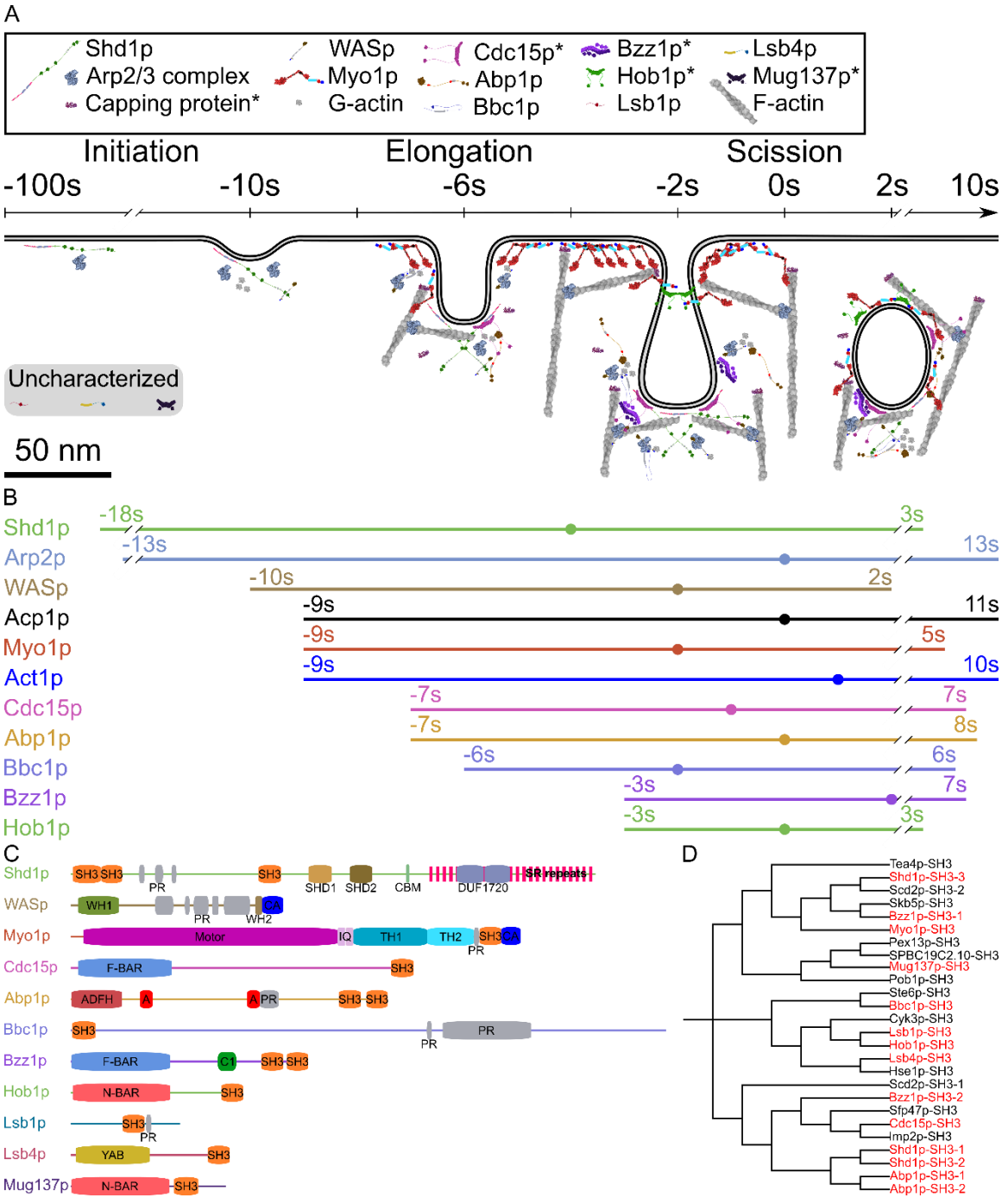

Figure 5. Endocytic proteins with SH3 domains arrive throughout endocytosis and their SH3 domains are not necessarily more closely related to other endocytic SH3 domains. (A) After an initial membrane deformation, nascent endocytic vesicles diffuse into the cytoplasm ~10s after a burst of actin polymerization. Depicted are SH3 domain containing proteins and other proteins of interest that do not have SH3 domains but are regulatory or binding targets of SH3 domains in endocytosis: actin (Act1p), WASp, and the Arp2/3 complex component, Arp2p. References for information in this schematic in Table 3. The number of molecules depicted

in the schematic is ~1/30th of the measured peak number of molecules and are pictured at the appropriate stage. *Asterisk indicates that the schematized protein is a dimer. (B) Total and peak assembly time of proteins of interest in endocytosis. 0-s represents scission of the endocytic pit. Dot in the line segment represents the time at which the maximum number of molecules is assembled into endocytosis for a particular protein. (C) Protein features for proteins of interest in endocytosis. (D) Evolutionary tree diagram shows the relationship between SH3 domains in *S. pombe*.

To determine if SH3 domains in endocytosis are more closely related than non-endocytic SH3 domains and whether SH3 domains with a particular endocytic role clustered together by sequence, we performed various sequence alignments. *S. pombe* endocytic SH3 domains have poor sequence identity, compared pairwise, to each other (**Figure 6**). Furthermore, some endocytic SH3 domains in *S. pombe* are distantly related (**Figure 5**). In contrast, *S. pombe* SH3 domains' core binding surfaces, namely, the hydrophobic motif and the WPY triad, are well conserved. This contrasts with the overall sequence identity of the entire domain, which may suggest specificity in SH3-domain mediated interactions (**Figure 6**). And yet, representative structures of endocytic SH3 domain orthologs from the Protein Data Bank (PDB) structurally align with low RMSD (**Figure 4**).

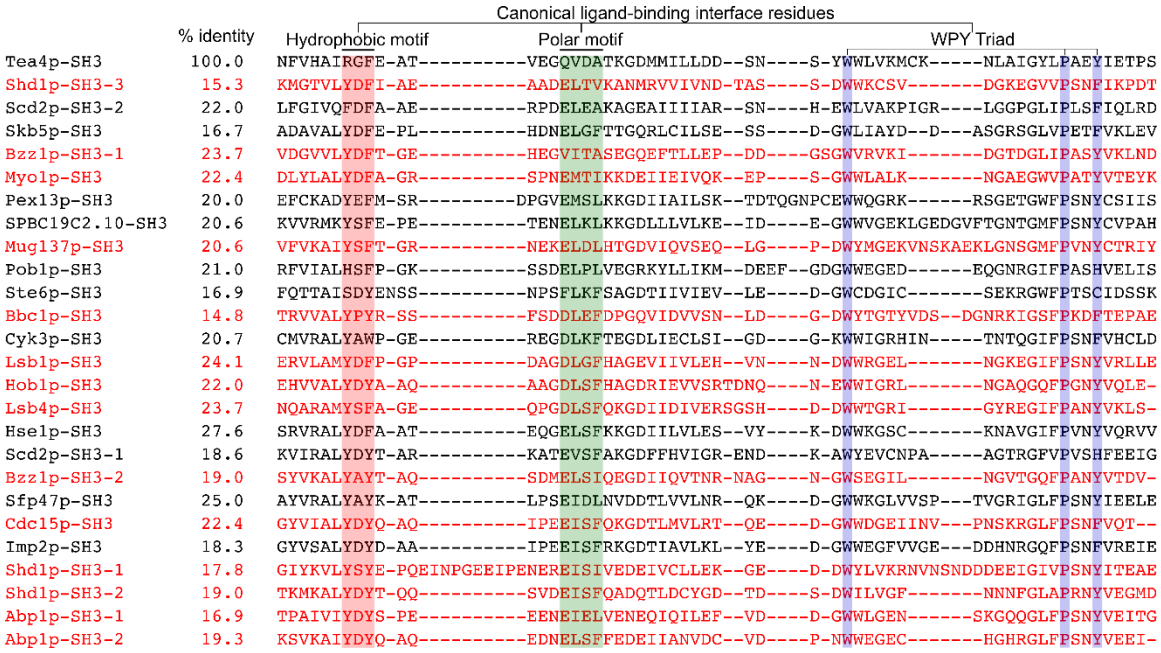

Figure 6. Sequence alignment of all SH3 domains in *S. pombe*. SH3 domains in known endocytic proteins are highlighted in red. SH3 domains bind PXXP motifs in proteins, interfacing with the well-conserved hydrophobic motif (red boxed residues) and WPY triad (blue boxed residues) while positive residues flanking the canonical peptide ligand motif interacts with SH3 domains' polar motif (green boxed resides). Protein order is ranked in evolutionary distance to Tea4p-SH3.

Proteins with SH3 domains also contain several other domains and features. It is common for SH3-domain containing proteins to possess proline-rich regions (PRs). Some of these proteins may be auto-inhibited since their PR may bind their own SH3 domain to prevent interactions. This kind of auto-inhibition can be regulated by phosphorylation (Kurochkina & Guha, 2013). SH3 domains are often found in proteins that have BAR domains, which serve to target proteins to sites of membrane curvature, for example, endocytic structures (Zhao et al., 2013). SH3 domains are also found in proteins with NPF activity, whose central or connecting (C) and acidic regions (A) bind and activate the Arp2/3 complex (T.D. Pollard & Borisy, 2003). Other proteins containing SH3 domains also contain actin-binding domains, such as the ADFH, YAB, and TH1/2 domains in Abp1p, Lsb4p, and Myo1p, respectively. Thus, SH3 domain-containing proteins in endocytosis can connect the membrane to actin through BAR domains and actin binding domains, may interact with many endocytic proteins, may play regulatory roles in endocytic assembly dynamics, may coordinate their interactions within the endocytic SH3 interactome, and may be regulatory targets (Verschueren et al., 2015).

2. Defining the sequence boundary of SH3 domains

The precise sequence boundary of a SH3 domain varies among known crystal and solution NMR structures and databases. To offer a precise definition, with independent, structurally functional cut-offs, we compiled a library of PDB structures of SH3 domains whose proteins are orthologous to *S. pombe* (**Figure 7**; for complete list of representative structures, see "SH3BoundaryDefinition.pdf" on git.yale.edu/ngr4). Then, we compiled a library of peptide sequences constructed with sequences for *S. pombe* SH3 domains from four databases: SMART, PROSITE, SUPERFAMILY, Pfam (Finn et al., 2016; Gough, Karplus, Hughey, & Chothia, 2001; Schultz et al., 1998; Sigrist et al.,

2002). I performed multiple sequence alignments of the structure sequences and the four database sequences and defined boundaries that contained all the structural features of SH3 domains and minimally overlapped across databases (**Figure 7**; for complete list of SH3 domain boundary definitions, see "SH3BoundaryDefinition.pdf" on git.yale.edu/ngr4). Previous approaches have used multiple sequence alignments between databases to define SH3 domain boundaries, typically between Pfam and SMART databases (Teyra et al., 2017; Verschueren et al., 2015). However, it has been noted that this approach to defining the boundaries of SH3 domains likely leads to poor boundary definitions and un-successful purification SH3 domains in the human proteome (<1/3 of SH3 domains in the human proteome were successfully purified in a recent study using only database overlap to define the boundary of SH3 domains) (Teyra et al., 2017). In contrast to these more limited approaches, we include solved structures of SH3 domains that are orthologous and representative of *S. pombe* SH3 domains and we use the sequences from these successfully purified and associated structural feature annotations in considering the boundary of SH3 domains. By using SH3 domain sequence boundaries from representative structures and structural features in selecting the SH3 domain boundaries, we increased the likelihood that the SH3 domains we defined could be purified and fold independently. Furthermore, we included additional databases in our alignments, compared to previous approaches (Verschueren et al., 2015). This novel SH3 domain boundary definition allowed us to confidently select the genetic sequence for deletion and avoid disrupting the folding of neighboring domains.

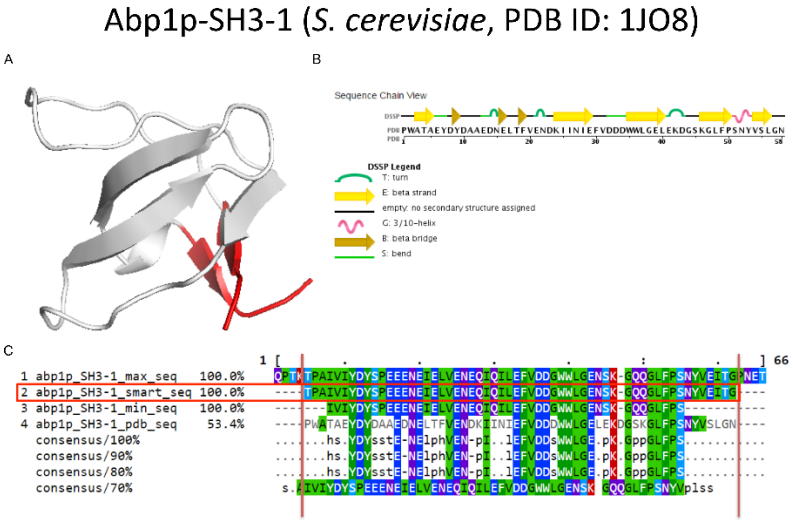

Figure 7. Definition of SH3 domain boundaries in the *S. pombe* genome based on alignments between multiple databases and sequence annotations of structural features as extracted from representative SH3 domain structures deposited in the PDB. See Methods for full details of boundary definition and "SH3BoundaryDefinition.pdf" on git.yale.edu/ngr4 for PDB IDs used as representative structures and for boundary definitions for all endocytic SH3 domains in *S. pombe*. (A) Representative PDB structure for the indicated *S. pombe* SH3 domain. Title parentheses: organism that the structure is derived from and the PDB ID of the structure. SH3 domains were annotated in PyMOL and red coloring represents N/C-termini of the representative structure. (B) Sequence of the representative SH3 domain structure with annotated structural features provided with PDB depositions (annotation figure provided by rcsb.org tools). (C) Clustal Omega alignment of the maximum peptide sequence overlap from multiple databases (1), the sequence of a SH3 domain from the SMART database (2), the minimum database overlap (3), the sequence of the PDB structure (3), and the consensus sequence for these alignments (bottom). Red box and vertical lines indicate sequence taken for the SH3 domain in S. pombe. Residues in alignments are colored, annotated, and arranged into consensus sequences using previously developed web-based tools (Brown, Leroy, & Sander, 1998).

3. Deletion of endocytic SH3 domains and quantification of assembly, dynamics, and the cell's regulation of endocytosis

In order to determine the role of each of the 14 SH3 domains in endocytosis, we deleted individual SH3 domains at their endogenous locus using CRISPR-Cas9 mediated gene editing and gap repair in *S. pombe* (**Table 4**) (Fernandez & Berro, 2016; Kostrub, Lei, & Enoch, 1998). In each strain, we tagged the Acp1p subunit of the canonical actin capping protein with green fluorescent protein (mEGFP) to monitor endocytosis using quantitative fluorescence microscopy. Acp1p (hereafter, capping protein) caps the barbed ends of actin filaments and is recruited almost exclusively to endocytic structures within the cell; though, during cytokinesis, a small percentage of capping protein localizes to the cytokinetic ring (~2%) (David R. Kovar, Wu, & Pollard, 2005). Monitoring the amount of capping protein assembled into endocytic structures allowed us to study actin assembly in endocytosis since capping protein is a reliable proxy for actin assembly (Julien Berro & Thomas D. Pollard, 2014; Sirotkin et al., 2010) (**Figure 19**). The peak of capping protein assembly was previously measured relative to other endocytic proteins and correlated with the motility of the endocytic patch, demonstrating that capping protein reproducibly accumulates a maximum of ~152 molecules at the time of scission (Julien Berro & Thomas D. Pollard, 2014; Sirotkin et al., 2010). By aligning the peak of capping protein's assembly into endocytic structures for individual tracks, we report the assembly dynamics of capping protein into endocytic structures relative to scission of nascent endocytic vesicles at t = 0s (**Figure 10 – Figure 14**).

Table 4. *S. pombe* strains used to investigate the influence of individual SH3 domains on actin assembly and endocytosis.

Strain	Genotype	Source
FY527	*ade6-M216 his3-D1 leu1-32 ura4-D18*	S. Forsburg
JBSp355	*fex1Δ fex2Δ ade6-M216 his3-D1 leu1-32 ura4-D18*	This study
JBSp366	*acp1-mEGFP fex1Δ fex2Δ ade6-M216 his3-D1 leu1-32 ura4-D18*	This study
JBSp337	*bbc1-SH3Δ acp1-mEGFP fex1Δ fex2Δ ade6-M216 his3-D1 leu1-32 ura4-D18*	This study
JBSp345	*bzz1-SH3-1Δ acp1-mEGFP fex1Δ fex2Δ ade6-M216 his3-D1 leu1-32 ura4-D18*	This study
JBSp379	*myo1-SH3Δ acp1-mEGFP fex1Δ fex2Δ ade6-M216 his3-D1 leu1-32 ura4-D18*	This study
JBSp427	*lsb4-SH3Δ acp1-mEGFP fex1Δ fex2Δ ade6-M216 his3-D1 leu1-32 ura4-D18*	This study
JBSp429	*mug137-SH3Δ acp1-mEGFP fex1Δ fex2Δ ade6-M216 his3-D1 leu1-32 ura4-D18*	This study
JBSp431	*shd1-SH3-3Δ acp1-mEGFP fex1Δ fex2Δ ade6-M216 his3-D1 leu1-32 ura4-D18*	This study
JBSp433*	*acp1-mEGFP bzz1-SH3-2Δ fex1Δ fex2Δ ade6-M216 his3-D1 leu1-32 ura4-D18*	This study
JBSp434*	*acp1-mEGFP cdc15-SH3Δ fex1Δ fex2Δ ade6-M216 his3-D1 leu1-32 ura4-D18*	This study
JBSp435*	*acp1-mEGFP hob1-SH3Δ fex1Δ fex2Δ ade6-M216 his3-D1 leu1-32 ura4-D18*	This study
JBSp437*	*acp1-mEGFP abp1-SH3-2Δ fex1Δ fex2Δ ade6-M216 his3-D1 leu1-32 ura4-D18*	This study
JBSp450	*shd1-SH3-1Δ acp1-mEGFP fex1Δ fex2Δ ade6-M216 his3-D1 leu1-32 ura4-D18*	This study
JBSp451	*abp1-SH3-1Δ acp1-mEGFP fex1Δ fex2Δ ade6-M216 his3-D1 leu1-32 ura4-D18*	This study
JBSp452	*lsb1-SH3Δ acp1-mEGFP fex1Δ fex2Δ ade6-M216 his3-D1 leu1-32 ura4-D18*	This study
JBSp457	*shd1-SH3-2Δ acp1-mEGFP fex1Δ fex2Δ ade6-M216 his3-D1 leu1-32 ura4-D18*	This study

*In these strains, JBSp355 or its complementary mating type, JBSp362, was used to first edit a protein to delete its SH3 domain, *protein-SH3Δ*, then, in positive strains, *acp1* was edited to *acp1-mEGFP*.

4. *The robustness of quantitative microscopy measurements of endocytosis in control experiments and sensitivity analysis of statistical significance testing*

To monitor actin assembly dynamics during endocytosis, we imaged *S. pombe* cells expressing capping protein tagged with monomeric enhanced green fluorescent protein (mEGFP or EGFP). I used a microfluidic perfusion system to provide optical stability during imaging and took advantage of automated spot tracking, identical to methodology which has been reported to be robust and reproducible over a wide-range experimental conditions (Lemière & Berroa, 2018). The control experiments reported in this study exhibit minimal variation in the average peak values (~1% variation across individual wells and multiple fields of view) (**Figure 8**). In particular, for the summary metrics reported (maximum capping protein assembled, maximum and minimum assembly rate, absolute displacement and cumulative path length 5s after scission), control experiments vary by <1% (corresponding peaks or troughs in relevant panels, **Figure 8**). This result supports the definition that any variation in the summary metrics for test strains corresponding to an order of magnitude higher than the variation observed in control experiments is a “small” or “relatively minor” effect. That is, given that the variation in control experiments is on the order of 1%, effects <10% different than controls are considered to be similar to control cells for that metric. Thus, similar to a previous report using the same methodology, the experimental and quantitative microscopy strategy described here allows us to achieve a high-degree of reproducibility across experimental conditions, especially fields-of-view and days of experimentation, facilitates un-biased collection of hundreds of endocytic events to observe endocytic behavior in individual strains, and allows us to detect small perturbations to endocytosis in a variety of strains that previous methods could not discern (Lemière & Berroa, 2018). Furthermore, measurements of capping protein in control experiments match previous findings,

namely, capping protein assembles and disassembles in ~15s and with a burst of patch motility occurring ~3s before scission (Julien Berro & Thomas D. Pollard, 2014; Sirotkin et al., 2010).

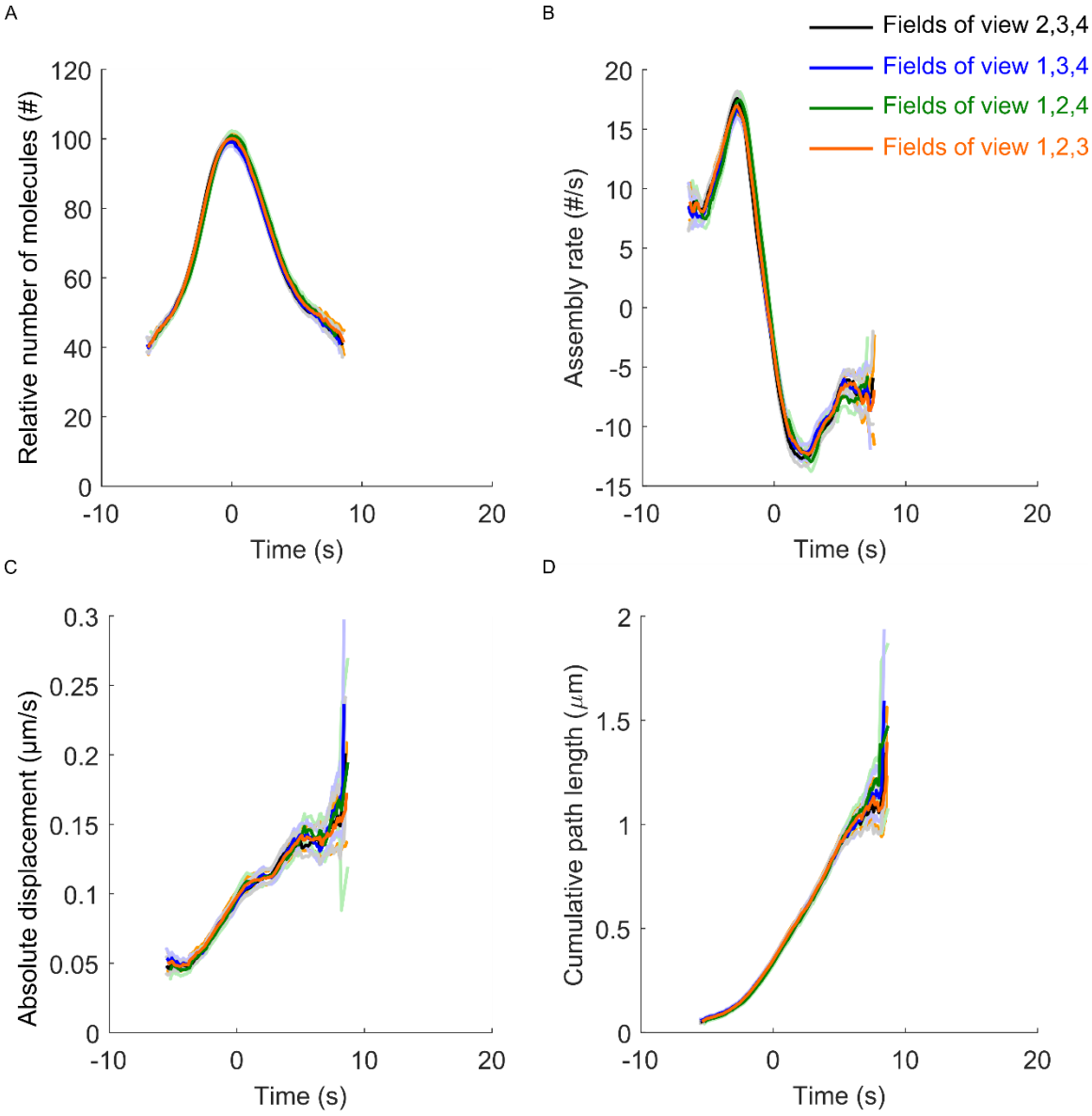

Figure 8. Variation in control experiments is less than 1% for metrics used to summarize quantitative microscopy data across SH3 domain deletion strains. In control experiments, >300 individual tracks from a single chamber across 3-10 fields of view are used to compare SH3 domain deletion effects. Black, blue, green, and orange curves correspond to averages for 476, 460, 377, and 460 individual tracks from a control strain (JB 366: capping protein tagged with EGFP, no SH3 domains deleted) relative to scission at t=0s. Ribbons show 95% CI. (A) The number of molecules versus time, relative to 100 for the first control experiment (black curve). (B) Associated assembly rate in time, expressed as relative number of molecules per second. (C) Mean absolute displacement in an interval of 1s at each time. (D) Cumulative path length up to indicated time.

Over the time range the data described in this study were collected, measurements for the peak assembly of capping protein into endocytic structures, represented as arbitrary units of fluorescence, can vary by as much as 12% (**Figure 9A**). Thus, for each experimental condition, measurements in arbitrary units of fluorescence are calibrated to number of molecules for the average peak value in control experiments, preserving the relationship between control and test strains and yielding average curves that are highly reproducible across experimental conditions (varying ~1%, see above and **Figure 8A**). The utilization of calibration to compare experiments is consistent with other quantitative microscopy methodologies (Akamatsu et al., 2019; Lemière & Berroa, 2018; Manenschijn, Picco, Mund, Ries, & Kaksonen, 2018; Andrea Picco et al., 2015; Sirotkin et al., 2010).

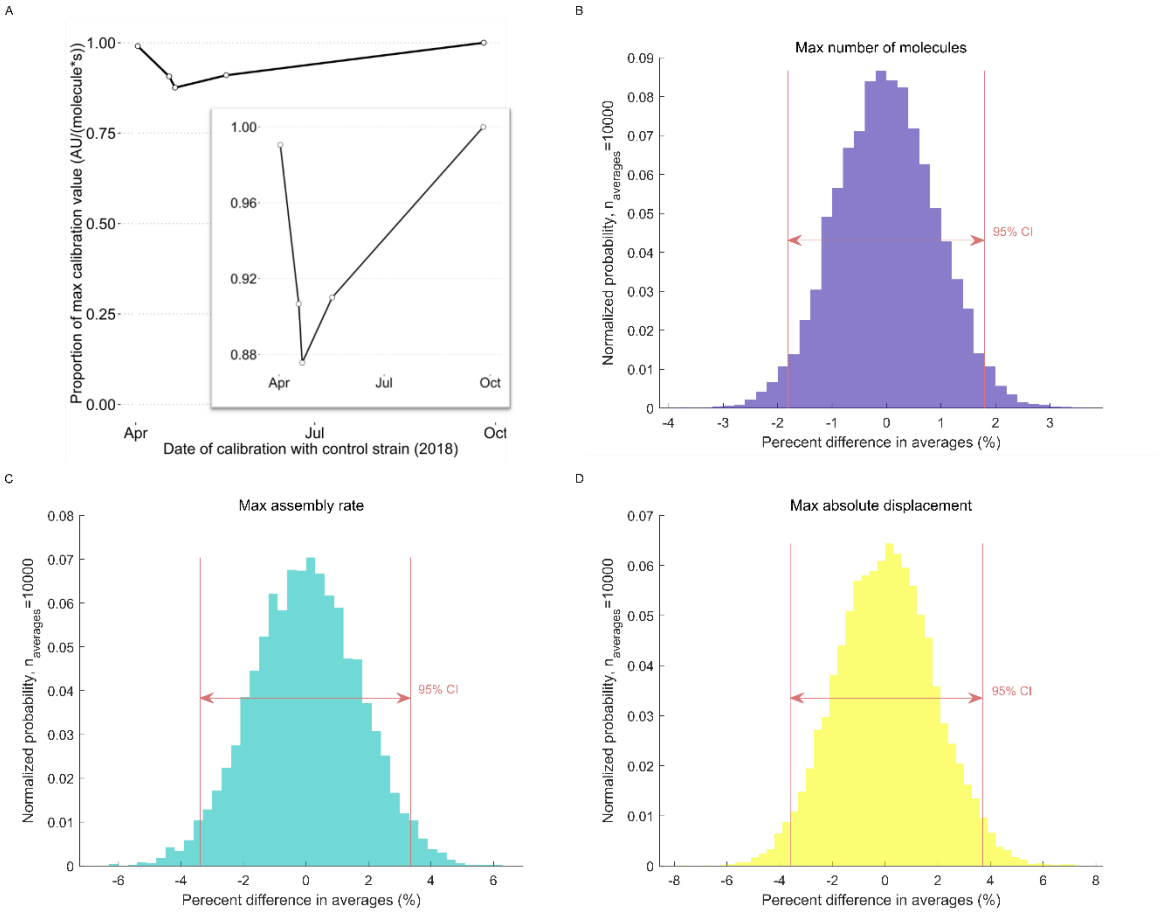

Figure 9. Pooling control experiments and averaging samples by bootstrapping with replacement demonstrates that average values for summary metrics of interest that differ by more than 3-4% from control will be statistically significant. Measurements from individual experimental conditions (same microfluidic plate and same day) are calibrated to a control strain, JB 366 (*S. pombe* cells expressing capping protein tagged with EGFP) with the indicated value (open circles), represented as the proportion of the maximum calibration value across the approximate time range for which data were collected. Inset: zoomed in plot. (B-C) Normalized probability distributions of averages in control experiments that were, prior to temporal alignment, bootstrapped with replacement from the set of control experiments reported in this study for the metric indicated in the panel title. Percent difference in the distribution is relative to the reported average for the indicated metric. Red, double-arrow indicates the 2.5% to 97.5% quantile (bootstrapped 95% CI). (A) Distribution of averages in control experiments for the maximum number of capping protein assembled into endocytic structures. (C) Distribution of averages in control experiments for the maximum assembly rate of capping protein assembled into endocytic structures. (D) Distribution of averages in control experiments for the maximum displacement of endocytic patches in 1s time intervals.

Typically, the standard deviation of the average number of molecules is on the order of 10 molecules (for a maximum number of molecules on the order of 100s of molecules). With 100s of tracks, this corresponds to standard errors of the mean yet another order of magnitude lower (on the order of single molecules). Even with few control experiments, for example n=4, the estimate of the mean value has 95% confidence at ~3.2 times the standard error, or ~3.2*1 molecule, corresponding to confidence in the mean that deviates less than 10 molecules from the reported average value. For 100s of molecules in the average peak value, this implies that deviations of greater than ~1% are statistically significant.

Temporal alignment contributes to the precision of quantitative microscopy measurements by minimizing comparisons of incomplete tracks and by linearly interpolating data. To account for true variation in the raw data, I sought to examine the variability in control experiments, for summary metrics of interest, prior to temporal alignment, especially in order to incorporate and account for this variation in assessing the statistical significance in my data (**Figure 9B-C**). For this sensitivity analysis, I constructed probability distributions based on averages from control experiments that were, prior to temporal alignment, bootstrapped with replacement from the set of control experiments reported in this study. This provided normalized probability distributions for summary of metrics of interest, whose area under 95% of the distribution can be used to assess the reported statistical significance of observed effects. Incorporating the variation in control experiments into this sensitivity analysis shows that for the maximum number of molecules assembled into endocytic structures, differences greater than ~2% from control (~3 molecules) will be statistically significant (non-overlapping, bootstrapped 95% confidence intervals, **Figure 9D**). This is consistent with the reported statistical significance (**Figure 10C**, **Table 7**). Without temporal alignment, the displacement 5s

after scission cannot be extracted from raw data in control experiments, as such, the variability in the maximum absolute displacement is evaluated, which typically has higher standard deviation than the absolute displacement 5s after scission for aligned data (**Figure 12**). Even with greater variability in the maximum absolute displacement compared to the reported summary metric (absolute displacement 5s after scission), this sensitivity analysis shows that differences greater than ~3-4% from control will be statistically significant, which is borne out by the reported p-values (**Figure 9D, Figure 12C**, **Table 7**). Thus, the variability in raw data from control experiments for the metrics of interest in this study are incorporated into the reported statistical significance analysis and are not sensitive to temporal alignment.

In control experiments, the variation in the maximum assembly rate is larger than the variation in the maximum number of molecules assembled (differences of ~4% from control, compared to differences of ~2% for max capping protein assembled, will be statistically significant) (**Figure 9C**). Indeed, one of the smallest effect sizes (effect size according to Cohen's definition, namely, Cohen's d~0.2) that is reported in this study to be statistically significant occurs in a comparison between Bzz1p-SH3-2Δ cells and control ($p = 0.01$; Figure 14**C**, **Table 7**) (Cohen, 1988). To incorporate variation in the raw data from control experiments into the validity of this significance test, I performed a random permutation test for this comparison (**Figure 13C-D**). Briefly, raw data from both Bzz1p-SH3-2Δ cells and control cells are pooled together into one sample. From this sample, tracks are randomly drawn with replacement and assigned to a control and test group, and the difference in the maximum assembly rate is calculated. This calculation is done for a random set of permuted samples for 10,000 iterations to construct a random probability distribution of differences between control and test strain. The actual observed difference between the control and test strain (Bzz1p-SH3-2Δ cells) is greater

than 99.9999% of the differences expected due to random chance incorporating variation in controls and test strains, as calculated in the permutation test, substantiating the reported p-value of p=0.01.

To further substantiate the incorporation of variation into the reported statistical significance tests, I performed a statistical power analysis for small effect sizes, and, in particular, for the comparison between Bzz1p-SH3-2Δ cells and control cells for the maximum assembly rate of capping protein (**Figure 13E**). Incorporating variation in control experiments and considering small effect sizes, (Cohen's d~0.2), to detect an effect using a two-sided, parametric statistical test that has 80% power (that is, an 80% chance of finding an effect that is there, or exhibiting a 20% false-negative or type-II error rate), ~190 tracks are required. In this study, statistical significance is conservatively set at $p < 0.01$, rather than $p < 0.05$. This reduces the likelihood of falsely identifying an effect, lowering the false positive or type-I error rate to 1%. Acquiring statistical power of 80% for tests incorporating this more conservative significance level requires that ~300 tracks are analyzed. Some strains are analyzed with fewer than 300 tracks, however, the power of statistical tests involving strains analyzed in this study is minimally 63% (for Bbc1p SH3 domain deletion cells) (Table 5). Only the likelihood of missing an effect that is there is compromised in tests with fewer than 300 tracks; the likelihood of detecting an effect is not compromised. For Bbc1p, the effect sizes are large (Cohen's d>0.5); therefore the number of tracks analyzed is appropriate to detect an effect using statistical analyses (**Figure 10B-C**, **Figure 21A**). Nonetheless, rather than statistical testing, a threshold for observations of test trains that differ from control measurements by more than 10% is used to determine whether an observation can be considered an effect. That is, in discussion and consideration of the results for individual SH3 domains, only those that far exceed the variation between control and test strains,

as assessed by statistical analysis, and that differ by more than 10% from control measurements are considered to have an influence on behavior for a particular metric of interest (**Figure 8**, **Figure 9B-D**, **Figure 13C-E**).

5. *Myo1p, Abp1p-1, Abp1p-2, Lsb1p, Bbc1p, and Cdc15p SH3 domains influence actin assembly in endocytosis*

Initially, we assumed that SH3 domains might play a role in recruiting other proteins to the endocytic patch, given that SH3 domains are thought to assemble molecular machineries by connecting proteins through protein-interactions, and, in so doing, bring together catalytic components to accomplish some function (Bhattacharyya et al., 2006; B. J. Mayer & Saksela, 2006). If that were the case in endocytosis, then without a SH3 domain, fewer proteins would be assembled. This might lead to less actin assembly, since factors like NPFs and other accessory factors that need to be concentrated for robust actin polymerization within endocytic structures *in vivo* would not be as abundant (A.E. Carlsson, 2010). However, we observed that endogenous, single SH3 domain deletions cause three phenotypes: one in which less actin is assembled into endocytic structures, one in which SH3Δ cells exhibit minor differences compared to control, and one in which SH3Δ cells result in more actin assembled into endocytic structures (**Figure 10**).

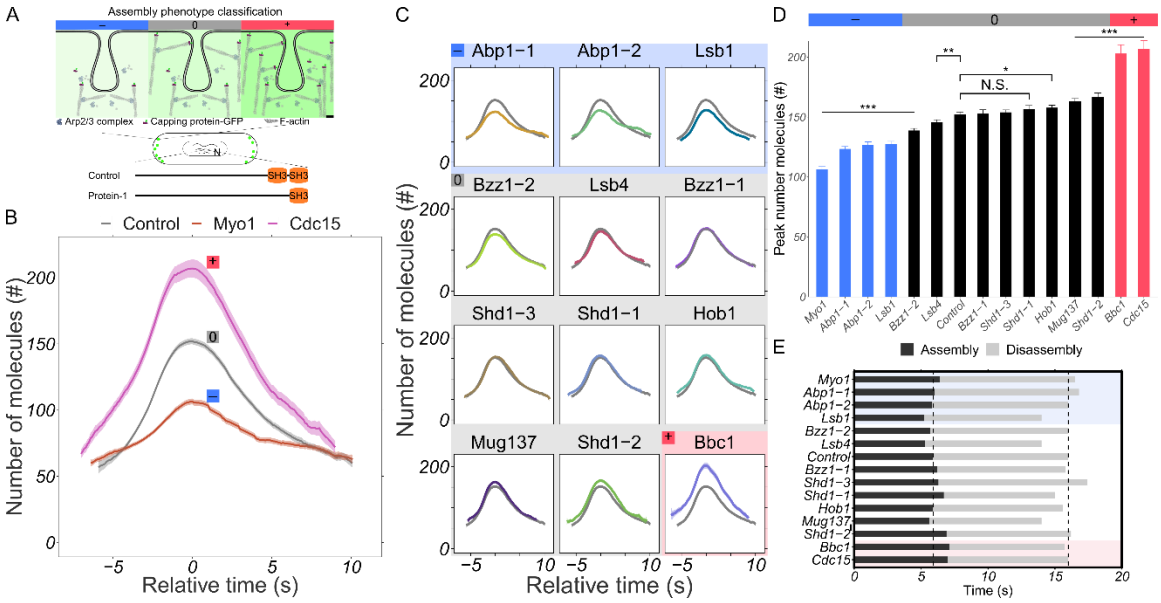

Figure 10. SH3 domains influence actin assembly in endocytosis. (A) Experimental overview and classification schema for observed for single, endogenous SH3 domain deletion phenotypes. Cells are genetically engineered to have a single SH3 domain deleted from a particular protein. Naming scheme used throughout paper: “Control” for no SH3Δ and capping protein tagged with GFP; “Protein-1,” for a strain with a protein’s most N-terminal SH3 domain is deleted and with capping protein fused with EGFP. Small effects are considered to be <10% different in the metric for control cells shown in (D). (B) Most striking assembly phenotype for endocytosis occurs in *myo1-SH3*Δ or *cdc15-SH3*Δ backgrounds, with assembly phenotype classification marked. N_{cells} for Control, Myo1 SH3Δ, and Cdc15 SH3Δ strains were 437, 322 and 800, respectively and N_{tracks} was 387, 246 and 124, respectively. (B-E) Ribbons or error bars represent 95% confidence interval (CI) and solid lines or bar represents average behavior. (C-E) Numbers used for statistics and single SH3Δ strain-wide measurements are in Table 5. (C) Assembly phenotypes, compared to control (gray) for all other SH3 domains in known endocytic proteins. Background color represents phenotype classifications based on statistics in (D). (D-E) p-values are based on Welch’s t-test and all test cases are compared to control. N.S.: $p>0.01$; *: $p<0.01$; **: $p<.001$; ***: $p<0.0001$. (D) The peak number of capping protein molecules assembled into endocytic structures for various SH3Δ strains and control. (E) The assembly time of endocytosis (black) is the time of appearance in (B) and (C) up to the maximum number of capping protein molecules and the disassembly time (gray) is the time between the peak number of capping protein molecules and the vanishing point; their sum, the total bar, is the total time of endocytosis for a particular SH3Δ strain. The appearance and disappearance times of capping protein in endocytosis for individual tracks

across all strains is summarized in Table 6. Background highlights the actin assembly phenotype classification from (D). Dashed line indicates assembly time for control and total time of endocytosis for control, from left to right, respectively.

If a particular SH3 domain plays a role in enhancing actin assembly in endocytosis, then the loss of that domain in the cell will result in lower amounts of actin assembled into endocytic structures. If the individual SH3 domain has minor or redundant roles in influencing actin assembly, then cells with this SH3Δ will have a similar amount of actin assembled into endocytic structures, relative to control, which has no SH3Δs. If the individual SH3 domain is responsible for restricting the amount of actin assembled into endocytic structures, then the loss of this domain will result in more actin assembled into endocytic structures. This corresponds with less dim, similar brightness, and bright spot-like objects in the microscope, relative to control cells (**Figure 10A**).

Table 5. Sample numbers for data used in investigating the influence of SH3 domains on actin assembly & endocytosis.

SH3Δ strain	N_{cells} for cell features	N_{cells} for endocytic features	N_{tracks} for endocytic features
Abp1-1	49	333	389
Abp1-2	87	485	233
Bbc1	61	79	106
Bzz1-1	79	271	235
Bzz1-2	75	570	588
Cdc15	48	800	124
Control	44	437	387
Hob1	60	780	496
Lsb1	81	378	321
Lsb4	78	452	407
Mug137	46	380	285
Myo1	55	322	246
Shd1-1	88	640	294
Shd1-2	81	620	179
Shd1-3	74	86	433

The Myo1p and Cdc15p SH3 domain deletion strains display the most striking actin assembly defects. Without the Myo1p SH3 domain, at most ~2/3 of actin is assembled into endocytic structures at the peak of assembly, relative to control. In contrast, without the Cdc15p SH3 domain, ~40% more actin is assembled at the peak of assembly, into endocytic structures (**Figure 10B**). Cdc15p-SH3Δ cells take longer to assemble actin, relative to control, but actin is disassembled more quickly, exhibiting an endocytic lifetime similar to control (**Figure 10E**, **Table 6**). Myo1p-SH3Δ cells have less actin within endocytic structures throughout endocytosis, compared to control, while Cdc15p-SH3Δ cells always have more actin within the endocytic structure. Other SH3 domains exhibit actin assembly phenotypes within the range of Myo1p-SH3Δ and Cdc15p-SH3Δ defects (**Figure 10C**).

Table 6. Summary of observed influences of endocytic SH3 domains on actin assembly & endocytosis.

Deleted SH3 domain	SH3Δ phenotypic feature					
	Peak assembly (#)	Mean absolute displacement @ t=5s (μm/s)	Assembly rate (#/s)	$N_{endocytosis}$ per cell length (#/μm)	Appearance time (s)	Disappearance time (s)
None (control)	152 ± 2	0.145 ± 0.008	30 ± 1	0.39 ± 0.02	-4.8 ± 0.2	7.0 ± 0.2
Shd1-1	157 ± 3	0.128 ± 0.008	28 ± 1	0.33 ± 0.01	-5.2 ± 0.3	6.6 ± 0.3
Shd1-2	166 ± 4	0.13 ± 0.01	29 ± 2	0.36 ± 0.01	-5.0 ± 0.3	6.6 ± 0.4
Shd1-3	154 ± 2	0.122 ± 0.007	30 ± 1	0.23 ± 0.01	-4.1 ± 0.2	8.3 ± 0.3
Myo1	106 ± 2	0.105 ± 0.009	12 ± 1	0.27 ± 0.03	-5.7 ± 0.4	7.3 ± 0.4
Cdc15	207 ± 7	0.14 ± 0.01	37 ± 3	0.16 ± 0.02	-5.1 ± 0.4	7.8 ± 0.5
Abp1-1	123 ± 2	0.098 ± 0.007	20 ± 1	0.56 ± 0.03	-4.8 ± 0.3	7.7 ± 0.3
Abp1-2	127 ± 3	0.11 ± 0.01	20 ± 1	0.46 ± 0.02	-4.9 ± 0.4	7.4 ± 0.4
Bbc1	203 ± 7	0.15 ± 0.01	34 ± 3	0.22 ± 0.02	-5.4 ± 0.8	7.8 ± 0.5
Bzz1-1	153 ± 3	0.16 ± 0.01	29 ± 1	0.40 ± 0.02	-4.9 ± 0.3	7.6 ± 0.3
Bzz1-2	139 ± 2	0.121 ± 0.006	27 ± 1	0.30 ± 0.01	-4.5 ± 0.1	7.8 ± 0.2
Hob1	158 ± 2	0.129 ± 0.007	30 ± 1	0.38 ± 0.01	-4.4 ± 0.2	6.9 ± 0.2
Lsb1	127 ± 2	0.136 ± 0.008	24 ± 1	0.46 ± 0.02	-4.4 ± 0.2	6.6 ± 0.2
Lsb4	146 ± 2	0.131 ± 0.007	27 ± 1	0.33 ± 0.01	-4.1 ± 0.2	6.4 ± 0.2
Mug137	163 ± 3	0.150 ± 0.009	34 ± 2	0.43 ± 0.02	-4.2 ± 0.2	6.5 ± 0.3

All values are reported as average value +/- 95% CI. Sample numbers for averages and error calculations are in Table 5. The appearance and disappearance time of capping protein and patch motion is relative to scission at *t* = 0-s.

We extracted the maximum number of capping protein molecules assembled into endocytic structures for each SH3Δ strain and ranked them for each SH3 domain (**Figure 10D**). We found that some SH3 domains have minor or redundant influences on actin assembly, though several significantly enhance actin assembly, including the Myo1p SH3 domain, the first and second SH3 domains of Abp1p, the second SH3 domain of Bzz1p (Bzz1-2), and Lsb1p's SH3 domain. Other domains appear to be important in restricting actin assembly into endocytic structures, including Bbc1p's and Cdc15p's SH3 domains. It is reasonable to expect that assembling less actin into endocytic structures would require shorter disassembly times; however, we observed that despite the actin assembly defect, the assembly, disassembly, and overall endocytic lifetimes are comparable (**Figure 10E**, **Table 3**). SH3Δ strains that have reduced amounts of actin assembled into endocytic structures take a similar length of time to assemble and disassemble capping protein, while SH3Δ strains that assemble more actin into endocytic structures take slightly longer times to assemble capping protein into endocytic structures but a shorter time to disassemble, resulting in comparable overall endocytic lifetimes.

Variations in capping protein expression do not explain observed differences in the accumulation of actin within endocytic structures across single SH3 domain deletions (negligible correlation, $r_S = 0.24$; $p = 0.40$) (**Figure 15E**, **Figure 18A**). Furthermore, the endocytic rate exhibits a low negative correlation with the maximum accumulation of capping protein into endocytic structures ($r_S = -0.45$; $p = 0.09$) (**Figure 15D**, **Figure 18A**). To determine whether the combination of capping protein expression and the number of endocytic events can explain differences in molecular assembly of actin across SH3 deletions, I performed multiple linear regression using the maximum number of capping protein molecules assembled into endocytic structures as a response variable

with expression and endocytic rate as predictor variables (normalized and expressed in unit percentage difference, relative to corresponding average metrics for control cells). Multiple linear regression reveals that capping protein expression and the number of endocytic events are poor independent predictors of molecular assembly across SH3 domain deletions (in independent predictor models, $R^2 = 0.07$, $p = 0.32$ for capping protein expression and $R^2 = 0.33$, $p = 0.02$ for the number of endocytic events) (**Figure 11**). Together, expression and endocytic rate predict maximal accumulation of capping protein with an adjusted $R^2 = 0.79$ ($p < 0.001$); however, for individual SH3 domain deletion cells, the model's predicted value differs from the actual value with residuals differing more than 1% from the observed value for control, Hob1p-SH3Δ, Abp1p-SH3-2Δ, Shd1p-SH3-1Δ, Shd1p-SH3-2Δ, and Shd1p-SH3-3Δ cells. Other multiple linear regression models, for example using the mean absolute deviation five seconds after scission and the maximum disassembly rate, the total time of endocytosis and the maximum assembly rate, or the length of cells and the maximum disassembly rate to predict the maximal accumulation of capping protein into endocytic structures yield better predictions than variations in capping protein expression and the endocytic rate (adjusted $R^2 = 0.94$, 0.82, and 0.94, respectively, versus adjusted $R^2 = 0.79$ for capping protein expression and the endocytic rate as predictors of maximum capping protein accumulation).

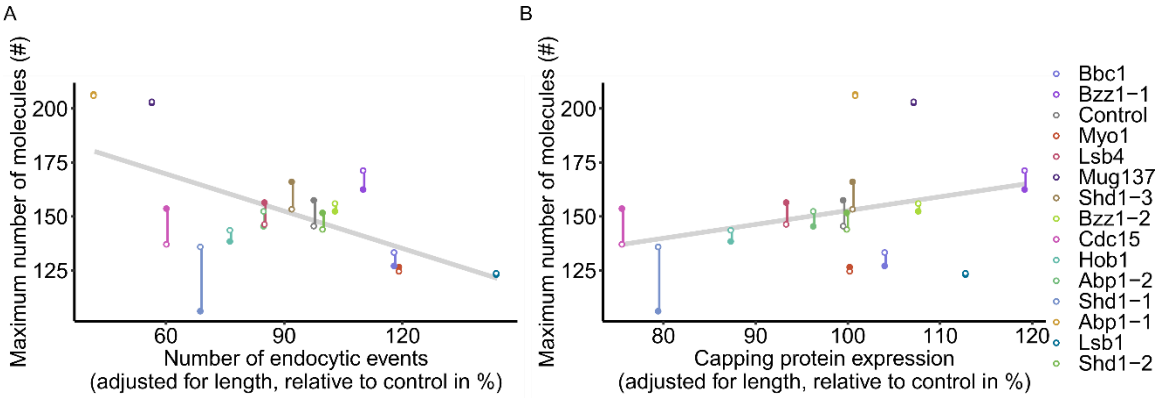

Figure 11. Multiple linear regression model predicting maximal accumulation of capping protein into endocytic structures shows that capping protein expression and the number of endocytic events are poor independent predictors of molecular assembly across SH3 domain deletions. Multiple linear regression model: maximum number of molecules (response variable) ~ capping protein expression + the number of endocytic events (predictor variables) where the averages of capping protein expression and the number of endocytic events for individual cells are normalized for each cell's length and each strain's average is represented in units relative to average corresponding metrics for individual control cells (%). See Table 4 for numbers used in this analysis. Estimated coefficient for capping protein expression is 2.0 number of molecules per unit percentage difference in capping protein expression, relative to control (95% CI, 1.2 – 2.7). Estimated coefficient for the number of endocytic events is -1.0 number of molecules per unit percentage difference in endocytic rate, relative to control (95% CI, -1.4 – -0.7). Adjusted R^2 = 0.79 for multiple linear regression model and for independent predictors, R^2 = 0.07 for capping protein expression and R^2 = 0.33 for the number of endocytic events. (A-B) Filled in circular points represent observed values for SH3 domain deletion strains shown in legend (right). Open circles represent predicted value from the multiple linear regression model. Vertical line segments represent residuals. Gray line represents linear relationship between plotted bivariate. (A) The maximum number of capping protein molecules assembled into endocytic patches in various SH3 domain deletion strains versus capping protein expression, relative to control (unit percentage). (B) The maximum number of capping protein molecules assembled into endocytic patches in various SH3 domain deletion strains versus the number of endocytic events, relative to control (unit percentage).

6. *Mug137p, Bzz1p-2, Myo1p, Abp1p-1, Abp1p-2, and Shd1p-3 SH3 domains influence the motility of endocytic structures in the cell*

Given that individual SH3 domains can alter the assembly of actin into endocytic structures, we wanted to investigate whether the altered assembly of actin disrupted the motility of endocytic structures *in vivo*. Endocytic structures move around during the process of endocytosis due to membrane fluctuations, diffusion, and an active cytoskeleton network. Furthermore, endocytic patch motion can be stabilized by an actin and coat protein network (Okreglak & Drubin, 2007). To investigate whether SH3 domains influence the motion of an endocytic patch, we quantified the motility of endocytic patches in time (**Figure 12**).

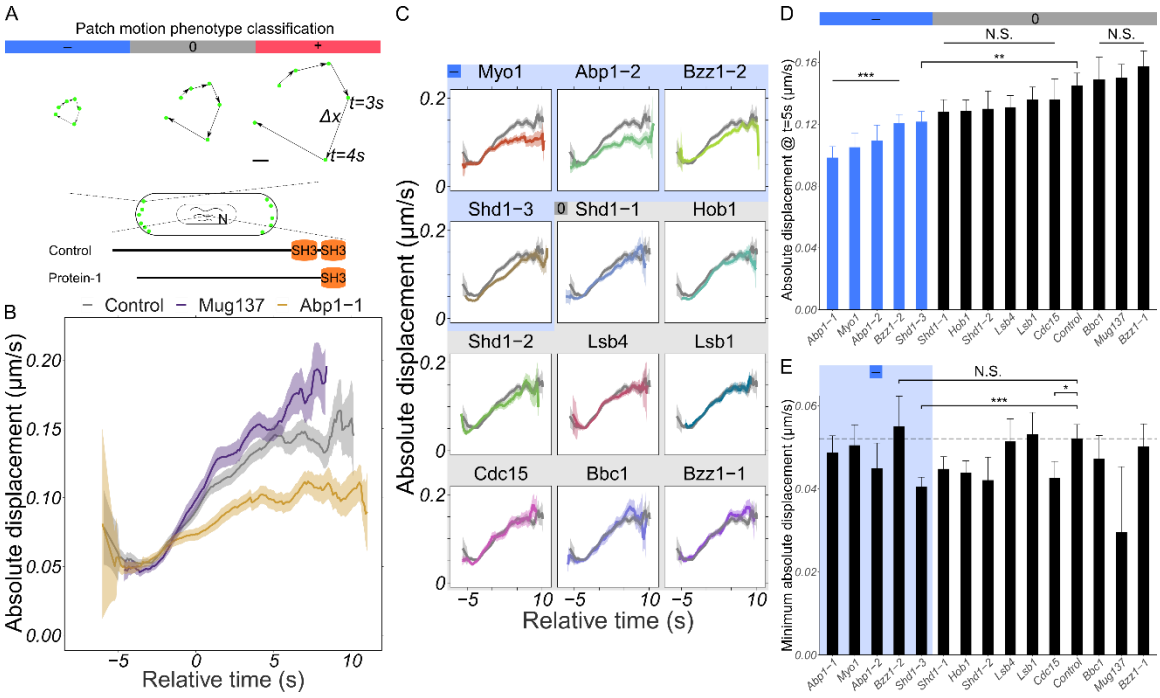

Figure 12. SH3 domains influence the motility of endocytic structures *in vivo*. The motility is considered to be the absolute displacement of a tracked endocytic structure between consecutive z-stacks (for $\Delta t=1s$). (A) Experimental overview and description of the phenotypic classification. Scale bar 1-μm. Small effects are considered to be <10% different in the metric for control cells shown in (D) or statistically insignificant. (B-E) Ribbons and error bars represent 95% confidence interval (CI); solid lines and bar represents average behavior. (B) SH3Δ strains that cause striking defects in the motion of an endocytic patch. N_{tracks} 387, 285, and 389 in N_{cells} 437, 380, and 333 cells for Control, *mug137-SH3*Δ, and *abp1-SH3*Δ*-1*, respectively. (C-E) Numbers used for single SH3Δ strain-wide measurements are in Table 5. (C) Patch absolute displacement and motility of endocytic patches for remaining SH3Δ strains, where background shading denotes classification of motility phenotype for a particular SH3Δ according to (D). (D-E) All statistical comparisons are made between a SH3Δ strain and control, by Welch's t-test. N.S.: $p>0.01$, **: $p<0.001$, ***: $p<0.0001$. (D) The mean absolute displacement at 5s after scission is extracted from (B) and (C) to analyze the motility of nascent endocytic vesicles in various SH3Δ background strains. Bar indicates that strains spanning the bar share the same p-value label. (E) The minimum mean absolute displacement obtained by the tracked endocytic structure for each SH3Δ strain. Dashed line indicates minimum mean absolute displacement of endocytic structures in control cells.

Single SH3 domain deletions influence the motion of the endocytic patch by either reducing, having no effect, or increasing the motility of endocytic patch motion at various stages of endocytosis (**Figure 12A-B**). Mug137p and Abp1p's first SH3 domain have the largest influence on patch motility (**Figure 12A**, **Figure 13**). Cells without Abp1p's first SH3 domain initially reduce the motility of endocytic structures, similar to control. Mug137p-SH3Δ cells lack this initial stabilization. After scission, Mug137-SH3Δ cells have higher mean absolute displacement, compared to control. In contrast, nascent vesicles in cells without Abp1p's first SH3 domain have reduced motility around and after scission, compared to control. This observed reduction in motility after scission is also observed for Abp1-SH3-2Δ, Myo1p-SH3Δ, Bzz1-SH3-2Δ, and Shd1p-SH3-3Δ (**Figure 12B**).

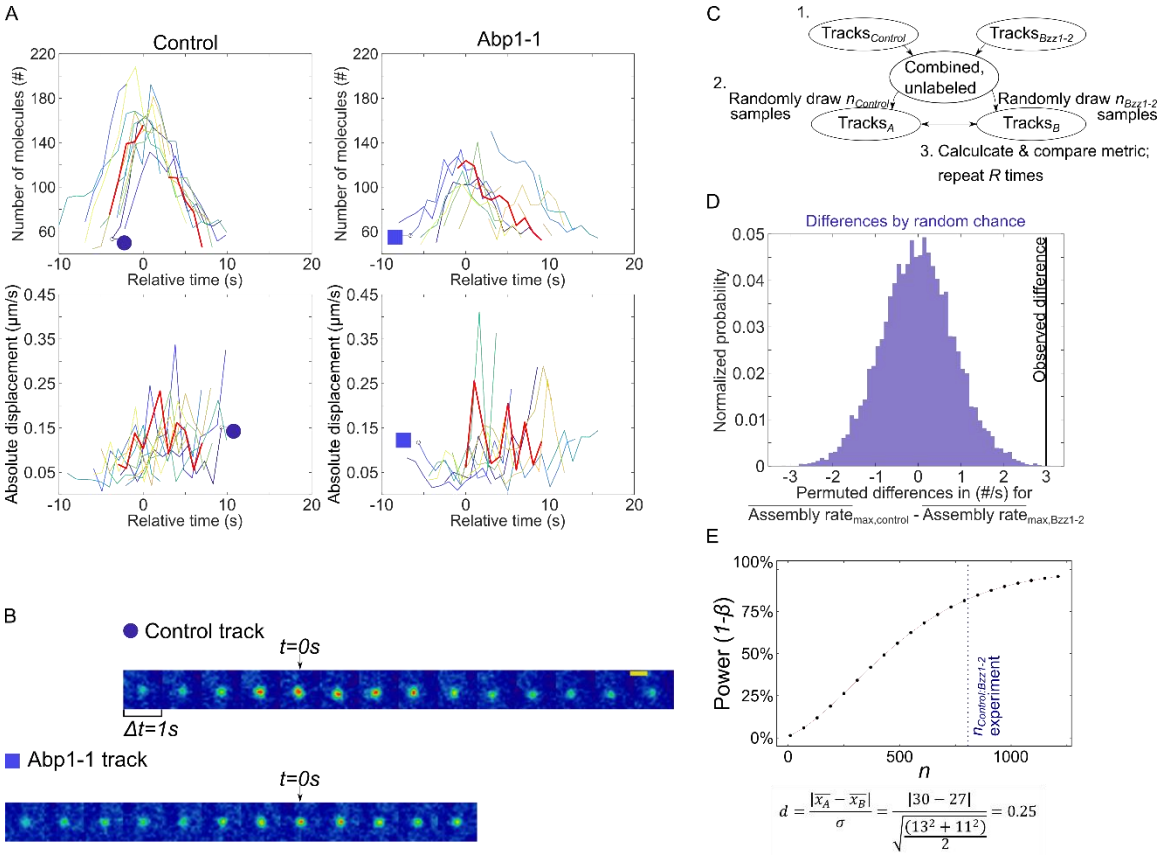

Figure 13. Non-motile endocytic patch contribution to absolute displacement versus time curves and validity Bzz1-2 assembly rate classification based on permutation tests of un-aligned track samples. (A) Random sample of tracks from control cells (A, left) or Abp1p-SH3-1Δ cells (A, right). (A, top) Number of capping protein molecules versus time for 10 random tracks and the average track (red). (A, bottom) Absolute displacement of tracked endocytic patch versus time for same tracks as in (A, top) with mean absolute displacement (red). (B) Montage of tracks annotated in (A) for equal contrast and brightness where each frame represents 1s and the aligned time of scission is indicated by *t=0s*. Scale bar 1-μm. (C) Algorithm for permutation test. (D) Permuted differences for R = 10,000 iterations. Histogram contains values for differences observed by random chance. Black line (D, right) shows the actual observed difference in our experiment. The probability, given a random chance model and the noise of our measurements before temporal-alignment of tracks, that the difference observed between control and Bzz1p-SH3-2Δ cells' max assembly rate is $p = 10^{-4}$. (E) Power for various sample sizes given significance level, α = 0.01 (Type I error rate) and small effect size, d (bottom equation), corresponding to Bzz1p-SH3-2Δ cells' max assembly rate comparison to control. Blue line indicates sample size of actual experiment reported in Figure 14. Power for comparison is high (~82%), corresponding to low (~18%) Type II error rate (Cohen, 1988).

After scission, the nascent vesicle diffuses inside the cell, proximal to the membrane, and its coat and actin network is disassembled. However, 5s after scission, vesicles in some SH3Δ strains are not moving as fast as vesicles in control cells (**Figure 12D**). Yet, the motion of SH3Δ cells after scission does not obviously correlate with the minimum mean absolute displacement achieved by initial assembly of the endocytic machinery (**Figure 12E**). In particular, though Myo1p-SH3Δ, Abp1p-SH3-2Δ, Hob1p-SH3Δ, and Lsb1p-SH3Δ cells do not exhibit the characteristic initial reduction of motion of the endocytic patch, they exhibit only minor differences in the minimum mean absolute displacement of the endocytic patch. The exception is Shd1p-SH3-3Δ cells, whose endocytic structures have reduced motion that differs significantly from control cells (*p<0.0001*). Yet, this effect cannot be explained by defects in actin assembly (**Figure 6C**).

7. *Cdc15p, Bbc1p, Bzz1p-2, Myo1p, Abp1p-1, and Abp1p-2 SH3 domains influence the rate at which actin is assembled into endocytic structures*

Given that SH3 domains influence the amount of actin assembled, we asked whether different SH3 domains alter the rate at which actin assembled into endocytic structures. To measure this rate, we took the derivative of the curve for the number of capping proteins within endocytic structures over time. To assess the validity of our phenotypic classification for small effect sizes, we performed random permutation tests on un-aligned tracks and power analyses (**Figure 13C-E**). We found that SH3 domains in endocytosis enhance, restrict, or have minor or redundant effects on the rate at which capping protein is assembled into endocytic structures (**Figure 14**).

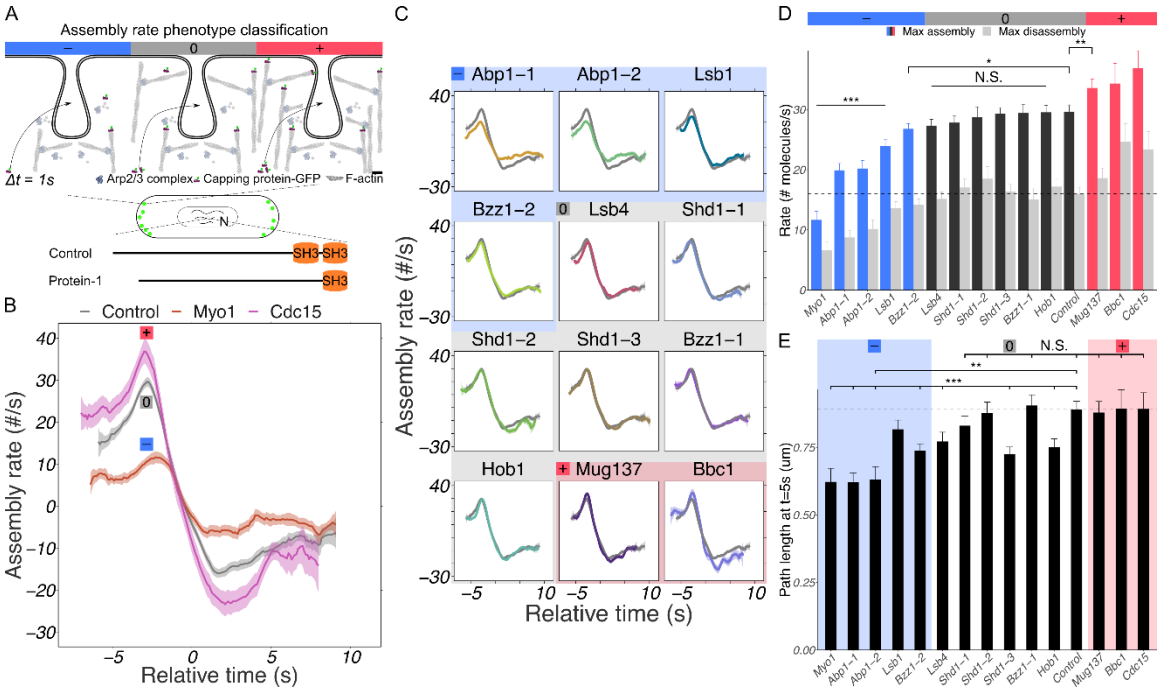

Figure 14. SH3 domains influence the rate at which actin is assembled into endocytic structures. (A) Schematic depicting classification of observed assembly rate phenotypes for various SH3Δ strains. Small effects are considered to be <10% different in the metric for control cells shown in (D). (B-E) Ribbon and error bars represent 95%CI; solid line and bar represents average behavior. (B) Striking differences in the assembly rate. N_{tracks} 387, 246, and 124 in N_{cells} 437, 322, and 800 for Control, *myo1-SH3*Δ, and *cdc15-SH3*Δ cells, respectively. (C-E) Numbers used for statistics and single SH3Δ strain-wide measurements are in Table 5. (C) Assembly rate versus time for remaining SH3Δ strains. (D-E) All statistical tests are compared to control by Welch's t-test for N.S.: *p>0.01*; *: *p<0.01*; **: *p<0.001*; ***: *p<0.0001*. (D) The maximum assembly rate (colored) and the maximum disassembly rate, i.e., the absolute value of the minimum assembly rate (gray) for various SH3Δ strains. (E) The cumulative path length of the average tracked endocytic structure for a particular strain, *t=5s* after scission, with assembly rate phenotype classification colored in the background.

Myo1p-SH3Δ and Cdc15p-SH3Δ cells have the most striking differences in the rate of assembling capping protein into endocytic structures, compared to control cells. Myo1p-SH3Δ consistently has a reduced rate of assembly, with only a small burst of actin polymerization just before scission (**Figure 14B**). In contrast, Cdc15p-SH3Δ cells consistently have a higher rate of assembling capping protein into endocytic structures, compared to control cells. All SH3Δ strains have stopped assembling capping protein around scission and quickly increase the rate of disassembly, which peaks ~2s after scission (negative assembly rate, **Figure 14B-C**). Myo1p-SH3Δ, Abp1p-SH3-1Δ, and Abp1p-SH3-2Δ cells do not increase and then reduce their disassembly rates, as other SH3Δ strains do but, rather, plateau. In general, SH3Δ strains with a lower assembly rate than control cells also have a lower maximum disassembly rate (**Figure 14D**). In contrast, SH3Δ strains that assemble more capping protein and do so more quickly than control cells have a higher maximum disassembly rate, compared to control.

Table 7. Statistics for reported endocytic phenotypes for various SH3Δ strains.

		p-value (Welch's t-test) for given variable					
SH3Δ strain	**…compared to**	**Peak number of molecules (#)**	**Peak assembly rate (#/s)**	**Peak disassembly rate (#/s)**	**Minimum mean absolute displacement (μm/s)**	**Mean absolute displacement @ t=5s (μm/s)**	**Path length @ t=5s (μm)**
Control	Control	1.00E+00	1.00E+00	1.00E+00	1.00E+00	1.00E+00	1.00E+00
Shd1-1	Control	3.15E-02	6.61E-02	3.31E-01	6.46E-03	1.17E-02	3.70E-02
Shd1-2	Control	1.58E-07	4.67E-01	7.09E-02	1.09E-02	7.35E-02	6.70E-01
Bzz1-1	Control	7.65E-01	8.45E-01	4.58E-01	6.13E-01	1.22E-01	6.31E-01
Bzz1-2	Control	8.45E-14	1.07E-03	4.04E-02	5.50E-01	3.68E-05	6.16E-10
Shd1-3	Control	2.74E-01	7.43E-01	6.85E-01	2.78E-06	1.93E-04	4.00E-11
Lsb4	Control	7.11E-04	1.41E-02	3.75E-01	8.47E-01	3.32E-02	2.62E-05
Mug137	Control	4.24E-07	5.75E-04	2.47E-02	3.84E-02	5.01E-01	7.12E-01
Hob1	Control	1.92E-03	9.28E-01	2.32E-01	1.90E-03	1.03E-02	2.03E-07
Bbc1	Control	2.06E-19	3.03E-02	2.09E-05	2.08E-01	6.99E-01	9.54E-01
Cdc15	Control	9.61E-25	1.88E-04	1.59E-04	2.61E-03	3.32E-01	9.64E-01
Abp1-1	Control	2.42E-46	3.63E-22	4.44E-14	2.82E-01	1.53E-12	4.98E-21
Abp1-2	Control	8.16E-30	3.86E-17	2.06E-07	8.67E-02	5.45E-06	3.62E-13
Lsb1	Control	2.69E-32	1.50E-09	1.13E-02	7.82E-01	1.82E-01	8.61E-03
Myo1	Control	2.70E-83	5.83E-46	2.28E-17	6.44E-01	5.23E-08	6.20E-13

Faster actin assembly and disassembly rates are associated with increased patch motility over time (Huckaba, Gay, Pantalena, Yang, & Pon, 2004). However, 5s after scission, SH3Δ strains that disassemble their actin coats more quickly than control cells do not have significantly different cumulative path lengths, compared to control (**Figure 14E**). Instead, reducing the maximum assembly and disassembly rates of actin throughout the process of endocytosis is associated with significant decreases in the total amount of vesicle motion, 5s after scission. However, some strains with minor defects in the max actin assembly rate also have reduced total path lengths.

8. Cdc15p, Bbc1p, Bzz1p-2, Myo1p, Abp1p-1, Abp1p-2, and Shd1p-3 SH3 domains influence the cellular regulation of endocytosis

Given the perturbation to the vital cellular process of endocytosis across our library of SH3Δ strains, we wanted to quantify whether endocytic SH3Δs affect cellular growth. Since the distribution of actin networks is tightly controlled by the cell, we also sought to determine if endocytic SH3Δs influence the ability of the cell to regulate the distribution and number of endocytic events in the cell in addition to altering the endocytic actin network (Blanchoin, Boujemaa-Paterski, Sykes, & Plastino, 2014). Given that endocytic events appear to be independent of one another and occur throughout all endocytic stages, we segmented cells and divided the cytoplasmic fluorescence by the average fluorescence of an endocytic event to yield the local number of endocytic events (**Figure 15**). We found that in SH3Δ cells, the number of endocytic events for a given cellular length is either reduced, unaltered, or increased, suggesting that endocytic SH3 domains influence the ability of the cell to regulate the number of endocytic events.

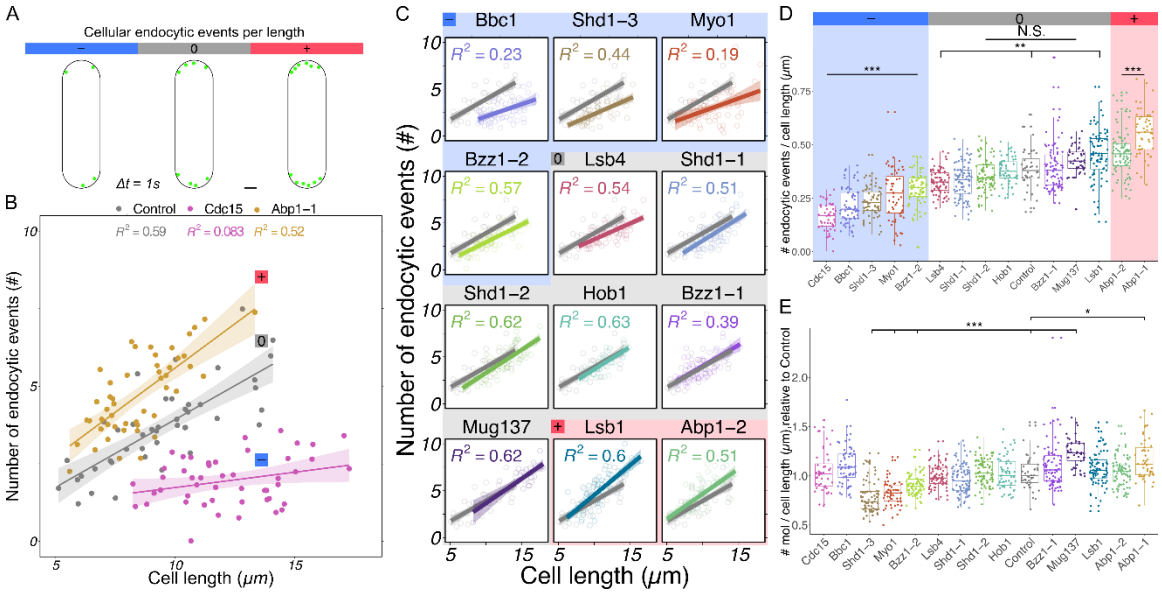

Figure 15. SH3 domains influence cellular regulation of the number of endocytic events per µm of cell length. (A) Description of cellular regulation of endocytosis phenotypes. Small effects are considered to be <10% different in the metric for control cells shown in (D). (B-C) Ribbon represents 95%CI; solid lines represent ordinary least-squares linear model fit; top indicates coefficient of determination. (B) Linear relationship between the number of endocytic events and the cell's length for the most striking phenotypes. N_{cells} 44, 48, and 49 were for Control, *cdc15-SH3Δ and abp1-SH3-1Δ,* respectively. (C-E) Numbers used for statistics and single SH3Δ strain-wide measurements are in Table 5. (C) The remaining SH3Δ strains are shown as compared to control (gray) with colored open circles as raw data points for linear fit. Mug137-SH3Δ cells shown on a reduced cell-length scale; full-cell length data is shown in **Figure 17**. (D-E) All statistical tests were performed with Welch's t-test, comparing a particular SH3Δ strain to control, according to N.S.: *p>0.01*; *: *p<0.01*; **: *p<0.001*; ***: *p<0.0001*. Box plots show the median (line) and box edges show the 25th and 75th percentiles, while the single upper and lower lines demark 1.5 times the interquartile range plus or minus the third and first quartile, respectively. (D) Ranked from lowest to highest value of the global number of endocytic events in a cell divided by that cell's length for individual single SH3 domain deletion strains. (E) The number of molecules in an entire cell divided by the length of that cell and normalized to control. Strains not assigned significance code do not differ significantly from control.

Cells exhibit a positive correlation between the number of endocytic events and the length of the cell (J. Berro & T. D. Pollard, 2014). We verify this for control cells, showing a very high positive correlation (Pearson's correlation coefficient, *PCC=0.77*) and show that cellular length is a reasonable predictor for the number of endocytic events (coefficient of determination, R^2=0.59) (**Figure 15B**). In particular, without Abp1p's first SH3 domain, cells had ~2x more endocytic events per micron of cell length compared to control cells, which cannot be explained by changes to capping protein expression (**Figure 15B**,**E**). In most cells, more endocytic events are associated with larger cells (**Figure 15C**). However, for Cdc15p-SH3Δ cells, in which more actin is assembled into endocytic structures, the relationship between the number of endocytic events and cell length is less pronounced (**Figure 15B**). Except for Cdc15p-SH3Δ, Bbc1p-SH3Δ and Myo1-SH3Δ, all other SH3Δ strains are able to maintain this relationship with moderate to high positive correlation (minimum *PCC* is Bzz1-1 at *PCC=0.6*, **Figure 15C**).

Table 8. Statistics for global, cell-wide phenotypes for various SH3Δ strains.

SH3Δ strain	...compared to	Variable	p-value (Welch's t-test)
Bzz1-1	Control	# mol / cell length	4.09E-02
Bzz1-2	Control	# mol / cell length	4.00E-05
Lsb1	Control	# mol / cell length	2.01E-01
Bbc1	Control	# mol / cell length	4.60E-02
Cdc15	Control	# mol / cell length	8.18E-01
Myo1	Control	# mol / cell length	5.11E-09
Abp1-2	Control	# mol / cell length	9.15E-01
Abp1-1	Control	# mol / cell length	1.40E-03
Shd1-1	Control	# mol / cell length	3.36E-02
Shd1-2	Control	# mol / cell length	8.33E-01
Lsb4	Control	# mol / cell length	2.18E-01
Mug137	Control	# mol / cell length	9.16E-08
Hob1	Control	# mol / cell length	9.06E-01
Shd1-3	Control	# mol / cell length	2.17E-11
Bzz1-1	Control	# events / cell length	5.34E-01
Bzz1-2	Control	# events / cell length	7.84E-07
Lsb1	Control	# events / cell length	4.81E-04
Bbc1	Control	# events / cell length	1.31E-14
Cdc15	Control	# events / cell length	5.67E-21
Myo1	Control	# events / cell length	3.31E-07
Abp1-2	Control	# events / cell length	9.00E-05
Abp1-1	Control	# events / cell length	3.01E-12
Shd1-1	Control	# events / cell length	1.15E-03
Shd1-2	Control	# events / cell length	7.55E-02
Lsb4	Control	# events / cell length	5.36E-04
Mug137	Control	# events / cell length	2.45E-02
Hob1	Control	# events / cell length	6.06E-01
Shd1-3	Control	# events / cell length	9.11E-14

Differences in cells' regulation of endocytosis do not directly correspond with defects in motility or actin assembly in the various SH3Δ backgrounds. For example, without Bbc1p's and Cdc15p's SH3 domains, the number of endocytic events is reduced for a given cell length (**Figure 15B-C**). This is consistent with the notion that for similar expression but more capping protein assembled into endocytic structures, there should be fewer endocytic events (**Figure 10B-C**). However, contrary to that notion, Myo1p-SH3Δ and Bzz1p-SH3-2Δ cells assemble less actin into endocytic structures and reduce the number of endocytic events. This can be explained, in part, by a reduction of capping protein expression in these cells (**Figure 15E**). However, capping protein expression does not change (<1% mean difference, relative to control) for Abp1p-SH3-2Δ cells even while these cells assemble less actin into endocytic structures and increase their rate of endocytosis in the cell (**Figure 15D-E**). Abp1p SH3Δ and Lsb1p-SH3Δ cells assemble less actin into endocytic structures and increase their expression and endocytic rate in contrast with Myo1p-SH3Δ, Lsb4p-SH3Δ, and Bzz1p-SH3-2Δ cells, which assemble less actin into endocytic structures and decrease their expression and endocytic rate, while Mug137p-SH3Δ and Bzz1p-1 SH3Δ cells assemble more actin into endocytic structures and increase their expression and rate of endocytosis in contrast to Bbc1p-SH3Δ and Cdc15p-SH3Δ cells, which assemble more actin into endocytic structures, increase capping expression but decrease their endocytic rate (**Figure 10C-D**, **Figure 15E**). Generally this suggests that there is poor concordance between capping protein expression, endocytic rate and molecular assembly across single SH3 domain deletions. This is borne out by a negligible correlation between the maximum number of capping protein molecules accumulated into endocytic structures and expression across the library of endogenous, single SH3 domain deletions (r_S = 0.24; p = 0.49) and a low correlation between the peak number of molecules and endocytic rate (r_S = -0.45; p

=0.09) and a low correlation between expression and endocytic rate (r_S = 0.51; p = 0.053) (**Figure 18A**).

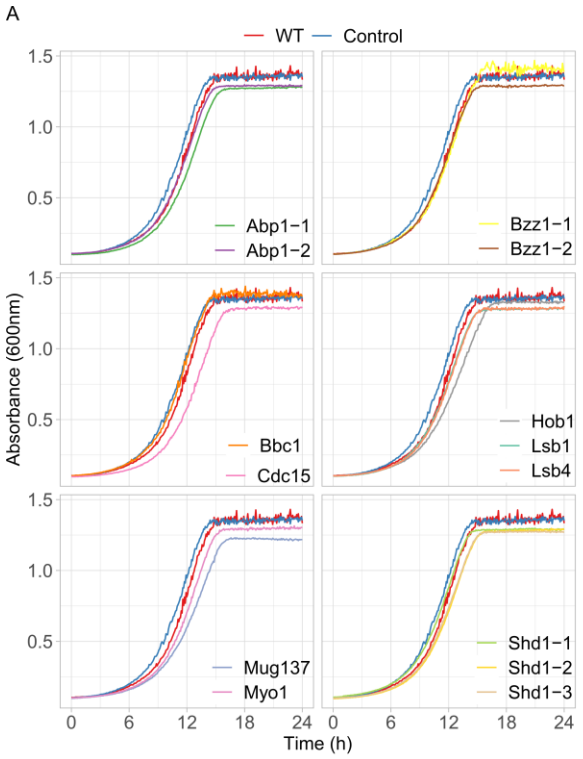

C

Strain	Growth rate (1/h)	(Lower, Upper) 95% CI	P-value
WT	0.34	(0.31, 0.37)	1
Control	0.34	(0.31, 0.37)	0.03
Abp1-1	0.32	(0.29, 0.35)	0.96
Abp1-2	0.33	(0.3, 0.36)	0.81
Bbc1	0.34	(0.32, 0.37)	0.54
Bzz1-1	0.31	(0.29, 0.34)	0.87
Bzz1-2	0.33	(0.3, 0.36)	0.38
Cdc15	0.31	(0.28, 0.34)	0.32
Hob1	0.27	(0.25, 0.3)	0.88
Lsb1	0.32	(0.3, 0.35)	0.33
Lsb4	0.33	(0.3, 0.36)	0.82
Mug137	0.28	(0.26, 0.31)	0.08
Myo1	0.32	(0.29, 0.35)	0.64
Shd1-1	0.32	(0.3, 0.35)	0.78
Shd1-2	0.32	(0.29, 0.35)	0.53
Shd1-3	0.32	(0.29, 0.35)	0.67

Figure 16. Single, endogenous SH3∆s do not cause significant growth defects for *S. pombe*. (A) Growth curves compared to WT and control (Acp1p-EGFP) strains. Cells were inoculated in rich media (YE5S) and these overnight cultures were diluted to 0.1 and then agitated at 32C for the duration of the growth assay. For growth assay absorbance at OD_{600} was measured every 5-minutes until saturation or after 32h. Different color lines represent different SH3∆ strains where the name of the protein indicates that its SH3 domain is deleted. (B) Growth curves from (A) fitted to the Gompertz growth model, shown as an inset where a = asymptote; b = time-lag; c = growth rate. (C) Non-linear least squares regression results for Gompertz growth model for each strain. P-value was calculated as two-tailed Z-tests comparing the Z-score of the indicated strain to WT. CI = confidence interval.

9. A role for uncharacterized proteins in endocytic actin assembly

Evidence suggests that Lsb1p and Lsb4p interact with WASp during endocytosis, while Mug137p is orthologous to endophilin, an endocytic protein in metazoans (Goode et al., 2015; Urbanek et al., 2015; Valerie Wood et al., 2012). Apart from its SH3 domain, Lsb1p has a PR and binds WASp through its SH3 domain (Madania et al., 1999). Lsb4p also has a SH3 domain that may bind WASp during endocytosis and it has an actin-binding domain, which binds actin only when Lsb4p binds WASp, signaling a possible role for Lsb4p in endocytic actin assembly (Robertson et al., 2009). Mug137p is an uncharacterized protein but it is homologous to endophilin proteins, which participate in endocytosis, and it has characteristic structural features of endocytic proteins: a BAR and SH3 domain (Arasada & Pollard, 2011). Mug137p-SH3Δ cells are significantly longer than normal cells (**Figure 17C**). The long length of Mug137p-SH3Δ cells is not associated with an absence of cellular division and causes only a slight delay in the onset of logarithmic-phase growth, relative to WT cells (**Figure 16**). Endocytic tracks in Mug137p-SH3Δ cells are, on average, similar to control cells (**Figure 10E**, **Figure 17B**). Yet, without the Mug137p-SH3 domain, more actin is assembled into endocytic structures, it is assembled at a faster rate, and endocytic patches are more motile after scission (**Figure 21**). Without the Mug137p SH3 domains, cells alter their regulation of endocytosis for a given length (**Figure 17A**). In Mug137p-SH3Δ cells, the length of the cell is a very high determinant of the number of endocytic events (coefficient of determination, $R^2=0.77$) while in control cells, the length only moderately determines the number of endocytic events.

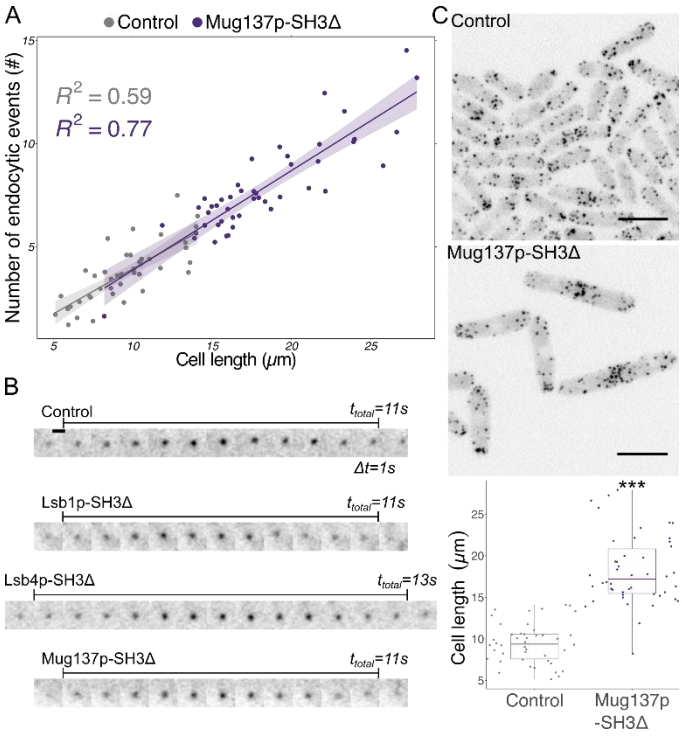

Figure 17. Measurements of endocytosis and its cellular regulation for SH3Δs in poorly characterized endocytic proteins reveals long length of Mug137p-SH3Δ cells relative to control. (A) The number of endocytic events in the cell versus the cell length for 44 control cells and 46 Mug137p-SH3Δ cells. (B) Tracked endocytic structures across the total time of an endocytic event for indicated strain. Consecutive frames are taken 1s apart and each frame is a sum-projection of 6-slices, each 500-nm apart. Contrast is the same for all representative track images. Scale bar 1-μm. (C) Representative fields-of-view for control and Mug137p-SH3Δ cells. Contrast is same for both images. Box edges show 25th and 75th percentiles; line shows median. Mug137p-SH3Δ cells are significantly longer than control cells (***: *p<0.0001*, Welch's t-test). Scale bar 10-μm.

Deletion of Lsb1p's and Lsb4p's SH3 domains decrease actin assembly in endocytosis, which may suggest that, when present, these SH3 domains enhance actin assembly in endocytosis (**Figure 21**). Without Lsb1p's SH3 domain, less actin is assembled into endocytic structures (**Figure 10**). Lsb4p-SH3∆ cells also assembly significantly (*p<0.001*) less actin into endocytic structures and endocytosis takes longer than control cells. Deletion of the SH3 domains of Lsb1p and Lsb4p do not alter patch motility, so their roles in stabilizing the endocytic machinery or anchoring endocytic structures to the membrane may be redundant (**Figure 5**). Lsb4p-SH3∆ cells have fewer endocytic events for a given cellular length, compared to control, while Lsb1p-SH3∆ cells have more endocytic events for a given cellular length; yet, although these are statistically significant, the differences are relatively minor (**Figure 15**). Typical endocytic tracks for Lsb1p-SH3∆ cells and Lsb4p-SH3∆ cells are comparable to endocytic tracks in control cells but, on average, endocytosis in Lsb4p-SH3∆ cells takes longer than control (**Figure 17B**, **Figure 10E**). Given the moderate effects of Lsb4p's SH3 domain on actin assembly and the dynamics of endocytic structures, we conclude that the Lsb4p-SH3 likely has overlapping or redundant roles with other proteins in endocytosis. The loss of the Lsb1p-SH3 domain significantly enhances actin assembly and, since it is known to bind WASp, we conclude that it has an NPF-enhancing role in endocytosis. For the first time, we report a role for Mug137p in endocytosis and, specifically, that its SH3 domain has a role in actin assembly, namely to restrict assembly, potentially through SH3-domain mediated interactions that regulate NPF activity.

10. Correlating all combinations of quantified features for perturbations to endocytosis by endogenous single SH3 domain deletions

Single, endogenous SH3 domain deletions do not alter cellular growth or prevent endocytosis from occurring (**Figure 13, Figure 16**). As such, tracking and quantifying the assembly dynamics of capping protein as an endocytic marker across a library of endogenous, single SH3Δs allowed us to quantify perturbations to endocytosis across many different quantitative features and identify patterns over the comprehensive single-SH3Δ library and across a range of endocytic behaviors (**Figure 18**).

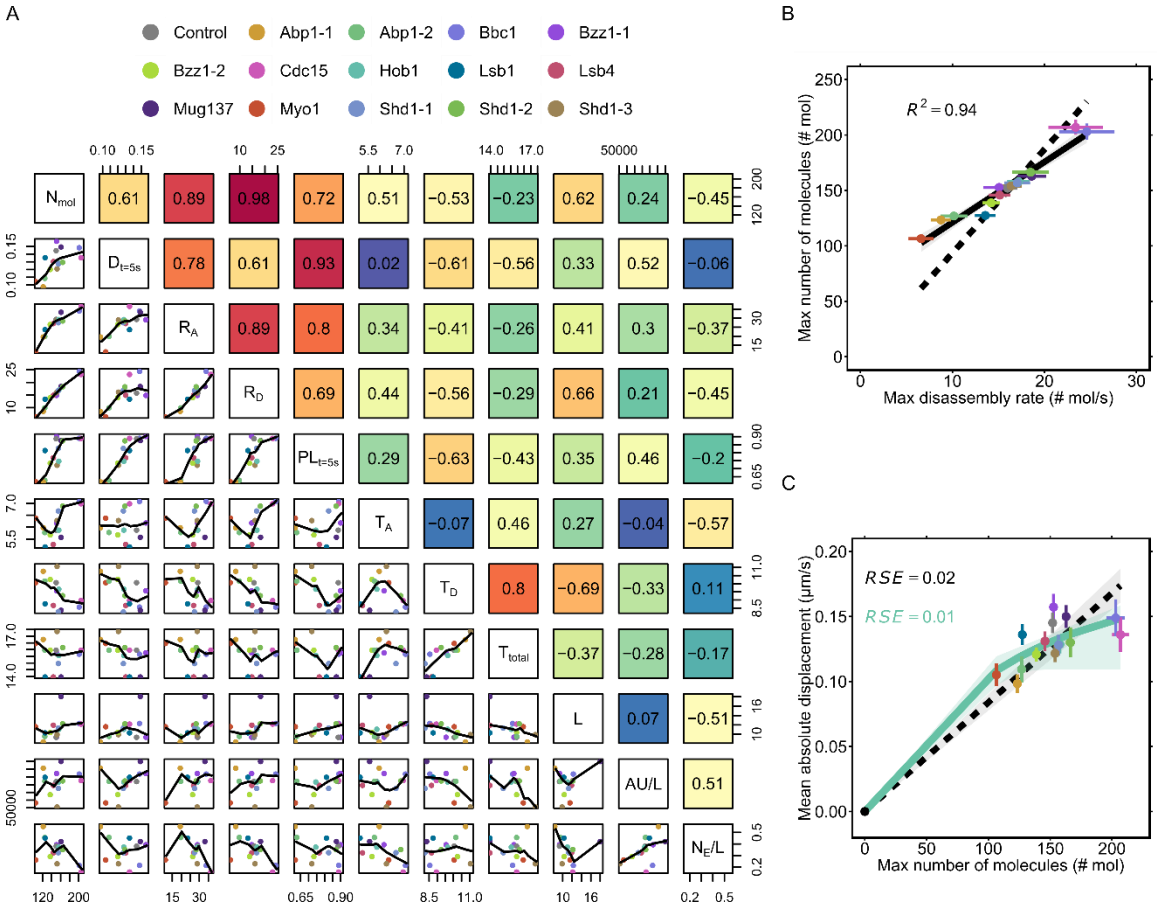

Figure 18. Pairwise correlations of 11 quantitative metrics across 14 perturbations to endocytosis by endogenous, single SH3Δs. (A-C) Legend indicates points in bivariate plots corresponding to measurements for a strain with the indicated protein's SH3 domain deleted. Points represent average values for the number of cells denoted in Table S4. (A) Abbreviations: N_{mol} = maximum number of capping protein molecules assembled (# mol); $D_{=5s}$ = endocytic patch mean absolute displacement 5s after scission (μm/s); R_A = maximum molecular assembly rate (# mol/s); R_D = maximum molecular disassembly rate (# mol/s); $PL_{t=5s}$ = cumulative endocytic patch path length achieved 5s after scission (μm); T_A = assembly time (s); T_D = disassembly time (s); T_{total} = total time of the average endocytic event; L = cell length (μm); AU/L = total arbitrary units of fluorescence in a cell adjusted for each cell's length (AU/μm); N_E/L = the number of endocytic events in a cell, adjusted for cell length (#/μm). (A, upper triangle) The value in [i (row), j (column)] is the Spearman's rank correlation coefficient, r_s, for the correlation between the variables denoted in the diagonal and intersecting with the i^{th} row and the j^{th} column along the diagonal. Box background color represents absolute value of r_s from 0 (blue) to 1 (red). (A, lower triangle) Scatter plot of measurements across endogenous SH3Δ strain library. Points in the plot at position [i,j] represent measurements from SH3Δ strains

for the variables denoted in the diagonal and intersecting with the i^{th} row and j^{th} column along the diagonal. Solid black line shows local regression fit (LOESS) for each bivariate association. (B-C) Horizontal and vertical error bars represent 95% CI for the metric denoted in the corresponding axis. (B) The maximum number of capping protein molecules assembled into endocytic structures compared to the maximum capping protein disassembly rate for each strain. Solid line shows linear fit; ribbon represents 95% CI for the fit, and R^2 indicates coefficient of variation for the linear fit with intercept at 67 molecules (95% CI, 54 – 80 molecules). Dashed line shows linear fit for an intercept coerced to the origin. (C) Endocytic patch mean absolute displacement 5s after scission compared to the maximum number of capping protein molecules assembled into endocytic structures for each strain in the endogenous, SH3Δ library. Dashed line indicates linear fit coerced to zero intercept with residual standard error (RSE) in black. Solid green line represents exponential fit, $D_{t=5s} = A\left(1 - e^{-\frac{N_{mol}}{k}}\right)$, coerced to intercept at the origin. Green ribbon represents 95% CI for exponential fit, calculated using a Monte Carlo simulation. Green RSE annotation denotes the residual standard error for the exponential fit.

The maximum capping protein disassembly rate has a very high positive correlation with the maximum number of capping protein molecules assembled into endocytic structures across perturbations to endocytosis by SH3 domain deletions (Spearman's rank correlation coefficient, $r_s = 0.98$; $p < 0.0001$) (**Figure 18A-B**). Across the SH3Δ library, the maximum disassembly rate exhibits a linear association with the maximum number of molecules assembled into endocytic structures (coefficient of variation, $R^2 = 0.94$; intercept, ~67 molecules, 95% CI, 54 – 80 molecules; slope, 5.5-s, 95% CI, 4.7 – 6.2-s) (**Figure 18B**). Compared to assembly, the endocytic disassembly phase appears to be more associated with measures of endocytic behavior: the disassembly time of the average endocytic event has a high positive correlation with the total time of endocytosis ($r_s = 0.80$; $p = 0.0004$) while the assembly time has a low positive correlation with the total time of endocytosis ($r_s = 0.46$; $p = 0.085$). Similarly, the speed and cumulative path length of endocytic structures five seconds after scission have moderate negative correlations with the disassembly time ($r_s = -0.61$ and $r_s = -0.63$, respectively; $p = 0.015$ and $p = 0.013$, respectively) but a negligible correlation with the assembly time ($r_s = 0.02$ and $r_s = 0.29$, respectively; $p = 0.955$ and $p = 0.289$, respectively).

Yet, despite the negligible correlation between the assembly and disassembly time of the average endocytic event ($r_s = -0.07$; $p = 0.793$), there is a high positive correlation between the maximum molecular assembly and disassembly rates of capping protein to and from endocytic structures ($r_s = 0.89$; $p < 0.0001$). This may partially be explained by a moderate negative correlation between the maximum disassembly rate and disassembly time ($r_s = -0.56$; $p = 0.029$) on the one hand and a low association between the maximum assembly rate and assembly time on the other ($r_s = 0.34$; $p = 0.218$). Complicating the potentially stronger association between molecular mechanism and variations in disassembly, the maximum number of capping protein molecules

assembled exhibits a moderate positive and moderate negative correlation with the assembly and disassembly time of the average endocytic event (r_S = 0.51 and r_S = -0.53, respectively; p = 0.053 and p = 0.043, respectively), in spite of a negligible association with the total time of endocytosis (r_S = -0.23; p = 0.406). Furthermore, the number of endocytic events exhibits a moderate negative correlation with the assembly time (r_S = -0.57, p = 0.025) but a negligible correlation with the disassembly time (r_S = 0.11; p = 0.685).

The maximum number of capping protein molecules assembled has a high positive correlation with the cumulative path length traveled by endocytic structures five seconds after scission (r_S = 0.72; p = 0.003). This suggests an association between endocytic molecular assembly and motility, which is borne out by a moderate positive correlation between the maximum number of capping protein molecules assembled and the instantaneous speed of endocytic patches five seconds after scission (r_S = 0.61; p = 0.015). This association may be non-linear, given that an exponential model fits the data with lower residual standard error (RSE) than a linear model (*RSE* = 0.01 versus *RSE* = 0.02, respectively) (**Figure 18C**). Reinforcing the connection between molecular assembly and motility, the speed and cumulative path length of endocytic patches five seconds after scission exhibits a high positive correlation with the maximum molecular assembly rate of capping protein (r_S = 0.78 and r_S = 0.80, respectively; p = 0.0006 and p = 0.0003, respectively).

Unexpectedly, the number of molecules assembled into endocytic structures exhibits a moderate positive correlation with cell length (r_S = 0.62; p = 0.013) but a negligible correlation with capping protein expression and a low negative correlation with the number of endocytic events (r_S = 0.07 and r_S = -0.45, respectively; p = 0.800 and p = 0.092, respectively). Both capping protein expression and the number of endocytic

events exhibit poor or negligible correlations with the maximum assembly rate, maximum disassembly rate, and cumulative path length five seconds after scission ($|r_s| < 0.46$, all; $p > 0.087$, all). Globally in the cell, even though capping protein expression is moderately correlated with endocytic patch motility (speed 5s after scission, $r_s = 0.52$; $p = 0.044$), the association between the number of endocytic events and patch speed is negligible ($r_s = -0.06$; $p = 0.830$). Furthermore, the total time of endocytosis is negligibly correlated with capping protein expression and the number of endocytic events in the cell ($r_s = -0.28$ and $r_s = -0.17$, respectively; $p = 0.308$ and $p = 0.536$, respectively). Collectively, these observations reveal novel associations, some of which may govern the pattern of variation given perturbations to endocytosis by endogenous, single SH3 domain deletions.

11. Mathematical modeling reveals Arp2/3 activation steps that may be regulated by SH3-domain mediated interactions in endocytosis

It is hypothesized that the role of SH3 domains in endocytosis is to regulate Arp2/3 activity but the mechanistic details are unclear and lack specificity given that regulation by SH3 domains has not been proposed or narrowed down to any single activation step (Sun et al., 2017). Conversely, SH3 domains are expected to recruit and accumulate proteins at sub-cellular locales to contribute to pathway assembly (B. J. Mayer, 2015; Pawson & Nash, 2003). A simplistic view of the latter hypothesis seems incongruent with our observation of over-assembly of actin upon SH3 domain deletion. Previous work took advantage of quantitative microscopy and the many kinetic parameters for actin associated proteins measured *in vitro* to describe a model for actin assembly in endocytosis with precise quantitative and mathematical detail as based on the dendritic nucleation hypothesis (Berro, Sirotkin, & Pollard, 2010; T. D. Pollard,

Blanchoin, & Mullins, 2000). Starting with this model, I reproduced simulations, based on our new data and looking in particular at the lifetime of capping protein within endocytic structures and at the maximum accumulation of capping protein in parameter scans, to compare variations to previously fitted data with the range of amplitudes I observed across the SH3 domain deletion library (Berro et al., 2010; Sirotkin et al., 2010). Use of this mathematical model allowed us to better understand which steps in the actin assembly pathway in endocytosis might plausibly be regulated by SH3-domain mediated interactions.

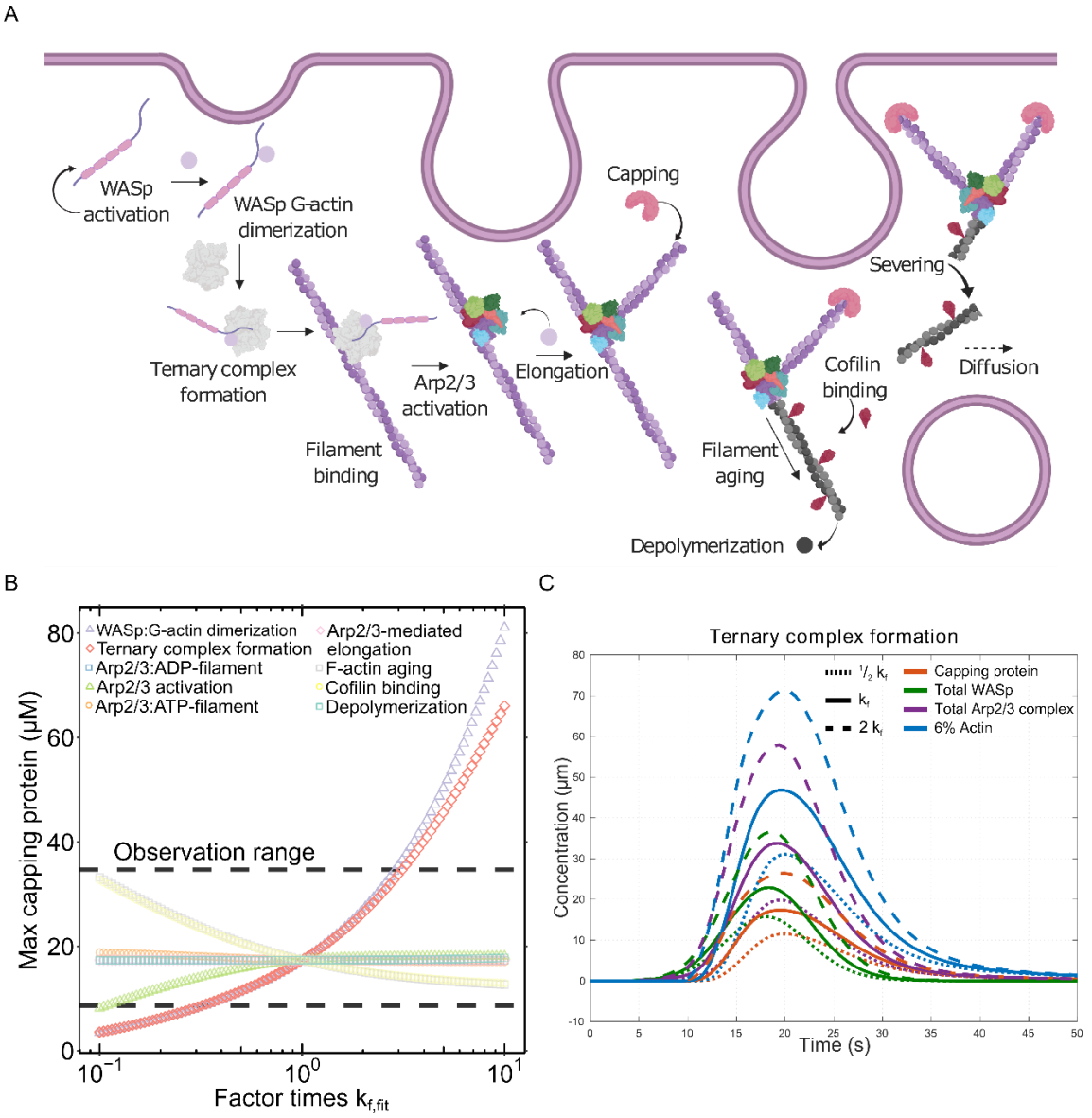

Figure 19. Mathematical modeling of actin assembly in endocytosis reveals which Arp2/3 activation steps may be regulated by SH3-domain mediated interactions. (A) Mechanism of actin assembly in endocytosis proceeds through Arp2/3-nucleated actin polymerization. Schematic was made using BioRender (BioRender.com) under an academic license. (B) Variation of all Arp2/3-activation steps (parameter scans across fitted k_f) across two orders of magnitude, plotting the resultant maximum concentration of capping protein in endocytic structures as based on data from (Sirotkin et al., 2010) and model from (Berro et al., 2010). Variations to the capping protein interaction step and the severing rate given that in some of these simulations, capping protein is not disassembled, which is inconsistent with *in vivo* observations. (C) Representative assembly, in concentration over time, of capping protein, WASp, actin (plotted as 6% of the

total actin within the endocytic structure), and Arp2/3 complex for various forward reaction rates of the ternary complex formation step in the Arp2/3 activation pathway for actin assembly in endocytosis. Kinetic model was previously implemented and parameters, here, were varied from fitted parameters described in previous work (Berro et al., 2010).

To extract insights from the kinetic model and identify which steps in this minimal mechanistic model of actin assembly during endocytosis might be singularly mediated by competitive SH3 domain-mediated interactions, we varied fitted forward reaction rate parameters in an attempt to recapitulate the amplitude of maximum capping protein molecules assembled into endocytic structures without significantly altering the lifetime of capping protein in endocytic structures, consistent with our data (**Figure 10**). In particular, we asked two questions: which steps, when varied, do not significantly change the lifetime of capping protein in endocytic patches but yield both over-and under-assembly of capping protein, relative to control. If we simply assume that SH3 domains are brought to endocytic sites and recruit other proteins into the endocytic structure, then we would expect that the loss of a single SH3 domain would reduce the amount of actin within endocytic structures. However, this view is not consistent with some of our data because, in some context, we observe an increase in actin assembly (**Figure 10**). Thus, we sought to test if the consensus mechanism of actin assembly in endocytosis can explain our observations of both over-assembly of actin and under-assembly of actin, given that increased assembly may be associated with concomitant increases in the rates of disassembly, preventing over-assembly from occurring. In particular, we varied fitted forward reaction rates of all reactions across two orders of magnitude (range of factor 10 or divided by 10 times the fitted forward reaction rate parameter) to identify which actin assembly steps can be modified to match our data (**Figure 19**). Using a minimal model of actin assembly during endocytosis, we found that by modifying the forward reaction rates of two actin assembly steps in the Arp2/3 activation pathway by a factor of two and the amount of active WASp, we could account for the range of observed SH3Δ data (**Figure 20**).

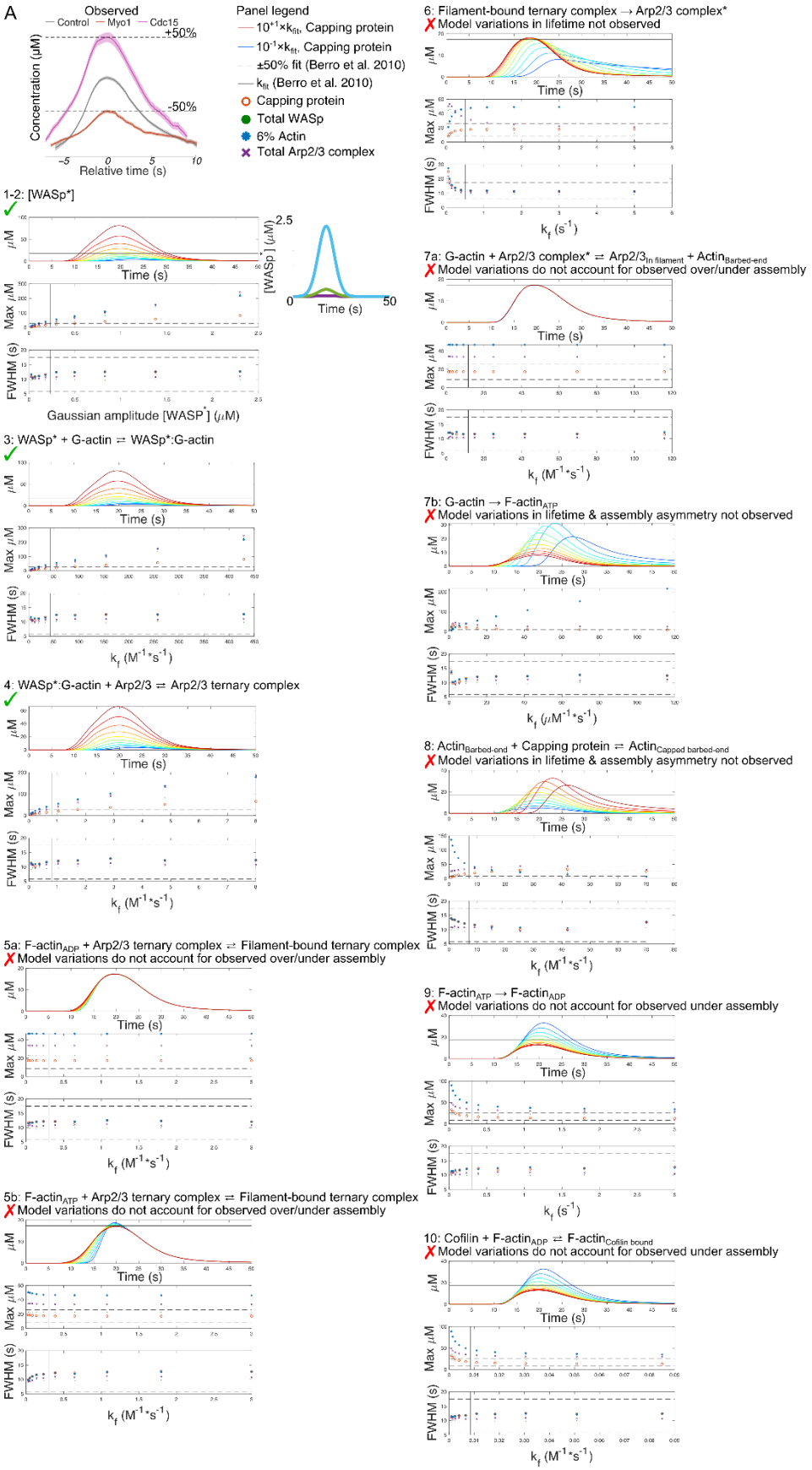
A
Observed
Control
Myo1
Cdc15
+50%
-50%
Concentration (μM)
Relative time (s)
Panel legend
10^+1×k_fit, Capping protein
10^-1×k_fit, Capping protein
±50% fit (Berro et al. 2010)
k_fit (Berro et al. 2010)
Capping protein
Total WASp
6% Actin
Total Arp2/3 complex
1-2: [WASp*]
Time (s)
Max μM
FWHM (s)
[WASp*] (μM)
Gaussian amplitude [WASP*] (μM)
3: WASp* + G-actin ⇄ WASp*:G-actin
k_f (M^-1*s^-1)
4: WASp*:G-actin + Arp2/3 ⇄ Arp2/3 ternary complex
5a: F-actin_ADP + Arp2/3 ternary complex ⇄ Filament-bound ternary complex
Model variations do not account for observed over/under assembly
5b: F-actin_ATP + Arp2/3 ternary complex ⇄ Filament-bound ternary complex
Model variations do not account for observed over/under assembly
6: Filament-bound ternary complex → Arp2/3 complex*
Model variations in lifetime not observed
k_f (s^-1)
7a: G-actin + Arp2/3 complex* ⇄ Arp2/3_In filament + Actin_Barbed-end
Model variations do not account for observed over/under assembly
k_f (M^-1*s^-1)
7b: G-actin → F-actin_ATP
Model variations in lifetime & assembly asymmetry not observed
k_f (μM^-1*s^-1)
8: Actin_Barbed-end + Capping protein ⇄ Actin_Capped barbed-end
Model variations in lifetime & assembly asymmetry not observed
9: F-actin_ATP → F-actin_ADP
Model variations do not account for observed under assembly
10: Cofilin + F-actin_ADP ⇄ F-actin_Cofilin bound
Model variations do not account for observed under assembly

Figure 20. Variation of reaction rates in a model of actin assembly in endocytosis identifies reactions that could plausibly be mediated by SH3 domains, given the extent to which simulated model variations account for observations. (A) Summary of observed actin assembly phenotypes for comparison. (A, right) Legend for numbered panels. (Numbered panels) Number and associated equation indicates reaction varied and simulated for comparison to observed data. Parameters fit for endocytic patch components, based off previous modeling for endocytosis in *S. pombe*, were varied across two orders of magnitude, and simulations were run for parameters logarithmically spaced across a range of 1/10 to 10 times the model's fit parameter (Berro et al., 2010; Sirotkin et al., 2010). Checkmark or "X" indicates whether model variations are consistent with observed data and text briefly indicates rationale. Solid vertical lines indicate model's fit parameter value. Dashed lines indicate ± 50% of corresponding value for capping protein in fit model. (Numbered panels, top) Individual simulation results for concentration of capping protein in an endocytic patch versus time. (Numbered panels, middle) Maximum concentration for proteins of interest for parameter scans. (Numbered panels, bottom) The full-width at half-maximum value of the simulation's concentration versus time, in seconds. (1-2, right) The assumed concentration of active WASp in the patch at the given time. Variations in the height of the Gaussian were simulated for this parameter scan.

For the Arp2/3 complex to nucleate the formation of a daughter filament, WASp and G-actin must form a dimer that binds the Arp2/3 complex in order to form a ternary complex, which, in turn, binds an actin filament (**Figure 19A**). In the Arp2/3 activation pathway, we found that modifying the forward reaction rate of WASp and adapter binding, the binding of the ternary complex to actin, and the activation of the F-actin bound Arp2/3 ternary complex do not alter the amount of actin assembled into endocytic structures. Once loaded onto the filament, reducing the reaction rate of Arp2/3 activation leads to significantly lengthened capping protein lifetimes (not disassembled within simulation time of 50s, despite assembling and disassembling in ~15s *in vivo*) within endocytic structures while increasing the Arp2/3 activation rate does not produce over-assembly of actin (**Figure 20**). Outside of the Arp2/3 activation steps in the actin assembly pathway, several steps either do not lead to over- and under-assembly of actin or significantly lengthen capping protein lifetimes in the patch, which is inconsistent with observed data (see details for each step's justification, **Figure 20**). Tracking only the the maximum capping protein concentration across all simulated parameter scans shows that the most sensitive activation steps are the WASp:G-actin dimerization and ternary complex formation step (**Figure 19B**). Furthermore, these are the only two steps which can be mediated to lead to both over- and under-assembly of actin within endocytic structures (**Figure 19B-C**). Other steps in the model, such as cofilin binding or activation of the Arp2/3 complex nearly cross the observation range threshold (amplitude of capping protein assembly measured *in vivo*) but they do not in fact cross it over the two orders of magnitude variation in fitted forward reaction rate and they, furthermore, cannot produce both over- and under- assembly of actin in the examined range.

Thus, the WASp:G-actin dimerization and ternary complex step in actin assembly during endocytosis are plausibly mediated by SH3 domain interactions. The WASp:G-

actin dimerization step was previously suggested to be mediated by the SH3 domains of Shd1p, suggesting that the insights gained from this model are plausible and coherent with current understanding of actin assembly in endocytosis (Feliciano & Di Pietro, 2012). Furthermore, variations to the WASp:G-actin dimerization step and the ternary complex formation step within a range of just a factor of ½ to 2 times the fitted forward reaction rate parameter can capture both the magnitude of over- and under- actin assembly, showing more sensitivity to perturbations than all other steps in the kinetic model (**Figure 19B-C**). Broadly, interfering with the WASp and G-actin dimerization step or preventing ternary complex formation can either reduce or increase actin assembly, dependent on the forward reaction rate, without significantly altering capping protein lifetimes in patches, consistent with the range of observations in our SH3 domain deletion library, and consistent with the hypothesized roles for SH3-domain containing proteins (**Figure 10**, **Figure 20**, **Figure 21**). In addition, modeling shows that even in conditions where Arp2/3 activation is disrupted, capping protein is a reliable marker for actin and other key components of the activation pathway such as WASp and Arp2/3 complex (**Figure 19C**). These results add to the notion that simple accumulation of NPFs are sufficient for initiating and regulating actin assembly during endocytosis, adding nuance to what might be going on within endocytic structures; namely, NPFs may be inhibited by competitive interactions such that disruptions to SH3 domains alter the balance of inhibiting or enhancing activities, leading to variation in whether SH3 domain deletions lead to increased facilitation or hindrance of interactions in the Arp2/3 activation pathway.

C. Discussion

We measured the influence of each SH3 domain on actin assembly and endocytosis. This revealed striking differences between individual SH3 domain deletion phenotypes, demonstrating that most endocytic SH3 domains are not redundant. Loss of a single SH3 domain from any of 8 endocytic proteins, and in particular the Shd1p-2, Shd1p-3, Cdc15p, Bbc1p, Mug137, Bzz1p-1, Bzz1p-2, Lsb1p, Myo1p, Abp1p-1, and Abp1p-2 SH3 domains, leads the cell to alter the amount of and the rate at which actin is assembled into endocytic structures, endocytic patch motility, and the number of endocytic events. Simulations support that the range of actin assembly defects we observed are consistent with perturbations to interactions in the Arp2/3-mediated actin nucleation pathway (**Figure 19**, **Figure 20**). Thus, our results are consistent with a role for SH3 domains in endocytosis as regulators of Arp2/3 activation.

A

Deleted SH3 domain	Peak assembly (#)	Patch motion (μm/s)	Max assembly rate (#/s)	$N_{endocytosis}$ per cell length (#/μm)
SH3Δ phenotypic feature				
Restricts actin assembly				
Cdc15	+	0	+	-
Bbc1	+	0	+	-
Mug137	+	+	+	0
Enhances actin assembly				
Bzz1-2	0*	-	-	-
Lsb1	-	0	-	0
Regulates NPF				
Myo1	-	-	-	-
Abp1-1	-	-	-	+
Abp1-2	-	-	-	+
Minor or redundant role in actin assembly dynamics				
Shd1-1	0	0*	0	0
Shd1-2	0*	0*	0	0
Shd1-3	0	-	0	-
Bzz1-1	0	0*	0	0
Hob1	0	0*	0	0
Lsb4	0	0	0	0

B

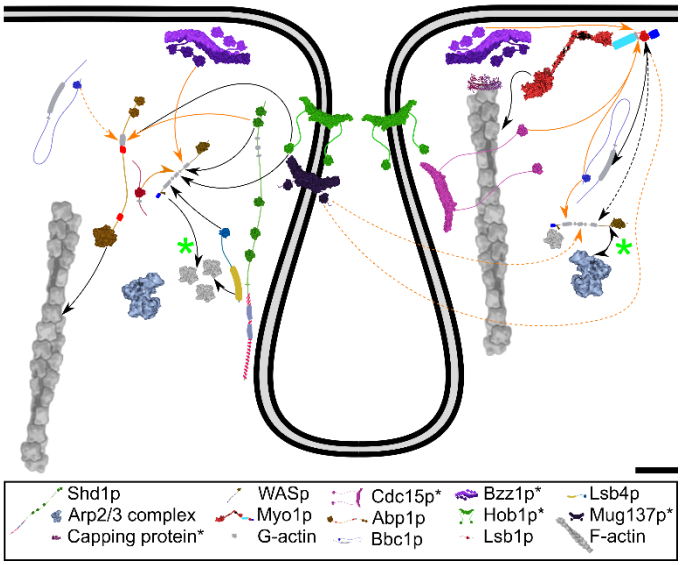

Figure 21. SH3 domains' role in endocytosis is consistent with mediation of interactions that influence Arp2/3 activation and may thus influence actin assembly in endocytosis and the cell's regulation of endocytosis. (A) Summary of results for the role of SH3 domains in actin assembly dynamics and the cell's regulation of the number of endocytic events. Asterisks indicate that effect is on the edge of the 10% difference cutoff threshold. (B, solid black lines) Known direct interactions. (B, dashed black lines) Known indirect interactions. (B, solid orange lines) SH3 domains with a novel interaction that may be functional and influence actin assembly. (B, dashed orange lines) SH3 domains that may exhibit functional, though perhaps indirect, interactions that have not been reported before. Asterisks indicates statistically significant just within 10% threshold for small and large effect classification schema. References for reported interactions are denoted in Table 9. (B, left hand side) WASp and G-actin dimerization step (green asterisk) and possible interactions that may interfere with this step and thus alter the forward rate of that reaction; (B, right hand side) depicts the ternary complex step and interactions that may interfere with ternary complex formation. Scale bar, 10-nm.

1. *Shd1p-2, Cdc15p, Bbc1p, and Mug137p SH3 domains restrict actin assembly in endocytosis*

In mammals, intersectin inhibits WASp and in *S. cerevisiae*, Pan1p-End3p-Sla1p (Pan1p-End3p-Shd1p in *S. pombe*) form a complex that may be the equivalent of mammalian intersectin (Goode et al., 2015). Intersectin contains multiple EH and SH3 domains and serves as a scaffold for multivalent interactions (Tang, Xu, & Cai, 2000). Yet, it was unclear which domains are important and whether endocytosis is robust to deletion of any single-valent SH3 domain-binding site in intersectin. The first SH3 domain of Shd1p does not exhibit striking endocytic defects upon deletion, suggesting that it is dispensable (**Figure 21**). The third SH3 domain of Shd1p exhibits reductions in motility and in the number of endocytic events for a given cell but, otherwise, does not alter actin assembly. In contrast, our data shows that Shd1p's second SH3 domain restricts actin assembly in endocytosis ($p < 0.0001$, though by defining small effects as <10% difference from max number of capping protein molecules accumulated in control, this effect is small) (**Figure 10**). Yet, how the second SH3 domain of Shd1p inhibits NPF activity remains unclear. One hypothesis is that the first two SH3 domains of Shd1p prevent monomeric actin from binding to WASp (Feliciano & Di Pietro, 2012). However, it is also possible that Shd1p's SH3 domains prevent the WASp and G-actin dimer from binding Arp2/3 to form the ternary complex (**Figure 20**). It also remains unclear how release of WASp inhibition is accomplished. In *S. cerevisiae*, Sla1p's third SH3 domain and Rvs167p's (Hob1p in *S. pombe*) SH3 domain competitively bind ubiquitin, which could limit Shd1p and WASp binding (Stamenova et al., 2007). It's also possible that other SH3 domains transiently compete with Shd1p for WASp but this explanation is complicated by fast re-association of Shd1p and WASp, given that Shd1p and WASp form a stable complex in the cytosol (Feliciano & Di Pietro, 2012).

Table 9. Summary of SH3 domain-mediated interactions between endocytic proteins of interest.

SH3 domain	Interactors	Organism	Reference
Shd1	Disrupts WASP:G-actin, Abp1p, WASp	S. cerevisiae	Feliciano et al. 2012, Costa et al. 2005
Myo1	Cdc15, WASp (indirect)	S. pombe	Carnahan et al. 2003, MacQuarrie et al. 2018
Cdc15	Myo1	S. pombe	Carnahan et al. 2003
Abp1	Hob1, F-actin	S. cerevisiae	Friesen et al. 2006; Lila et al. 1997
Bbc1	WASp, Myo1	S. cerevisiae, S. pombe (proposed)	Rodal et al. 2003, MacQuarrie et al. 2018
Bzz1	Myo1, WASp	S. cerevisiae	Soulard et al. 2002, Arasada & Pollard 2011
Hob1	WASp, Abp1p	S. cerevisiae	Goode et al. 2015
Lsb1	WASp (NPF-inhibitor?)	S. cerevisiae	Spiess et al. 2013
Lsb4	WASp, F-actin	S. pombe	Robertson et al. 2009
Mug137	NA	NA	

Cdc15p participates in endocytosis during interphase and cytokinesis during mitosis (Arasada & Pollard, 2011; Carnahan & Gould, 2003). Our results show that deleting Cdc15p's SH3 domain results in more actin assembled into endocytic structures, in contrast with previously reported Cdc15p full-length depletion (**Figure 10**) (Arasada & Pollard, 2011). In endocytosis, Cdc15p localizes around the base of the tube when and where myosin-I activates Arp2/3 in a membrane-proximal polymerization zone (Arasada & Pollard, 2011). There, it is possible that Cdc15p's SH3 domain sequesters verprolin, decreasing Myo1p binding to Arp2/3. In this case, Cdc15p's SH3 domain restrict NPF activity, which could explain how Cdc15p-SH3Δ cells restrict actin assembly (**Figure 21**) (Oh et al., 2013; G. Ren et al., 2005).

Full-length Bbc1p deletion causes increased actin nucleation (M. Kaksonen et al., 2005). Deleting Bbc1p's SH3 domain phenocopies Bbc1p's full-length deletion defect, suggesting that Bbc1p's SH3 domain is sufficient for Bbc1p' overlapping role with Shd1p in restricting actin polymerization (**Figure 21**). Bbc1p localization to endocytic structures depends on myosin-I and when Bbc1p is deleted, verprolin accumulates in the patch (MacQuarrie et al., 2018; Sirotkin et al., 2005). As such, Bbc1 may also restrict actin assembly in endocytosis by competing with verprolin for myosin-I.

Mug137p is an uncharacterized protein in yeast but its mammalian orthologs, endophilin A1-3, are involved in endocytosis (Kjaerulff et al., 2011). Mug137p's SH3 domain restricts actin assembly in endocytosis and restricts the length of endocytic cells, though it remains unclear whether it exerts these influences on the cell directly or indirectly (**Figure 17**). Given that its SH3 domain influences actin assembly in endocytosis, we predict that Mug137 directly or indirectly interacts with NPFs during endocytosis. Future work will have to parse Mug137p's activity *in vitro* and quantify its

spatiotemporal assembly into endocytic structures in order to further resolve its role in endocytosis.

2. Bzz1p-2 and Lsb1p SH3 domains enhance actin assembly in endocytosis

Bzz1p arrives concurrently or slightly before the beginning of actin assembly, binds WASp through its SH3 domain and promotes WASp NPF activity *in vitro* (Arasada & Pollard, 2011; Tonikian, Xin, Toret, Gfeller, & Landgraf, 2009). Bzz1p also interacts with myosin-I and Bzz1p's SH3 domains, myosin-I, and verprolin are sufficient to recruit and create branched actin networks *in vitro* (Soulard et al., 2002). It was previously shown that deletion of Bzz1p's SH3 domains increases actin assembly but we showed that the deletion of only Bzz1p's second SH3 domain has significant reductions in the amount of actin assembled into endocytic structures and a reduction in the rate of assembling actin into endocytosis (**Figure 10**, **Figure 14**) (Arasada & Pollard, 2011). Our results are consistent with Bzz1p's purported NPF-enhancing activity (Goode et al., 2015).

S. cerevisiae Lsb1p and Lsb4p were identified as Las17p (WASp in *S. pombe*) binding proteins in a two-hybrid screen (Madania et al., 1999). Lsb1p inhibits Arp2/3 polymerization *in vitro* while Lsb1p overexpression blocks endocytosis *in vivo* (Spiess et al., 2013). However, Lsb1p's influence on actin assembly in endocytic structures *in vivo* is unknown (Goode et al., 2015). Without Lsb1p's SH3 domain, less actin is assembled into endocytic structures and actin is assembled at a reduced rate (**Figure 10**, **Figure 14**). This suggests that Lsb1p enhances actin assembly *in vivo*, in contrast to its reported activity *in vitro*. Our results may help to explain why Lsb1p over-expression blocks endocytosis: through its SH3 domain, Lsb1p may competitively relieve inhibition of endocytic NPFs, such that over-expression disrupts this balance and restricts actin

assembly in endocytosis. Alternatively, because Lsb1p forms homo-and hetero-oligomeric complexes, it may help WASp dimerize, enhancing its NPF activity (Padrick et al., 2008). More studies into Lsb1p are needed to distinguish between these actin assembly enhancing activities *in vivo* and restrictive activities *in vitro*.

3. Myosin-I's and Abp1p's SH3 domains regulate their NPF activity in endocytosis

Myosin-I has a CA domain that binds Arp2/3 and its SH3 domain binds verprolin, which has an N-terminal WH2 (V) domain (Evangelista et al., 2000). Together, Myosin-I and verprolin have a VCA domain that promotes branched-actin network assembly (Sirotkin et al., 2005). In deleting myosin-I's SH3 domain, we observed reduced myosin-I localization to endocytosis (data available in previous version). We also found that actin assembly in endocytosis is reduced in Myo1p SH3∆ cells (**Figure 10**). Full-length myosin-I deletion is viable and cells increase the number of actin patches (Petrini et al., 2015). However, we found that deleting myosin-I's SH3 domain reduces the number of actin patches in the cell (**Figure 15**). This is consistent with the observation that endocytic structures lacking myosin-I motor activity exhibit compromised internalization (Sun et al., 2006).

Abp1p has moderate NPF activity *in vitro*, relative to WASp (Goode, Rodal, Barnes, & Drubin, 2001; Sun et al., 2006). Abp1p is a poorly understood NPF that may have important effects on actin assembly in the presence of binding partners *in vivo* (Goode et al., 2015). Its activity is a regulatory target: its SH3 domain interacts with Aim21p, which negatively regulates actin assembly (Farrell et al., 2017; Shin, van Leeuwen, Boone, & Bretscher, 2018). Deletion of Abp1p's SH3 domains increases the number of endocytic events in the cell (**Figure 15**). This consistent with full-length Abp1p deletion, which

lengthens disassembly time (M. Kaksonen et al., 2005). *S. cerevisiae* Abp1p's SH3 domain binds and localizes a disassembly factor, the cyclase-associated protein Srv2p/CAP, to endocytic structures, which may explain why Abp1p SH3Δ cells exhibit extended disassembly times despite assembling less actin (**Figure 10E**, **Table 6**) (Freeman et al., 1996). There is only one SH3 domain in the *S. cerevisiae* Abp1p but there are two SH3 domains in the *S. pombe* Abp1p: the reason for this difference or possible redundancy in the SH3 domains of *S. pombe* Abp1p is unclear. In *S. cerevisiae*, Abp1p's SH3 domain is essential in Sla1p (Shd1p in *S. pombe*) deletion backgrounds, suggesting that the Abp1p SH3 domain has an overlapping function with Shd1p (Quintero-Monzon, Rodal, Strokopytov, Almo, & Goode, 2005). However, since each *S. pombe* Abp1p SH3 domain significantly contributes to actin assembly during endocytosis, we showed that the two *S. pombe* SH3 domains are not redundant and that they have a functional role since, contrary to functional overlap, we observed opposite effects between Abp1p's and Shd1p's SH3 domains (**Figure 21**).

4. *Some SH3 domains have minor or redundant effects on actin assembly in endocytosis*

Abp1p, Bzz1p, and Shd1p have multiple SH3 domains (**Figure 5**). If multivalency is vital to the function of these proteins, then disruption of single SH3 domains should lead to defects in actin assembly. However, Shd1p-1, Shd1p-3, and Bzz1p-1 SH3 domains are dispensable to actin assembly and Shd1p-1 and Bzz1p-1 SH3 domains are dispensable to cellular adjustment of the number of events (**Figure 21**). This suggests that Shd1p and Bzz1p have redundant copies of SH3 domains. At the scale of the entire endocytic structure, some SH3 domains also exhibit redundant functions in actin assembly and endocytosis. Full-length Hob1p deletion cells exhibit disruptions to actin

polymerization, internationalization defects and failed scission (Friesen et al., 2006; Gallego et al., 2010; M. Kaksonen et al., 2005) Yet, we see no evidence of failed scission in Hob1p-SH3∆ cells and no striking defects in actin assembly, suggesting either that its SH3 domain is not essential to Hob1p's function or that its SH3 domain has a redundant role in endocytosis (**Figure 21**). Lsb4p binds and bundles F-actin and its SH3 domain binds WASp, whose presence increases bundling activity (Robertson et al., 2009; Urbanek et al., 2015). However, we found that Lsb4p's SH3 domain has only a minor contribution to actin assembly, relative to other SH3 domains, which may suggest that it has a largely redundant or minor role in actin assembly and endocytosis (**Figure 10**, **Figure 21**).

5. SH3 domains in endocytosis

By perturbing endocytosis and quantifying local endocytic and global cellular features for each endogenous, single SH3 domain deletion, we revealed a number of relationships between endocytic molecular assembly dynamics, motility, and cellular regulation of endocytosis (**Figure 18**). Perturbations to endocytic molecular assembly correlate with variations in patch motility, which may suggest that assembly of the endocytic actin network controls the motion of the endocytic patch or vice versa. In particular, the disassembly phase of endocytosis has stronger associations with motility than the assembly phase, which may indicate that SH3∆s disrupt assembly without significantly disrupting the molecular mechanisms associated with disassembly of the endocytic actin network. Global cellular features, such as the expression of capping protein and the number of endocytic events poorly or negligibly correlate with most local endocytic measurements, which may indicate that perturbations to endocytosis by deleting different SH3 domains indirectly effect cellular phenotypes. However, despite

these novel associations, it remains unclear whether these observations reveal patterns unique to SH3 domains or whether they generalize to any perturbations to endocytosis. Suggesting their generalizability, a recent study reports a dose-dependence between an endocytic patch's speed and the number of myosin-I molecules assembled into endocytic structures (Manenschijn et al., 2018). This relationship appears to be non-linear, consistent with our observation of the non-linear, dose-dependent relationship between the number of capping protein molecules and patch motility (**Figure 18C**). Future quantitative experiments and analyses that perturb endocytosis in ways orthogonal to those reported here will need to be performed and compared with ours results in order to decouple SH3-specific patterns from rules governing endocytic behavior.

SH3 domains regulate actin polymerization in endocytosis but it is unclear how these domains do this in spite of the degeneracy of SH3 domains in endocytosis and within several endocytic proteins. In a model where all SH3 domains have only a protein binding molecular function, degeneracy may enable multivalent interactions that form functional, phase-separated structures. If this is true, then deleting a SH3 domain will reduce the propensity to phase separate. However, if the valency of proteins in the macromolecular complex remains high, then deletion of a single valent unit may not produce noticeable effects. In the latter case, if we assume that phase-separation influences function, then deletion of a single valent unit should not produce diverse effects on endocytosis. Furthermore, it should not matter which SH3 domains are deleted. To the contrary, we found that SH3 domains have diverse influences on actin assembly and endocytosis. We showed that our observations are consistent with a role for SH3 domains in regulating actin assembly by mediating interactions that influence Arp2/3 activation (**Figure 19**, **Figure 20**). Determining how competition and promiscuity

of SH3-domain interactions accomplish the effects we observed will require future investigations into the specificity of SH3 domains *in vivo*. In addition, because so many SH3-domain containing proteins in endocytosis have intrinsically disordered regions, determining whether a transient, phase-separated structure alters the kinetic parameters of the Arp2/3 activation pathway may yet reveal a functional role for phase-separation in endocytosis. Given the broad interest of SH3 domains in assembling molecular pathways, our findings may lend insight into how single components can be brought together for emergent biological activities, which may inform synthetic pathway design (Nash, 2012).

D. Limitations

1. Genetic engineering in S. pombe

The variability in the fraction of colonies with positive editions, typically screened by colony PCR amplicon size, depends on the gene being modified and the selected Cas9 target site. For example, in my hands ~1/60 colonies will be positive for C-terminal tagging of fimbrin with EGFP while C-terminally tagging capping protein (Acp1p) with EGFP yields ~3 positively edited colonies out of every 4 screened. The reason for this variability is a topic of active research but one possibility is that Cas9's ability to access the genome is influenced by chromatin organization and regulation (Horlbeck et al., 2016; Yarrington, Verma, Schwartz, Trautman, & Carroll, 2018).

Colonies identified as positive by size (or by restriction digest and other PCR-based screening methods) are sequenced around the edited genetic region (~0.5 – 1-kbp in the

edited genome are sequenced; note, EGFP insert is ~700-bp). Sequencing around the edited region seldom reveals an error, suggesting that indels and frame-shift mutations are rare. To my knowledge, no one using CRISPR-Cas9 mediated genetic engineering in S. pombe has fully sequenced the genome of positively edited strains to assess the frequency of off-target mutations in this model organism. Therefore, I cannot rule out the presence of additional, un-intentional mutations in the organisms I study (note, all strains studied in Chapter VI were created by homology-directed repair, not CRISPR-Cas9 mediated gene editing).

However, there are a number of reasons to temper concern regarding the confounding effects of potential, off-target mutations. Cas9 target specificity is mediated by interactions between the 5'-end of the gRNA and protospacer DNA, especially in the 12-mer region 5' to NGG (Tsai & Joung, 2016; Tsai et al., 2015; Q. Wang & Ui-Tei, 2017). In S. pombe, the genome is significantly smaller than in mammalian cells so it is much easier to find unique 20-bp sequences to target Cas9 (human genome, ~3,000 Mb; S. pombe genome, ~10 Mb). To increase the likelihood that Cas9 is targeted specifically in the strains created for this dissertation, unique 12-mer sequences (5' to the NGG site) were selected to target Cas9 in all genetic editing approaches in these studies (Y. Naito, K. Hino, H. Bono, & K. Ui-Tei, 2015). In contrast, in humans, where most of the reported off-target effects are reported, >50% of the genes do not have unique 12-mer sequences, suggesting that for the majority of human genes, there are no targets free of the potential for off-target effects (Q. Wang & Ui-Tei, 2017). This is far from the case in S. pombe. Indeed, some organisms have even been shown not to exhibit off-target mutations (X. H. Zhang, Tee, Wang, Huang, & Yang, 2015).

In addition to a reduced potential for off-target effects in S. pombe relative to humans, yeast cells have innate systems to control the number of plasmids they retain

whereas transfection of human cells with lentiviral vectors may contribute to off-target mutations and stabilization of Cas9 copy number, further complicating the attribution of off-target edition risk estimated for human gene editing to S. pombe (Lavillette, Russell, & Cosset, 2001; Y. T. Liu et al., 2014).

To substantiate this moderating rationale, I compared strains created by CRISPR-Cas9 mediated genetic editing to strains edited with homology directed repair in a patch tracking assay (**Figure 37**). This shows that even in the case where background, off-target mutations likely exist (as determined by a phenotype in mating assay), there is no detectable difference in local endocytic behavior in strains edited by CRISPR-Cas9 mediated genetic engineering and strains with a comparable genotype created by homology-directed repair. In addition, strains in all chapters except for Chapter IV, were derived from strains in which backcrossing did not reveal any defects (data not shown, experiments done by Ronan Fernandez and communicated to NGR). Nonetheless, a pressing future direction of study ought to be to sequence the whole genome, perhaps of a handful of genetically modified S. pombe strains, in order to estimate the frequency of off-target mutations expected in the utilized library of strains (**Table 13**).

2. *Effect of SH3 domain-containing protein expression and capping protein expression in various SH3 domain deletion genetic backgrounds*

Capping protein expression, relative to control cells and adjusted for cellular length, can be decreased by as much as 24% (for Shd1-3 SH3 domain deletion cells, relative to control cells) and increased by as much as 19% (for Mug137p SH3 domain deletion, relative to control cells), compared to ~30% decrease in actin assembly (for Myo1p SH3 domain deletion, relative to control cells) and ~40% increase in actin assembly (for

Cdc15p SH3 domain deletion cells, relative to control cells) (**Figure 10A**, **Figure 15E**). This might cause concern that the primary influence of SH3 domains is to alter protein expression rather than directly influence actin assembly and endocytosis. However, contrary to this concern, there is a negligible correlation between capping protein expression and the number of capping protein molecules assembled into endocytic structures across SH3 domain deletion strains (r_S = 0.24; p = 0.49) (**Figure 18A**). Furthermore, capping protein expression does not predict the maximal number of capping protein molecules assembled into endocytic structures (linear model, R^2 = 0.07; p = 0.32) and performs poorly compared to other predictors of actin assembly in endocytosis (**Figure 11A**, **Figure 18B-C**). These results suggest that, despite the fact that SH3 domains alter capping protein expression in the cell, these alterations do not explain the reported observations. Thus, deleting single SH3 domains appears to have influences beyond simply altering expression.

In addition to altering capping protein expression, SH3 domains may alter the expression of other endocytic proteins or influence the expression of their own protein. We have not quantified the expression of each of the over 60 proteins known to be involved in endocytosis in each of the 14 SH3 domain genetic deletion backgrounds. However, we have quantified the dependence of some SH3-domain containing proteins on their SH3 domain (**Figure 23** – **Figure 26**). Most SH3 domains either do not alter the expression of their protein upon deletion or have small influences (<10%) on their protein's expression upon deletion (**Table 10**). Yet, some SH3 domains, in particular Shd1p-SH3-1Δ cells express Shd1p at levels >50% than that of control cells (**Figure 27**). However, in our measurements, Shd1p-SH3-1Δ cells exhibit relatively minor influences on actin assembly and endocytosis (**Figure 12B-C**, **Figure 21A**). This discrepancy between alteration to expression and influence on actin assembly and endocytosis

seems to suggest that expression is not a significant confounder to these results and may indicate that the cell compensates SH3 domain deletion by altering expression in order to maintain successful endocytic events throughout the cells. However, a more comprehensive analysis, perhaps using regression approaches to evaluate multiple predictors of actin assembly in endocytosis, may yet disentangle which alterations to expression can explain some of the results we observe across the endocytic SH3 domain single deletion library.

Global cellular features (capping protein expression and the number of endocytic events in the cell) are poorly or negligibly correlated with local endocytic behavior across the SH3 domain deletion library (maximum r_S = -0.57, between the endocytic rate and the time of assembly; average r_S = 0.31) while variations in local endocytic behavior exhibit very high correlations with each other (maximum r_S = 0.98 between maximum disassembly rate and maximum number of capping protein molecules assembled) (**Figure 21A**). This may suggest that perturbations to SH3 domains alter endocytic behavior and that the effects of these deletions are indirectly communicated to the cell, thus exhibiting poor correlations in variations for global compared to local measurements. Regardless, these patterns weaken the likelihood that capping protein expression dictates the variety of influences that we observe SH3 domains have on local endocytic behavior. Nonetheless, it is still possible that deletions of SH3 domains perturb the cell, which, in turn, causes variations in local endocytic behavior, potentially indicating that SH3 domains' influence on actin assembly is indirect. Independently, capping protein expression and endocytic rate do not predict the magnitude with which capping protein is accumulated within endocytic structures (linear regression, R^2 = 0.07 and R^2 = 0.33, respectively) (**Figure 11**). Treating these global measurements as predictors in a multiple linear regression model, we find that expression and endocytic

rate, taken together, reasonably predict the maximal accumulation of capping protein (adjusted $R^2 = 0.79$). However, in this model, control cells as well as several other SH3 domain deletion cells have large residuals, suggesting that capping protein expression and alterations to the endocytic rate fail to explain specific observations, despite globally performing well. Furthermore, other multiple linear regression models, for example using the mean absolute deviation five seconds after scission and the maximum disassembly rate (adjusted $R^2 = 0.94$), the total time of endocytosis and the maximum assembly rate (adjusted $R^2 = 0.82$), or the length of cells and the maximum disassembly rate to predict the maximal accumulation of capping protein into endocytic structures (adjusted $R^2 = 0.94$) also yield reasonable predictions of the maximal accumulation of capping protein into endocytic structures. Including all of these predictors in a multiple linear regression model yields yet more accurate predictions of the maximum number of capping protein found within endocytic structures for various SH3 domain deletions (adjusted $R^2 = 0.98$). Yet, in this model, capping protein expression and the relative endocytic rate do not significantly contribute to the model's fit (Z-test, $p = 0.46$ and $p = 0.31$, respectively; see "salient_bivariates.rmd" on git.yale.edu/ngr4, authored by NGR).

These predictive models are limited by the size of the endocytic SH3 domain deletion library and thus, are based on a limited number of data points. Furthermore, they lack temporality, failing to indicate whether global cellular phenotypes occur before or after variations in local endocytic behavior. Yet, even if the expression matched changes in molecular assembly one-for-one across SH3 domain deletion strains, this would still be a result and require consideration of several explanations beyond merely ascribing alteration to expression and assembly as a confounding effect. For example, one way that cells might modify the molecular assembly of endocytosis would be to increase expression of actin assembly accessory factors to accomplish endocytosis in a

perturbed or comprised environment. This is not akin to erroneous control experiments but rather something that is monitored, in particular, to quantitatively measure and describe if and how cells adjust expression and assembly in response to perturbations to endocytic SH3 domains. It remains plausible that to compensate for a perturbation, cells alter expression and thus assembly of its pathways.

However, because this is an observational study, the pattern of variations we report across the SH3 domain deletion library cannot provide temporality to the correlations we observe, for example between the maximum disassembly rate of capping protein from endocytic structures and the maximum accumulation of capping protein into endocytic structures (**Figure 18B**). In addition, the strength of the dose-response we relationships we observe are limited across a narrow range of magnitudes, given that changes in any metric by several orders of magnitude is likely biologically or physically infeasible. Some relationships we observe are consistent with other studies, for example, the relationship between molecular assembly and patch motility, and many relationships have plausible explanations, for example between the maximum assembly rate and the maximum accumulation of capping protein into endocytic structures (**Figure 18**) (Manenschijn et al., 2018). Yet, we do not address the specificity in many of the alterations to the metrics we observe; for example, we do not know if a change in molecular assembly is only produced by a change in patch motility or vice versa, especially since, upon SH3 domain deletion, there are many changes in the cell. Thus, inferences to causality based on the results in this study are weak but, by tempering claims and concluding only that SH3 domains' presence seems not to be associated with the range of activities we observe when we delete each SH3 domain, this study provides a detailed and quantitative record of the cell's response to deleting single SH3 domains across several metrics to suggest their influence. Future work will need to expand the breadth of experimentation and

combine observations with mathematical modeling based on a larger number of individual data points to limit the number of plausible alternative explanations based on these data and to better tease out which alterations cause others.

3. *Effect of recruitment-timing on interpretation of individual SH3 domain influences on actin assembly and endocytosis*

The timing of recruitment and accumulation of SH3 domain-containing proteins into endocytic structures has, for the most part, been measured in *S. pombe* or *S. cerevisiae* (**Figure 5B**, **Table 3**). The observations for some SH3 domain deletion strains, such as Myo1p, Cdc15p, and Bbc1p, can be explained in terms of their recruitment timing and effect on actin assembly: they arrive before or concomitant with a burst of actin polymerization, ~3s before scission. As such, these SH3 domains plausibly regulate WASp, which is present during that time. Similarly, Hob1p arrives after a burst of actin assembly and exhibits minor influences on actin assembly, which might be expected, given that Hob1p is assembled into endocytic structures after actin assembly has initiated (**Figure 5B**, **Figure 21A**). Furthermore, Hob1p cells exhibit decreased motility after endocytosis, which is also consistent with its known endocytic timing (cumulative displacement, **Figure 14E**).

However, a significant limitation in this study is that we cannot confidently rely on previous reports of recruitment timing to interpret our results because we do not measure the effect of individual SH3 domain deletions on the recruitment and assembly dynamices of WASp, the Arp2/3 complex, or other SH3-domain containing proteins of interest. Scission occurs just after an increase in patch motility and concomitant with diffusive motion of the endocytic patch (J. Berro & T. D. Pollard, 2014). Thus, across the

SH3 domain deletion library, we can conclude that capping protein's recruitment timing does not change in different SH3 domain genetic deletion backgrounds (**Figure 12A-B**). However, when Shd1p's SH3 domains are deleted, the recruitment timing of Shd1p does appear to change, relative to scission at t=0s (**Figure 29A**). Thus, it is plausible that the assembly dynamics of proteins that are not measured are different in the various SH3 domain deletion backgrounds.

In order to evaluate how un-measured disruptions to the recruitment timing of proteins of interest might alter the interpretations in this study, we can focus primarily on the role of the full-length protein, rather than the influence of the individual SH3 domain, to interpret the range of activities observed across SH3 domain deletion cells. For example, Bbc1p is thought to inhibit actin assembly, which here we propose it accomplishes by competitively binding WASp through its SH3 domain, thus inhibiting WASp from activating the Arp2/3 complex (M. Kaksonen et al., 2005). If Bbc1p SH3 domain deletion alters the recruitment or timing of Bbc1p into endocytic structures, as it appears to do, then Bbc1p can no longer inhibit WASp at the right time or at all and, as a result, actin assembly is expected to increase (all else held constant). This is what we observe (**Figure 10B**, **Figure 24A**). Other than a SH3 domain, Bbc1p does not have many known functional structural features (**Figure 5C**). However, myosin-I has many structural and functional features and its motor domain activity may be independently critical to successful endocytosis (Lechler, Shevchenko, Shevchenko, & Li, 2000). When the SH3 domain of myosin-I is deleted, myosin-I no longer robustly localizes to endocytic structures (**Table 10**). Thus, myosin-I's SH3 domain may primarily play a regulatory and localization role for myosin-I. Given that myosin-I is also a NPF, both of these possibilities are considered for myosin-I (see discussion).

The approach of using previous literature and a consensus-based understanding of the full-length protein, rather than the influence of the SH3 domain in isolation, can be extended in the example of Cdc15p's SH3 domain deletion results. The Cdc15p SH3 domain may autoinhibit Cdc15p, preventing its BAR domain from creating membrane tubules (Kumar et al., 2009; Rao et al., 2010; Q. Wang et al., 2009). In control cells, its SH3 domain may bind myosin-I, thus relieving inhibition of its BAR domain's tubulation activity, which, in turn, may be connected to actin assembly (Arasada & Pollard, 2011; Kumar et al., 2009; Rao et al., 2010). However, if Cdc15p inhibits myosin-I activity through binding Myo1p with its SH3 domain, then deletion of the SH3 domain might reduce Cdc15p localization to endocytic structures and relieve inhibition of NPF activity within endocytic structures, resulting in the observed increase in actin assembly (**Figure 12A**, **Figure 21B**). However, if the SH3 domain is dispensable for Cdc15p localization to endocytic patches, then the Cdc15p SH3 domain's regulatory activity, rather than its assembly and localization role, would be a more critical determinant in increasing actin assembly. The assembly dynamics of Lsb4p, Mug137p, and Lsb1p have not been reported and, even for those whose recruitment timing has been studied, additional experiments are required to distinguish between localization and regulatory roles for individual SH3 domains. As a result of these limitations, in this study, we can only conclude that SH3 domains, indirectly or directly, influence the ability of individual endocytic proteins or of the endocytic pathway to function similarly to control cells.

E. Methods

1. Protein feature annotations and schematization

Protein features not included in curated databases were included in this study, consistent with the field's work on particular endocytic proteins (Goode et al., 2015). Translated protein sequences were downloaded from PomBase (V. Wood et al., 2002). The translated sequence was used to check proline-rich annotations and other features and extract their position in the sequence to determine range of a particular feature using InterProScan (Jones et al., 2014). Representative structures were found for each domain and converted into cartoon images using the Protein Model Portal (Haas et al., 2013). To identify sequence coordinates of protein features that were important in the literature but not in any database, such as Shd1p's SHD2 domain, its CBM and SR repeats, Myo1p's TH2 domain and its IQ motifs, and Wsp1p's, Myo1p's, and Abp1p's central or acidic domains, references were identified from the literature and domain diagrams in indicated references were used to estimate length and position of domain in amino acids.

Scaling for schematization of proteins was done according to structural measurements when available or by sequence length when structures were not available (Henne et al., 2007; Jiménez et al., 1999; Carsten Mim et al., 2012; Mullins, Stafford, & Pollard, 1997; Phillips, Kondev, & Theriot, 2009; T.D. Pollard & Borisy, 2003). Proteins are represented at the endocytic stage for where they reach their peak within endocytic structures at ~1/30th of their true accumulation number, constructed according to Table 4.

2. Sequence analysis of S. pombe SH3 domains

Using the Simple Modular Architecture Research Tool (SMART), *Schizosaccharomyces pombe* (972h-) SH3 domains were queried and their sequences were compiled automatically into a text file (Letunic & Bork, 2018). Proteins were named according to their PomBase name (Valerie Wood et al., 2012). The SMART SH3 domain sequences were used for a multiple protein sequence alignment using Clustal Omega via European Bioinformatics Institute (EMBL-EBI) web-services (Sievers et al., 2011). The multiple sequence alignment was visualized with EMBL-EBI's MView (Brown et al., 1998). Alignment, structural, and important SH3-feature annotation was based off comparisons to Myo1p in a yeast SH3 multiple sequence alignment (Verschueren et al., 2015). To calculate the significance at which SH3 domain containing proteins are found in a particular gene ontology category, we used gene enrichment analysis and calculations provided by the database for annotation, visualization, and integrated discovery (DAVID) (D. W. Huang, B. T. Sherman, & R. A. Lempicki, 2009). The Gene Ontology biological process annotation for endocytosis did not include 4 proteins with SH3 domains that are known to be involved in endocytosis, namely, Bbc1p, Lsb1p, Abp1p, and Cdc15p (Arasada & Pollard, 2011; Goode et al., 2015). Regardless, using GO annotations, there is a significant enrichment of SH3 domain containing proteins in endocytosis; however, as a consequence, the reported p-value is an overestimate, i.e., the p-value should be smaller (**Figure 4**). To do a pairwise sequence alignment comparing the percent identity and similarity of each endocytic SH3 domain to every other endocytic SH3 domain, I used a custom MATLAB script that aligned peptide sequences using the progressive method, which is included in the MATLAB Bioinformatics toolbox. The script to align, pair-wise, all combinations of endocytic SH3 domains, "sequence_alignment.m," is available through GitHub at

<https://git.yale.edu/ngr4> (authored by NGR). Structural alignment of SH3 domains was done in PyMOL using representative structures from the Protein Data Bank (PDB) (for complete list of representative structures, see “SH3BoundaryDefinition.pdf” on git.yale.edu/ngr4). PomBase tools were used to visualize, in totem, the list of genes known to play a role in endocytosis and to search for the canonical binding motif PXXP within endocytic proteins, providing the data for an empirical cumulative distribution function of the number of endocytic proteins that could be bound by SH3 domains (script “ECDF_of_PRM_number.m”available at <https://git.yale.edu/ngr4>) (authored by NGR) (Lacy et al., 2018; Valerie Wood et al., 2012).

3. Growth measurements

To assess whether or not a particular SH3 domain deletion compromised the ability to grow in rich liquid media, relative to a strain with all of its SH3 domains and only capping protein tagged with GFP, all single SH3 domain deleted cells were compared to control in a growth assay. To measure the growth of all strains, overnight cultures were diluted to a 1-mL, yeast-extract with 5 supplements (YE5S) culture of $OD_{595}=0.1$ in a 24-well tissue culture plate (FALCON, Corning Incorporated). The absorbance (OD_{600}) value for each strain in YE5S was measured every 5-min for 24-h, or until growth plateaued, using a BioTek Synergy 4 plate reader, which maintained temperature throughout growth at 32C with continuous agitation. Growth curves were plotted as absorbance over time and fit to a Gompertz growth model. Each strain was compared to control using 95% confidence intervals for the fitted coefficients and two-tailed Z-tests using a custom R script, “growthCurves.R,” which is available at <https://git.yale.edu/ngr4> (authored by NGR).

4. SH3 domain sequence boundary definition

To define the amino acid sequence boundary of SH3 domains, we aligned the sequences of each SH3 domain to itself across multiple database sources for the sequence of the domain, each of which had a different boundary for the SH3 domain (Finn et al., 2016; Gough et al., 2001; Schultz et al., 1998; Sigrist et al., 2002). In addition to including sequences from various protein databases, a sequence of a representative structure for each SH3 domain was taken from the PDB to ensure that at least one sequence would be sufficient for folding (**Figure 7**; for complete list of representative structures, see "SH3BoundaryDefinition.pdf" on git.yale.edu/ngr4). To draw cut-offs for each SH3 domain, N-terminally and C-terminally, structural features were annotated and boundaries were drawn such that all structural features were included in the SH3 domain (Saksela & Permi, 2012). After this criterion was met, the minimal database overlap was chosen as the SH3 domain sequence. If not all structural features were contained within the minimal database overlap sequence, then the sequence that aligned with and overlapped with the representative structure was chosen. If not all structural features were contained within the representative PDB structure, then the SMART sequence was chosen. If the SMART domain sequence lacked any structural features, then the maximal database overlap sequence was taken. The last condition was applied for only 3 domains, Shd1p's 1st SH3 domain, Bbc1p's SH3 domain, and Cdc15's SH3 domain. For all others, the SMART sequence was chosen since this was commonly the minimal database overlap sequence that contained all structural features. To process all the sequence alignments, a custom-script was

written, “functions_seq_align.py,” which is available at <https://git.yale.edu/ngr4> (authored by NGR).

5. S. pombe strain construction

To create a library of single SH3 domain deletion strains with an endocytic protein tagged with GFP, we used CRISPR-Cas9 mediated gene editing and gap repair (Fernandez & Berro, 2016; Kostrub et al., 1998). Briefly, a stretch of genetic sequence ~110-bp 5’ and 3’ of each SH3 domain were prepared by PCR, then ligated together by overlap extension PCR. This ligated PCR cassette was blunt end-ligated into a vector (CloneJET PCR Cloning Kit, ThermoFisher Scientific) for sequencing and robust amplification from a miniprep (NucleoSpin Plasmid, Takara Bio Inc) to use as donor DNA. To construct gRNA that targets Cas9, first a unique cut site with only 1 PAM +20mer sequence in the *S. pombe* genome and <8 PAM +12mer sequences in the *S. pombe* genome was identified using CRISPRdirect (Yuki Naito, Kimihiro Hino, Hidemasa Bono, & Kumiko Ui-Tei, 2015). To express the target sequence as RNA in a transformed *S. pombe* cells, the target DNA sequence was inserted into a plasmid, pJB166, which contains a RNA Pol III promoter element and cleavable leader RNA (Jacobs, Ciccaglione, Tournier, & Zaratiegui, 2014). To insert the target DNA sequence into pJB166, we used a natural gap repair process in *S. pombe* or Gibson assembly to create a modified pJB166 closed vector for gRNA expression in transformed *S. pombe* cells (Gibson et al., 2009; Kostrub et al., 1998). To make use of gap repair, a circular plasmid, pJB166, is digested by a restriction enzyme, CspCI. PCR products containing annealing ends for the open plasmid and the Cas9 target sequence are then transformed into *S. pombe* cells. The yeast cell repairs the gaps between the open

vector and the annealing ends of the PCR product. To collect a high-quantity of plasmid for linearization, we used a midi-prep (Genopure Plasmid Midi Kit, Roche). We transformed the donor DNA and gRNA into a master strain, JB355, in which two fluoride channels, *fex1* and *fex2*, were deleted from FY527 (Fernandez & Berro, 2016). To genetically edit cells, we used the lithium acetate transformation method, using ~250-ng of gRNA-containing plasmid and ~1µg of donor DNA for homology-directed repair and grew transformed cells on YE5S + 1 mM NaF at 32C for 3-4 days (Moreno, Klar, & Nurse, 1991). After colonies appeared, 16 colonies were re-streaked and grown for another 2-3 days. Each of these colonies were screened for insertion of mEGFP, in the case of JB366, or for deletion of a SH3 domain, by size difference, compared to control, of a colony PCR product. Positive gene edited strains were grown in liquid culture for genomic DNA extraction by ethanol precipitation. The genetic region around their edition sites was amplified and the resultant PCR product was sequenced by the Yale School of Medicine Keck Biotechnology Resource Laboratory to ensure positive gene editing. Strains containing capping protein EGFP in WT backgrounds and in Shd1-SH3-1Δ, Shd1-SH3-2Δ, Abp1-SH3-1Δ, and Lsb1-SH3Δ backgrounds were created by Ronan Fernandez; all other strains used for this chapter were created by NGR.

6. Imaging

We used a spinning-disk confocal microscope to image *S. pombe* cells, making use of a TiE inverted microscope (Nikon) with a Yokogawa CSU-W1 spinning disk (50-µm pattern). We used an oil immersion, 100X, 1.45 numerical aperture objective (Plan Apo λ series, Nikon) with 1X tube lens magnification. We imaged GFP exclusively and used a 525/36-nm filter cube to pass emission light to an Andor iXon Ultra 888 EM-CCD camera with a 1024x1024 pixel field of view at 130-nm per pixel. To excite GFP tagged

molecules within cells, we used a triggered 488-nm laser with an approximate power of ~130-mW at the light source's optical fiber tip. Imaging was performed with 40% of the possible 488-nm laser power. We imaged cells with 50-ms 488-nm light exposure per z-slice, collecting 6 z-slices every 1s for 1 minute. Each z-stack had a z-spacing of 500-nm between consecutive z-slices; thus, we acquired 1 z-stack across 2.5-µm every 1s and used electron multiplying gain to collect signal, namely, 300 EM gain at 16 MHz, and 1.1 µs camera frame-transfer. We imaged the bottom half of *S. pombe* cells, i.e., the part of the cell closes to the objective and coverslip, collecting ~½ of a *S. pombe*'s fluorescence, which are typically 3-µm in diameter and roughly cylindrical, at an approximate z-resolution of 600-nm. We used a motorized xy piezo stage (using a National Instruments data acquisition device, NIDAQ) to cycle through z-positions during image acquisition and, to reduce photobleaching, during movement we used a shutter to prevent exposing the sample to 488-nm light. Images were acquired by utilizing NIS Elements software (Nikon) and using the ImageJ Bioformats plugin, 16-bit .nd2 image files were converted into single-precision floating-point format and copied as .tif images. To find fields of view to image cells, we used phase contrast with trans-illuminated light (Prior) and selected at least 6 independent fields of view, spaced at least 400-µm apart in any direction (~3 fields of view separating each acquired field of view to prevent reduction in quantification due to photobleaching) and randomized the imaging order each day to prevent bias. Each day, a control image (*acp1-mEGFP* cells, JB 366) was acquired to quantify the number of proteins in the patch, which is highly-reproducible (see sensitivity analyses in results section), and calibrate the number of electrons in our collected signal to previously reported value for the peak number of Acp1p assembled into an endocytic structure (Julien Berro & Thomas D. Pollard, 2014).

To image cells, cells were inoculated in YE5S 1d prior to imaging, grown overnight, and diluted to OD_{595} the morning of imaging and allowed to grow to $OD_{595} < 0.5$ before imaging. If any cells were past exponential growth (OD_{595} ~0.5), imaging was canceled in order to ensure that growth defects did not affect measurements. Once cells reached 0.2-0.5 OD_{595}, cells were spun down at 2350g and washed three times in minimal media (EMM5S), which contributes minimal amounts of background fluorescence during imaging.

To control our cells and their environment, we used a microfluidics perfusion system (CellASIC ONIX2 Microfluidic System, Millipore Sigma), which spatially stabilized our samples, provided them with oxygenation and fresh imaging media (EMM5S) throughout imaging, and provided optical stability for our samples. To load our cells into the Y04C plate imaging chamber, we flowed cells at 55-kPa into the imaging chamber and trapped them in a 3.5-μm ceiling area. During time-lapse imaging, liquid media (EMM5S) was flowed through the chamber at 10-kPa. To correct images for camera noise and uneven illumination, we immersed AlexaFluor 488-nm organic dye (ThermoFisher Scientific) in our imaging media and used the Y04C plate marker to select an appropriate height and took images with and without 488-nm laser light illumination for camera noise correction and flat-field correction, respectively. After imaging a flat field correction image, dye was washed from the chamber for 2 minutes at 30-kPa, after which, cells were loaded into the imaging chambers of the Y04C plate.

7. Image analysis

Time-lapse images were analyzed with ImageJ plug-ins and macros bundled into a custom toolset, “PatchTrackingTools,” which is freely available for download, with

documentation, at <https://campuspress.yale.edu/berrolab/publications/software/> (J. Berro & T. D. Pollard, 2014). Post-processing of images tracked using ImageJ plugins was performed with custom scripts in MATLAB and visualization and statistics of data was performed in R (authored by NGR). MATLAB scripts and compilation files for output from PatchTrackingTools, and scripts for data transfer, visualization, and statistics of these data are available at <https://git.yale.edu/ngr4> (source scripts authored by Julien Berro and modified for specific use by NGR). To control and calibrate each reported measurement, I calibrated the microscope each day by imaging JB 366, a control cell expressing capping protein EGFP, and scaled tracks from individual strains to preserve the relationship between the average of control images for each experimental condition and test samples.

Endocytic structure identification and tracking

To automatically track endocytic structures, which are spot-like objects, we used the ImageJ plugin, TrackMate (Tinevez et al., 2017). Image correction, tracking endocytic structures, and compiling data for quantification of tracked structures was performed in PatchTrackingTools (J. Berro & T. D. Pollard, 2014). Before identifying endocytic structures in imaged cells, time-lapse images were corrected for camera noise and uneven illumination and the z-slices were summed to project the 4D image to a 3D image, and the corrected and z-summed image was used to track endocytic structures (Lemière & Berroa, 2018). To identify endocytic structures, which appear as spot-like objects in our images when capping protein is tagged with GFP, we used a Laplacian of Gaussian detector, which applies a LoG to the image and finds maxima in Fourier space with size, $\sigma = 0.3\text{-}\mu m$, corresponding to the approximate size of endocytic structures in diffraction limited images given a numerical objective of 1.45 and 100X magnification

with diffraction limit is ~250-nm and expected vesicle diameter ~50-nm. We used a value of 100 for TrackMate's quality-threshold to retain high-quality tracks with minimal overlap between tracks. To track spots, a median filter was also applied to the image and we used sub-pixel localization. To track identified endocytic structures, we used the Linear Assignment Problem in a "simple" implementation that prevents track-splitting and merging but allowed us to define the spatial range for searching for the same spot in the next time-frame, linking only spots that are less than 0.5-μm in consecutive images after 1s, including only those spots that do not disappear for a single time-frame, and keeping tracks that have at least a minimum of 6 spots in consecutive time frames. To estimate the background using a donut, we used a donut of 1 pixel, .13-μm around a spot and rejected tracks that have 20% of spots that are bad, i.e., either too close to other spots or missing fluorescence. To ensure that high-quality tracks were automatically identified, we manually sorted through each track to confirm that the identified and tracked spot-like objects were isolated and plausible endocytic structures. The cytoplasmic background contribution to intensity was calculated using a median filter with a radius of 0.9-μm and subtracted from the endocytic structure's intensity (J. Berro & T. D. Pollard, 2014; Julien Berro & Thomas D. Pollard, 2014). Images were thresholded with the Moments threshold in ImageJ to identify ROIs whose intensity in time was used to fit a single exponential and estimate the photobleaching rate. This photobleaching rate was used, by division, to correct the intensity of each tracked endocytic structure in a given time-frame, thus correcting for photobleaching.

Aligning tracks of endocytic structures in time

To align tracks of an endocytic structure, in time, with other tracks from the same time-lapse image, we used a temporal super-resolution, continuous-alignment method

(J. Berro & T. D. Pollard, 2014). Briefly, a track of median total time is selected to as a reference. Other tracks are aligned to this reference track by minimizing the difference between the linear interpolations of a particular track with the reference track across 4s at 0.1-s intervals. This is akin to selecting the time offset, for each track, that minimizes the mean square difference between that track and a reference, i.e., minimizing $\frac{1}{N}\sum_{i=1}^{N}\left|f_{reference}(x_i) - f(x_i, t_{offset})\right|^2$ where *f* represents the number of molecules of a track at a particular x value, and $f(x_i, t_{offset})$ is a linear interpolation of a track shifted by a temporal offset, t_{offset}. Doing this for all tracks allows tracks to be aligned in time, despite sampling endocytosis at different times and stages of the process. To improve alignment, the continuous-alignment method is run iteratively, selecting an average track for the reference in iterations subsequent to the first. In this paper, we used 7 iterations of the continuous-alignment method to measure average behavior of endocytosis across multiple tracks. Aligned tracks from a single-day of imaging in samples containing Acp1p-mEGFP were used to calibrate intensity values, since we expect 152 molecules of Acp1p at the peak of recruitment in endocytic structures, as previously measured (Julien Berro & Thomas D. Pollard, 2014). A control strain was used (JB366) and test strains, containing a single SH3∆, were imaged and tracks from a single day were pooled such that endocytic structures, across 6-10 time-lapse images were tracked and pooled to measure endocytic behavior for each strain. A minimum of 5 tracks, corresponding to ~5% of tracks for the smallest strain sample, was used to create average curves comparing the number of molecules, patch mean absolute displacement, or assembly rate versus time.

Measuring the number of endocytic events in the cell

To estimate the number of endocytic events in the cell, globally and locally, we relied on the fact that the total fluorescence of the cell is the sum of the cytoplasmic intensity and the intensity from all endocytic events (J. Berro & T. D. Pollard, 2014). Thus, the total fluorescence intensity of all endocytic structures in the cell at any given time is equal to the number of endocytic events times the average fluorescent intensity of one patch, i.e., the total cell intensity is given by, $\sum_{i=1}^{N} I_i = I_{cytoplasm} + N_{endocytosis} * \langle I_{endocytosis} \rangle$, for *i* pixels and *N* pixels in a segmented cell. We measure the total fluorescent intensity of the entire cell by assuming that across 2.5-µm in z, we collect ½ the fluorescence of the cell in our time-lapse spinning-disk confocal microscopy images. We automatically segment cells using the watershed algorithm, applying it to a single time frame in a summed, z-projected, and camera noise and uneven illumination corrected image. We manually link regions in single cells that are over-segmented by watershed segmentation using a custom-made script in the Jupyter Notebook environment, "cellLength_endocyticRate_segmentation.ipynb," which is available through <https://git.yale.edu/ngr4> (authored by NGR). After segmenting all cells, we estimate the cytoplasmic fluorescence by taking a z-slice from the middle of the cell, eroding the segmented cell by 1.04-µm, and then taking the cytoplasmic fluorescence per pixel as the average of pixel intensity values between the 1st and 3rd quartiles. The fluorescent intensity of a patch over time is ergodic so the temporal average of the average endocytic event, measured from PatchTrackingTools and aligned with the continuous-alignment method, is equal to the average fluorescent intensity of all endocytic events in the cell at any given time (J. Berro & T. D. Pollard, 2014). The major-axis length and area of each cell is extracted from segmentation. These calculations can be implemented using a custom python script, "endocyticRate.py," available at <https://git.yale.edu/ngr4> (authored by NGR).

8. Mathematical modeling

We used a previously established kinetic model of actin assembly in endocytosis to identify which steps in the mechanism might be influenced by SH3-domain mediated interactions (Berro et al., 2010). As the basis for fitting our model, we varied each forward reaction rate across 2 orders of magnitude above and below parameters fitted from a previous study's measurements (Sirotkin et al., 2010). To vary the level of active WASp in the simulations, we varied a Gaussian amplitude across two orders of magnitude, using the Gaussian as a representation of the concentration of active WASp in the system. To compare the study's observations, we searched for deviations of the peak capping protein assembly to +/- ~50% of the simulated data for each parameter scan. We also used deviations in lifetime, taken as the full-width at half maximum (FWHM) of assembly, as a criteria to evaluate the consistency between simulation and observation. We used MATLAB's SimBiology package for these parameter scans. Code for the SimBiology project, including parameter scans, is available through "jb2010model_withSevering.sbproj" on <https://git.yale.edu/ngr4> (model project file authored by Julien Berro, parameter scans and other tasks for simulations authored by NGR).

III. Localization of endocytic proteins with and without their SH3 domains

A. Introduction

SH3 domains have oft been an object of study for synthetic biologists, especially to engineer specific protein-interaction sequences or to take advantage of the singular property of SH3 domains as modules of protein-interactions (W. A. Lim, 2002; B. Mayer & Saksela, 2005; Nguyen et al., 2000; Nguyen et al., 1998). Despite limited specificity of SH3 domain and peptide binding *in vitro*, SH3 domains must achieve interaction specificity *in vivo* in order to avoid overlap between cellular pathways and to avoid confounding signaling in the cell; indeed SH3 domain mediated interactions may diverge within a single organism, while overlapping between organisms (Kelil, Levy, & Michnick, 2016; Ali Zarrinpar, Park, & Lim, 2003). It is assumed that the role of SH3 domains in cellular pathways is to recruit proteins to an ensemble of other molecules or to bring its protein, which may have other functional domains, to a molecular complex and effect some biological activity (Pawson & Nash, 2003). However, it has not been tested whether SH3 domains play a predominant and exclusive recruitment and localization role in the cellular pathway of endocytosis.

It has long been appreciated that SH3 domains are involved in cytoskeleton signaling and remodeling. Notably, even viruses take advantage of this fact. For example, the *Vaccina virus* outer membrane protein is phosphorylated once it penetrates the cell and this phosphosite recruits and binds the SH2 domain of the Nck protein (non-catalytic region of tyrosine kinase), which also contains 3 SH3 domains that can recruit the WASp interacting protein (WIP), which, in turn, recruits WASp, activating the Arp2/3 complex to assemble branched actin networks, internalizing the virus in a hijacked endocytic viral entry pathway (Pawson & Nash, 2003). This begs the question, can scaffolded,

multivalent SH3 domains be used to internalize membrane and vesicles even at non-endocytic sites?

More significantly, the complexity in signaling involving SH3 domains can provide a deeper understanding of physiology and perhaps elucidate principles of molecular assembly. This claim stands for the following reasons. We can think of cells as a dynamic system with a variety molecular components that act as sensors and/or processors, such that the cellular system dynamically integrates a multitude of molecular circuits to respond to a, perhaps, continuous infinite set of context clues and proliferate according to an adaptable program (Good, Zalatan, & Lim, 2011; Wendell A. Lim, 2010). Focusing on the molecular components, we can further organize our thinking. The cell's molecular components have structural or functional modularity in the sense that molecules are composed of structural units that can independently fold or have unstructured segments (structural modularity) and biological molecules contain units with discrete, biological activities (functional modularity) (Bhattacharyya et al., 2006). These modular, molecular domains can broadly be classified into two groups: (1) catalytic elements and (2) regulatory or localization elements (Bhattacharyya et al., 2006; B. Mayer & Saksela, 2005). SH3 domains are thought to only possess regulatory and localization roles in the cell (Kay, 2012; Saksela & Permi, 2012). While it seems unlikely that SH3 domains possess catalytic functionalities, they may possess an emergent property of catalytic functionality (Case et al., 2019; Li et al., 2012). The understanding that dichotomizes molecular components into catalytic or regulatory domains and that conceptualizes a pathway's circuit into discrete sensing and processing activities may need to be discarded. If SH3 domains recruit and localize proteins to macromolecular assemblies in a way that leads to a higher-order catalytic property, then molecular components can sense and process, catalyze and regulate. And perhaps multivalent,

modular protein-interactions assemble molecules in such a way that facilitates dynamic molecular assembly and cellular response, elucidating a general principle of molecular assembly that can be utilized, to more success, for synthetic biology.

Substantiating this potentiality is the recently appreciated role of SH3 domains in forming phase-separated structures *in vivo* with catalytic and biological activity (S. Banjade & M. K. Rosen, 2014; Case et al., 2019). Multivalent SH3 domains can bind PRMs to aggregate and form liquid-liquid de-mixed structures *in vitro* and *in vivo* (Li et al., 2012). Within phase-separated structures created by multivalent SH3-domain mediated interactions, actin assembly and Arp2/3-mediated actin polymerization can be drastically increased, suggesting higher-order catalytic activity of SH3 domains (Sudeep Banjade & Michael K. Rosen, 2014; McCall et al., 2018). Multivalency of the modular protein-interaction domains seems to be more important than linker length, while linker length determines whether phase separated structures undergo gelation transitions (Harmon, Holehouse, Rosen, & Pappu, 2017). The question of whether multivalency needs to be within a macromolecular complex or within a single protein in order to induce higher-order structure formation remains un-answered. In particular, on what length scales can a multitude of localized SH3 domains be considered to be multivalent? Recent reports suggest that even single SH3 domains can induce phase-separations when the single SH3 domain interacts with disordered regions in partner ligands (Amaya, Ryan, & Fawzi, 2018). My own results showed that single SH3 domains can have diverse influences on actin assembly *in vivo* and, while remaining agnostic on the question of whether SH3 domains induce phase-separation during endocytosis with catalytic activity for molecular assembly, I showed that the complexity of competitive SH3 domain-mediated interactions may yield a kinetic program that influences

assembly, adding yet another higher-order effective catalytic role to SH3 domains' pedigree.

This mixture of functionalities attributed to SH3 domains muddles the clean framework of understanding cells as dynamic systems of integrated molecular circuits composed of regulatory or functional modules, suggesting that we need to deepen our understanding of SH3 domains, if only to resolve this confounding picture and perhaps to elucidate a principle of biological molecular assembly. It seems plausible that SH3 domains possess a higher-order, emergent role in influencing actin assembly, broadly and during endocytosis. Yet, how they localize actin-associated proteins and their own protein to macromolecular complexes *in vivo* is important because it may reveal how they simultaneously possess localization and catalytic functionality in cellular pathways. As such, I sought to more deeply study protein localization to endocytic structures by SH3 domains *in vivo*. In particular, I sought to study whether SH3 domains are required to localize their protein to endocytic structures and to determine if recent insights regarding molecular assembly and multivalency could be hacked to assemble molecules at non-native sites in the cell. Ultimately, in the latter approach, I sought to unify recent observations in cell biology with applications in synthetic biology and to demonstrate that, in principle, we can predictably manipulate endocytosis by synthetic design of SH3 domain scaffolds and, in so doing, regulate membrane receptor turnover or increase the propensity of cellular entry and drug delivery in cells with engineered pathways.

There are many avenues and descriptors that can be added to the list of roles of SH3 domains in endocytosis. To develop a simple footing for future studies, in collaboration with Ronan Fernandez, I began by comprehensively deleting single-copies of SH3 domains and tagging SH3-domain containing proteins are tagged with a GFP reporter. This allowed me to comprehensively describe the localization of SH3-domain

containing proteins with and without their SH3 domain. I show that for most endocytic, SH3 domain containing proteins, the SH3 domain influences localization of the SH3-domain containing protein to endocytic structures. Building off these studies, I sought to test if endocytic proteins can be assembled at non-endocytic sites by fusing multiple SH3 domains together and attaching the multi-valent SH3 ensemble to a membrane scaffold. Colocalization experiments combined with quantification of depleted molecular resources at endocytic sites suggests that multivalent SH3 domains can be fused to a scaffold to aberrantly recruit endocytic proteins to non-endocytic structures in the cell. These results collectively suggest that SH3 domains can be used to manipulate molecular assembly within the cell. Future studies will need to resolve whether endocytic proteins assembled at non-endocytic scaffolds in the cell promote actin assembly and internalization. In any case, these results support the nuanced view that SH3 domains possess both regulatory and higher-order catalytic functions, integrating localization and biological activity, and that they may yet be useful in engineering synthetic molecular circuits.

B. Results

1. *The endocytic localization dependence and influence of SH3 domains on their native protein's endocytic assembly dynamics*

Comparing endocytosis in cells with and without single SH3 domains reveals that SH3 domains have diverse influences on actin assembly and endocytosis. However, these studies do not indicate whether SH3 domains in endocytosis are responsible for recruiting other proteins, localizing their own protein or both. Seeking a comprehensive

description of SH3 domains in endocytosis to complement the revelation that a competitive sequalae of interactions and/or induction of phase-separation influences actin assembly, in collaboration with Ronan Fernandez, we created a library where a GFP reporter was fused to endocytic SH3 domain containing proteins in strains with and without single-copies of each endocytic protein's SH3 domains. This library comprises 24 strains, 14 strains with single-copy deletions of each SH3 domain within an endocytic protein and 10 control strains with GFP fused to the endocytic SH3 domain containing protein.

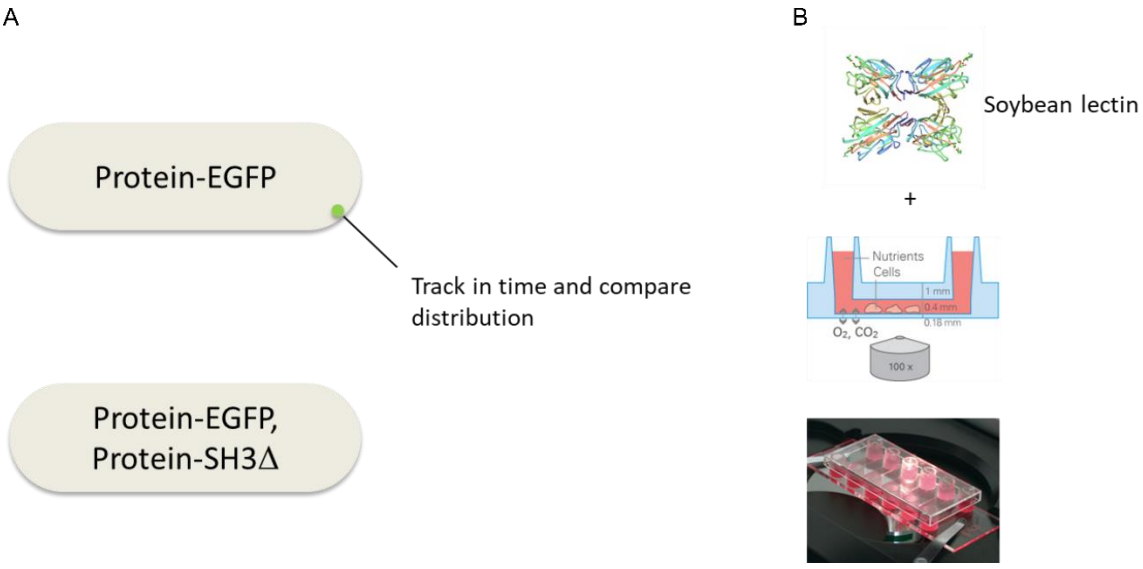

Figure 22. Approach to study the endocytic localization dependence and influence of SH3 domains on their native protein's endocytic assembly dynamics. (A) An initial library of strains is constructed in which all SH3-domain containing proteins involved in endocytosis are N- or C-terminally fused with EGFP. Then, in these strains, an additional library is made by deleting single-copies of each SH3 domain such that 14 additional strains contain a native protein tagged with EGFP and at least one SH3 domain deletion. (B) To provide optical stability and nutrition during image acquisition, cells are loaded into ibidi microfluidic chambers and coated for 30 minutes with 1:1 solution of ddH_20:soybean lectin from *Glycine max*. Cells are imaged with an inverted, spinning disk confocal microscope system. Bottom two schematics are from the microfluidic chamber manufacturer's website, animalab.eu/partners/ibidi.

To measure the influence of each SH3 domain on its protein's endocytic localization and assembly dynamics, first I created a library of EGFP fusions to SH3-domain containing proteins involved in endocytosis (**Figure 22**). Then, from these strains, I deleted single-copies of each endocytic SH3 domains. Rather than relying on a microfluidic perfusion system with costly imaging conditions, I relied on ibidi microfluidic chambers which provide excellent optical stability and nutrition during live cell imaging. Given that endocytic patches from diffraction limited puncta in fluorescent images, of ~0.3-μm diameter, I expected that labeling single proteins would provide adequate information to distinguish between the propensity to form puncta or diffuse in the cytoplasm. By comparing each SH3 domain deletion strain to a control, I was able to determine whether deleting the SH3 domain reduces the propensity of the native protein to form puncta and to determine whether SH3 domain deletion reduces cellular expression of the SH3-domain containing protein. I sought to measure both localization and expression for each SH3 domain deletion protein to assess its SH3 domains' influence on expression and localization.

2. *Most endocytic SH3 domains are required for robust localization of their protein to endocytic structures in vivo*

I previously showed that deletion of the myosin I SH3 domain reduces the localization of myosin I to endocytic puncta in the cell (data available in previous version). Myosin I, N-terminally fused with EGFP, is assembled into ~10 endocytic events per half-cell at any given time. When its SH3 domain is deleted, most myosin I is diffuse in the cytoplasm. Myosin-I SH3Δ is associated with decreased expression for cells of a given length ($p < 0.01$, data available in previous version) but the effect size is small (~10% reduction in expression). Some myosin I puncta (~2-5 per cell) appear to

form but the copy number in myosin I SH3 deletion cells is not comparable to control, supporting that myosin I's robust localization to endocytic structures requires its SH3 domain.

Cdc15p contributes to contractile ring assembly and cytokinesis by localizing to the contractile ring and recruiting cytoskeleton proteins but, during interphase, Cdc15p interacts with Myo1p during endocytosis at the base of nascent endocytic invaginated pits (Rajesh Arasada, Wasim A. Sayyad, Julien Berro, & Thomas D. Pollard, 2018; Willet et al., 2015). To determine whether its SH3 domain is important for localization, I tagged Cdc15p with GFP and deleted its SH3 domain (**Figure 23**). Cells in interphase with EGFP fused to Cdc15 appear to have slightly shorter lengths than typical *S. pombe* cells. Many cells also appear to have contractile rings. Regardless, in interphase, ~0.5-µm puncta form, suggesting that Cdc15p localizes to endocytic patches. When Cdc15p's SH3 domain is deleted, no puncta in cells without a contractile ring. There is slightly increased contrast near the tips of growing cells. Thus, robust localization of Cdc15p depends on its SH3 domain. The cellular expression of Cdc15p, however, does not depend on its SH3 domain ($p > 0.05$). Thus, deleting the Cdc15p SH3 domain alters its localization but not expression.

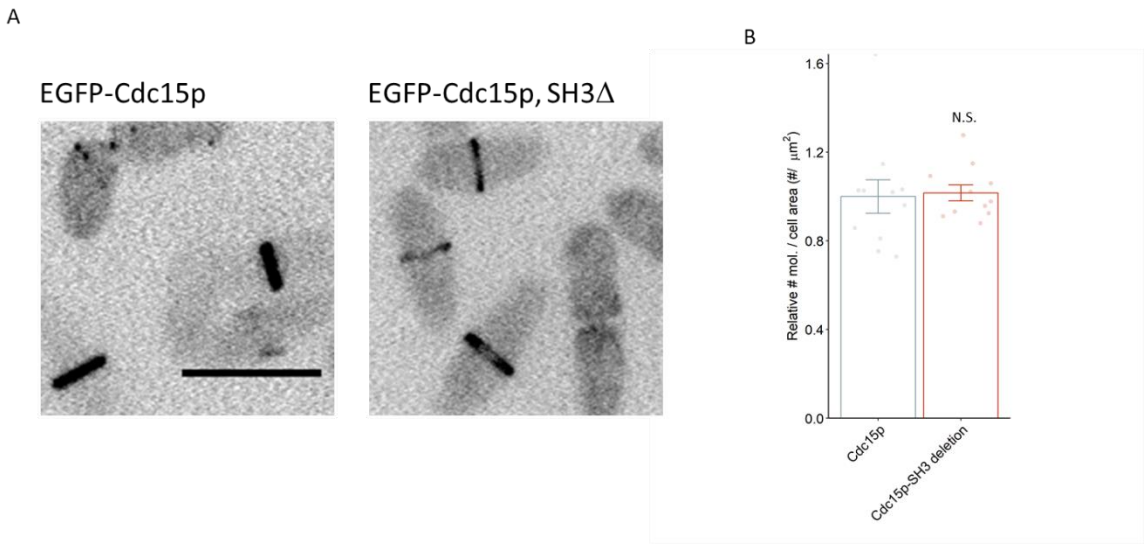

Figure 23. Robust localization of Cdc15p depends on its SH3 domain but its expression and localization to the cytokinetic ring is not affected by SH3 domain deletion. (A) Summed z-projections of spinning disk confocal fluorescence microscopy images of cells expressing EGFP-Cdc15p with and without the Cdc15p SH3 domain. Scale bar 10-µm. (B) Cells are automatically segmented and their fluorescence is converted to number of molecules based on calibration to capping protein EGFP. The number of molecules is adjusted for the segmented cell area and then compared to control (number of molecules per cell area, relative to control). Bar height shows average and error bars represent 95% CI. Welch's t-test assuming unequal variance, significance codes: N.S. = $p > 0.05$; . = $p \leq 0.05$; * = $p \leq 0.01$; ** = $p \leq 0.001$; *** = $p \leq 0.0001$.

During endocytosis, Bbc1p may regulate WASp and myosin I NPF activity by releasing Myo1p from interacting with Vrp1p and, in so doing, allow Wsp1p to bind Vrp1p and activate the Arp2/3 complex (Dawson, Legg, & Machesky, 2006; MacQuarrie et al., 2018). Bbc1p interacts with Myo1p through its SH3 domain. To determine if this interaction is important to Bbc1p's localization to endocytosis, I deleted Bbc1p's SH3 domains (**Figure 24**). During cell division, Bbc1p localizes to the contractile ring. Tagging Bbc1p C-terminally with EGFP appears to result in a shortened cell lengths. Endocytic spots appear less bright, in comparison to marking endocytic patches with other endocytic proteins. However, patches are visible at cell tips. When Bbc1p's SH3 domain is deleted, localization to puncta is lost and no patches are discernible. Bbc1p is still expressed without its SH3 domain but, relative to control, there is a ~20% decrease in Bbc1p expression (Welch's t-test, $p < 0.0001$). This suggests that Bbc1p's SH3 domain localizes Bbc1p to endocytic structures and influences its expression level in the cell.

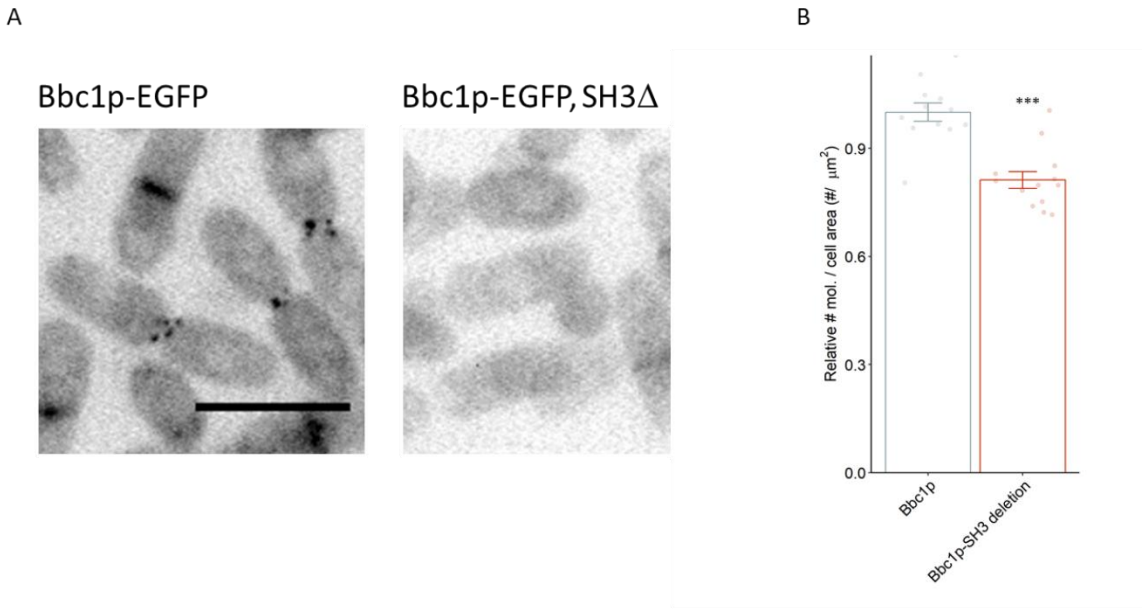

Figure 24. Bbc1p's SH3 domain influences its expression and localization to endocytic patches. (A) Summed z-projections of spinning disk confocal fluorescence microscopy images of cells expressing Bbc1p-EGFP with and without the Bbc1p SH3 domain. Scale bar 10-μm. (B) Cells are automatically segmented and their fluorescence is converted to number of molecules based on fluorescence calibration to capping protein EGFP. The number of molecules is adjusted for the segmented cell area and then compared to control. Bar height shows average and error bars represent 95% CI. Welch's t-test assuming unequal variance, significance codes: N.S. = $p > 0.05$; . = $p \leq 0.05$; * = $p \leq 0.01$; ** = $p \leq 0.001$; *** = $p \leq 0.0001$.

Lsb1p is not a well characterized endocytic protein but *in vitro*, it inhibits WASp-mediated actin polymerization and in *S. cerevisiae*, it forms puncta that co-localize with endocytic proteins and its over-expression causes internalization defects (Ali et al., 2014; Spiess et al., 2013). To tease out its role in endocytosis further, I fused Lsb1p to EGFP in *S. pombe* (Figure 25). Lsb1p localizes in a few puncta but may also aggregate in the cytoplasm. However, in these localization experiments, I have not performed extensive control experiments to determine whether tagging the native protein with a fluorescent protein alters the proteins' expression or behavior. Lsb1p has been C-terminally fused with fluorescent proteins *in vivo* before, with no reported defect, but to my knowledge, these controls have not been performed in *S. pombe* (Spiess et al., 2013). Barring these complications, deleting Lsb1p's SH3 domain does not entirely abrogate Lsb1p localization to puncta but the number of spherical, ~0.5-µm puncta per cell is reduced. Lsb1p SH3 domain deletion alters the distribution of Lsb1p in the cell, showing aggregation with increased penetrance relative to control. However, the Lsb1p SH3 domain is dispensable for Lsb1p expression in the cell (Welch's t-test, $p > 0.05$). This may suggest that Lsbp1p's SH3 domain influences its localization and distribution in the cell but does not influence Lsbp1p expression; however, the unknown effect of tagging Lsb1p with a reporter confounds any interpretation.

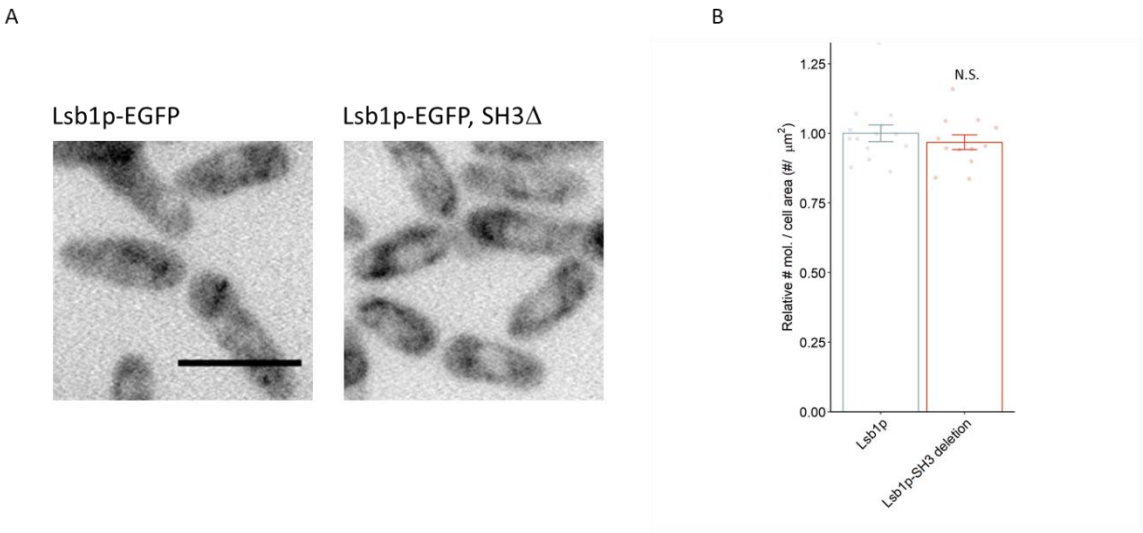

Figure 25. Lsb1p's SH3 domain influences its distribution in the cell without altering expression but its assembly into endocytosis is difficult to robustly track. (A) Summed z-projections of spinning disk confocal fluorescence microscopy images of cells expressing Lsb1p-EGFP with and without the Lsb1p SH3 domain. Scale bar 10-μm. (B) Cells are automatically segmented and their fluorescence is converted to number of molecules based on fluorescence calibration to capping protein EGFP. The number of molecules is adjusted for the segmented cell area and then compared to control. Bar height shows average and error bars represent 95% CI. Welch's t-test assuming unequal variance, significance codes: N.S. = $p > 0.05$; . = $p \leq 0.05$; * = $p \leq 0.01$; ** = $p \leq 0.001$; *** = $p \leq 0.0001$.

Bzz1p is an actin regulator and may stimulate Arp2/3 activity by binding WASp but it may also stabilize the invaginated pit's geometry and promote scission with other BAR proteins (Burston et al., 2009; Kishimoto et al., 2011b; Merrifield & Kaksonen, 2014). It has two SH3 domains. To determine the role of these SH3 domains on influencing the localization of Bzz1p, I deleted each SH3 domain in cells where Bzz1p was tagged with EGFP (**Figure 26**). Bzz1p localizes to endocytic structures, forming puncta at the cell periphery and tips during interphase. During cytokinesis, Bzz1p seems to primarily localize to the contractile ring. Without Bzz1p's first SH3 domain (most N-terminal), its localization to ~0.5-µm puncta is lost, showing no discernible puncta but only diffuse fluorescence in the cytoplasm. Similarly, when Bzz1p's second SH3 domain is deleted (most C-terminal), no puncta are visible and Bzz1p fluorescence is diffuse in the cytoplasm. For a given cell length, Bzz1p expression is reduced by 10-20% when deleting single-copies of the Bzz1p SH3 domain. This suggests that each of Bzz1p's SH3 domains influence Bzz1p's localization to endocytic structures and influence its expression in the cell.

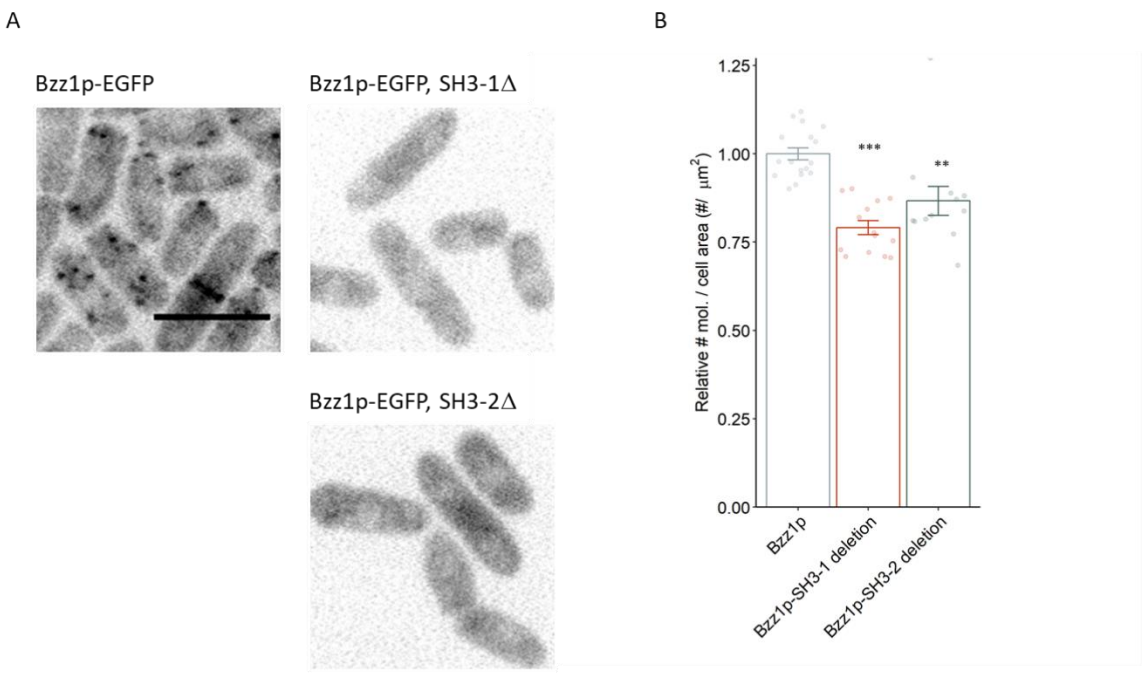

Figure 26. Both of Bzz1p's SH3 domains individually influence Bzz1p's localization to endocytic patches and both domains reduce Bzz1p expression when singly deleted. (A) Summed z-projections of spinning disk confocal fluorescence microscopy images of cells expressing Bzz1p-EGFP with both Bzz1p SH3 domains (top, left), without the most N-terminal Bzz1p SH3 domain (top, right), and without the most C-terminal Bzz1p SH3 domain (bottom, right). Scale bar 10-μm. (B) Cells are automatically segmented and their fluorescence is converted to number of molecules based on fluorescence calibration to capping protein EGFP. The number of molecules is adjusted for the segmented cell area and then compared to control. Bar height shows average and error bars represent 95% CI. Welch's t-test assuming unequal variance, significance codes: N.S. = $p > 0.05$; . = $p \leq 0.05$; * = $p \leq 0.01$; ** = $p \leq 0.001$; *** = $p \leq 0.0001$.

In *S. cerevisiae*, Abp1 localization to endocytic structures depend on its SH3 domain (Soheil Aghamohammadzadeh, Smaczynska-de Rooij, & Ayscough, 2014; Fazi et al., 2002). Thus, likely the Abp1p, Bbc1p, both Bzz1p, Cdc15p, Lsb1p, and Myo1p SH3 domains are required for robust localization of their protein to endocytic structures. This suggests that in endocytosis, most SH3 domains are responsible for at least localizing their own protein to endocytic structures. How they coordinate their recruitment timing remains unclear. The deletion of SH3 domains does not entirely abrogate the expression of SH3 domain-containing proteins in the cell. But, the deletion of SH3 domains can significantly alter expression of SH3 domain-containing proteins in some contexts. Regardless, expression is not reduced by more than ~30% across the library of single-copy SH3 domain deletions. This suggests that while SH3 domains are important for their protein's distribution in the cell, they may not be necessary for its other cellular roles.

3. *In contrast to other endocytic SH3 domain-containing proteins, the SH3 domains of the most multivalent SH3-domain containing protein in S. pombe, Shd1p, are dispensable for Shd1p localization to endocytic structures and expression*

Shd1p, or the SH3 homology domain protein, has the three SH3 domains, making it the most multivalent protein in *S. pombe* (**Figure 27**). It also has two Sla1p homolog domains, which adopt a structure similar to SH3 domains, enticing the supposition that this adaptor protein has as many as 5 modular protein-interaction domains and concentration NPFs within endocytic structures to trigger actin-assembly in a 'switch-like' manner (**Figure 27**) (Mahadev et al., 2007; Sun et al., 2017). With such a high number of SH3 domains, I sought to determine how each affects the localization, expression, and assembly dynamics of Shd1p. In contrast to most other endocytic, domain-

containing proteins, no single, individual SH3 domain is required for robust localization of Shd1p to endocytic structures. When Shd1p is tagged with EGFP, strains with single-copy deletions of its SH3 domains show approximately the same number and size of puncta in the cells, most ~0.5-μm puncta concentrating at the cell tips.

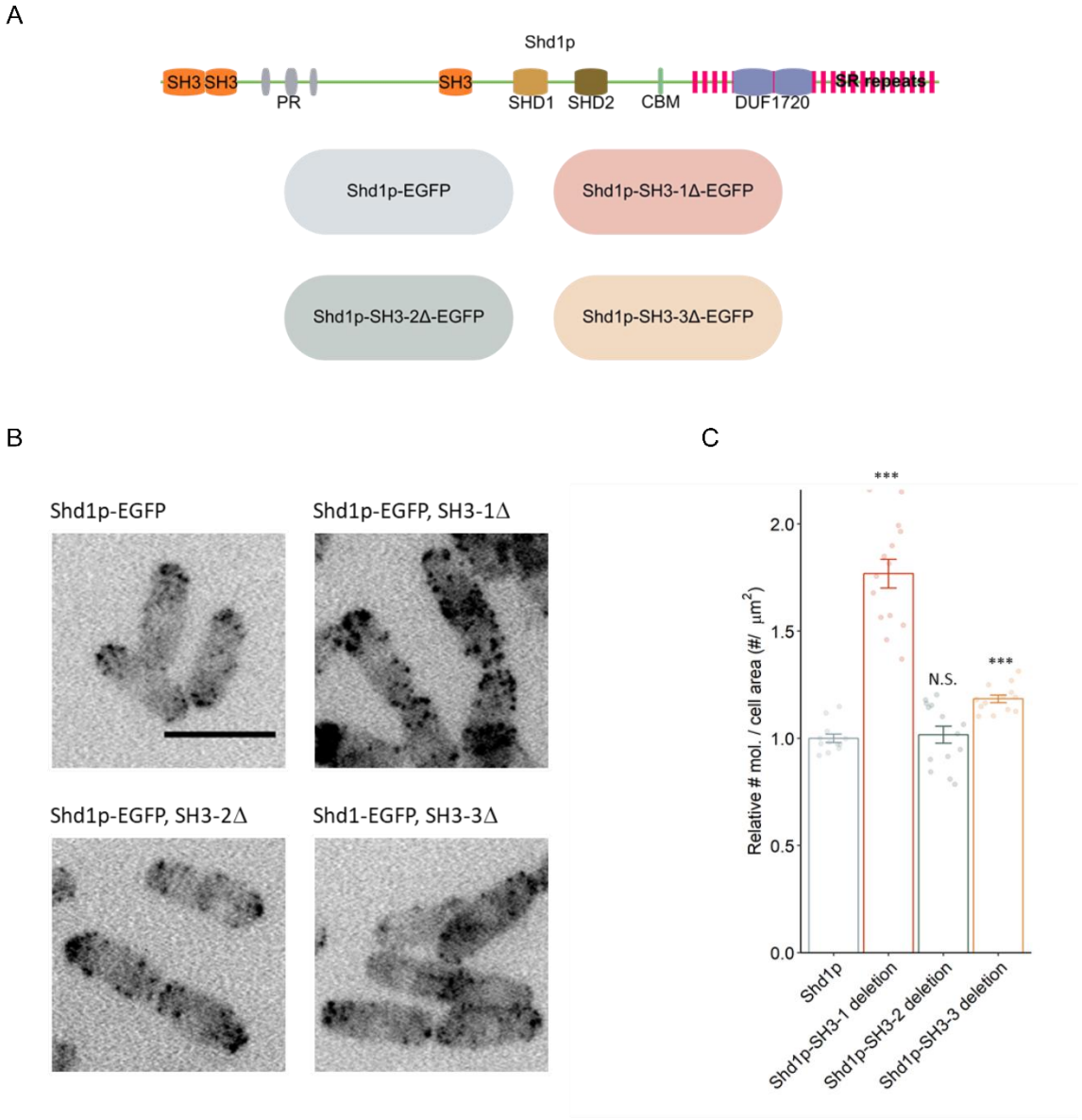

Figure 27. In contrast to most other proteins, single-copy SH3 deletions do not mis-localize the most multivalent SH3-domain containing protein, Shd1p, to endocytic structures within the cell, though SH3 deletions increase Shd1p expression. (A) Shd1p has the highest number of SH3 domains, relative to other *S. pombe* SH3-domain containing proteins. Domain diagram and over-view of experimental approach to study each Shd1p SH3 domain's influence on the endocytic assembly and dynamics of Shd1p. PR = proline-rich region; SHD1/2 = Sla1 homology-like domain 1/2; CBM = clathrin binding motif; DUF1720 = domain of unknown function; SR repeats = unstructured serine-arginine repeats. (B) Summed z-projections of spinning disk confocal fluorescence microscopy images of cells expressing Shd1p-EGFP with all Shd1p SH3 domains (top, left), without the most N-terminal Shd1p SH3 domain (top, right), without the second most N-terminal

Shd1p SH3 domain (bottom, left), and without the most C-terminal Shd1p SH3 domain (bottom, right). Scale bar 10-μm. (C) Cells are automatically segmented and their fluorescence is converted to number of molecules based on fluorescence calibration to capping protein EGFP. The number of molecules is adjusted for the segmented cell area and then compared to control. Bar height shows average and error bars represent 95% CI. Welch's t-test assuming unequal variance, significance codes: N.S. = $p > 0.05$; . = $p \leq 0.05$; * = $p \leq 0.01$; ** = $p \leq 0.001$; *** = $p \leq 0.0001$.

Most SH3 domains within endocytic, SH3 domain-containing puncta either do not influence or slightly decrease expression of their protein in the cell. In contrast, removing the SH3 domains of Shd1p increases the expression of Shd1p (**Figure 27B**). In particular, when the first Shd1p SH3 domain (most N-terminal) is removed, ~60% more Shd1p is expressed in the cell (Welch's t-test, $p < 0.0001$). The second SH3 domain is dispensable for WT expression levels of Shd1p and deletion of the third SH3 domain (most C-terminal) increases expression of Shd1p expression by ~15% in the cell. The effects of the Shd1p SH3 domains on their protein differ from the rest of the endocytic SH3 domain group influences on their protein's localization and expression. Though the reasons for this are still elusive, this suggests that, in contrast to most other proteins, the Shd1p SH3 domains do not influence Shd1p localization to endocytic structures in the cell but they are important for its function and cellular expression.

4. *Tracking endocytic SH3 domain proteins that have not been characterized reveals that each Shd1p SH3 domain influences the assembly dynamics, timing, and lifetime of Shd1p assembly into endocytic structures*

Some endocytic proteins are difficult to track as assemblies within endocytic structures, given their low expression in cells and low accumulation in endocytic structures, relative to highly assembled endocytic proteins such as fimbrin, capping protein, and myosin I (**Figure 23** - **Figure 26**). Patch tracking and quantitative microscopy can be usefully applied to my strain library because the assembly and dynamics of some SH3 domain-containing proteins have never been quantified in endocytosis (Bbc1p, Hob1p, Lsb1p, Lsb4p, Mug137p) and the influence of each SH3 domain on their protein's assembly dynamics has not been quantified for any endocytic, SH3 domain-containing protein. Yet, given the complexity of interactions mediated by

SH3 domains in endocytosis, and the demonstrate that their presence can have diverse influences on actin assembly and endocytosis, the question remains open as to how SH3 domains alter their protein's assembly dynamics, which may elucidate how SH3 domains' influence on endocytosis propagates to actin assembly defects.

Shd1p single-copy SH3 domain deletion strains, where Shd1p is tagged with EGFP, are amenable to patch tracking and quantitative microscopy measurements while SH3 domain deletions in other proteins reduce their localization to endocytic structures, making their dynamics difficult to characterize by quantitative imaging and tracking. The assembly dynamics of Shd1p's ortholog, Sla1p, in *S. cerevisiae* has been reported but the influence of its SH3 domains on Sla1p's endocytic assembly dynamics is unknown (Andrea Picco et al., 2015). To elucidate the assembly of Shd1p into endocytic structures in *S. pombe* and determine the influence of its SH3 domains on Shd1p assembly dynamics, I imaged, tracked, and quantified the assembly of Shd1p-EGFP in single-copy SH3 domain deletion backgrounds (**Figure 28**). When the first SH3 domain of Shd1p is deleted, Shd1p begins to appear in patches much earlier than Shd1p in control cells. Up to 35s before scission, Shd1p appears within endocytic structures while, with all its SH3 domains, Shd1p is assembled ~20s before scission. This suggests that Shd1p's first Sh3 domain may inhibit its other SH3 domains from interacting with an earlier coat protein such as Syp1p or Ede1p or facilitate autoinhibition. Nonetheless, once Shd1p appears, its accumulation in endocytic structures increases such that by the peak of assembly, 3-4s before scission, significantly more Shd1p is assembled in cells without its first SH3 domains than in control cells (non-overlapping confidence intervals). By the peak of assembly, ~30% more Shd1p molecules are assembled into endocytic structures, even though deletion of the other two Shd1p SH3 domains does not influence

the maximum number of Shd1p molecules assembled into endocytic structures ($p < 0.0001$, Shd1p SH3-1 deletion, $p > 0.01$, others).

However, the other two SH3 domains alter the recruitment timing of Shd1p. When the second SH3 domain is deleted, Shd1p is assembled far in advance of scission, relative to control and similar to Shd1p SH3-1 deletion cells. However, unlike Shd1p SH3-1 deletion cells, the assembly rate is slower such that the maximal number of Shd1p molecules in the patch matches control cells. In contrast to leading to earlier recruitment when Shd1p's first two SH3 domains are deleted, when Shd1p's third SH3 domain is deleted, Shd1p is recruited to endocytic structures slightly before control cells (~3-4s closer to scission, relative to control). Despite these differences, the second and third SH3 domains do not influence the time at which Shd1p is removed from the patch since Shd1p adaptor protein is removed from the nascent vesicle shortly after scission. Perhaps due to the over-assembly of Shd1p when its first SH3 domain is deleted, Shd1p remains on nascent vesicles ~4-5s after scission in Shd1p SH3-1 deletion cells. Using the FWHM of the number of molecules versus time curves as an indicator for assembly, disassembly, and net endocytic lifetime supports that each of Shd1p's SH3 domains alters the recruitment and lifetime of Shd1p molecules in the endocytic patch, suggesting that they do in fact influence Shd1p localization. In particular, Shd1p SH3-1 deletion cells assembly for longer than control cells but disassemble faster, resulting in slightly lengthened overall endocytic lifetimes. Shd1p SH3-2 deletion cells assemble for even longer than Shd1p SH3-1 deletion cells and disassembly faster. In contrast to the first two SH3 domains, Shd1p SH3-3 cells exhibit faster Shd1p molecular assembly times and overall shortened endocytic lifetimes, relative to control. These results suggest that each Shd1p SH3 domain influences the localization, assembly dynamics, and lifetime of Shd1p molecules in endocytic structures.

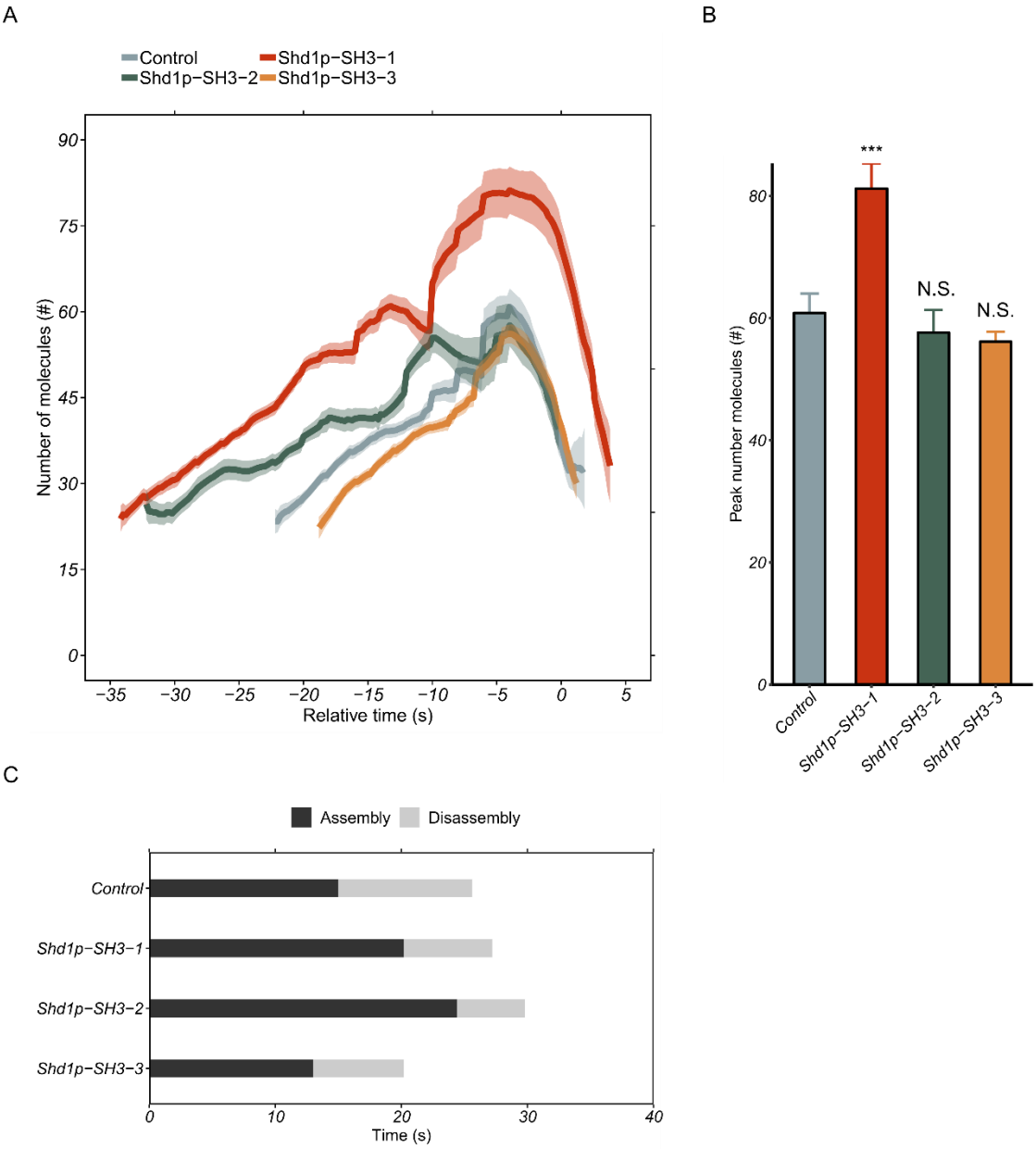

Figure 28. Only Shd1p's first SH3 domain influences the maximum number of Shd1p molecules assembled into endocytic structures but each Shd1p SH3 domain influences the assembly dynamics and lifetime of Shd1p in endocytosis. (A) Endocytic patches in cells with all Shd1p SH3 domains (control, N_{tracks} = 132), without the most N-terminal Shd1p SH3 domain (Shd1p-SH3-1, N_{tracks} = 137), without the second most N-terminal Shd1p SH3 domain (Shd1p-SH3-2, N_{tracks} = 50), and without the most C-terminal Shd1p SH3 domain (Shd1p-SH3-3, N_{tracks} = 155) are labeled with Shd1p-EGFP and tracked for imaging and analysis by quantitative microscopy. The number of Shd1p molecules assembled into endocytic structures is measured, in time relative to scission at t=0s, based off orthologous Shd1p measurements in *S. cerevisiae* (see methods).

Solid lines show average endocytic measurements and ribbon represents 95% CI. (B) The maximum number of Shd1p molecules endocytic structure is compared for each single-copy Shd1p SH3 domain deletion strain, relative to control by Welch's t-test, significance codes: N.S. = $p > 0.05$; . = $p \leq 0.05$; * = $p \leq 0.01$; ** = $p \leq 0.001$; *** = $p \leq 0.0001$. Bar height represents average and error bars represent 95% CI. Note: peak Shd1p molecular assembly occurs prior to scission. (C) Full-width time at half-maximum of Shd1p assembly (FWHM) for each single-copy Shd1p SH3 domain deletion strain. Assembly time represents the first passage time at Shd1p's assembly HM to the time at maximum assembly; disassembly time represents the maximum assembly time to second passage time at HM. Overall FWHM lifetime is represented by the sum of assembly and disassembly time. Bar height represents average across all tracks.

Given that the assembly of Shd1p differs so much when its SH3 domains are perturbed, I sought to determine whether the differences in adaptor protein assembly affected the motility of the patch, often thought to be strongly influenced by branched actin network assembly (**Figure 29**). The assembly rate of Shd1p fluctuates considerably amongst aligned tracks, leaving to fluctuating net assembly rates prior to scission across all Shd1p SH3 domain deletion strains. In any case, the maximum assembly rate of Shd1p molecules is comparable across single-copy Shd1p SH3 domain deletion cells, suggesting a weak influence of the SH3 domains on the maximum rate at which Shd1p molecules can be assembled into endocytic structures. The maximum disassembly rate is comparable for second and third SH3 domain deletions, relative to control, consistent with their dispensability in maximal assembly of Shd1p molecules. The increased disassembly rate of Shd1p SH3-1 cells may result from its over-assembly throughout endocytosis, relative to control. Thus, SH3 domains do not strikingly alter the assembly rate dynamics of Shd1p molecules, despite exhibiting altered Shd1p assembly. Throughout assembly of Shd1p molecules, regardless of whether or not single SH3 domains are deleted, the endocytic structure moves slowly. Deleting Shd1p's third SH3 domain seems to exhibit slightly increased motility prior to scission, which may indicate disruption to the actin network. Prior to scission, as the actin network is assembled, in all single-copy Shd1p SH3 domain deletion strains, there is a burst of motility, consistent with endocytic structures in other cells. This burst of motility typically occurs just before scission but in Shd1p SH3-1 cells, the burst of motility occurs just as scission is occurring. Since the point of scission is enforced and based off previous measurements, assuming that the perturbations do not affect the association between motility and scission, this may indicate that scission occurs later in Shd1p SH3-1 cells. Despite these slight differences in motility at different endocytic stages, around scission, the cumulative path length of endocytic structures overlaps with control cells

and after scission, the nascent vesicle moves around to comparable extents, suggesting that Shd1p SH3 domains do not considerable influence the motility of endocytic patches within the cell.

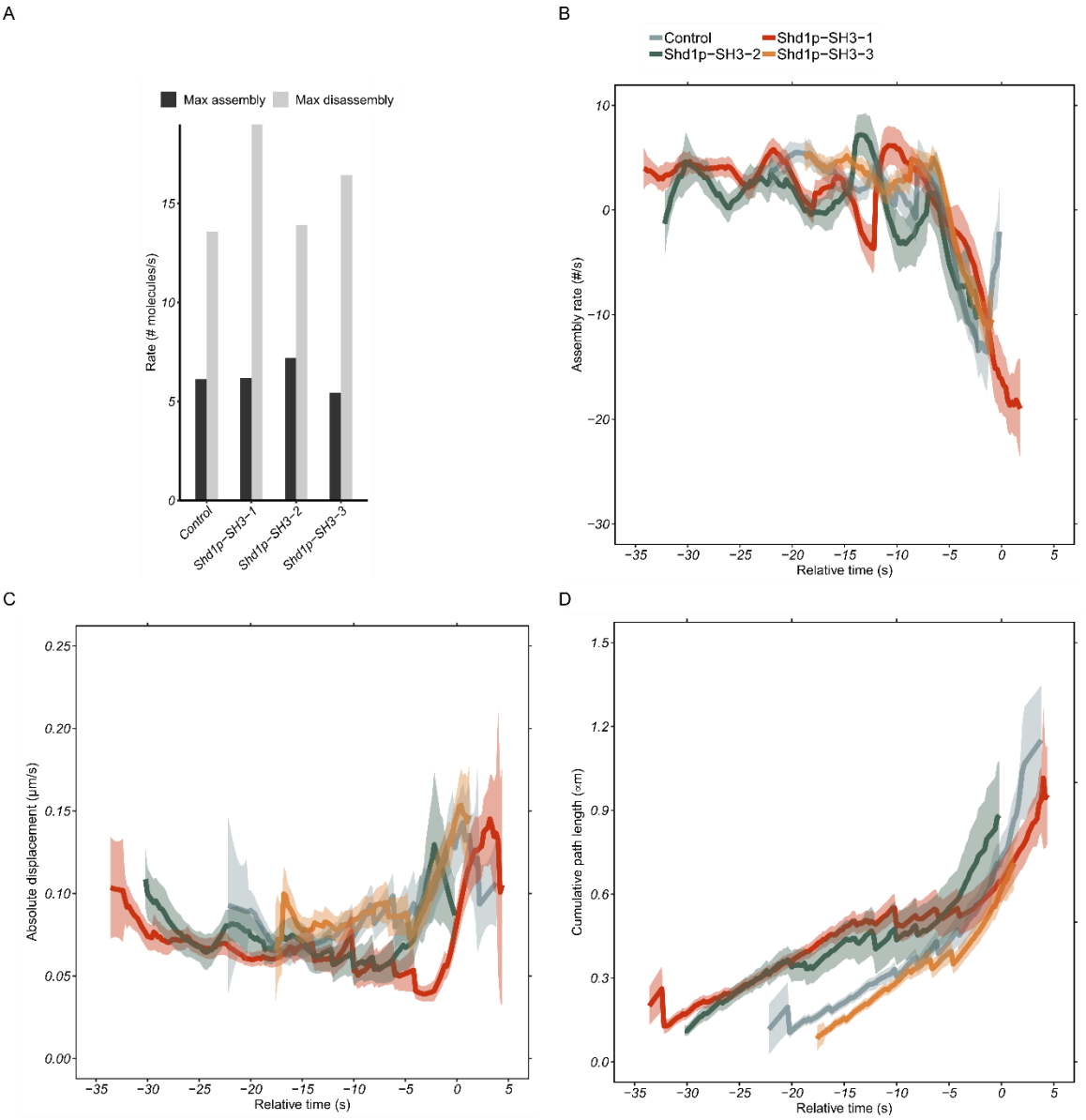

Figure 29. Single-copy Shd1p SH3 domain deletions exhibit similar patch motilities and molecular assembly rates but Shd1p SH3 domains influence the time at which Shd1p is assembled into endocytic structures. (A) Endocytic patches in cells with all Shd1p SH3 domains (control, N_{tracks} = 132), without the most N-terminal Shd1p SH3 domain (Shd1p-SH3-1, N_{tracks} = 137), without the second most N-terminal Shd1p SH3 domain (Shd1p-SH3-2, N_{tracks} = 50), and without the most C-terminal Shd1p SH3 domain (Shd1p-SH3-3, N_{tracks} = 155) are labeled with Shd1p-EGFP and tracked for imaging and analysis by quantitative microscopy. The maximum Shd1p instantaneous molecular assembly and disassembly rate achieved in each strain (gray, black, respectively). The time at which the maximum and minimum differs amongst strains. Bar height shows average across all tracks. (B-D) Solid lines show average endocytic measurements and ribbon

represents 95% CI. (B) Net Shd1p molecular assembly rate in time, relative to scission at t=0s, based off orthologous Shd1p measurements in *S. cerevisiae* (see methods). (C) The absolute displacement in 1s of tracked endocytic patches for each strain in time. (D) The cumulative path length traveled by tracked endocytic structures at the indicated time.

5. *Modeling suggests that the number of valent sites on a synthetically engineered, in vivo scaffold and the scaffolded SH3 domain's preference for particular PRMs may lead to drastically different recruitment amongst endocytic proteins*

To determine how increasing the number of valent sites, tethered to the membrane, might affect the quantities of endocytic proteins recruited to the non-endocytic membrane scaffold, I modeled how a single SH3 domain might recruit 3 different endocytic proteins, each with multiple SH3 domain-interacting motifs (PRMs = proline-rich motifs), across a range of apparent affinities, modeled as an interaction between a SH3 domain and an endocytic protein, with different specificities for each interaction (**Figure 30**). These results show that even for moderate affinity (100-μM) for each endocytic protein, a single, membrane-scaffolded SH3 domain can recruit 10-40% of the maximum number of molecules of Pan1p, WASp, and Vrp1p recruited to endocytic patches ($\alpha = 1$). If the SH3 domain exhibits 5-fold increase in affinity for these endocytic proteins relative to all others containing PRMs, then scaffolded SH3 domains can recruit between 50%-200% of the endocytic protein to non-endocytic sites. Given that there are ~10,000 Pan1p, Vrp1p, or WASp molecules in the average yeast cell (on the order of 10 times the peak assembly of each endocytic protein in endocytosis), SH3 domain membrane scaffolds may recruit significant quantities of PRM-containing, endocytic proteins (Carpy et al., 2014). In particular, assuming a simple model for multi-valency of additive affinity, this suggests that for 10-fold affinity preference, a 2x tandem repeated and scaffolded SH3 domain will deplete the cell of all Pan1p. If multi-valency works according to a multiplicative avidity, then a multivalent scaffold will quickly deplete even poorly expressing proteins, such as WASp, in the cell. These estimations suggest that specificity, affinity, and the mode of multi-valent binding may have significant influences on the quantities of endocytic proteins recruited to engineered scaffolds.

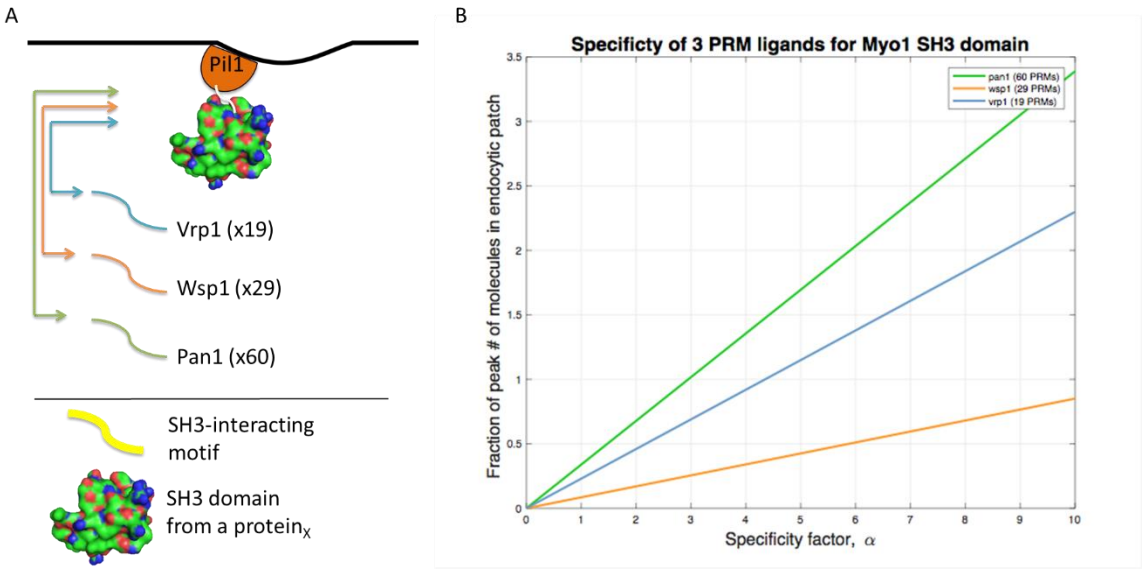

Figure 30. The number of valent sites on a hypothetical in vivo SH3 domain membrane-tethered scaffold and the scaffolded SH3 domain's preference for particular PRMs leads to different recruitment quantities amongst endocytic proteins. (A) An endocytic SH3 domain tethered do a non-endocytic, stable membrane structure, for example Pil1p, an eisosome component, may recruit a number of different endocytic proteins (Moreira et al., 2012; Walther et al., 2006). SH3 domains interact with PRMs (peptide sequence of PXXP) and the endocytic proteins Vrp1, Wsp1, and Pan1 have 19, 29, 60 PRMs within their protein, which could interact with a SH3 domain. (B) Given the cellular concentrations of endocytic proteins, across a range of effective affinities between the SH3 domain and each endocytic protein, enforced by defining a specificity factor for each interaction, the number of molecules recruited to non-endocytic sites is expressed as a fraction of the maximum number of molecules assembled at endocytic sites.

6. *Engineering tandem SH3 domain fusions to determine the connection between multi-valency and phase-separation*

If multi-valency simply increases the propensity to phase-separate, which indirectly increases actin assembly and (or) if multi-valency increases recruitment of actin assembly factors to endocytic patches, then tandem repeats of SH3 domains within endocytic proteins should lead to an increase in actin assembly during endocytosis. However, the opposite seems to be the case (**Figure 31**). Tandem fusion of the myosin I SH3 domain N-terminal to its native SH3 domain results in reduced assembly of capping protein in endocytosis, phenocopying myosin I SH3 domain deletion. Despite the increased multivalency of the myosin I NPF, the assembly of capping protein into endocytic structures is reduced, relative to control. The motility of endocytic structures in myosin I SH3 domain deletions is reduced, relative to control, prior to scission. Prior to scission, cells expressing two instead of one myosin I SH3 domain have similar motility to control. However, after scission, myosin I SH3 domain deletion cells exhibit motility similar to control while the motility of cells expressing tandem repeats of myosin I SH3 domains is reduced after scission. This may suggest normal assembly of the endocytic branched actin network and delayed or partially aborted endocytic patches within the cell when myosin I has two, rather than one, SH3 domain. An alternative possibility is that tandem fusions prevent folding of either SH3 domain, phenocopying myosin I SH3 domain deletion cells.

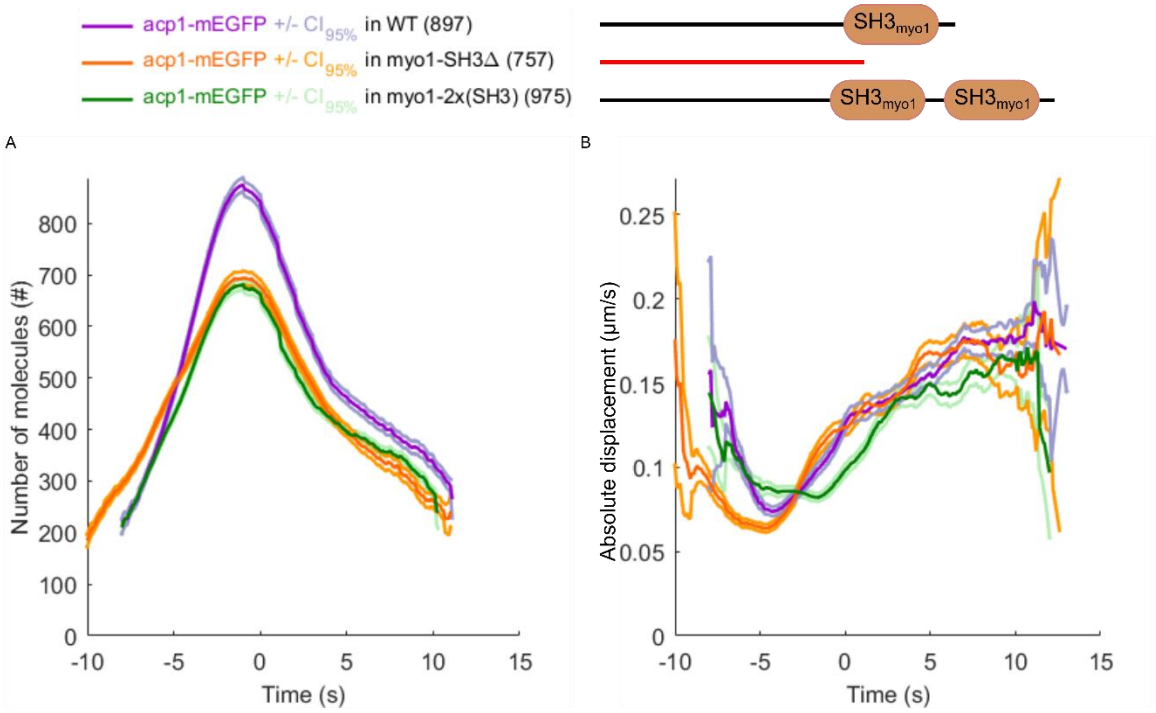

Figure 31. Tandem repeats of the myosin I SH3 domain do not increase actin assembly within endocytic structures but rather disrupt actin assembly, phenocopying SH3 domain deletion. Endocytic patches are labeled with capping protein tagged with EGFP in strains in which myosin I is unperturbed myosin I (WT), myosin I's SH3 domain is deleted (myo1-SH3Δ), or myosin I's SH3 domain is repeated, in tandem, with the peptide sequence of its native SH3 domain (myo1-2x(SH3)). (n) represents number of tracks used to construct average curves (solid lines) and 95% CI (transparent lines). (A) Number of capping protein molecules assembled into endocytic structures in time, relative to scission at t=0s. (B) The absolute displacement of endocytic patches, in a 1s time-interval, for each strain.

C. Discussion

SH3 domains, as modules to connect proteins in the cell, are generally thought to recruit a set of proteins and assemble macromolecules for biological activity (Skår, Coveney, & Pawson, 2003). Yet, for individual domains, it is not clear if a particular SH3 domain is primarily responsible for recruiting its own protein to a particular sub-cellular structure, whether it recruits other proteins, or whether it recruits both itself and other proteins to a macromolecular complex, for example, an endocytic patch. At sites of endocytosis, the early coat proteins Syp1p and Ede1p are perhaps the earliest arriving endocytic proteins and have several SH3 domain-interacting motifs (2 and 8 PRMs, respectively), which may suggest that the first SH3 domain-containing protein to arrive to endocytic sites, Shd1p, may plausibly require its SH3 domains to be localized to endocytic structures while all other endocytic, SH3 domain-containing proteins have overlapping timing, so it is not clear how they are localized (Lu & Drubin, 2017; Reider et al., 2009). Yet, contrary to this simple logic, I found that no individual SH3 domain is required to localize Shd1p to sites of endocytosis (**Figure 22** - **Figure 27**). In particular, when Shd1p's two most N-terminal domains are individually deleted, Shd1p arrives earlier to sites of endocytosis than endocytic arrival in full-length Shd1p expressing cells. Nonetheless, Shd1p's endocytic assembly dynamics are influenced by its SH3 domains (**Figure 28**). In further contrast to the simple logic, most other endocytic, SH3 domain-containing proteins require their SH3 domain for robust localization to endocytosis.

Uncovering, domain-by-domain how molecular assembly during endocytosis is mediated by individual SH3 domains is challenging because any perturbation to the system can incur local and global changes and there is a paucity of obvious and simple ways to distinguish whether an observed effect is local, global, indirect, or direct (Ruan, Wülfing, & Murphy, 2017; Vilela & Danuser, 2011). While this conundrum plagues any

correlative and causative experiment within the context of a living cell biological system, it is especially problematic in endocytosis which rapidly assembles and disassembles within cells while requiring a high-degree of connectivity between proteins in order to function, possibly with redundancy, and likely with extensive feedback and compensation. Adding to the set of observations centered around SH3 domains in cell biological systems, though perhaps still lacking convincing explanation, is a recent hypothesis that SH3 domains induce the formation of phase separated structures *in vivo* and, in so doing, concentrates assembly factors that can boost local actin polymerization within the higher-order structure (Case et al., 2019; Li et al., 2012). To begin to study this hypothesis, I modeled the dependency of valency, specificity, and affinity for a hypothetical SH3 domain membrane-tethered scaffold within cells and expressed a tandem repeat of the myosin-I SH3 domain (**Figure 30**, **Figure 31**). The extent to which endocytic proteins with different PRMs are predicted to be recruited to a non-endocytic engineered scaffold depends on the mechanism of avidity for multivalent linkers and the selective preference of the SH3 domain for particular PRMs. In addition, tandem repeats of SH3 domains within native proteins do not simply lead to increases in actin assembly within endocytic structures. Relying on a network view of endocytic molecular assembly may provide utility in narrowing down recruitment effects of engineered, SH3 domain membrane-tethered scaffolds or tandem repeats of SH3 domains within endocytic proteins. For example, if a single SH3 domain is deleted, it may reduce or abrogate localization of that protein or others to endocytic structures. Mapping out a detailed network of protein interactions may indicate which proteins in endocytic molecular assembly respond to perturbations of SH3 domains. Future studies will require numerous additional experiments but, given that SH3 domains plausibly organize actin cytoskeletal structures and robustly assemble the endocytic machinery, detailed investigations into how it achieves these assembly functions may yet provide

translational and clinical researchers with the knowledge to manipulate and regulate cellular structures responsible for cellular internalization, motility, and division (Fletcher & Mullins, 2010).

In the immediate future, a number of studies can be expanded upon to resolve the extent to which individual SH3 domains are required for their protein's localization to endocytic structures (**Table 10**). The assembly and dynamics of Bbc1p, Hob1p, Lsb1p, Lsb1p, Mug137p, and Shd1p have not been quantitatively studied in *S. pombe*. For all endocytic, SH3 domain-containing proteins, the quantitative assembly and dynamics dependent on each SH3 domain has also not been studied. I have developed the tools to study these assembly dynamics and have reported Shd1p's assembly dynamics, in addition the influence of each of its SH3 domains on Shd1p's assembly dynamics (**Figure 27** - **Figure 29**). However, from deleting SH3 domains in other proteins, it is clear that one cannot quantify the extent to which the SH3 domain is required for its protein's localization to endocytosis with only one-color imaging. Rather, studying the endocytic assembly dynamics dependent on SH3 domains may require another library of two-color strains, where in each strain, an endocytic, SH3 domain has a fluorescent reporter, and a well-studied endocytic protein has another, orthogonal reporter. However, even with such a system, patch tracking and quantitative microscopy of some SH3 domain-containing proteins will be difficult due to their poor localization to endocytic structures without their SH3 domain. In these cases, complementary assays, such as bulk-lipid or dye uptake may suggest whether the cell adapts and compensates to the loss of the protein or whether the loss of the protein to endocytic structures disrupts localization in addition to endocytosis.

Table 10. Summary of SH3 domain influence on their native protein's localization to endocytic structures, cellular expression, and endocytic assembly dynamics.

SH3 domain	Required for robust localization to endocytic structures	Influences expression	Assembly & dynamics tracked	Patch tracking straightforward	2-color alignment needed to strengthen conclusion
Abp1p-1	✓	?	×	✓	×
Abp1p-2	✓	?	×	✓	×
Bbc1p-1*	✓	✓	×	×	✓
Bzz1p-1	✓	✓	×	✓	×
Bzz1p-2	✓	✓	×	✓	×
Cdc15p-1	✓	×	×	×	✓
Hob1p-1*	?	?	×	✓	?
Lsb1p-1*	✓	×	×	×	✓
Lsb4p-1*	?	?	×	?	?
Mug137p-1*	?	?	×	×	✓
Myo1p-1	✓	×	✓	✓	×
Shd1p-1*	×	✓	✓	✓	~×
Shd1p-2*	×	×	✓	✓	~×
Shd1p-3*	×	✓	✓	✓	~×

"?" indicates that experiment has not been performed yet. "~" indicates ambivalence for the position stated, for example, in some cases, it is clear that two-color microscopy may be useful but also that it might not be necessary to make the simpler point that a SH3 domain is important for WT localization of the endocytic protein in question. "*" indicates that the dynamics of the protein's assembly into endocytic structures has not been reported in the literature for endocytosis in *S. pombe*.

D. Methods

1. Measuring whole-cell fluorescence

Spinning disk confocal fluorescence microscopy images of cells expressing EGFP fusions of SH3 domain-containing endocytic proteins with or without single-copies of its SH3 domain(s) were acquired with a 100X, oil-immersion 1.45 NA objective. Cells were loaded into ibidi microfluidic chambers (Slide VI, plastic bottom). Microfluidic chambers were washed 3x with imaging media and then incubated at room temperature for 30min with 1:1000 grams sterile ddH_2O to grams of lyophilized lectin from *Glycine max* (Sigma). Cells were grown in overnight cultures with rich media and spun down at 2350g, washed 3x in imaging media (EMM5S), and resuspended in imaging media (500 microliter resuspension for cells spun down at OD_{595nm}=0.5). To measure whole-cell fluorescence consistently, even across strains with low signal due to poor expression, single z-slices were acquired at 200-ms 488-nm exposure with EM 16MHz gain = 300 AU. DIC mode was used to find the cell mid-plane and then 500-nm slices starting 10 microns below and above the cell mid-plane were acquired. Then, an error function was used to define the whole-cell z-slice locations. A subset stack was extracted and summed to produce a 2D summed z-projection image of the whole cell. Only one time-frame was used, and the microscope variably acquired an entire z-stack at around ~10s.

2. Quantitative microscopy and tracking un-aligned, poorly expressing proteins

The assembly dynamics of several endocytic SH3 domain-containing proteins have not been quantified and thus, the temporal alignment of the molecule's peak assembly relative to scission is not known. In particular, Shd1p's endocytic molecular assembly has not been tracked in endocytosis. To align Shd1p tracks relative to scission, I relied

on measurements of Shd1p's ortholog in *S. cerevisiae*, Sla1p, which indicates that the peak of molecular assembly occurs 4s before scission (Andrea Picco et al., 2015). With this information, the peak assembly time is aligned to 4s for all Shd1p tracks, even though no data exists in any organism as to how perturbing its SH3 domains affect Shd1p's temporal alignment relative to scission.

A 0.1s sampling rate is used for temporal alignment. This is the sampling rate assumed for other quantitative microscopy measurements reported here but to capture enough signal for SH3 domain-containing endocytic proteins fused to EGFP, 200-ms, rather than the typical 50-ms exposure times were taken. The microscope cannot acquire z-stacks every 1s at this lengthened exposure time so z-stacks are taken every 2s instead of 1s. The calibration is also constructed by comparison to endocytic assembly of capping protein at a z-stack acquisition rate of 1s. Thus, the calibration AU/molecule*s value was divided by 2 to adjust for 4 times the test-group fluorescent signal acquired in 200ms, compared to collection of the calibration-group at 50ms exposures, and acquired at half-the rate of the calibration signal.

3. *Expression and localization measurement of endocytic, SH3 domain-containing proteins*

To quantify expression, whole-cell images, pre-processed to contain only a z-stack subset of the entire cell (see above) were projected into a 2D, summed z-projection image. All images were corrected for uneven illumination and camera noise. Then, the 2D whole cell projection was manually segmented in ImageJ and fit to an ellipsoid to determine its long-axis length. Area was calculated based off the number of pixels in the segmented area. The total integrated signal was converted to number of molecules and

adjusted for the segmented area. Then, each SH3 domain deletion strain was compared to control ratiometrically.

To determine localization, summed z-projection images of the whole cell were inspected by eye. Representative images were reported. Endocytosis forms ~0.3-µm puncta in diffraction-limited images (Error! Reference source not found.). Thus, the formation or absence of such puncta in cells was used as a determinant of endocytic localization. The number of cells in a field of view lacking puncta or containing allowed for phenotype penetrant quantification.

4. Loading cell samples into holders for imaging

For localization studies of endocytic proteins tagged with EGFP, all cells were loaded into ibidi microfluidic chambers. For all other studies in this chapter, cells were loaded onto gelatin pads. In each case, flat-fields were collected by loading 1:500 stock Alexa488 dye solution (ThermoFisher) to imaging media in empty flow-channels or onto an empty (no cells) gelatin pad. For quantitative microscopy on gelatin pads, images were analyzed using previously described temporal super-resolution method; script authored by Julien Berro) (Berro et al., 2010). Nonetheless, the striking assembly dynamic and motility phenotypes are not dependent exclusively on the temporal alignment and gelatin pads are associated with comparatively higher variability and poor reproducibility.

5. *Tandem repeats of SH3 domains within endocytic proteins and strain construction to track dependence of sub-cellular localization on individual SH3 domains*

To construct tandem repeats of SH3 domains tethered to the membrane, CRISPR-Cas9 mediated genome engineering with Ura selection was used. Constructing tandem repeats of SH3 domains was difficult and relied on chance. To produce donor DNA with two SH3 fragments, SH3 domains were amplified from gDNA and then blunt-end ligated into pJET1.2 (ThermoFisher). Several transformed colonies were screened for double insertions of the SH3 domain amplicon, yielding poor efficiencies of double inserts. Positive colonies were cultured and extracted plasmids were sequenced to verify tandem repeated insertion. Then, long-primers (110-bp) were used to amplify the double-insert vectors with homology tails for genomic integration. Strains created to analyze the distribution of cellular fluorescence in various single SH3 domain deletion backgrounds, and in which SH3 domain containing proteins were also tagged with a fluorescent reporter, were constructed with methods described in chapter II. Strains in the single SH3 domain localization sections with the SH3-domain containing protein tagged with EGFP were primarily created by Ronan Fernandez.

IV. Interchangeability of SH3 domains in endocytosis

Some sections are partially adapted from Ruth L. Kirschstein National Research Service Award (NRSA) Individual Predoctoral Fellowship (Parent F31) application, submitted December 2017.

A. Introduction

Protein-interaction domains assemble pathways by connecting proteins through binding interactions. One highly conserved protein-interaction domain, the SH3 domain, is involved in the assembly of several cellular pathways. SH3 domains' interaction partners comprise as much as 25% of the proteome, so it is a challenge to comprehend how they exhibit specificity in their interactions. A key question is *how do individual SH3 domains specifically interact with a unique set of proteins to assemble a pathway with distinct cellular functions*?

The interactions mediated by SH3 domains are important to study because they assemble many vital cellular pathways, including several associated with cardiovascular disease and stroke (Bowles, Bowles, & Towbin, 2000; Chang et al., 2016; Hagiwara et al., 2008; Haling et al., 2011; Hammad, Barth, Knaak, & Argraves, 2000; Herron et al., 2005; C. S. Lim et al., 2001; C.-Z. Liu et al., 2016; Maurer & Cooper, 2006; Mulkearns & Cooper, 2012; Poon et al., 2001; Prokic et al., 2014; Prudente et al., 2011; Ram & Blaxall, 2010; L. Tian et al., 2006). Yet, because SH3 domains are found in over 200 human proteins and potentially interact with ~25% of the proteome, it is a challenge to comprehend their unique role in various pathways (Carducci et al., 2012; S. Li, 2005). A key question is *how*

do individual SH3 domains interact specifically with proteins in distinct pathways without cross-reactivity? For example, many proteins involved with endocytosis contain SH3 domains but it is unclear how they interact exclusively with binding partners in this pathway without cross-reacting with proteins in a different pathway.

Interaction specificity can be attained through: (1) *domain-mediated specificity*, where an individual domain has unique biophysical features that enables it to interact specifically with its ligands; (2) *contextual specificity*, where an individual domain has overlapping biophysical features with other domains but its biochemical, regulatory, or cellular localization encodes additional information to facilitate unique domain-ligand interactions (**Figure 32**). In the same context, domains exhibiting predominantly contextual specificity will be functionally interchangeable whereas domains exhibiting domain-mediated specificity will not be interchangeable since their substitution would disrupt normal binding interactions.

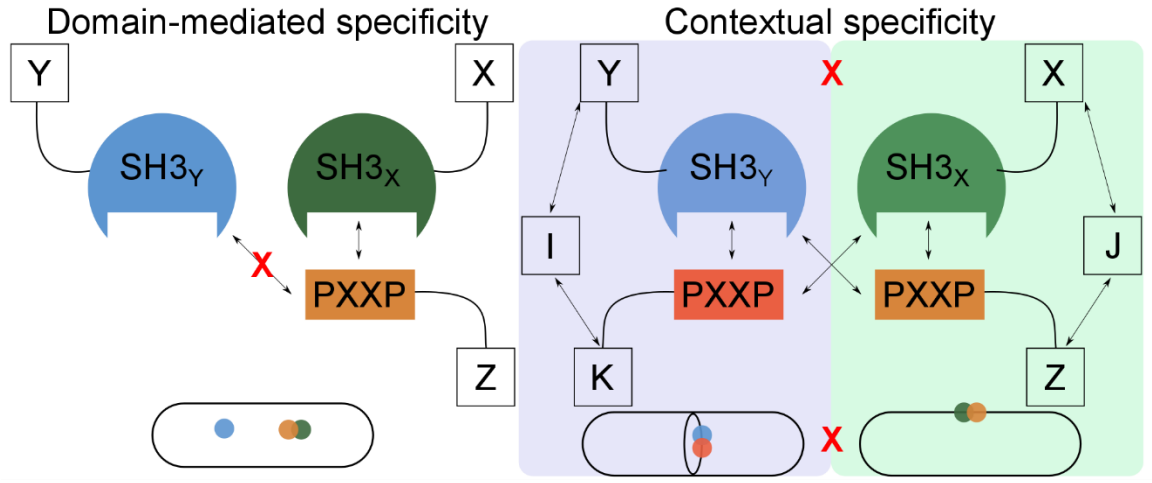

Figure 32. Mechanisms for achieving interaction specificity. (A) *Domain-mediated specificity*: SH3 domains from protein X and Y have distinct biophysical features and cannot bind the same ligand Z even though it has a core-SH3 domain-binding motif. Even if X and Y have overlapping cytoplasmic cellular localizations (bottom), Y's SH3 domain will not bind Z's motif. (B) *Contextual specificity*: Protein X's and Y's SH3 domains share common biophysical features and both can bind ligand K and Z but X and Y localize to different places in the cell, e.g., the cytokinetic ring (left) and the plasma membrane (right), through intermediary proteins I and J, respectively. Non-overlapping molecular and cellular contexts limit cross-reactivity between SH3 domains in separate pathways (bottom) (Ali Zarrinpar et al., 2003).

A large body of work assumes the first model but few studies have explored the plausibility of the second model (Freund, Kühne, Yang, & Embo …, 2002; Stein & Aloy, 2008). Studies focused on describing SH3 domain binding interfaces often operate within a framework with an underlying assumption that specificity can be achieved through a domain-mediated specificity mechanism. However, challenging this underlying assumption, these studies reveal that, in general, SH3 domains bind multiple binding partners and have weak affinities for their peptide ligands (S. Li, 2005; Saksela & Permi, 2012; Tossavainen, Aitio, Hellman, Saksela, & Permi, 2016). This highlights that these studies do not explain how the majority of SH3 domains achieve binding specificity within pathways *in vivo*, since non-specific binding is expected in highly concentrated contexts with weak affinities (Carbonell, Nussinov, & del Sol, 2009; Karlsson, Sundell, Andersson, Ivarsson, & Jemth, 2016). The few studies that report strong affinities *in vitro* do not indicate that a SH3 domain will interact specifically *in vivo*, where it may be in competition and interact non-specifically with other ligands, lowering the apparent affinity. Thus, it remains unclear how individual SH3 domains exhibit strong enough relative binding affinities to achieve specificity.

SH3 domains have been grouped into three different ligand specificity classes based off of their preference for residues flanking a core SH3 domain-binding motif, PXXP (proline and X for any amino acid) (see Figure 5B).(Erik et al., 2015; Saksela & Permi, 2012; Tonikian et al., 2009; Xin et al., 2013) However, most human SH3 domains cannot be grouped into any specificity class because they exhibit indistinguishable selectivity and weak binding *in vitro*.(Kazlauskas et al., 2016) These studies rely on high-throughput techniques, which often miss transient interactions that may be important *in vivo*. Furthermore, these studies and are not quantitative, conflating differences in specificity with relative differences in affinity. This makes it difficult to determine whether an individual

SH3 domain will exhibit its apparent preference for ligands of a particular specificity class *in vivo*, where pathways involving SH3 domains are present in local concentrations high enough that small differences in affinity will not prevent cross-reactivity. Lastly, motifs from multiple classes can be found within one protein, suggesting that domain-mediated protein binding may still occur, regardless of specificity class. Thus, it is not clear if SH3 domain ligand specificity classes are relevant to SH3 domains' biological function or whether the affinity differences between classes are large enough to prevent non-specific inter-class binding.

Fewer studies have explored the plausibility of contextual specificity as a mechanism for interaction specificity (Freund et al., 2002; Stein & Aloy, 2008). For proteins observed to interact *in vitro*, a lack of observed binding *in vivo* is sometimes attributed to a difference in cellular localization (Freund et al., 2002). However, this does not explain how interaction specificity is achieved in the same reaction volume. Several pathways, like endocytosis, operate in a single cellular context so it is unclear how SH3 domains could mediate specific interactions within this pathway.

Eukaryotic cells use endocytosis to internalize nutrients, membrane, and other cargo and it facilitates cell size control and signaling receptor regulation (McMahon & Boucrot, 2011). In endocytosis, a highly conserved molecular machinery reproducibly assembles and disassembles in ~20 sec to form a ~50-nm diameter vesicle from the membrane (Doherty & McMahon, 2009; Sirotkin et al., 2010). Fission yeast endocytosis is an ideal model system to study SH3 domains because only 21 proteins have SH3 domains, and 11 of them are associated with endocytosis (Carducci et al., 2012). In fission yeast, ~60 proteins are involved in the endocytic pathway and over 40 of these proteins contain SH3 domains binding motifs. Thus, the majority of the endocytic machinery may interact through SH3 domain-mediated binding. The degeneracy of each SH3 domain's

binding in endocytosis isn't well studied even though it may play a salient role in the assembly of the endocytic pathway.

I developed an experimental strategy to examine the specificity of SH3 domains *in vivo*. I replaced some endocytic proteins' SH3 domain with non-native SH3 domains and examined how these replacements affected endocytosis. I hypothesized that SH3 domains achieve interaction specificity predominantly through context and that most SH3 domains are interchangeable in the same context. The overall approach sought to distinguish between two mechanisms of achieving interaction specificity, which is a dichotomy that has evaded resolution.

My experiments support the hypothesis that SH3 domains achieve interaction specificity through domain-mediated specificity. In particular, exchanging proteins based on a peptide binding specificity classification for individual *S. pombe* SH3 domains revealed that the myosin I SH3 locus exhibits a deletion phenotype that cannot be rescued by specificity class I or II SH3 domains (Verschueren et al., 2015). However, multiple domain swaps in sensitized strains and replacing the *S. pombe* myosin I with either of the two myosin I paralogs from *S. cerevisiae* exhibit partial rescues. These results do not rule out context-mediated specificity. Reciprocal replacements, namely replacing specificity class I and II domains with myosin I's SH3 domain, and SH3 domain insertions with a series of flexible linkers to reduce the likelihood of protein stability or folding effects as confounders, will be necessary to more conclusively elucidate the modularity and interchangeability of SH3 domains.

B. Results

1. *Multiple endogenous SH3 domain deletions in single strains support that SH3 domains are important for normal endocytic assembly*

Single SH3 domain deletions alter the recruitment dynamics of actin assembly in endocytosis, compared to control (**Figure 10**). Single SH3 domain deletions, across all endocytic SH3 domains, alter endocytic assembly in the cell as well as the rate of endocytosis per cell length but single-copy SH3 deletions do not abrogate successful endocytosis entirely, nor do single-copy SH3 deletions significantly affect cell growth ($p > 0.05$, all) (**Figure 15**, **Figure 16**). In search of significant perturbations to endocytosis, especially ones in which the presence of a SH3 domain (or SH3 domains) was critical to cell growth, albeit not so detrimental that survival following genetic manipulation was too unlikely to obtain positive mutants, I deleted multiple copies of various SH3 domains within endocytic proteins in a single strain.

In single copy deletions, the motility of the endocytic patch varies, generally resulting in either increased, decreased, or similar stabilization prior to scission and increased, decreased, or similar mean absolute displacement after scission, with the combined effect on cumulative path length of the endocytic vesicle variable across SH3 deletions (**Figure 12**, **Figure 14**). One of the most striking single-copy deletion defects is observed when tracking capping protein in the myosin I SH3Δ genetic deletion background. When tracking fimbrin in myosin I SH3 deletion backgrounds, there is a lack of initial stabilization in the motion of the endocytic patch, relative to control (**Figure 33A**, top). However, the initiation of a diffusive phase of motion overlaps with control. Yet, after scission, endocytic patches without myosin I's SH3 domain exhibit reduced motility and lower overall cumulative path lengths. Though the deletion of multiple SH3 domains results in defects in actin assembly,

strains without either of Bzz1p's SH3 domains exhibit an initial stabilization of the patch (**Figure 33A**, bottom). The motility of the patch after scission exhibits no difference to control. The extended lifetime of the 2 SH3 domain deletion strain, relative to control, accounts for the lengthened cumulative path length of its endocytic structures in the cell.

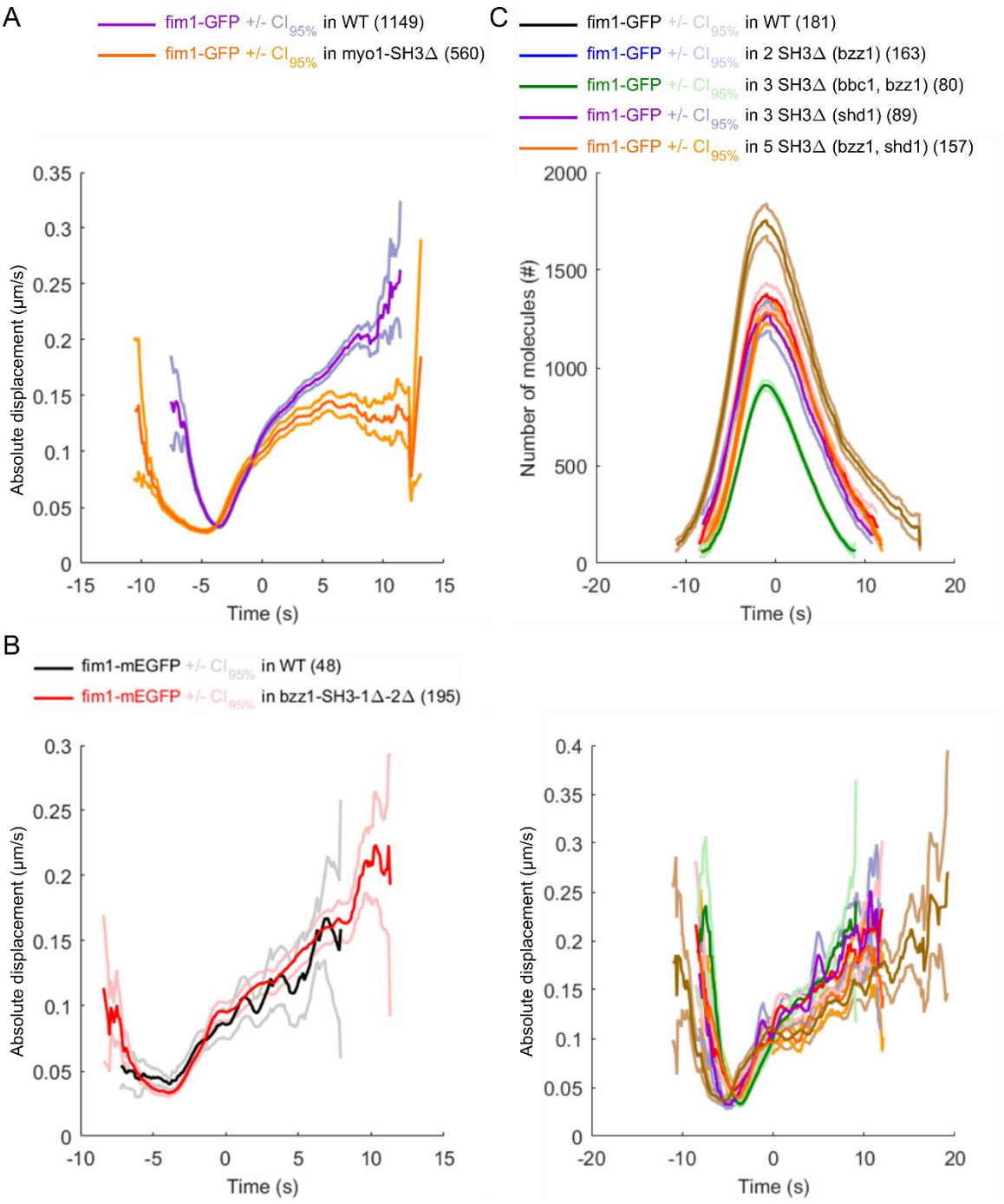

Figure 33. Multiple SH3 domain deletions within single strains substantiates the influence of SH3 domains on actin assembly and endocytosis. Influence of SH3 domains on endocytosis for endogenous, multi-copy deletions of various endocytic SH3 domains measured by quantitative microscopy. (A) Endocytic patch absolute displacement in 1-s time interval as measured by tracking patches of fimbrin, an actin-cross linker involved in endocytosis, fused with EGFP (fim1-GFP) in WT (control) and myosin I SH3 domain deletion

backgrounds. (A) Endocytic patch absolute displacement in 1-s time interval, relative to scission at t=0s for 2 SH3 domain deletion strain comparing deletion of both Bzz1p SH3 domains to control (WT background). (C, top) Number of fimbrin molecules in endocytic structures for various multiple SH3 domain deletions within a single strain. (C, bottom) Absolute displacement of endocytic patches in 1-s time interval for various multiple SH3 domain deletions within a single strain; line color according to legend in C, top. (n) represents # of tracks, time is relative to scission of nascent endocytic vesicles at t = 0s. Solid lines represent averages and ribbons represent 95% CI.

Multiple SH3 domain deletions, regardless of the domain, leads to over-recruitment of actin, as tracked by the proxy, fimbrin, suggesting that actin assembly is increased in response to deletion of multiple SH3 domain deletions. In particular, Bzz1p's SH3 domains increase the amount of actin assembled into endocytic structures since, without the SH3 domains, the rate of capping actin filaments and the overall assembly of capping protein into endocytic structures is reduced without the Bzz1p-2 SH3 domain (**Figure 21**). Yet, when both Bzz1p SH3 domains are deleted, ~50% more fimbrin molecules are assembled into endocytic structures at the peak of assembly (**Figure 33B**). Indeed, when Bzz1p's and Shd1p's SH3 domains are deleted (5 total corresponding to 2 Bzz1p SH3 domains and 3 Shd1p SH3 domains), there is ~2-fold increase in the amount of fimbrin required for successful endocytosis.

Throughout the tracked process of endocytosis, multiple SH3 domain deletions assemble more fimbrin into the endocytic structure, compared to control. The number of molecules is roughly symmetrical about scission for control cells but the disassembly time, relative to the assembly time, is slightly lengthened for the 5 SH3 domain deletion strain. All multiple SH3 domain deletions exhibit longer total endocytic lifetimes. In the case of 5 SH3 domain deletions, endocytosis takes nearly twice as long as control cells, correlating with the peak number of molecules assembled into the patch. There trend is that for 2 towards 5 SH3 domain deletions, there is an increasing amount of fimbrin assembled into endocytic structures and lengthened endocytic lifetimes. However, there are few cases and deleting both Bzz1p's SH3 domains phenocopies deleting 3 SH3 domains, whether by deleting both Bzz1p's SH3 domains and Bbc1p's SH3 domain or 3 Shd1p SH3 domains (overlapping 95% CI, all).

2. *Poor efficiency of genetic engineering of endogenous, multiple copy deletions of SH3 domains despite negligible growth defects*

In haploid genetic editing, single-copy deletions of SH3 domains are viable. However, this does not provide evidence that multiple copy SH3 domain deletions will also be viable. If the deletion of multiple SH3 domains is lethal, then no positives can be identified, as was the case for deleting both Abp1p's SH3 domains in a genetic background with two Bzz1p SH3 domain deletions. However, in general, the efficiencies of multiple SH3 domain deletion strains, defined as the ratio of positive mutants over all mutants screened at the relevant genetic loci, is low compared to single SH3 domain deletion strains (**Figure 34**). Deleting Bzz1p's SH3 domains and Shd1p's SH3 domains can be done with efficiencies of ~15% and 40%, respectively. However, deleting additional domains on top of these either produces so few colonies that the total number of screening is reduced: deleting both Abp1p SH3 domains in a strain where both Bzz1p's Sh3 domains are deleted, 7 colonies screened, or, the efficiency is reduced, 3-6% in strains where positives could be identified. Even taking the intermediate step of cloning the deletion cassette into a vector and amplifying from there fails to produce positives, while all single copy deletions could be successfully edited in this way (data not shown).

# SH3 domains deleted	Parent protein(s)	Efficiency*	SH3Δ cassette cloned into vector**
1	abp1	4/26	Yes
1	abp1	0/23	Yes
1	bbc1	0/15	Yes
1	bzz1	5/32	Yes
1	bzz1	0/16	No
1	myo1	1/46	Yes
1	lsb4	0/16	Yes
1	mug137	0/16	Yes
1	cdc15	0/14	Yes
1	SPBC19C2.10	0/15	Yes
1	hob1	4/11	Yes
1	lsb1	6/16	Yes
2	abp1	0/29	Yes
2	bzz1	1/7	Yes
3	shd1	6/16	Yes
3	bzz1, bbc1	1/31	-
3	bzz1, myo1	0/11	-
4	abp1, bzz1	0/7	-
5	bzz1, shd1	1/16	-
6	bzz1, bbc1, shd1	0/16	-
7	abp1, bzz1, shd1	0/44	-

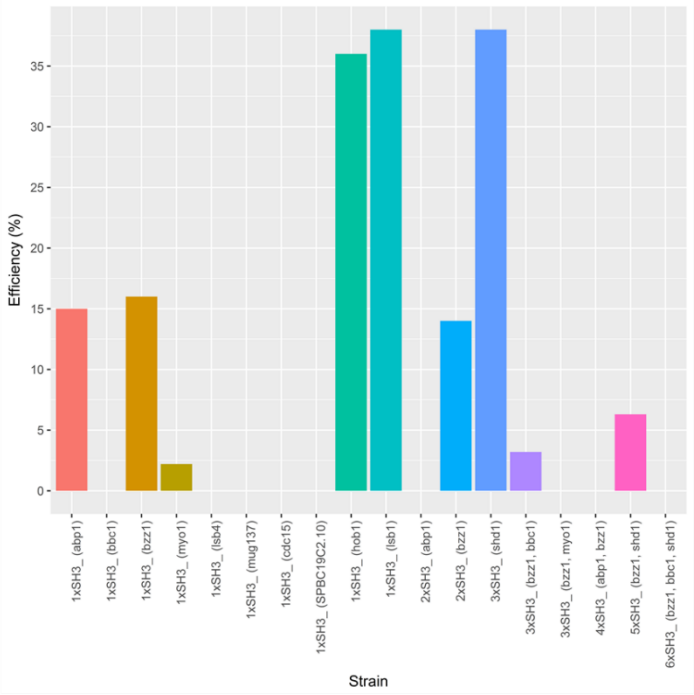

Figure 34. Efficiency of genetically deleting multiple copies of SH3 domains using CRISPR-Cas9 mediated gene editing and gap repair in *S. pombe*. Efficiency is defined as the ratio, expressed as a percentage, of the number of colonies screened by colony PCR containing the intended genetic edition at the relevant locus over the total number of colonies screened. (Left) Table for library of multiple SH3 domain deletions, compared against identical genetic backgrounds but with single SH3 domain deletions' efficiency indicated. * = efficiency of deletion by CRISPR-Cas9 and gap repair as # positives/total screened (%). ** = indicates that construction of SH3Δ cassette to serve as donor DNA at high concentrations was a rate limiting step, necessitating the intermediate step of cloning the deletion cassette into a vector from which to amplify donor DNA. (Right) Efficiency for indicated number of SH3 domain with specific SH3 domains targeted for deletion in parentheses.

Despite poor efficiencies, and low colony growth in some cases, post-transformation, the positive strains with multiple SH3 domain deletions do not exhibit severe growth defects (**Figure 35**). There is some variability in the initial OD across all strains, cultured over-night in rich media, then diluted before beginning the measurement. For example, the 5 SH3 domain deletion strain has the highest starting OD and enters the logarithmic phase of growth first. Taking the growth rate and ignoring the lag time, the slopes of the logarithmic phase of growth is similar across control and multiple SH3 domain deletion strains. The saturation point of the different strains varies but even in the Fex1, Fex2 deletion strain, the saturation value differs from WT cells. There is no clear trend in low saturation values as the 5 SH3 domain deletion strain has a comparable value to a 2 SH3 domain deletion strain while a 3 SH3 domain deletion has a slightly higher saturation value.

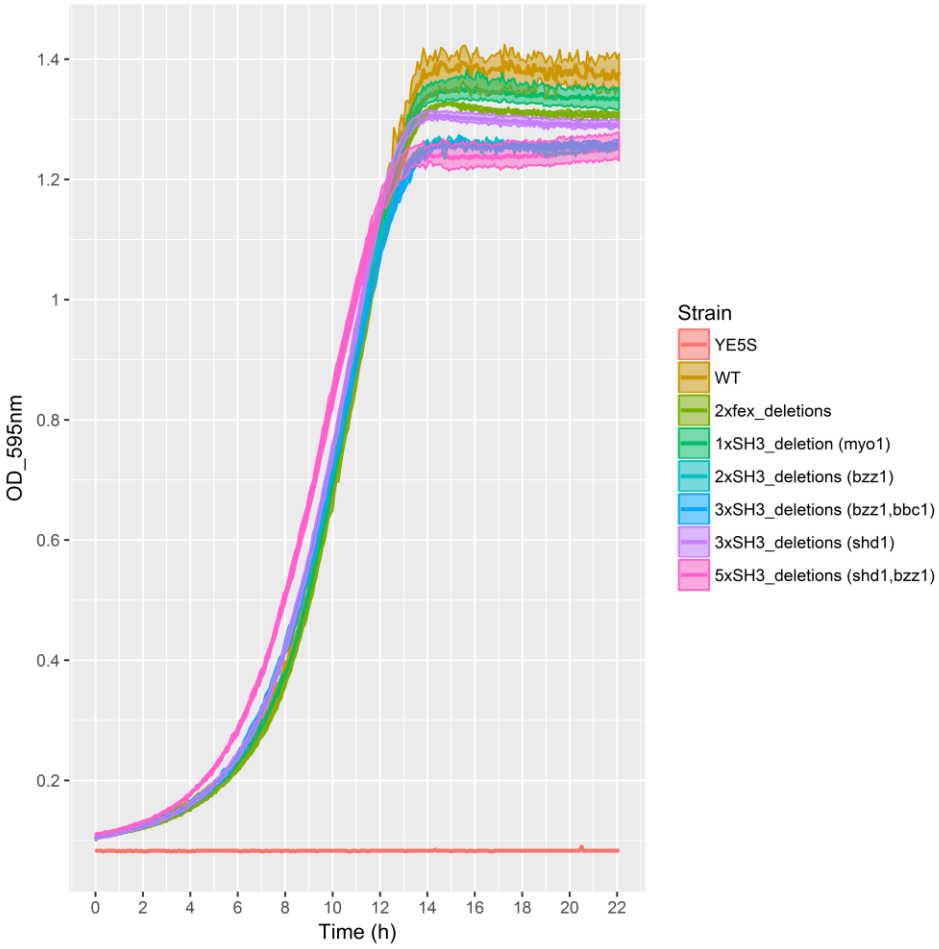

Figure 35. Growth curves for multiple SH3 domain deletion strains. Growth curves for various strains in rich media (YE5S) over 24h with an 595nm absorbance measurement taken every 5 minutes. The number of SH3 domains deleted in the strain for the specific proteins in parentheses is indicated in the legend. Line represents average across 3 biological replicates and ribbon represents the minimum and maximum value across replicates at any given time.

Multiple SH3 domain deletion strains were created from a parent strain. First, FY527, the WT strain isolated by Urs Leupold and used as a standard laboratory strain, was edited to remove the fluoride transporters Fex1 and Fex2, leading to the strain JB 300 (Forsburg, 2003). JB 300 was then used to create an EGFP fusion protein to fimbrin, JB 311. JB 311 served as the parent strain for all multiple SH3 domain deletion strains. Back-crossing JB 300 with the WT strain of the opposite mating type, FY528, revealed growth defects in isolated spores (**Figure 36**). The growth of isolated spores varied amongst tetrads for JB300, while an intermediate strain, JB224, did not exhibit variability in spore colony size.

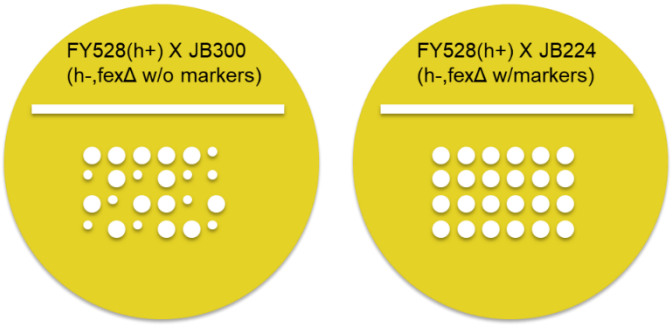

Figure 36. Backcrossing and isolating spores reveals a mating phenotype in parent strain used to construct endogenous, multiple-copy SH3 domain deletion library. Summary of backcrosses for strains used to build a library of multiple SH3 domain deletion strains. FY528 = WT strain; JB300 = strain in which Fex1p and Fex2p are deleted, without markers. JB224 = strain in which Fex1p and Fex2p are deleted but, C-terminal to the deleted coding domain sequence is a sequence for antibiotic selection, KanMX6 and NatMX6, respectively. JB300 was used to create multiple SH3 domain strain library. (Left) Summary of spore phenotypes for cross of JB300 with FY528 on nitrogen-poor media. Spores exhibit variable sizes, notably in pairs or triplicate, where some are small and some are large. This is contrast to typical crosses, where spore colonies grow to equal length (right). Each column represents 1 tetrad, from which 4 spores are picked and isolated into rows. Experiments performed with Ronan Fernandez.

To determine if strains derived from JB300 exhibit defects in endocytosis, in addition to mating, I compared strains fused with EGFP and the same endocytic protein but in different genetic backgrounds, namely, either derived from the WT strain, FY528, or the strain JB300. Quantitative microscopy revealed no significant differences in the peak number of molecules of fimbrin assembled into endocytic structures (**Figure 37**). Throughout endocytosis, the assembly of fimbrin is the same as control, despite the mating phenotype observed on its parent strain. The motility of patches in the mating phenotype exhibiting strain does not show as striking of an initial stabilization as control cells but these region is noisy and limited by the different number of tracks between control and test strain, thus leading to differences in detection limits between strains. Otherwise, the motility of the patch does not significantly differ between control and the strain with marker-less Fex1p and Fex2p deletion.

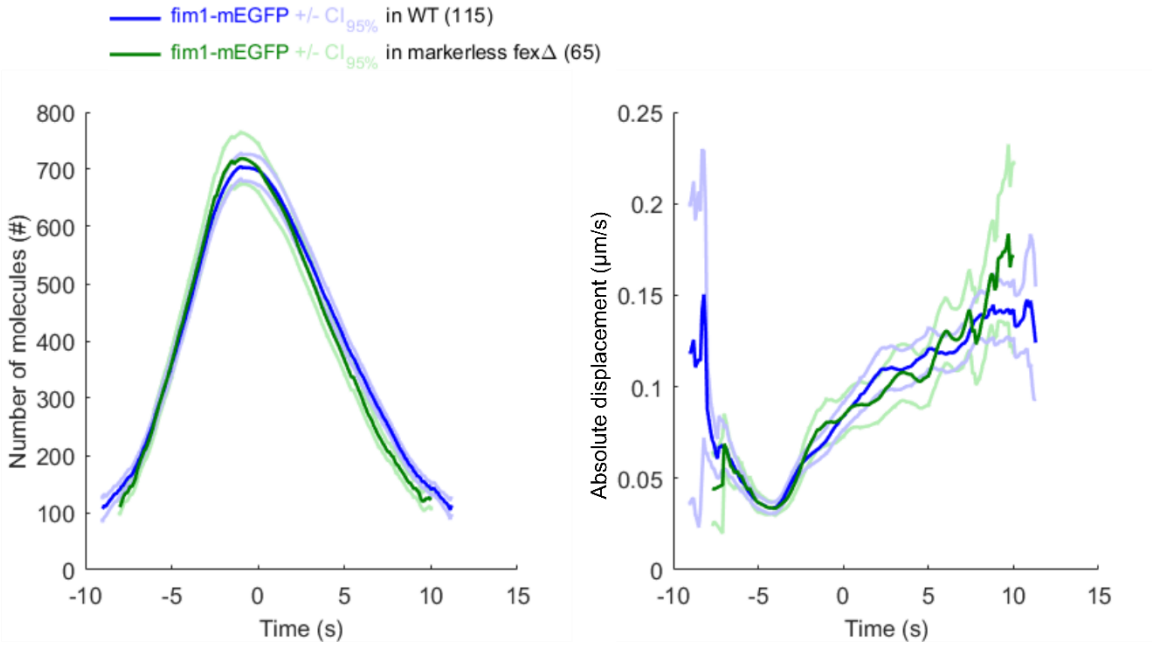

Figure 37. Endocytosis in strain exhibiting mating phenotype. Quantitative microscopy measurements of fimbrin tagged with EGFP in a WT strain (FY528) compared to fimbrin tagged with EGFP in a marker-less Fex1p, Fex2p deletion strain (JB300), which exhibits a mating phenotype. (Left) The number of fimbrin molecules assembled into an endocytic patch versus time for each strain, relative to scission at t = 0s. Faded lines show 95% confidence intervals. (Right) Absolute displacement of aligned tracks of endocytic patches, showing their motility throughout the process of endocytosis. Transparent lines indicate 95% CI.

While there is no association between defects in endocytosis, as measured by quantitative microscopy, and mating phenotype, microscopy reveals differences between strains derived from WT and strains derived from JB300, the marker-less Fex1p and Fex2p deletion strain that exhibits mating phenotypes (**Figure 38**). In cells where fimbrin is fused with EGFP and derived from the WT strain, FY528, nearly all cells are around 10 microns or less in long-axis length. In contrast, nearly all cells derived from JB300, the strain exhibiting a mating phenotype, exhibit long-axis lengths greater than 10 microns. In cells derived from JB300, namely JB311, there is also increased contrast in the cytoplasmic regions, slightly increased sizes of endocytic patches, and more contrast per cell, albeit in lower penetrance the long-axis length elongation relative to control.

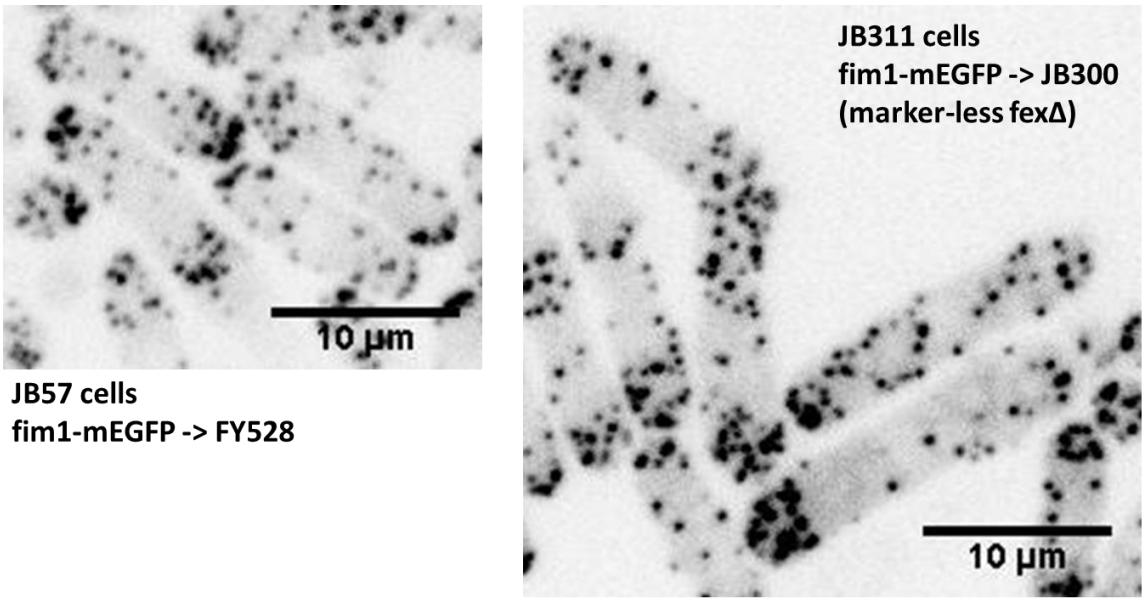

Figure 38. Elongated length of cells derived from a strain exhibiting mating phenotypes. Summed z-projection of fluorescent images of fimbrin fused with EGFP for cells derived from WT (left) or from a strain exhibiting mating phenotypes (right). Contrast is fixed for both images so that intensity is comparable. Scale bar 10 microns.

3. Insertion of exogenous SH3 domains into multiple SH3 domain-deleted loci partially rescues endocytic defects

Deleting both Bzz1p SH3 domains is associated with ~2 fold increase in the maximal number of fimbrin molecules assembled into endocytic patches at the peak while deleting all three Shd1p's SH3 domains is associated with ~3 fold increase in the maximal number of fimbrin molecules assembled into endocytic patches (**Figure 39**). In these strains, replacing Bzz1p's deleted SH3 domains with the SH3 domains from Bzz1p phenocopies the Bzz1p SH3 domain deletion defect, suggesting that the endocytic phenotype resulting from deletion of Bzz1p's SH3 domains cannot be rescued by replacement with Shd1p's two most N-terminal SH3 domains. Similarly, replacing Shd1p's two most N-terminal SH3 domains with Bzz1p's SH3 domains phenocopies the triple SH3 domain deletion of Shd1p's SH3 domains. Deletion of all of the SH3 domains of Bzz1p and Shd1p is associated with the largest over-assembly of fimbrin molecules in endocytic patches (**Figure 33**). Yet, in the 5 SH3 domain deletion strain, replacement of Shd1p's SH3 domains with Bzz1p's SH3 domains phenocopies the 3 SH3 domain deletion strain, suggesting partial rescue of this endocytic defect, given that Shd1p's third SH3 domain is dispensable for assembling actin into endocytic structures in cells (**Figure 10**).

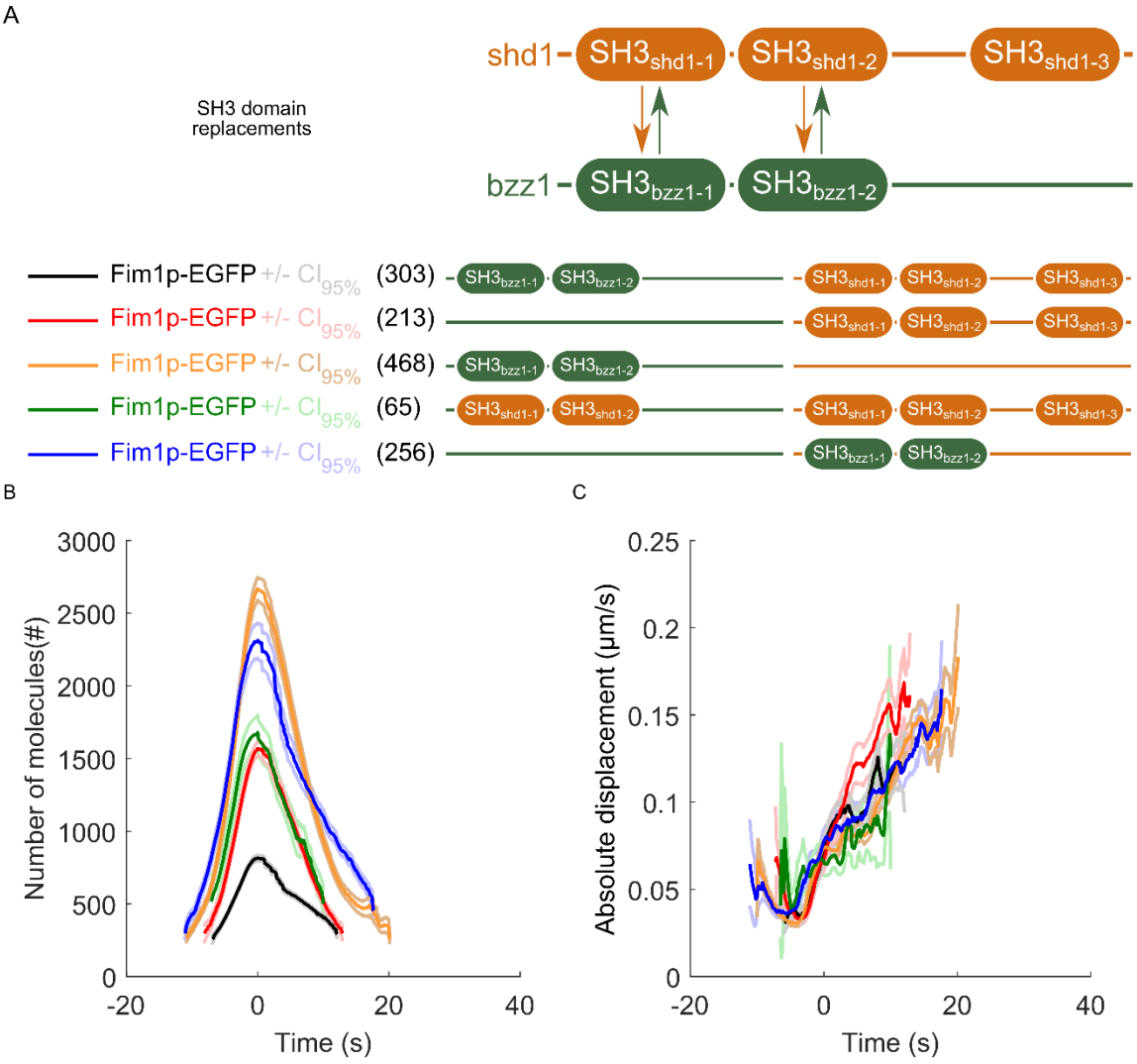

Figure 39. Replacing multiple SH3 domains with non-native SH3 domains. Quantitative microscopy tracking patches marked by fimbrin tagged with EGFP for various, endogenous, multiple-copy deletions of SH3 domains replaced with non-native SH3 domains. (A) Schematic of overall interchangeability experiments shown swapped Bzz1p and Shd1p SH3 domains. (Legend) (n) represents number of tracks used to construct average curves (solid lines); ribbon shows 95% confidence interval. Green line represents Bzz1p genetic locus and orange represents Shd1p (locus). In control cells, Bzz1p and Shd1p have two and three SH3 domains, respectively. Multiple SH3 domain deletions for each protein are shown. Interchangeability experiments are replacement of Bzz1p's SH3 domains with the first two Shd1p SH3 domains (two most N-terminal, green curve), and replacement of Shd1p's first two SH3 domains with Bzz1p's SH3 domain (blue curve). (B) Number of molecules in time, relative to scission at t=0s for strains indicated in legend above. (C) Absolute displacement of endocytic patches in 1-s time for strains indicated in above legend.

Deletion of 2 SH3 domains in the endocytic, actin-associated protein Bzz1p and 3 SH3 domains in the coat protein Shd1p increases the lifetime of endocytosis and overall actin assembly, relative to control (**Figure 33**). Deleting all 5 SH3 domains of Bzz1p and Shd1p exhibits the largest overall assembly of fimbrin into endocytic patches, with the longest total endocytic lifetimes. Inserting Bzz1p's SH3 domains into Shd1p's two most N-terminal SH3 domain locus in the 5 SH3 domain deletion strain results in a partial rescue of the 5 SH3 domain deletion (**Figure 40**). The 5 SH3 domain deletion strain is associated with ~2 fold increases in the maximal amount of fimbrin assembled into the patch and twice as long of a lifetime. When Bzz1p's SH3 domains are inserted into the Shd1p triple deletion locus, the increase in the amount of fimbrin assembled into the patch is less than 50% higher than control. In addition, compared to the 5 SH3 domain deletion strain, there is an ~40% reduction in the overall endocytic lifetime.

The number of SH3 domain deletions is associated with an approximately increasing amount of actin assembly in patches and lengthened endocytic lifetimes, such that 5 SH3 domain deletions exhibits larger magnitudes of these effects relative to triple SH3 domain deletions. Insertion of Bzz1p's two SH3 domains into Shd1p's N-terminal SH3 loci amounts to three overall SH3 domain deletions in that strain. Replacement of Shd1p's first two SH3 domains with Bzz1p's SH3 domains phenocopies the triple deletion strain in which all of Shd1p's SH3 domains are deleted and Bzz1p's SH3 domains are intact. For most times throughout endocytosis, regardless of the location of Bzz1p's SH3 domains in the genome, namely, whether it is in the Bzz1p coding domain sequence or in the Shd1p SH3 domain sequence, endocytosis behaves identically. This suggests that the first two SH3 domains of Shd1p and Bzz1p's two SH3 domains are interchangeable.

Contrary to this, there is significantly more fimbrin assembled in endocytic patches 10s before scission for the when Bzz1p's SH3 domains are integrated into Shd1p rather than Bzz1p (**Figure 40A**, non-overlapping 95% CI of average curves). There is also more variability in the time at which enough fimbrin is assembled into endocytic patches to pass the detection threshold. The derivative of the number of molecules, with respect to time, represents the assembly rate of fimbrin into endocytic patches. When Bzz1p's SH3 domains are integrated into Shd1p, the assembly rate of fimbrin into patches is depressed, relative to when Bzz1p's SH3 domains are within their native protein. There is no significant difference during disassembly between the strains, either in rate or number of fimbrin molecules; though, the swapped strain takes ~1s longer disassembly takes.

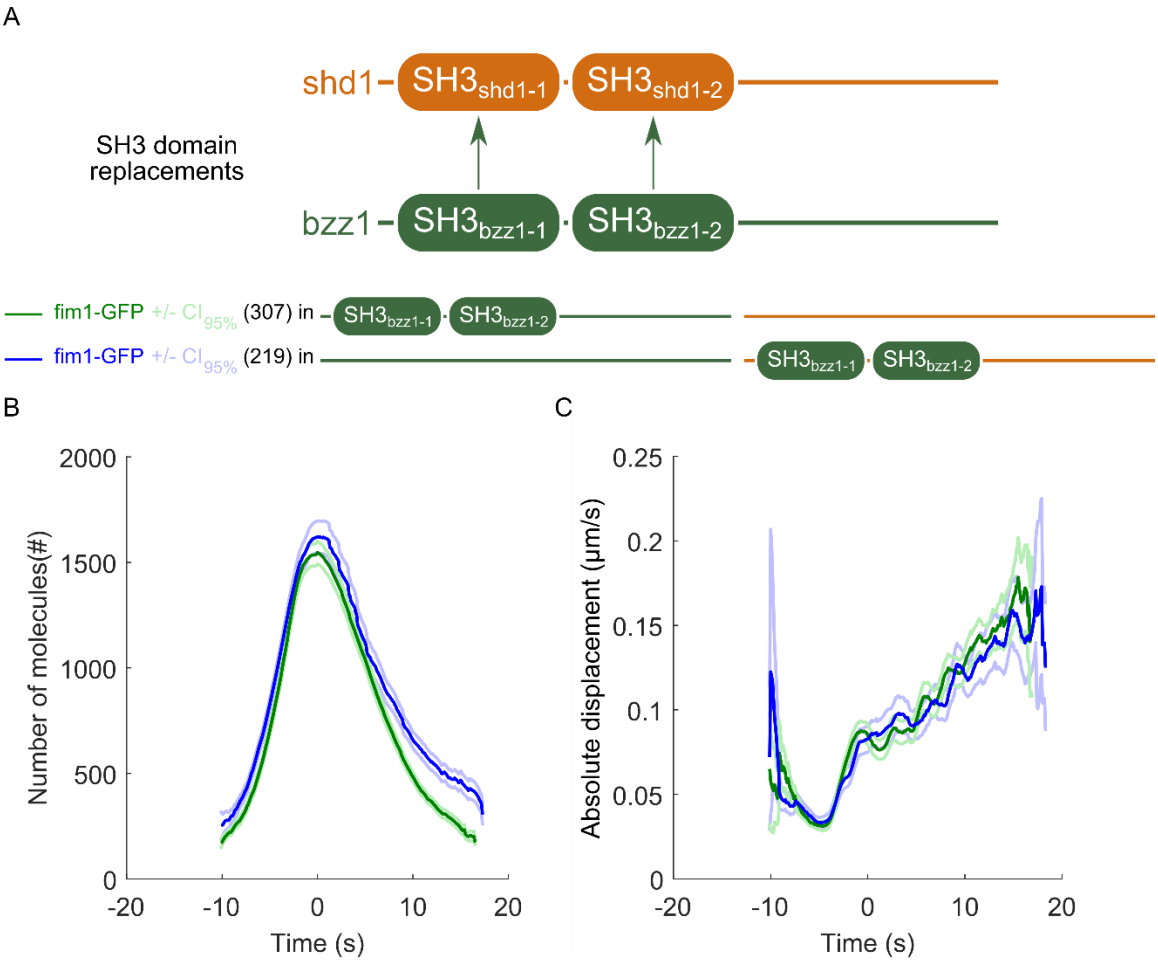

Figure 40. Partial rescue of 5 SH3 domain deletion phenotype by replacing Bzz1p's SH3 domains with Shd1p's two most N-terminal SH3 domains and vice versa. (A) Domain architecture of Bzz1p and Shd1p and replacement strategy. Bzz1p's SH3 domains are inserted in the two most-N-terminal SH3 loci of Shd1p. (B) Number of molecules within endocytic patches in time, relative to scission at t=0s, of fimbrin when Bzz1p's SH3 domains are inserted into Shd1p (blue curve, 3 SH3 domain deletions total) compared to deletion of Shd1p's SH3 domains (green curve, 3 SH3 domain deletions total) demonstrating partial recovery of defect from deletion of all 5 SH3 domains of Bzz1p and Shd1p. (C) Absolute displacement of endocytic patches in a time interval of 1-s for strains shown in legend above. Solid lines show averages; ribbon shows 95% CI.

4. Replacements by three different SH3 domains do not fully rescue Myo1p SH3 domain deletion phenotype

An alternative hypothesis to the dominance of contextual specificity is that SH3 domains have overlapping functionality when they share the same peptide-binding-motif specificity class *and* cellular context. To test this, I replaced the Myo1p class III SH3 domain with Bbc1p's Class II SH3 domain and two Class I SH3 domains, Cdc15p's and Shd1p's third SH3 domain, based off previously reported peptide-binding-motif specificity classes in *S. pombe* (Verschueren et al., 2015). Myosin I's SH3 domain deletion cells exhibit striking defects in actin assembly, patch motility, myosin I localization, and alter the cell's regulation of endocytosis overall (**Figure 21**). Having identified this as a good candidate SH3 domain to query the extent of interchangeability, I endogenously replaced its SH3 domain with endocytic SH3 domains in different specificity classes, which led to viable cells amenable to analysis by quantitative microscopy (**Figure 41A**).

The control strain, in which capping protein is tagged with EGFP, the peak assembly of the average endocytic structure is calibrated to previous measurements of Acp2p (Sirotkin et al., 2010). Based off these measurements, capping protein is assembled and disassembled within tracked endocytic structures in ~14s. Compared to control, when myosin I's SH3 domain deleted, ~150 capping protein molecules are maximally assembled into the patch (**Figure 41B**). Replacing the native myosin I SH3 domain with three other SH3 domains, from different specificity classes and proteins, phenocopies myosin I SH3 domain deletion quantitative microscopy measurements. In all cases, the insertion of a non-native SH3 domain is associated with consistently lower assembly of capping protein, relative to control, assembling maximally ~150 capping

protein molecules into endocytic structures, constituting a ~30% reduction in capping protein assembly.

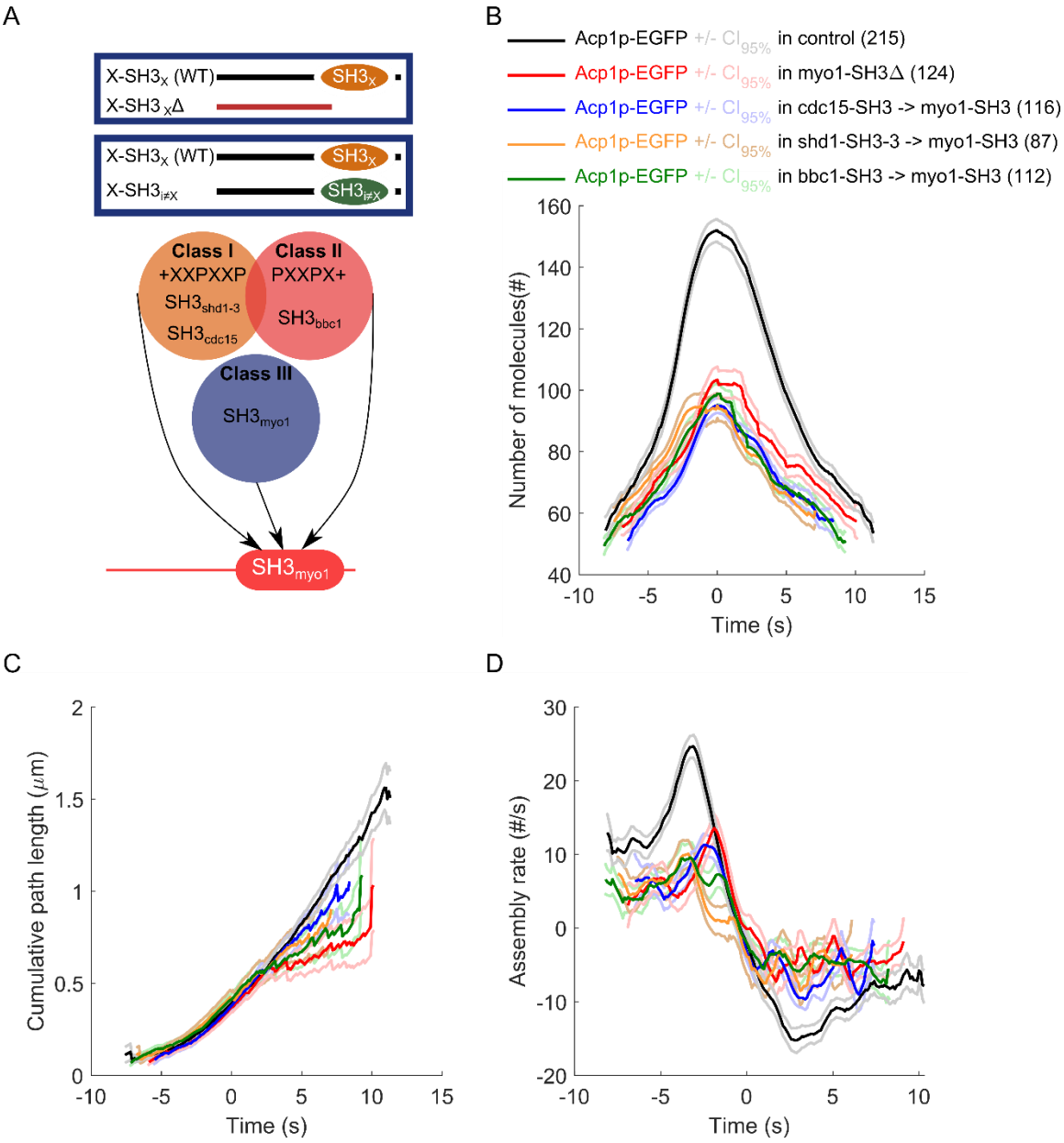

Figure 41. Interchangeability of myosin I's SH3 domain by peptide-binding specificity class. Myo1p SH3 domain deletion and replacements according to specificity class. (A) Overall strategy to determine interchangeability of a domain: identify a phenotype by SH3 domain deletion, replace the domain with non-native domains. Replacement of myosin I's SH3 domain (myo1) according to peptide binding specificity class (bottom). Arrow indicates which protein's SH3 domain was inserted. (B-D) Quantitative microscopy measurements for strains modified according to legend (top) where the endogenous replacement and ligand specificity class is indicated. (n) represents the number of tracks used to produce the average curve. Transparent lines show 95% confidence intervals. (A) Number of molecules capping protein in endocytic

structures for various strains, relative to scission at t=0s. (B) Cumulative mean absolute displacements as cumulative path length up to indicated point in time. (C) The net assembly rate throughout endocytosis for various strains.

In contrast to SH3 domain deletion phenotype rescue by insertion of non-native SH3 domains, endocytic assembly proceeds as if no SH3 domain is present within myosin I even while sequencing confirms the intended insertion (data not shown). Deleterious effects of non-native SH3 domain insertion are not observed. In control cells, capping protein is assembled at a maximal rate of ~30 molecules per second. Without the myosin I SH3 domain, only ~10 molecules per second are maximally assembled (**Figure 41B**, bottom). Control cells achieve a high disassembly rate, removing maximally removing ~20 capping protein molecules per second, while without the myosin I SH3 domain, only 10 capping protein molecules are removed per second. When non-native SH3 domains are inserted into the myosin I SH3 locus, the net assembly rate throughout endocytosis phenocopies the myosin I SH3 domain deletion assembly rate, exhibiting reductions in capping protein assembly relative to control, albeit without displaying worse defects than the myosin I SH3 domain deletion phenotypes.

5. S. cerevisiae myosin I SH3 domains partially rescue S. pombe myosin I SH3 domain deletion phenotypes

SH3 domains from different peptide-binding-motif specificity classes failed to rescue myosin I SH3 domain deletion phenotypes. In order to determine whether the myosin I SH3 domain was interchangeable to SH3 domains in its peptide-binding-motif specificity class, I could not rely on other *S. pombe* SH3 domains, as the myosin I SH3 domain is the only class III SH3 domain in yeast (Verschueren et al., 2015). It has also been suggested that within a single organism, SH3 domains evolve different specificity classes and furthermore that, within a single pathway, SH3 domains may have evolved different peptide-binding preferences in order to linearly and consistently translate signal into output (Kelil et al., 2016; Ali Zarrinpar et al., 2003). Though this hypothesis has not

been verified experimentally, myosin I orthologs from *S. cerevisiae* have been shown to function in endocytosis similarly to the *S. pombe* myosin I SH3 domain, its sequence is conserved between yeast species, and both paralogs (Myo3p and Myo5p) of the *S. cerevisiae* myosin I contain class III SH3 domains (East & Mulvihill, 2011; Verschueren et al., 2015).

As a control for the experimental approach to query interchangeability, to partially examine the veracity of suppositions that orthologous SH3 domains fail to co-adapt specificity and to determine the interchangeability of myosin I's SH3 domain with respect to orthologous SH3 domains, I replaced the *S. pombe* myosin I SH3 domain with the *S. cerevisiae* Myo3p and Myo5p SH3 domain (**Figure 42**). Control cells are calibrated to previous measurements of the maximal number of capping protein (Acp1p) molecules assembled into endocytic structures (Julien Berro & Thomas D. Pollard, 2014). Relative to control, when myosin I is deleted in *S. pombe* cells, there is a reduction in the overall amount of capping protein assembled into endocytic structures at the point of scission, constituting an ~30% reduction in the maximal number of capping protein molecules assembled into endocytic structures. When paralogous SH3 domains from the orthologous myosin I in *S. cerevisiae* are inserted into the *S. pombe* myosin I SH3 locus, replacing the native SH3 domain, there is a partial rescue of this capping protein assembly defect. Though there is still a significant difference ($p < 0.0001$, both) from control, significantly more ($p < 0.0001$, both) capping protein maximally assembled into endocytic structures relative to the *S. pombe* myosin I SH3 domain deletion strain. Relative to control, replacement of *S. pombe's* myosin I SH3 domain with either of *S. cerevisiae's* paralogous myosin I SH3 domains maximally reduces the amount of capping protein assembled into endocytic structures by ~15%, although the reduction of capping protein is not as pronounced at all stages of endocytosis. The Myo3p SH3

domain has assembled more capping protein at scission than the Myo5p SH3 domain, though, the maximal assembly rate achieved between strains does not differ (Welch's t-test, $p = 0.083$).

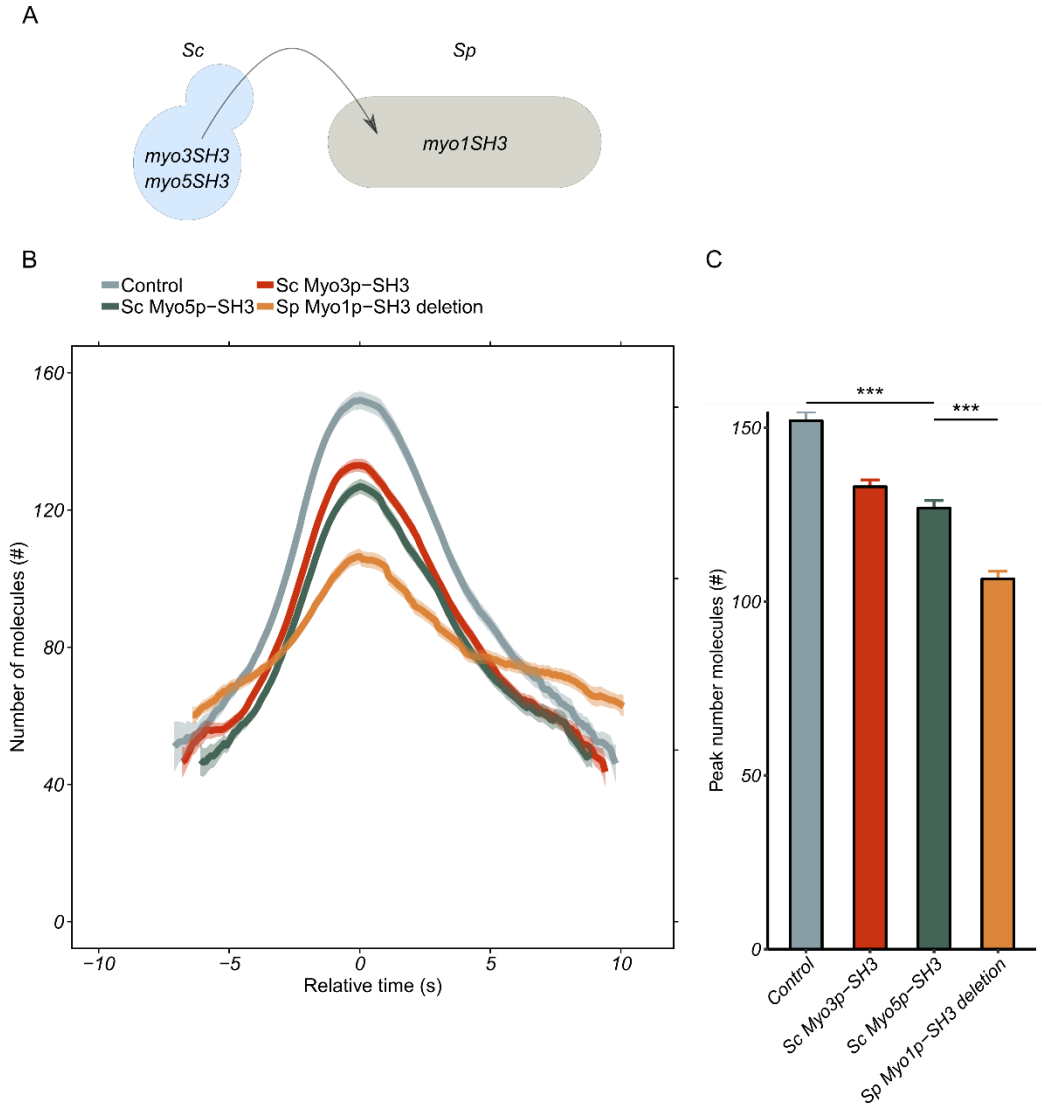

Figure 42. *S. cerevisiae* myosin I SH3 domains partially rescue *S. pombe* myosin I SH3 domain deletion phenotypes. (A) Replacement of the *S. pombe* (brown cell) myosin I SH3 domain (*myo1SH3*) with either the myosin I paralog, Myo3p, SH3 domain (*myo3SH3*) or the paralog, Myo5p, SH3 domain (*myo5SH3*) from *S. cerevisiae* (blue cell). (B) Number of capping proteins assembled into endocytic structures in time relative to scission at t=0s. Ribbon shows 95% CI. In all strains, capping protein is fused with EGFP for tracking in quantitative microscopy but in control cells, there are no modifications to SH3 domains. Sc = *S. cerevisiae*; Sp = *S. pombe*. (C) The peak number of molecules for various strains. Error bars show upper 95% CI. Welch's t-test significance codes: NS = $p > 0.05$; * = $p \leq 0.01$; ** = $p \leq 0.001$; *** = $p \leq 0.0001$.

The *S. cerevisiae* myosin I SH3 domains rescue *S. pombe* myosin I SH3 domain deletion lifetime defects and partially rescue assembly rate defects (**Figure 43**). ~5s before scission, there is a burst of actin assembly, associated with a linear increase of capping protein up until scission. In myosin I SH3 domain deletion cells, this burst of capping protein assembly is delayed and the slope in increasing the rate per unit time before scission is also depressed, relative to control. However, in replacing the *S. pombe* SH3 domain with both paralogs of the *S. cerevisiae*, the assembly defect in the myosin I SH3 domain is rescued. The maximal capping protein assembly rate of myosin I SH3 domain deletion exhibits an ~3-fold reduction relative to control, while with the *S. cerevisiae* myosin I SH3 domains, cells exhibit only 10-20% reduction in the maximal assembly rate of capping protein into endocytic structures, though this is a significant reduction compared to control ($p < 0.001$, both). These results are mirrored by the maximally achieved capping protein disassembly rate, which is significantly reduced for all SH3 replacements and deletions ($p < 0.001$, all). Despite this, the overall disassembly rate of capping protein is between 15-20 molecules per second throughout disassembly of the actin coat for control and *S. cerevisiae* myosin I SH3 domain replacements but 4-6 molecules per second in myosin I SH3 domain deletion cells. This imbalance between assembly and disassembly rates leads to slightly longer disassembly times compared to assembly times and a right-skewed number of molecules distribution in time.

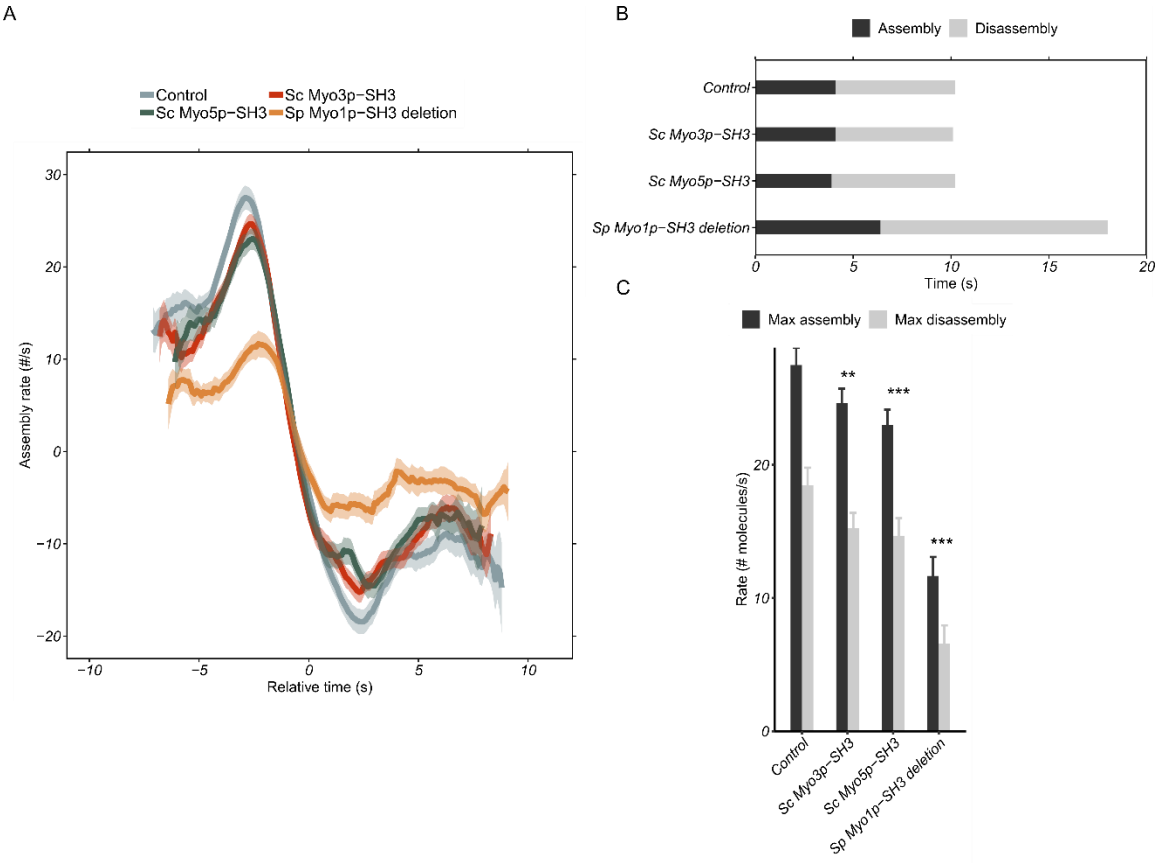

Figure 43. Rescue of lengthened endocytic lifetimes in *S. pombe* myosin I SH3 domain deletion by replacements with both paralogs of myosin I SH3 domains from *S. cerevisiae*. (A) The net assembly rate of capping protein into endocytic structures in time, relative to scission at t=0s. Ribbon represents 95% CI. (B) Full-width at half-maximum of the number of capping protein molecules assembled in time where dark bar represents the assembly time and gray bar represents the disassembly time for the indicated strain, such that their sum is the total endocytic time. (C) The maximum assembly and disassembly rate of capping protein achieved by each strain. Error bars show 95% CI. Welch's t-test significance codes: NS = $p > 0.05$; * = $p \leq 0.01$; ** = $p \leq 0.001$; *** = $p \leq 0.0001$.

The overall endocytic lifetimes can be determined by either relying on the detection limit or by taking the full-width time at half the maximum number of molecules (FWHM) after alignment. The FWHM total endocytic lifetime in myosin I SH3 domain deletion cells is dramatically increased, given long and dim tracks identified in these cells (data available in previous version). Myosin I SH3 domain deletion cells exhibit lengthened assembly times, relative to control, and dramatically longer disassembly times, perhaps due to a reduced disassembly rate throughout uncoating of the nascent endocytic vesicle. On average, the lifetime of endocytosis in myosin I SH3 domain deletion cells is ~80% longer, than control cells. Insertion of both paralogs of *S. cerevisiae* myosin I SH3 domains rescues both of these defects, exhibiting similar assembly times, compared to control, and similar disassembly times and similar overall endocytic lifetimes.

In addition to rescuing endocytic lifetime defects by replacing the myosin I SH3 domain with an orthologous domain from a different organism, the patch motility in cells where *S. cerevisiae* SH3 domains have replaced the native *S. pombe* myosin I SH3 domains are indistinguishable from control cells (**Figure 44**). As a network of actin is assembled, there is a moderate stabilization of endocytic structures just prior to scission in control cells. This is exhibited regardless of whether the cell's myosin I SH3 domain from *S. pombe* or *S. cerevisiae*. However, without its SH3 domain, the motility of endocytic structures in the cell remains small, near the detection threshold. Around scission, the endocytic structure is detached from the membrane and moves diffusively as a nascent vesicle. In myosin I SH3 domain deletion cells, around scission, the motility increases but saturates and does not move to the same extent that control cells do. In cells where the *S. pombe* myosin I SH3 domain is replaced with both paralogs of the *S. cerevisiae* myosin I SH3 domains, the motility of the patch does not significantly differ from control throughout endocytosis. The full rescue of motility defects in the myosin I

SH3 domain deletion strain by insertion of *S. cerevisiae* myosin I SH3 domains is reflected by overlapping cumulative path lengths of endocytic structures such that the average endocytic structure moves to the same extent and at every stage of endocytosis regardless of whether its myosin I SH3 domain is endogenous to *S. pombe* or exogenous with *S. cerevisiae* SH3 domains. Given the reduced motility of myosin I SH3 domains after scission, the average cumulative path length of endocytic structures is significantly reduced after scission, relative to control. Thus, the *S. cerevisiae* myosin I SH3 domains fully rescues *S. pombe* myosin I SH3 domain deletion motility defects, suggesting interchangeability of myosin I SH3 domain with orthologous SH3 domains.

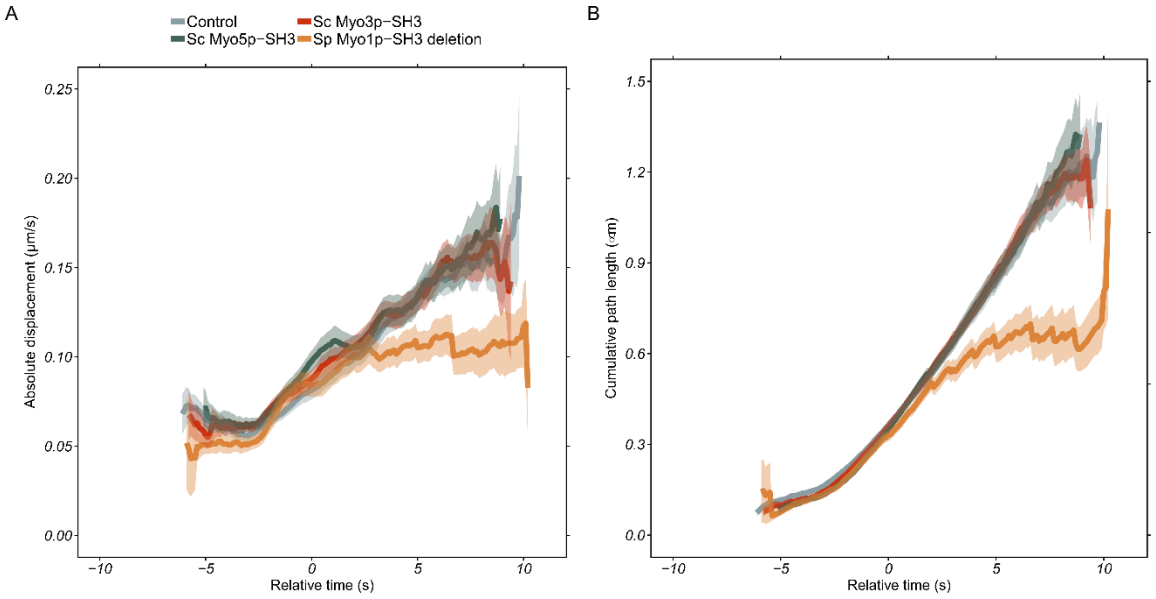

Figure 44. *S. cerevisiae* myosin I SH3 domains do not exhibit altered endocytic patch motility, fully rescuing *S. pombe* Myo1pSH3Δ defects. (A) Absolute displacement of tracked endocytic structures for indicated strains in time, relative to scission at t=0s. Line shows mean absolute displacement of tracks for a particular strain at the indicated time; ribbon represents 95% CI. (B) Average cumulative path length traveled by moving endocytic patches throughout endocytosis for indicated strains. Ribbon shows 95% CI.

6. *Determining the range of SH3 domains' affinity and specificity sufficient for pathway assembly using mathematical modeling.*

Consider a SH3 domain that binds two ligands, namely proteins containing a Proline Rich Motif (PRM). The extent that this SH3 domain binds each ligand depends on the ligands' concentrations and the affinity of the SH3 domain for each ligand. If this domain is responsible for recruiting one of the ligands to a particular sub-cellular structure *in vivo* but not the other, then the SH3 domain must balance its affinity and local concentration to specifically interact with one ligand over the other in the appropriate cellular context. As a proof of principle, I used mathematical modeling to determine the range of affinity, specificity, and concentration that SH3 domains can exhibit in order to recruit proteins to endocytic structures *in vivo*.

A precise, mathematical definition of specificity helps elucidate how SH3 domain interactions are balanced in order to accomplish binding that is sufficient for pathway assembly. The specificity of a SH3 domain for a particular ligand can be described as a comparison between the extent that the SH3 domain binds one ligand compared to all others, which is a function of its ligand affinities and concentrations. The specificity of a SH3 domain for a particular ligand (PRM) can be defined as:

$$\alpha_{SH3_i:PRM_j} = \frac{[SH3_i \cdot PRM_j]}{\sum_{k \neq j}^{all\ PRMs} [SH3_i \cdot PRM_k]} \quad (1)$$

where α describes the specificity of the i^{th} SH3 domain for the j^{th} SH3 domain ligand, PRM_j. This specificity is defined as the fraction of the i^{th} SH3 domain that binds the j^{th} ligand compared to all other ligands. This formulation makes the assumption that SH3 domains do not appreciably bind other peptide motifs, which is reasonable given previous phage-display experiments to identify the sequences of linear peptide motifs bound to SH3 domains (Cheadle et al., 1994).

To develop numerical simulations based on this formulation, I relied on previously collected binding data and quantitative microscopy measurements, which allowed me to constrain the concentrations of reactants and affinities of SH3 domain interactions (Arasada & Pollard, 2011; Julien Berro & Thomas D. Pollard, 2014; Sirotkin et al., 2010). I used Equation (1) to vary the specificity and ligand affinities in order to predict the range that each SH3 domain needs to recruit the number of ligand molecules observed within endocytic structures.

In my numerical simulations, I initially assumed that one SH3 domain is responsible for recruiting all of its partner protein to endocytic structures. In some cases, this is a reasonable assumption, given that there are several reports in which a protein's localization to a sub-cellular structure is dependent on binding the SH3 domain within another protein (Krendel, Osterweil, & Mooseker, 2007; Pawson & Nash, 2003). The mechanism by which SH3 domains achieve interaction specificity influences the model. One possibility is that if contextual specificity dominates over domain-mediated specificity, then, in the shared context of endocytosis, many of the endocytic SH3 domains will recruit the same protein. This implies that there will be a high-degree of cross-reactivity. These overlapping binding interactions will constitute terms in the denominator of the specificity parameter for individual SH3 domains. However, this ignores consideration of timing as a term in the formulation and complicates modeling of assembly dynamics. Of course, different SH3 domain-containing proteins or their ligands localize to endocytic structures at different times and in different quantities. To account for this, without formulating a poorly constrained and overly complex model, I increased the local concentration of SH3 domains in sub-cellular structures to represent the situation of overlapping recruitment interactions, treating different SH3 domains as an ensemble. This allowed me to

recalculate the range of affinities and specificities required for a particular protein's recruitment.

7. Recruitment of Wsp1p by Myo1p's SH3 domain

There are 16 predicted binding sites of the myosin I (Myo1p) SH3 domain in the actin NPF WASp (Wsp1p) (Verschueren et al., 2015). This binding interaction has not been tested *in vitro* and it is unknown how Wsp1p is recruited, given that it potentially interacts with many SH3-domain containing proteins through its numerous proline-rich regions (PRs). There may be cross-talk between the myosin I actin assembly pathway and the WASp-mediated actin assembly pathway, suggesting an interaction *in vivo* (Sirotkin et al., 2010). I asked, *what affinity and specificity is required for Myo1p to recruit Wsp1p to endocytic structures*? This is an especially pertinent question because given the complexity, spatial scale, and speed with which the endocytic machinery is assembled, it is difficult to predict what the apparent affinity between molecules will be and it is hard to know the extent of cross-reactivity, given the high local concentrations of molecular components within endocytic structures compared to the cytoplasm (Sirotkin et al., 2010). Affinities, even if they were reported *in vitro*, may not be relevant *in vivo*, yet, measuring the affinity between Myo1p and Wsp1p *in vivo* is challenging. Thus, the question framed in this way allows us to answer the question what affinities and specificities can account for the observed recruitment in endocytosis.

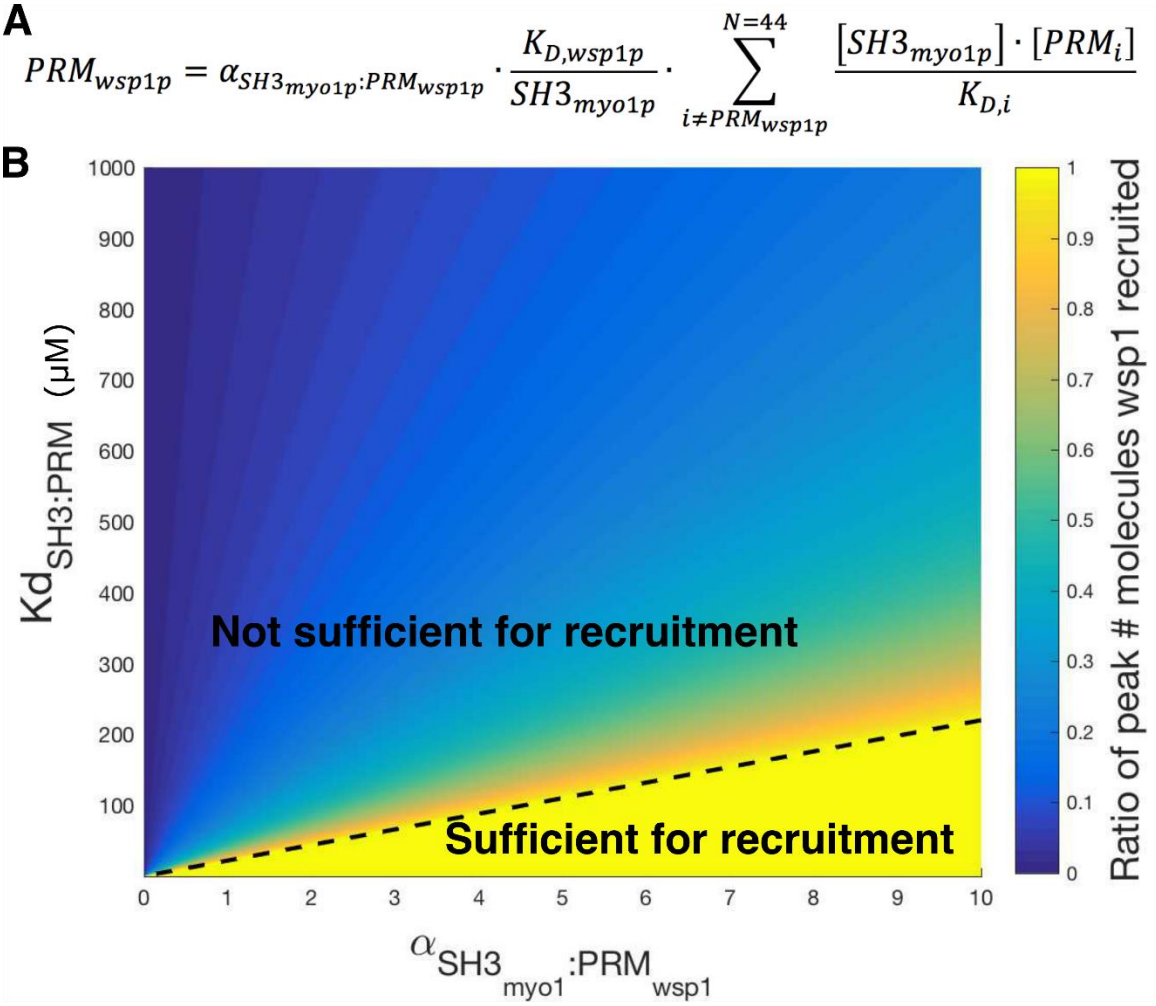

Figure 45. Numerical simulations describe range of affinity and specific sufficient for recruitment of WASp by myosin I's SH3 domain or vice-versa. (A) Formulation of the amount Wsp1p recruited, derived from Equation 1 and taking into account specificity, affinity of the binary interaction, concentration of myosin I within endocytic structures at the peak, the peak concentration of WASp, and the estimated amount of the myosin I SH3 domain binding all other PRM-containing proteins in endocytosis as based off previous measurements (Sirotkin et al., 2010). (B) Affinity and specificity yielding peak number of molecules of Wsp1p expected within endocytic structures, expressed as a ratio of the observed peak number of molecules of WASp in endocytic structures. Abline represents points at which the ratio of the numerically simulated concentration of WASp in the patch, given the affinity of the WASp and myosin I reaction with the indicated specificity of myosin I's SH3 domain for WASp, over the experimentally observed maximal concentration of WASp in the endocytic structure is equal to 1.

To answer this question, I developed a mathematical model based on the relationship of specificity, affinity, and concentration (Equation 1, **Figure 45A**). The results of my simulation show that for strong affinities (<1 μM), poor specificities ($\alpha \leq 1$) do not significantly deter Wsp1p's recruitment (**Figure 45B**). In this case, poor specificity indicates that relative to the ~44 other PRM-containing proteins in endocytosis, the myosin I SH3 domain interacts with a higher proportion of non-WASp proteins compared to WASp. Thus, even if the affinity of the myosin I SH3 domain is very high, the presence of a multitude of competitive interactors will dominate and fail to recruit WASp in sufficient concentration. When the binding preference of myosin I's SH3 domain for WASp is comparable to that of all other PRM-containing proteins in endocytosis, i.e., $\alpha = 1$, a greater than 100-fold increase in the binding affinity, from ~100 μM to <1 μM is sufficient for myosin I's SH3 domain to recruit WASp to endocytic structures. For relatively poor specificities, $\alpha \sim 1$, SH3 domains require strong affinities (<1 μM), in order to assemble and recruit proteins into pathways and sub-cellular structures. However, SH3 domains exhibit characteristically poor (~100 μM) affinities for their ligands. It is estimated that the strongest SH3 domain and PRM interaction is ~50 nM, although this affinity varies considerably and is only observed when the peptide is isolated, notably, when the SH3 domain is tested against the full-length protein, the interaction dissociation constant is weaker, ~10 μM (Desrochers et al., 2017; Desrochers, Lussier-Price, Omichinski, & Angers, 2015).

Due to conformational, regulatory, molecular or cellular contexts, a SH3 domain may exhibit high specificity for a particular PRM-containing protein compared to all other PRM-containing proteins. Given the high-degeneracy of the problem, the preference for one protein over all others is difficult to quantify in the context of the cellular pathway *in vivo*. These numerical simulations show that for high specificities ($\alpha > 1$), relatively low

affinities (>1 μM) are sufficient for a SH3 domain to assemble a protein into the pathway and recruit it to the relevant sub-cellular structure. In the range expected for SH3 domain interactions, if myosin I SH3 domain exhibits a 5 to 10 fold preference for WASp compared to all other PRM-containing proteins in endocytosis, then it will account for the entirety of WASp's recruitment to endocytic structures. If myosin I exhibits a 10-fold preference for WASp compared to other PRM-containing proteins, then even with a very low affinity (~1 mM), myosin I's SH3 domain will still recruit ~20% of the amount of WASp assembled into endocytic structures. This is significant because in that range, such an interaction would not be detected in phage-display or in *in vitro* binding experiments, even this model reveals that there is expected to be a biologically significant role for myosin I's SH3 domain in recruiting WASp (Hoffmann et al., 2010).

C. Discussion

1. Alternative approaches to identifying candidate SH3 domains to interrogate interchangeability

The goal of the first step in parsing out the extent to which SH3 domains are module that can be interchanged is to associate how binding interactions mediated by SH3 domains relate to the assembly of a particular pathway. Previous literature can be used to identify vital SH3 domains (Ali Zarrinpar et al., 2003). However, approaches that target only one SH3 domain for complementation by replacement with non-native SH3 domains are vulnerable to favoring one mode of achieving interaction specificity without ruling out the alternative. Yet, many pathways involving SH3 domains contain several SH3 domains, for example, in endocytosis there is a high degeneracy in the number of

SH3 domains and it is likely that the pathway evolved this degeneracy so that assembly of the necessary molecules is robust to perturbation (Kelil et al., 2016; Kurochkina & Guha, 2013; S. Li, 2005; B. Mayer & Saksela, 2005; B. J. Mayer & Saksela, 2006). Deleting single domains may not always produce observable defects. Workarounds include identifying sensitive genetic backgrounds or deleting and replacing multiple copies. However, the combinatorial of deleting and replacing is much larger, scaling with $\sim N^2$, which increases the amount of genetic engineering and strain creation and detailed quantitative analyses to unfeasible proportions. Instead, endogenous, single-copy deletions with a precise measurement, can be used as a first-pass to identify potential candidates.

Nonetheless, this approach has flaws because, in endocytosis for example, deleting a single SH3 domain may have deleterious effects not attributable solely to the loss of the SH3 domain. This can occur if the SH3 domain is required for a protein's localization, fold, or expression. As reported in chapters II and III, the localization of several SH3-domain containing proteins seems to be reduced, if not abrogated, upon deletion of the SH3 domain. However, expression does not seem to be affected by SH3 deletion. Thus, the identified defects stemming from endogenous, single-copy deletions of SH3 domains, while originally caused by deletion of a particular SH3 domains may have other proximal causes. For example, it could be the case that by deleting a particular SH3 domain, a single interaction is lost. That lost interaction is required for localizing the SH3-domain containing protein to endocytosis. Without the other domains in that protein, endocytosis exhibits observable defects. In this case, the replacement strategy is still valid: complementing the observed defect with a non-native domain implies that the non-native domain can rescue the lost interaction. However, the measurement is indirect and thus, more vulnerable to noise and less reproducible in other systems, *in vitro*, *in silico*,

or in other organisms *in vivo*. Thus, an experiment less vulnerable to confounders and easier to control may be to query localization of the protein. It is clear that, for example, myosin I requires its SH3 domain for robust localization to endocytic structures (data available in previous version). Thus, in some cases, clear localization phenotypes, rather than the extensive and time-consuming quantitative microscopy analysis can be used to query complementation of deletion phenotypes by non-native SH3 domain replacements and, thus, serve as an alternative, albeit complementary, approach to interrogating the extent of interchangeability between SH3 domains.

Regarding other controls, one concern is that replacement of the native SH3 domain with non-native SH3 domains is that the non-native SH3 domain will not fold as well as the SH3 domain. To limit this possibility, and thus limit the frequency of negative results, SH3 domains' peptide sequences were chosen such that that sequence used for replacement and deletion aligned and overlapped with a SH3 domain that had been purified, crystallized, and had its structure reported to high resolution (< 3 Angstroms, all). In addition, misfolded domains within a protein can lead to increased protein degradation (Goldenzweig & Fleishman, 2018; Parsell & Sauer, 1989). Thus, to control indirect and deleterious effects associated with the proposed approach to identify single SH3 domain candidates for replacements, I used image segmentation and quantitative fluorescence microscopy to ensure that proteins whose SH3 domain was deleted expresses at similar levels, regardless of its protein's localization with and without its SH3 domain. To date, no defects in expression were observed, suggesting that protein stability is not significantly affected by SH3 domain deletion or replacement; however, in the generalized approached to determining the extent of modular protein-interaction domains' interchangeability, if indirect and deleterious defects upon deletion are observed, one can make single point mutations in SH3 domains' WPY triad, which

disrupts binding interactions without affecting the domains' fold (Heim et al., 2017). I made such point-mutations in myosin I but did not extensively characterize the phenotypic effects of these point mutations in *S. pombe*, which have not been reported (Cheng, Grassart, & Drubin, 2012; Sun et al., 2006). If there is a significant difference between the SH3 domain deletion and these mutants, then a library of these mutants, rather than a deletion library, can be constructed and used to generate a library of non-native SH3 domain replacements to query complementation. This approach is more time consuming than deletion, as it requires more trial and error; however, it more directly determines how binding interactions mediate endocytic assembly compared to the current experimental approach.

2. *Challenges to interpreting measurements of endogenous, multiple copy SH3 domain deletion strains*

Deleting multiple copies in order to identify contexts in which native SH3 domains could be replaced by non-native SH3 domains to complement striking phenotypes is challenging. For one, creating a multiple SH3 domain deletion has to be done in series, given that the efficiency of single genetic editions is low and the chance of two simultaneous genetic editions is small (**Figure 34**). Given the genetic variability of lab strains, which pick up mutations when temporarily stored prior to or post-transformation, a standard strain quality control test is to back-cross genetically edited strains with a WT strain of the opposite mating type to check for spore growth variability. This should be done in addition to sequencing the genetic insert for positive editing. After creating up to 6 SH3 domain deletions, nearly 50% towards full deletion of endocytic SH3 domains in a single strain, a backcross revealed that the parent strain exhibited mating defects

(**Figure 36**). Thus, the multiple domain deletion library was compromised. These risks persist in a multiply edited strain and may challenge the extent to which precursor strains are comparable to strains later derived from those strains. In addition to the natural rate of mutation and the passing down of these variations, non-specific cutting by Cas9 may lead to an accumulation of indels or other mutations, perhaps more deleterious, in multiply edited strains. There is sparse literature on the effect of Cas9 on cells in single generations for fission yeast, let alone for multiple generations and rounds of genetic editing (Lemos et al., 2018).

Regardless of these challenges, strains positive for multiple SH3 domain deletions do not exhibit severe growth defects (**Figure 35**). Though the multiple SH3 domain deletions have accumulated mutations that result in variability in spore size, endocytosis does not appear to be affected by this accretion of variability between haploid strains (**Figure 37**). In some cases, endocytic SH3 domain-containing proteins have an intron within the SH3 genetic sequence and in mammals, this alternative splicing can lead to novel functions and cell-type specific isoforms (Gerth et al., 2019). In my multiple-copy SH3 domain deletion strains, these introns are deleted along with the domain and ignored, perhaps contributing additional artifacts.

When multiple endocytic SH3 domains are deleted within one cell, there tends to be an increase in actin assembly and lengthened endocytic lifetimes. However, it is hard to establish a SH3 domain dose-endocytic assembly response curve, partially due to limited variability in the combinations of different SH3 domains deleted within in the cell, but in large part due to the observation that double SH3 domain deletions phenocopy triple SH3 domain deletions. Consistent with the notion that individual SH3 domains regulate actin assembly during endocytosis (**Figure 21**), it is difficult to predict the combined effect of two SH3 domain deletion or three in the same pathway. While some

SH3 domains within proteins, for example Abp1p's SH3 domains, tend to exhibit overlapping influences on actin assembly and endocytosis, it is unclear whether their combined deletion will be additive or synergistic. In particular, using quantitative microscopy to determine the combined effects of multiple SH3 domain deletions is challenging. For example, deleting single-copies of Abp1's SH3 domains causes the cell to assemble less actin into cells but double SH3 domains cause more actin to be assembled into cells. In this case, the sign of the effect, relative to control, opposes simplistic interpretations of the combined deletion as additive or synergistic.

One explanation may be that deleting multiple SH3 domains severely disrupts the mediation of actin assembly in endocytosis. Given that endocytosis is a vital process for cells, the cells may respond to dysregulation of actin assembly or defects in the initiation of actin assembly by increasing actin assembly as compensation (S. L. Schmid, Sorkin, & Zerial, 2014). Alternatively, it may be that disrupting SH3 domains perturbs the competitive balance of interactions that mediate actin assembly primarily by removing barriers and inhibition to assembly and allowing WASp to activate the Arp2/3 complex without regulatory control. While many SH3 domains can be deleted without influencing actin assembly in endocytosis, most SH3 domains produce an effect on actin assembly, patch motility, or the cell's regulation of the number of endocytic events. This challenges the robustness of endocytosis to single-copy SH3 domain deletions and suggests that further perturbations to endocytic SH3 domains may incur more significant defects in endocytosis. However, without more precise understanding of the complex interplay of interactions, regulatory or recruitment, between SH3 domains and their binding partners during endocytosis, it is difficult to estimate the effect of deleting more than two SH3 domains. Given the additional challenge of genetically engineering multiple copy SH3 domain deletions in multiply edited cells, the utility of multiple SH3 domains will remain

limited until future work paints a more complete picture of the molecular systems biology mediated by endocytic SH3 domains *in vivo* and the effect of multiple rounds of CRISPR-Cas9 mediated genetic editing is resolved.

3. Limitations in determining the extent of interchangeability by complementation of deletion phenotypes with non-native SH3 domain replacements

If a SH3 domain cannot be replaced with another SH3 domain, it may be because the domain does not fold, which prevents it from exposure to the endocytic context. To control for this, one could use glycine-serine linkers, or any flexible linker inserts, to flank the termini of inserted SH3 domains into non-native endogenous loci. These kinds of insertions may allow for the stable non-native SH3 domain to fold without constraints from the native proteins' structure. Furthermore, for each domain, the effect of various linker lengths on endocytosis can be assayed to optimize the length of the flexible linker while simultaneously assessing the extent to which mis-folding contributes to phenotype. These experiments were not performed but were planned, given the partial rescue of myosin I SH3 domain deletion phenotype with orthologous protein's SH3 domains from a different organism (**Figure 40** - **Figure 44**). For example, both paralogs of the orthologous myosin I in *S. cerevisiae* can be tested with various flanking linkers in search of full complementation each of the *S. pombe* myosin I SH3 domain deletion phenotypes.

One challenge with screening linker lengths to validate negative deletion complementation by replacement results is that there is no obvious metric with which to determine an optimum linker length for insertion. Re-inserting the myosin I SH3 domain into a strain in which the myosin I SH3 domain was deleted does not exhibit any differences. Thus, one possibility is that linkers can be added to the N and C termini of the native SH3 domain and lengthened until a phenotype is detected. However, because there

is no example in which a non-native SH3 domain fully complements a native SH3 domain deletion phenotype across all endocytic quantitative microscopy metrics, it is difficult to identify a SH3 domain with which flanking its termini with linkers helps to stabilize the fold of the SH3 domain in the targeted locus. It may be possible to estimate the stability of a non-native SH3 domain in a non-native molecular context, namely within the protein it is being inserted into, via molecular dynamics. But, still lacking is a negative control in which an optimum linker length flanking the non-native SH3 domains will exhibits no differences from the WT protein in function or fold. Orthologous proteins are good candidates, and despite the uniqueness of the myosin I SH3 domain, it can partially be rescued by both paralogs of the orthologous myosin I SH3 domain in *S. cerevisiae*. Previous studies suggest that SH3 domains from other organisms may be more likely to complement deletion phenotypes than SH3 domains from within the same organism (Ali Zarrinpar et al., 2003). However, there is no demonstration that such a scenario exists in the context of endocytosis and given the extensive experimental controls that must be considered for each locus, a more feasible approach will be to identify a small number of loci, optimize the linker length for SH3 domains at those loci, and then, according to the combinatorial, insert non-native SH3 domains with the determined linker length. To reduce the likelihood that each SH3 locus has drastically different constraints and requires different linker lengths, SH3 domains flanked by unstructured regions within the proteins should be favored candidates for querying interchangeability. While higher-throughput methods to screen a larger number of SH3 replacements may provide more data to address the question, controls will need to carefully considered and implemented in order to ensure that a negative complementation result is really caused by the lack of some particular SH3 domain's interactions before domain-mediated specificity can be supported over contextual specificity.

Despite these limitations, if many SH3 domains, which are known to be stable in isolation, are not interchangeable in endocytosis, then at least a qualified explanation that SH3 domains' function is primarily dictated by contextual specificity will be warranted. Here, the qualification may be that the poor-sequence conservation in the non-binding regions may, in part, be due to the adaption of the SH3 domain its native context, namely balancing stability with the constraints of the native protein's conformational bounds. In that case, the development of linkers may yet allow SH3 domains to be used as interchangeable modules in synthetic biology. However, whatever the case, a modified hypothesis to the general explanation that SH3 domain-mediated interactions are only contextual specific still needs to be tested. A modified hypothesis is that, *for SH3 domains in the same specificity class, contextual specificity dominates domain-mediated specificity and only SH3 domains within the same specificity class are interchangeable*. This modified hypothesis is plausible, even in consideration of the underlying assumptions in the current literature, given that SH3 domains in the same specificity class can bind peptide motifs found in many unstructured positions within proteins, suggesting that, at least in principle, SH3 domains in the same specificity class could bind overlapping sets of proteins (Saksela & Permi, 2012; Verschueren et al., 2015). This modified hypothesis can be subjected to experimentation by a similar approach: one can replace SH3 domains with non-native SH3 domains from each of the three ligand specificity classes and determine whether intra-class replacements more frequently rescue deletion phenotypes than inter-class replacements. I have begun this set of experiments but first, the priority is to determine the appropriate linker length to flank non-native SH3 domain insertions in at least 3 loci (according to specificity class) so that the non-native SH3 domain genetic replacement strategy can be standardized and enough replacements can be tested to compare frequencies between and within specificity classes.

On the other hand, if individual SH3 domains in fact exhibit domain-mediated specificity within and despite its ligand specificity class, then I will use my existing SH3 domain deletion library to more fully characterize the influence of each SH3 domains on endocytosis, especially by completing the tracking and quantification of the assembly of SH3 domain-containing endocytic proteins. The completion of these studies will allow one to construct a constrained system of differential equations to predict assembly, which would yet allow the manipulation of endocytosis and SH3 domain-mediated interactions in synthetic pathways to proceed, as envisioned, albeit, with considerable nuance and precision hitherto not appreciated (Bhattacharyya et al., 2006; B. Mayer & Saksela, 2005). Further characterizing the influence of SH3 domains in endocytosis could involve tracking other endocytic markers, for example, other actin associated proteins involved in endocytosis, such as fimbrin or early-stage endocytic proteins, like Clc1p (clathrin light-chain) or End4p (Huntingtin interacting protein), and late-stage endocytic proteins, like Crn1p (coronin) or Hob1p (BAR adaptor protein) in SH3 domain deletion or mutant strains (M. Kaksonen et al., 2005). This progression of studies encompasses future work that will allow us to more deeply determine the role of each SH3 domain in the assembly of the endocytic pathway, regardless of their specificity, while advancing the prospects of using SH3 domains in synthetic biology.

4. SH3 domains do not solely achieve interaction specificity from context

Given that replacing myosin I's SH3 domain with other endocytic SH3 domains does not rescue deletion phenotypes, we might rule out the possibility that SH3 domains achieve interaction specificity through context alone. However, this would be a mistake, and limited by the same scope as previous queries into the extent to which SH3 domains are interchangeable in the cell (Ali Zarrinpar et al., 2003). The issue is that the myosin I

SH3 domain swap results only indicate that the myosin I SH3 domain might not be interchangeable. Of particular note is that myosin I's SH3 domain is the only class III SH3 domain in yeast, at least across four yeast species (Verschueren et al., 2015). Previous reports in the budding yeast *S. cerevisiae* show that only the Sho1p SH3 domain is not interchangeable while failing to query other SH3 domains (Ali Zarrinpar et al., 2003). Thus, how generalizable are such particular findings? This remains an open question.

Yet, the overall interchangeability approach may have a limited capacity to fully address this question because, in investigating the interchangeability of SH3 domains, we need to assume that SH3 domains' only function is to interact with other proteins, namely, in order to connect its native protein to others in the right place and at the right time (Bhattacharyya et al., 2006; B. Mayer & Saksela, 2005; B. J. Mayer & Saksela, 2006). This is generally accepted, but difficult to exhaustively and comprehensively verify. There are some examples in which SH3 domains are phosphorylated or alternatively spliced, which enable the SH3 domain to exhibit different behaviors in the cell or different interaction partners such that replacement with a non-native SH3 domain would fail to complement phenotypes partially caused by influences of the SH3 domain in the pathway that extend beyond simple binding (Gerth et al., 2019). Given that the third peptide binding specificity class is reserved for SH3 domains that bind non-canonical peptide motifs, i.e., linear peptide motifs that extend beyond the classic PXXP binding motif, it is possible that myosin I may have an influence on the endocytic pathway that cannot be complemented solely by rescuing its interaction partners. In that case, then no SH3 domain can replace the native domain.

The extent to which this generalizes to other SH3 domains remains unclear. Yet, given that single SH3 domain deletions significantly influence actin assembly and

endocytosis, it seems likely that their sequence adapts to their molecular context, under the assumption that SH3 domains possess one function: overlapping protein-interactions. The extent to which the phenotypes observed from single- and multi-copy SH3 domain deletions within cells can be explained by overlapping protein-interactions and their variance determined by the differential timing and roles of the other domains in SH3-domain containing proteins can be addressed by mathematical modeling. This may address the feasibility of contextual specificity. However, current results suggest that there is, to some extent, domain-mediated specificity. Even orthologous domain replacements exhibit some defects in actin assembly and endocytosis. Furthermore, replacements with non-native, non-orthologous SH3 domains phenocopies myosin I single-copy SH3 deletion. In the condition in which the molecular context requires a certain SH3 domain sequence for function, which seems to be the case, then even if no *in vivo* binding specificity is realized, there remains room for domain-mediated specificity of SH3 domains because a specific SH3 domain sequence is required for interchangeability. Though weakening the initial hypothesis, there remains the possibility that structural information and prediction can be used to predict which SH3 domains are likely to be interchangeable at a given genetic locus. Then, the question, are SH3 domain binding interactions in the same cellular context specific, remains open.

5. Interchangeability in the case of partial rescues

When Bzz1p's SH3 domains are inserted into Shd1p's two most N-terminal SH3 domain loci, and vice versa, cells still have 3 SH3 domains, in total, deleted but, nonetheless, there is a partial rescue of the quintuple SH3 domain deletion actin assembly defect (**Figure 40**). In contrast, when Shd1p's two SH3 domains replace Bzz1p in cells where, overall no SH3 domains are deleted, but endocytosis in the Bzz1p

SH3 domain replaced cells phenocopy a strain in which the Bzz1p SH3 domains are deleted (**Figure 39**, red and green curve). This begs the question, are Bzz1p and Shd1p SH3 domains interchangeable? Further complicating the interpretation of these results is that, in single-copy replacements and deletions, there can be partial rescue for some phenotypes, for example, motility and cumulative path length of endocytic structures, but not for other defects, namely, actin assembly. In these cases, what dictates whether, overall, these domains are interchangeable?

It is a challenge to un-ambiguously interpret multiple SH3 domain replacement data as a way determine interchangeability because it is difficult to test every combinatorial and incremental replacement experimentally. However, in the single-copy replacement strategy, the differential results of partial and complete rescue across different metrics supports domain-mediated rather than contextual specificity. Indeed, it seems plausible that the *S. pombe* myosin I SH3 domain is uniquely required for normal actin assembly in cells. However, the domain is interchangeable with the *S. cerevisiae* SH3 domain insofar as the SH3 domain influences the overall lifetime of endocytosis and the motility of endocytic structures. In the latter case, contextual specificity is important and in the former, domain-mediated specificity is critical.

This seems to leave open the possibility that contextual specificity is not critical because, if the myosin I SH3 domain does not influence patch motility or the lifetime of an endocytic event, or indirectly does so, then replacement should not matter. However, the myosin I SH3 domain exhibits significantly different endocytic patch motility and lifetime upon deletion and even in the case that the influence is indirect, it stands that replacing the SH3 domain with a non-native domain rescued some but not all phenotypes. Rather than concretely and summarily favoring one mechanism of SH3 domain interaction specificity, my results highlight the nuance that one should consider

interchangeability as an independent predictor in the phenotypic response for a particular pathway. If one can decouple the different phenotypes resulting from a single SH3 domain deletion, then the interchangeability with respect to each phenotype can be expressed in fractional form. The overall interchangeability of a particular SH3 domain for the pathway can then be approximated as a combination of the collected phenotypes: $Interchangeability\ in\ endocytosis \sim \beta_{Phenotype\ 1} * Interchangeabilty_1 + \beta_{Phenotype\ 2} * Interchangeabilty_2 + \cdots + \beta_{Phenotype\ n} * Interchangeabilty_n$, where interchangeability adopts a value between 0 and 1, and the β coefficients can be determined by weighted regression (nonlinear, multiple linear, or logistic regression) for each phenotype against a pre-determined response, e.g., the weight of motility versus the number of endocytic events obtained by regressing the number of molecules versus motility and the number of endocytic events.

In this sense, it is unlikely that a particular pathway has a SH3 domain that is perfectly, 100% interchangeable. If interchangeability was near unity for the overall pathway, the question would remain to what extent can all SH3 domains replace that particular SH3 domain. Nonetheless, the experimental approach and methodological tools I've developed can sufficiently answer particular questions and determine the interchangeability of a set of SH3 domains for a particular phenotype. For example, one goal of the project was to determine the extent to which endocytic SH3 domains are interchangeable with each other for assembly. While endocytic SH3 domains are not entirely interchangeable in this respect, their replacement produces a variety of different effects and, as a result, the overall rate of endocytosis can be manipulated without incurring growth defects. In that regard, the prospect for using SH3 domains to manipulate the process of endocytosis and for using interchangeability to learn more about the different interactions mediated by SH3 domains remains open.

6. Future directions and outlook

I have developed an approach to determine the extent to which SH3 domains are interchangeable in a pathway. This can allow one to either (A) target poorly interchangeable loci for study and therapeutic manipulation or (B) build synthetic pathways from SH3 domains that are interchangeable. The realized utility of this approach has highlighted the need for a nuanced notion, namely, that interchangeability depends on the phenotype and context. For example, SH3 domains may be interchangeable in modulating patch motility but not actin assembly. Furthermore, non-native SH3 domains may rescue severe phenotypes but fail to fully complement deletion phenotypes. It remains a challenge to clearly distinguish between domain-mediated and contextual specificity. However, partial rescue of deletion phenotypes by orthologous SH3 domains provides an avenue with which to optimize non-native SH3 domain insertions. Implementation of these measures could validate the failure of non-native SH3 domain replacements to complement deletion phenotypes and strengthen support of the hypothesis that SH3 domains participate in unique pathways by exhibiting unique, domain-mediated specificities, regardless of the context. Thus, the immediate next steps of the project are to optimize the linker for inserting orthologous SH3 domains into the myosin I SH3 domain locus and simultaneously testing if the frequency of inter-class interchangeability is lower or higher than intra-class interchangeability.

D. Methods

1. Identifying good candidates for replacement in a cellular pathway

For each SH3 domain in a pathway, it is not immediately obvious that single deletions domain deletions will produce observable defects. As such, it follows that for those domains which do not produce clear deletion phenotypes, rescue by interchanging the native domain with a non-native SH3 domain cannot be queried. Thus, the first step is to identify conditions in which the native SH3 domain is essential. In a typical genetics experiment, this may take the form of identifying a sensitive genetic background such that deletion of the SH3 domain produces an observable phenotype. However, given the high degeneracy in the number of SH3 domains in pathways, and in particular, in endocytosis, a more reliable and precise method is quantitative microscopy, which is sensitive to detecting small defects in the assembly of a pathway upon SH3 deletion.

Thus, the first step is to identify and determine the influence of each SH3 domain in a pathway using quantitative microscopy in fission yeast and endogenous, single-copy deletions of SH3 domains. If this produces an observation than replacing the deleted locus with a non-native SH3 domain can determine whether the domain or the context of the protein is essential to this influence.

In the context of endocytosis, my working hypothesis was that SH3 domains help assemble the endocytic pathway by recruiting proteins through binding. To test this hypothesis, I deleted endocytic SH3 domains in fission yeast and used quantitative fluorescence microscopy to spatiotemporally track endocytic structures. This allowed me to determine the influence of each SH3 domain on the assembly and dynamics of endocytosis. Moreover, it allowed me to identify SH3 domains in different specificity classes that are good candidates to interrogate the importance of the particular domain

and context of that domain via replacement of the native SH3 domain with non-native SH3 domains to query rescue of the observed phenotype.

These studies have the potential to establish a novel, albeit low-throughput, approach to rule out or substantiate the domain-mediated specificity model of SH3 domain binding to quantitative precision, which would overcome prior limitations in our understanding and inform synthetic pathway designs that use protein-interaction domains. Moreover, these studies clarify explanations that describe basic principles of how protein-interaction domains assemble proteins into vital cellular pathways and, in particular, these results provide a single framework for understanding the role that SH3 domains play in assembling cellular pathways, namely as mediating interactions particular to individual domains.

2. Distinguishing between domain-mediated and contextual specificity

To determine the interchangeability of SH3 domains in a single context, I endogenously replaced endocytic SH3 domains with SH3 domains from other proteins, organisms, and pathways. The rationale is that if SH3 domains can achieve binding specificity to assemble proteins into distinct pathways through (1) *domain-mediated* or (2) *contextual specificity*, then replacing a native domain with a non-native domain, which has the same molecular and cellular context, will either (1) fail or (2) succeed to rescue the native domains' deletion phenotype(s). If exchanging a native SH3 domain for the SH3 domain of a different protein partially complements a deletion phenotype, then context may not be more critical than domain-mediated specificity (**Figure 46**).

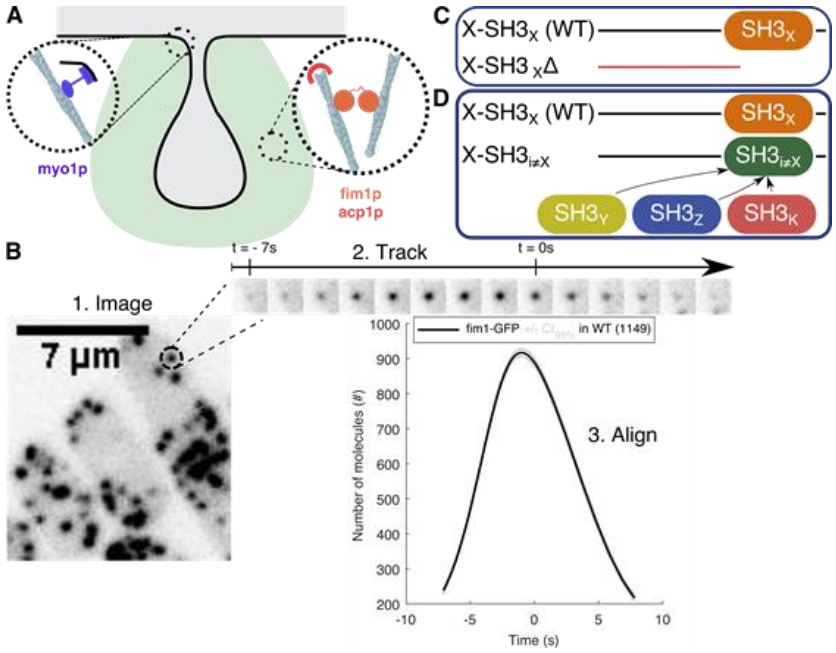

Figure 46. Overview of experimental approach to distinguish between domain-mediated and contextual specificity. (A) Proteins of interest in the context of endocytosis ~2s before scission. (Left) Myosin I localizes near the base of the invagination before scission and binds actin and membrane. (Right) Proteins used to monitor endocytosis in the context of various perturbations to endocytosis, e.g., by endogenous single-copy SH3 domain deletion. Fim1p is an actin cross-linking protein with 2 actin-binding domains. Acp1p is an actin capping protein the caps the barbed ends of polymerizing actin-filaments. (B) Quantitative fluorescence microscopy in S. pombe to monitor the assembly & dynamics of the endocytic pathway. Live cells are imaged, tracked, and then temporally aligned relative to scission at t=0s. (n) represents number of tracks used to produce average curve. (C) Identification of good candidates for replacing the indicated native SH3 domain, $SH3_X$ with non-native SH3 domains. The SH3 domain is a good candidate if perturbing it, e.g., by deletion, displays an observable defect. (D) This phenotype can be complemented by rescue with non-native SH3 domains. This involves endogenously replacing the native SH3 locus with the SH3 domain sequence from non-native proteins, e.g., $SH3_Y$, $SH3_Z$, or $SH3_K$. This approach tests interchangeability because the replacements can either (1) complement the quantitative microscopy observed defect, in which case, the particular domain is less critical than the context for the particular SH3 domains' assembly role, favoring contextual over domain-mediated specificity, or the replacements can (2) fail to complement the deletion phenotype, in which case, the particular domain is responsible for the native SH3 domains' influence on pathway assembly, favoring domain-mediated over contextual specificity.

In examining the mechanism by which SH3 domains achieve interaction specificity, I used the fission yeast *Schizosaccharomyces pombe* as a model organism to monitor the localization and influence of each SH3 domain in endocytosis (results reported in chapter II). Briefly, using CRISPR-Cas9 mediated genome editing, I deleted each endocytic SH3 domain in fission yeast. In each of these strains, I fused a green fluorescent protein (GFP) to an endocytic protein. To assess endocytosis, I relied on the actin capping protein Acp1p because this protein is a good proxy for actin assembly in endocytosis, which is required for endocytic pit elongation, vesicle scission, and vesicle movement (J. Berro & T. D. Pollard, 2014; Mooren, Galletta, & Cooper, 2012). I imaged these strains using spinning-disk confocal microscope, which allowed for fast, z-stack imaging; this is critical since endocytosis takes ~20s. This analysis revealed good candidates for replacement, especially the SH3 domains of Cdc15p, Bbc1p, and Myo1p, which exhibit striking deletion phenotypes and have been grouped into the peptide-interaction specificity class I, II, and III, respectively (Verschueren et al., 2015).

To broadly scope out the limits of the extent to which SH3 domains are interchangeable, I replaced SH3 domains that influence endocytic assembly with SH3 domains from (a) other endocytic proteins in different ligand specificity classes, (b) non-native endocytic proteins from a different organism (*S. cerevisiae*), and (c) multiple different native SH3 domain replacements with a single, non-native SH3 domain. In the future, these studies could be extended to replace native SH3 domains with (d) a non-endocytic protein's SH3 domain from *S. pombe*, and (e) human proteins associated with disease (especially, **Table 2**).

For non-native SH3 domain-replaced strains, I used CRISPR-Cas9 mediated gene editing to endogenously integrate non-native SH3 domains into native SH3 domain genetic loci, replacing these domains endogenously. To ensure that the insertion of a non-

native SH3 domain did not affect the localization and expression of the protein, I fused GFP to the domain-replaced protein and used quantitative microscopy to check its localization and expression. I controlled my replacement strategy by swapping native SH3 domains of select *S. pombe* proteins with the SH3 domain of orthologous proteins from *S. cerevisiae*. The rationale behind this control is that I expect that endocytosis for orthologous domain replacements will be identical as in wild-type cells since orthologous SH3 domains have a high sequence identity and are in the same ligand specificity class (Verschueren et al., 2015).

Strains for multiple SH3 domain deletions and swapping were created by NGR. Strains in which myosin I's SH3 domain from *S. cerevisiae* (Myo3p and Myo5p SH3) were integrated into myosin I's SH3 domain locus in *S. pombe* were created by Ronan Fernandez.

3. Using mathematical modeling to design a complex system of interacting proteins

Specificity can be defined mathematically for a particular ligand as parameter equal to the ratio of the amount of that ligand bound by a particular molecule over the amount of all other ligands bound by that molecule (Equation 1). To relate interaction specificity to macromolecular assembly and using the well-defined concept of affinity and quantitative microscopy experiments to inform assembly dynamics, we used systems of differential equations to determine the range of SH3 domains' affinity and specificity sufficient for endocytic assembly (Berro et al., 2010; Tonikian et al., 2009). We used numerical simulations to describe how SH3 domains recruit proteins to endocytic structures across a range of affinities and specificities. This model and its predictions allow one to determine what SH3 domain binding specificities are required for endocytic assembly.

An assumption that underlies this model is that the peak amount of protein assembled, as measured in quantitative microscopy experiments, represents the total amount of protein required to be assembled (Sirotkin et al., 2010). This will not be the case if there is significant turnover of the endocytic machinery during the process of endocytosis (Francis et al., 2015). However, in the case in which the machinery is turned over approximately a constant number of times, as suggested by a recent study, then the range of affinity and specificity required to recruit a SH3 domain-containing protein by a PRM-containing protein or vice versa will only be changed by a constant factor (Lacy, Baddeley, & Berro, 2019).

To perform these numerical simulations, I relied on specificity class data in which a particular SH3 domain, for example, myosin I is known to interact with ligands carrying a particular linear peptide motif, based of purification of its SH3 domain and a series of synthetic peptide binding assays (Verschueren et al., 2015). In the case of myosin I, it is predicted to bind multiple sites in Wsp1p, and there is expected to be cross-talk between myosin I and WASp-mediated actin assembly pathways (Sirotkin et al., 2005). Other candidate SH3 domain ligands were identified using motif searches within endocytic proteins, which identified non-specific interactions. Using measurements that correlate affinity with yeast-two hybrid assays, an affinity for each of these ligands was estimated (Tonikian et al., 2009). Then, using the formulation in equation (1), the concentrations of components in the patch was calculated and the affinity and specificity was varied. These models allowed me to quantitatively describe SH3 domains' role in endocytic assembly and predict previously unmeasured SH3 domain-ligand binding affinities (Arasada & Pollard, 2011). Modeling was executed in MATLAB and Python, available as "affinityVSspecificity.py" and "myo1SH3_WASp_specificity.m" at https://git.yale.edu/ngr4 (authored by NGR).

4. Patch tracking and temporal-super-resolution alignment

The number of molecules was calibrated to previous measurements of (Acp1p, ~ 152 molecules at the peak assembly; Acp2p, ~250 molecules at the peak of assembly; or, fimbrin ~800 molecules at the peak of assembly) during one day of calibration imaging and later fixed for all subsequent quantitative microscopy experiments (Julien Berro & Thomas D. Pollard, 2014; Sirotkin et al., 2010). Due to day-to-day and longer time-scale variability in the effective laser power illuminating cell samples, the absolute number of molecules can differ for the marker across different reported experiments. Instead of adjusting for these variabilities, all experiments are compared to measurements from a control strain. Comparisons are only analyzed if all strains were imaged in a single day. A custom-made temporal alignment software was used to analyze some experimental data (J. Berro & T. D. Pollard, 2014). Patch tracking was primarily done for cells loaded onto gelatin pads. Recent data, specifically for replacing myosin-I's native SH3 domain with the SH3 domain sequence from *S. cerevisiae* were performed using a microfluidic perfusion system (described above and reported to be robust and reproducible in detecting small differences across a range of experimental conditions) (Lemière & Berroa, 2018).

V. Summary

The studies described in this dissertation broadly focus on molecular assembly within living cells. To effect biological function in cellular processes, molecules must be spatiotemporally brought together to interact and actualize a higher-order phenomenon of emergent biological activity. Biological molecules can be assembled to effect such function through a coordinated sequence of protein interactions. Recently, these sequelae have been associated with the emergent phenomenon of phase separation and one of the components associated with inducing this molecular ensemble, the SH3 domain, is one of the most ubiquitous modular protein-interaction domains within cells and cellular pathways.

To study the role of modular protein-interaction domains on endocytic molecular assembly, I observed and experimented with SH3 domains in the cellular context of endocytosis, which is significantly enriched for SH3 domain-containing proteins. In endocytosis, molecules are assembled within ~20s at the plasma membrane to overcome mechanical barriers to internalization, fold in the membrane and ingest macromolecules, including nutrients, proteins, and lipids, and other material from the extracellular space, such as viruses and bacteria. The dynamic molecular assembly of the endocytic pathway is a vital cellular process that influences many different biological activities that impact human health across a variety of spatiotemporal scales. As such, understanding how molecules are assembled into the endocytic pathway may have broad impacts.

In these studies, I revealed that individual SH3 domains have diverse influences on actin assembly and endocytosis in the cell. While observational studies are limited in their mechanistic insight, I described a range of endocytic SH3 domain activities within the cell that future explanations will need to account for. In particular, diversity of

influence, rather than idiosyncratic and overlapping phenotypes across a library of endogenous, single SH3 domain deletion strains, adds nuance to the purported role of SH3 domains in inducing phase separations within the cell that promote local actin assembly.

Degeneracy in the copy-number of SH3 domains within endocytic proteins and within the endocytic pathway may enable multivalent interactions to form functional, phase-separated structures. But if this were true, then deleting a single SH3 domain would reduce the propensity of the endocytic molecular machinery to phase separate, barring compensation. Some SH3 domains, including Lsb1p's, Myo1p's, Abp1p's first and second, and Bzz1p's second SH3 domain promote actin assembly in the cell. However, Cdc15p's, Bbc1p's, and Mug137p's SH3 domain restrict actin assembly during endocytosis. These results indicate that deletion of SH3 domains, which is predicted to reduce the propensity to phase separate, does not necessarily reduce actin assembly in local endocytic structures.

On the other hand, deleting a single SH3 domain may not significantly reduce the valency of SH3 domains within the endocytic pathway. If this were true, then deleting a single valent unit may not produce observable effects because endogenous, single deletions would not noticeably perturb the formation of endocytic localized, phase separated structures that promote actin assembly. However, on the contrary, deletion of individual SH3 domains reveals noticeable defects in actin assembly during endocytosis. Some SH3 domains do not exhibit striking phenotypes upon deletion, leaving open the possibility that they form phase-separated structure at endocytic sites. But, if phase-separation is functional and plays a role in promoting local actin assembly, then deletion of single valent units should not produce diverse effects on actin assembly in

endocytosis. To the contrary, I observed that SH3 domains have diverse influences on actin assembly during endocytosis.

In any case, if SH3 domains' role in endocytosis is to promote the formation of localized, phase-separated structures that facilitate a burst of actin polymerization, then the results described here suggest that this explanation needs to be expanded in order to contend with the fact that altering the kinetics of actin assembly factor interactions in endocytosis can also explain the observed range of SH3 domain influences on actin assembly during endocytosis. The observed range of SH3 domain influences on actin assembly is consistent with perturbations to a minimal model of actin assembly during endocytosis and leaves open the possibility that a plethora of competitive and overlapping interactions amongst nucleation promoting factors within endocytic structures effectively regulates the activity of the Arp2/3 complex, an actin nucleator. By coordinating the activity of the Arp2/3 complex activators, SH3 domains may regulate actin assembly during endocytosis in addition to playing recruitment and assembly roles.

By observing the patterns of variation for several different quantitative metrics across a library of endogenous, single endocytic SH3 domain deletions, I found that perturbations to molecular assembly correlate with variations in patch motility. This suggests that molecular assembly may control the motion of the endocytic patch during endocytosis. On the other hand, given that these analyses cannot resolve the temporality of this dose-response relationship, the motility of endocytic patches may feedback into molecular assembly. Despite a local association between patch motion and molecular assembly, global cellular features, such as capping protein expression and the rate of endocytosis in various SH3 domain deletion cells, exhibit low or negligible correlations with variations in local endocytic behavior. This may indicate that SH3 domains indirectly effect cell-wide phenotypes. These analyses don't strongly

suggest causality but their dose-response relationships motivate future study, especially to distinguish between whether these patterns of variation are idiosyncratic to SH3 domains or whether they reveal rules governing endocytosis. In particular, analyzing these patterns across distinct genetic, mechanical, or chemical perturbations to the cell may reveal which effects are peculiar to SH3 domains while providing consistency to strengthen the supposed causal relationships between properties whose variations do not depend on the type of perturbation.

In addition to influencing local actin assembly within endocytic structures, I showed that several SH3 domains influence their protein's assembly and localization to endocytic structures and influence the overall rate of endocytosis in the cell. Relative to other modular protein domains found within endocytic proteins, SH3 domains are highly connected and mediate a large number of interactions between endocytic proteins. Thus, SH3 domain-mediated interactions offer a plausible answer to how molecules are assembled and recruited into the endocytic pathway within cells. Yet, analysis of the endocytic SH3 domain interaction network remains limited by the lack of temporality and directionality; as such, insight into the flow of information through the endocytic protein interaction network remains obscured and future work will need to disentangle whether SH3 domains primarily recruit other proteins or are themselves recruited for other regulatory activities within endocytic structures.

That individual SH3 domains are specific and have unique functions or roles in the cell is consistent with my observation that SH3 domains have a diverse influence on actin assembly, endocytosis, and the cell's regulation of the endocytic rate. However, this runs counter to data from *in vitro* literature, which suggests overlap in ligand recognition amongst individual SH3 domains in the cell. Despite an apparent discrepancy between the lack of interaction specificity and diversity of influence, by

endogenously deleting single SH3 domains, I did not test for the possibility that the unique molecular context of individual SH3 domains might lead single SH3 domain deletions to exhibit a diversity of influences on actin assembly and endocytosis even while lacking selectivity in interacting with specific proteins. This ambiguity is reflected in a broader challenge to the use of SH3 domains in synthetic biology, namely, that the specificity of individual SH3 domains *in vivo* is poorly understood and it remains unclear how distinct sets of SH3 domains assemble distinct molecules into various cellular pathways.

To clarify how SH3 domains might assemble distinct sets of proteins into separate pathways in the cell, I proposed two modalities through which SH3 domains might achieve interaction specificity: through domain-mediated specificity and/or through contextual specificity. In domain mediated specificity, SH3 domains selectively interact with specific partners because individual domains display non-overlapping biophysical properties, relative to other SH3 domains. In contextual specificity, domains selectively interact with specific partners because individual SH3 domains are exposed to non-overlapping molecular and cellular environments, limiting the range of partners an individual domain can interact with. Given that SH3 domains bind PRMs with characteristically weak affinity, I originally hypothesized that SH3 domains primarily achieve binding selectivity through contextual specificity. This implies that individual SH3 domains are interchangeable in the cell, since, in this model, what matters to the activity of a pathway is not the domain but the context in which the domain is expressed; thus, replacing SH3 domains with non-native SH3 domains at the name genomic locus preserves contextual specificity and, therefore, the role of that SH3 domain in the pathway. To test this hypothesis and disentangle domain-mediated interaction specificity modalities from contextually-mediated interaction specificity modalities, I sought to

determine the interchangeability of SH3 domains in the cell. I replaced native endocytic SH3 domains with non-native SH3 domains from other proteins and organisms. Contrary to my suppositions, my findings support the hypothesis that SH3 domains achieve binding selectivity primarily through domain-mediated specificity. However, my results do not entirely rule out contextually-mediated interaction specificity modalities. Given that I have not tried all combinations of replacements, some endocytic SH3 domains may primarily exhibit contextual specificity. Broadly, my results advocate for a nuanced view of interchangeability: for some functions in the cell, but not others, SH3 domains may be interchangeable. Optimizing the replacement approach, perhaps by employing flanking and flexible linkers to preserve folds in the native protein and replaced SH3 domain, may improve the interchangeability of SH3 domains. Future work will have to tease out the extent to which individual SH3 domains are "modular," that is, the extent to which they can be used as interchangeable parts, and decipher which phenotypes, across SH3 domain replacements, are critical to the functioning of the pathway in the cell and which are dispensable, merely appearing to suggest that a SH3 domain is interchangeable.

Of the fourteen SH3 domains participating in endocytosis, six SH3 domains exhibit relatively minor influences on actin assembly during endocytosis. It is possible that some of these SH3 domains are working in parallel with each other or with other endocytic proteins. As such, these SH3 domains may reveal influences on endocytosis under different experimental conditions. However, as a group, endocytic SH3 domains appear to have both a regulatory and assembly role in endocytosis and individual SH3 domains do not have entirely overlapping and redundant roles in endocytosis. Kinetic models describing the balance and interplay of competitive interactions may yield fruitful and specific predictions as to how SH3 domains regulate the Arp2/3 complex during

endocytosis but the extent to which individual SH3 domains recruit endocytic proteins to endocytic structures within the cell remains an open question.

In investigating the influence of individual SH3 domains on localizing their protein to sites of endocytosis in the cell, I found that several SH3 domains are required for robust localization of their protein to endocytic structures. However, none of the Sla1 homology domain protein (Shd1p) SH3 domains are required for Shd1p localization to endocytic structures. Despite this fact, the assembly dynamics of Shd1p into endocytic structures appears altered when different Shd1p SH3 domains are deleted. Thus, most SH3 domains appear to influence the localization of endocytic, SH3-domain-containing proteins to endocytic structures. As such, in addition to reducing the localization of SH3 domain-containing proteins to endocytic structures, SH3 domain deletions may also indirectly prevent other endocytic proteins from being recruited to endocytic structures.

Collectively, these studies test various explanations and determinants of molecular assembly within living cells and support the idea that SH3 domains can be used to manipulate molecular assembly within the cell. The findings of this dissertation provide precise quantitative insights into molecular assembly during endocytosis and, as such, may inform manipulation, control, or correction of endocytosis for synthetic cell or molecular circuit design in the future.

VI. Appendix

A. Forces in endocytosis

Adapted from Lacy MM, Ma R, Ravindra NG, Berro J. (2018). Molecular mechanisms of force production in clathrin-mediated endocytosis. *FEBS Letters*, 592(21), pp.3586-3605. Text written by NGR is indicated by an accompanying vertical bar.

1. Introduction

Eukaryotic cells create endocytic vesicles from the plasma membrane to import extracellular molecules and regulate cell surface components. This process enables a variety of vital cellular functions including nutrient uptake, cell size control, signaling protein regulation, and recycling of membrane components. Clathrin-mediated endocytosis (CME), the primary endocytic pathway, has been a subject of study in cell biology for decades, and many of the biochemical components are well understood (Gaidarov, Santini, Warren, & Keen, 1999; M. Kaksonen, Sun, & Drubin, 2003; McMahon & Boucrot, 2011; B. M. Pearse, 1976; Roth & Porter, 1964). What remains poorly understood is precisely how the macromolecular components cooperate to perform this mechanical work to deform the membrane.

CME involves an initial bending of the plasma membrane, elongation of the invagination, and scission of the tubule neck to form a ~50-nm diameter membrane vesicle that is released into the cytoplasm. The robust, regulated self-assembly of endocytic proteins in cells has been quantitatively measured in several studies and has been shown to be highly reproducible across events (Boettner, Chi, & Lemmon, 2011; A. Picco, Mund, Ries, Nedelec, & Kaksonen, 2015; Sirotkin et al., 2010; M. J. Taylor et al., 2011) (**Figure 2**). Over 60 proteins are self-assembled at the endocytic site (**Table 1**),

including a dynamic meshwork of cytoskeletal actin filaments. Approximately 100 sec before vesicle formation, clathrin and a number of membrane-binding proteins bind to a site on the plasma membrane. Recruitment of other membrane-associated proteins, followed by a burst of actin polymerization leads to the formation of a dense meshwork of short, Arp2/3-branched actin filaments. The actin assembly phase leads to membrane elongation and scission of the membrane invagination within ~10 sec. The actin meshwork and coat proteins are rapidly disassembled as the vesicle is released and diffuses into the cytoplasm (Julien Berro & Thomas D. Pollard, 2014). A variety of these protein modules are capable of producing force, and a number of theoretical efforts have aimed to explain how the protein machinery develops over time (Berro et al., 2010; Mogilner, Allard, & Wollman, 2012) and how the membrane is deformed (A.E. Carlsson, 2018; Hassinger, Oster, Drubin, & Rangamani, 2017). In recent years, several models of force production have been explored but a comprehensive account of how force is produced to achieve CME is lacking. Currently, we do not know how the various proposed force production mechanisms cooperate, synergize, and coordinate mechanical work on the membrane in a spatially and temporally controlled manner.

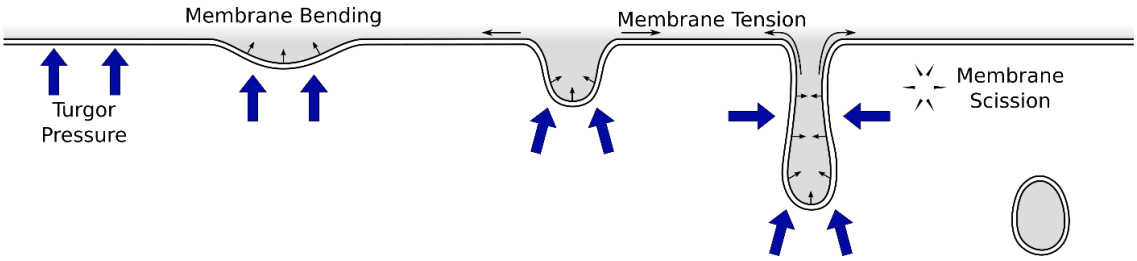

Figure 47. Forces counteracting endocytosis in yeast. Forces opposing CME. Turgor pressure, membrane bending and membrane tension pose significant energy barriers that must be overcome to generate a clathrin-coated pit and vesicle. Note that turgor pressure is applied isotropically to all membrane surfaces, favoring collapse of the pit and tubule, and membrane scission passes through a high-energy intermediate. Arrows are drawn to indicate the direction and order of magnitude of forces opposing CME.

In this review, we focus on the model organisms budding yeast and fission yeast (*Saccharomyces cerevisiae* and *Schizosaccharomyces pombe*, respectively) which exhibit many valuable similarities and a few differences compared with other eukaryotes such as mammals. Yeast has been historically used in cell biology studies, since they are amenable to genetic manipulation, easy to handle and their proteins are well conserved with higher eukaryotes (Boettner et al., 2011). Yeast CME is of special interest because membrane invagination is opposed by much larger forces than in mammalian cells, due to their high turgor pressure (**Figure 47**), and therefore successful CME in yeast requires actin dynamics–highlighting its role in force production (S. Aghamohammadzadeh & Ayscough, 2009; Boulant, Kural, Zeeh, Ubelmann, & Kirchhausen, 2011).

We discuss the energetic barriers to endocytosis and a variety of models that explain how cells produce sufficient force to carry out CME, focusing first on actin-based models and then on other mechanisms acting on the membrane. The redundancy and cooperation of multiple mechanisms can make CME more robust but the multitude of overlapping mechanisms often obscures our understanding of the underlying mechanisms and complicates direct experimental study or comprehensive modeling. By quantitatively assessing the experimental and theoretical support for each model, we hope to synthesize the various hypotheses and evaluate their potential for force production comprehensively.

2. Force and energy barriers for membrane deformation during CME

CME involves a series of morphological changes in the membrane that are opposed by the bending stiffness and surface tension of the membrane, as well as the

turgor pressure of the cell. Initially, forces must be applied to bend the membrane and begin the invagination of a tubule into the cytoplasm (**Figure 47**). Later, the clathrin-coated pit (CCP) must be elongated and the tubule neck must be constricted to induce scission and release the vesicle into the cytoplasm.

Using the theory of elastic membranes developed by Helfrich (Helfrich, 1973), one can estimate that the energy required to create a vesicle from a flat membrane is larger than 500 k_BT (Kozlov et al., 2014; Kozlovsky & Kozlov, 2003). The required energy is even higher in cells with increased membrane tension or turgor pressure. For instance, creating a cylindrical tube of 50 nm in diameter and 120 nm in length against a 1 MPa turgor pressure (Goldenbogen et al., 2016; Minc, Boudaoud, & Chang, 2009) requires an energy around 6×10^4 k_BT and a force around 2000 pN.

In mammalian cells, where the turgor pressure is low, the largest energetic barrier to endocytosis is overcoming a cell's membrane tension. Simulations with high membrane tension (~0.5 pN/nm) indicate that the force to pull the membrane into an elongated tube is ~100-200 pN (Walani, Torres, & Agrawal, 2015) (**Table 11**). This force can be reduced to tens of piconewtons with the assistance of coat proteins that impose a specified curvature on the membrane (Hassinger et al., 2017). When membrane tension is low (0.002 pN/nm), increasing the area covered by curvature-generating proteins is sufficient to induce vesiculation without applying other external forces (Hassinger et al., 2017). In yeast cells, under realistic conditions of membrane tension and turgor pressure (0.2-1 MPa, (Goldenbogen et al., 2016; Minc et al., 2009)), the force required to deform the membrane into a tube is ~3000 pN (Dmitrieff & Nedelec, 2015; Tweten, Bayly, & Carlsson, 2017). Theory and experiments (Campillo et al., 2013; Dmitrieff & Nedelec, 2015; Koster, Cacciuto, Derényi, Frenkel, & Dogterom, 2005; Aurelien Roux, 2013) demonstrate that the main force barrier for the formation of a CCP comes from the initial

deformations of the plasma membrane into a small tubule while maintaining the tubule elongation requires a relatively smaller amount of force.

Table 11. Force requirements for endocytosis, estimated from simulations.

Turgor pressure	Membrane tension	Curvature generating proteins	Pulling force required	Reference
0	0.02 pN/nm (low)	clathrin	15 pN	(Hassinger et al., 2017)
1 kPa (low)	0.5 pN/nm (high)	no	190 pN	(Walani et al., 2015)
1 kPa (low)	0.5 pN/nm (high)	BAR and clathrin	130 pN	(Walani et al., 2015)
1 kPa (low)	0.5 pN/nm (high)	clathrin	0	(Walani et al., 2015)
0.2-1 MPa (high)	0	clathrin	3000 pN	(Dmitrieff & Nedelec, 2015)

3. Differences between yeast and mammals

Turgor pressure in yeast is significantly larger than in mammals, and, therefore, a dynamic actin network is always required for successful CME in yeast (S. Aghamohammadzadeh & Ayscough, 2009) but is not necessarily required for CME in mammals. However, actin is required in mammalian CME in conditions where the membrane tension is increased (Boulant et al., 2011). Recent studies of mammalian CME have revealed that actin is often involved - if not required in some physiological conditions (Watanabe et al., 2013; X. S. Wu et al., 2016). Actin is also involved in clathrin-independent endocytic pathways in mammals (Hinze & Boucrot, 2018) but we will not discuss these pathways in this review.

Another major difference is that dynamin is required for membrane scission in mammals (Hinshaw, 2000) but is not required for CME in yeast (Sirotkin et al., 2010) . Because the precise molecular mechanism of membrane scission is not fully understood, it is possible that dynamin itself is not strictly required for CME in all organisms, especially since dynamin appeared quite late in evolution (Field, Gabernet-Castello, & Dacks, 2007), and key aspects of its function could be performed instead by BAR domain proteins, the actin machinery, and other factors (Daumke, Roux, & Haucke, 2014; Simunovic et al., 2017).

The ease of genetic manipulation in and the handling of yeast has enabled detailed quantitative microscopy studies (J. Berro & T. D. Pollard, 2014; Mund et al., 2017; A. Picco et al., 2015; Sirotkin et al., 2010). In contrast, experimental results from mammalian cells have been difficult to quantitatively interpret due to the presence of redundant isoforms, incomplete knock-down experiments, and variable gene expression profiles across cells and cell lines - although these challenges are being mitigated with new genome-editing tools (Doyon et al., 2011).

4. Actin-based mechanisms

Many lines of evidence have suggested that the actin meshwork assembled at sites of endocytosis is responsible for producing the forces necessary for membrane deformation (Goode et al., 2015). The CME machinery assembles and disassembles very rapidly (~20 sec) and on a very short length scale (~250 nm), posing challenges both for experimental observation and for adapting established theories from other actin systems. Simulations of the dynamic evolution of actin during endocytosis demonstrated that the observed fast actin assembly can be explained by autocatalytic dendritic nucleation of filaments (Berro et al., 2010; X. Wang, Galletta, Cooper, & Carlsson, 2016). This model also indicated that key steps of Arp2/3 nucleation and filament capping are faster in the cell than previously reported *in vitro* and that severing of filaments into short pieces (rather than depolymerization alone) is necessary to account for the fast disassembly in 10 sec. Thus, while actin's biochemistry is tightly controlled and concomitant with rapid deformations of the membrane, how this biochemistry is coupled to mechanical utility is unclear. Here, we address models seeking to describe the molecular mechanisms of force production by actin, which are complex and remain unresolved.

I. Actin filament polymerization

Polymerization of individual actin filaments can generate forces, and can power many forms of cell motility, such as the movement of *Listeria monocytogenes* and the leading edge of lamellipodia (T.D. Pollard & Borisy, 2003; Theriot & Mitchison, 1991). In the Brownian Ratchet model, thermal fluctuations can create a gap between the

filament's polymerizing barbed end and the object against which actin polymerizes (**Figure 48A**), allowing the addition of an actin monomer in that gap, which generates a net force on the object (Mogilner & Oster, 1996, 2003; Peskin, Odell, & Oster, 1993).

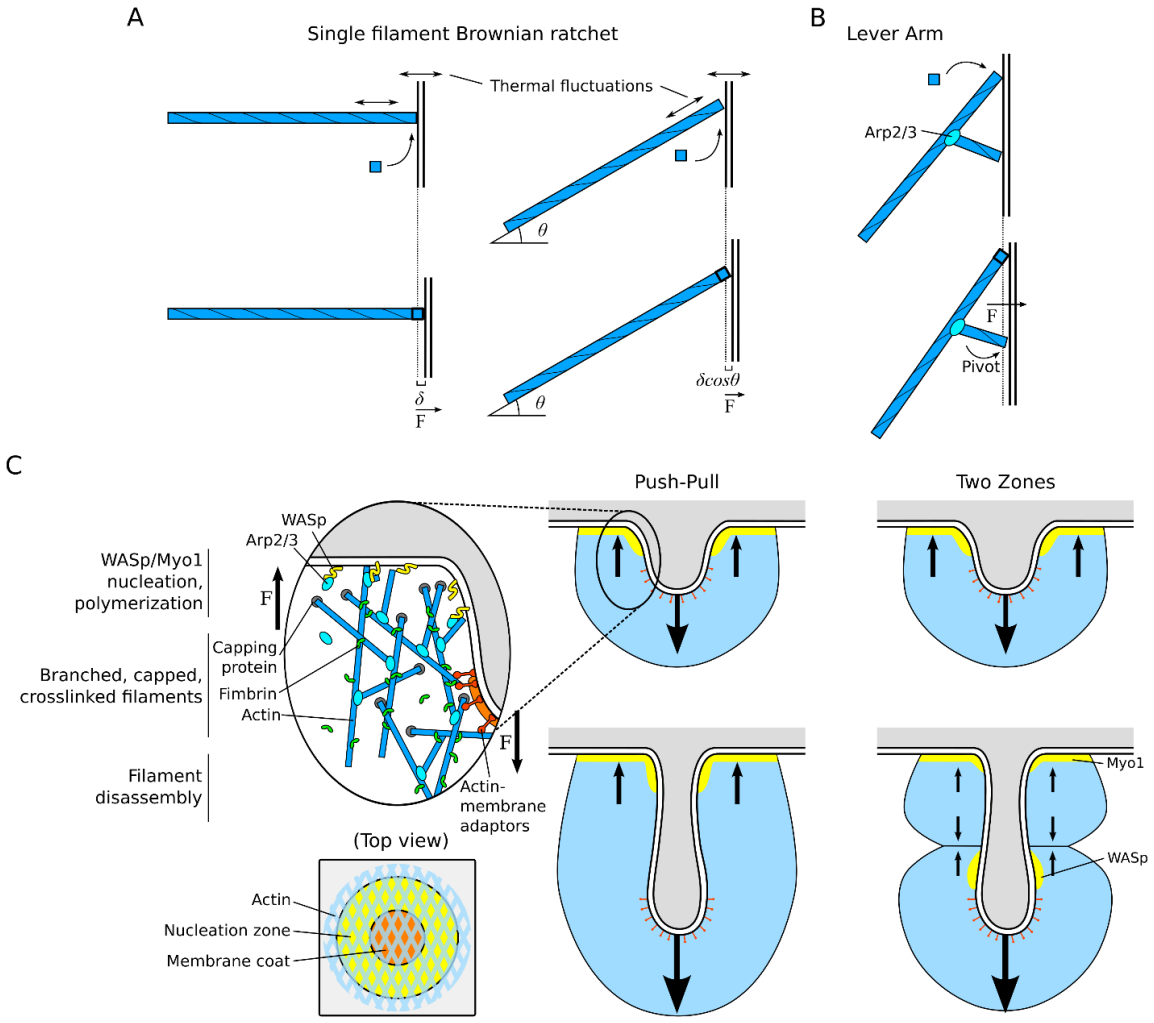

Figure 48. Actin force produced by polymerization. (A) Brownian Ratchet model for force production from polymerization of a single filament. Left: A single filament polymerizing against a barrier or object exerts force related to the single polymerization step distance δ. Right: A filament at an angle exerts force related to the step distance $\delta cos\theta$. If the filament is maintained at an angle (e.g. as one branch in a meshwork), the stall force is higher but the velocity of the barrier object is lower compared with the perpendicular filament. (B) Actin polymerization force can be distributed through pivot points. Polymerizing filaments exert force not only at their barbed end but may generate torque with branched or crosslinked filaments or membrane-bound proteins acting as a lever arm. (C) Schematic of the dendritic nucleation model for the endocytic actin meshwork. Left inset: Force production can be achieved by WASp/Myo1 nucleation at the membrane surface, actin filament branching and polymerization, capping and crosslinking, and attachment to the invaginating CCP tip to transmit force from the growing meshwork. Right: The Push-Pull model proposes an actin meshwork nucleated at the base membrane pushing towards the cytoplasm and attachment to the CCP tip pulling the membrane.

Far right: The Two-Zone model proposes that, as the CCP elongates, two distinct zones of nucleation (by Myo1 and WASp) generate two actin meshworks that push against each other, resulting in pulling the CCP tip toward the cytoplasm. Arrows are drawn to indicate the direction of forces generated and propagated by actin filaments or meshwork.

An actin filament experiencing a load force F from the object reduces its polymerization velocity. This force-velocity relationship is $V = V_p e^{(-F\delta/k_B T)} - V_d$, where V_p is the polymerization velocity in the absence of force, V_d is the depolymerization velocity, and δ is the elongation length of the filament by incorporation of one actin monomer. The first term of this equation describes the negative effect of a load force on the polymerization velocity. Actin polymerization is related to the concentration of monomeric actin by the relation $V_p/V_d = c/c^*$, where c is the free actin monomer concentration and c^* is the critical concentration above which polymerization dominates over depolymerization. The stalling force, which represents the maximum force that can be produced from actin polymerization and the force at which the net polymerization velocity vanishes, is $F_s = (k_B T/\delta)\, ln(c/c^*)$.

In fission yeast, the cytoplasmic actin concentration is c ~ 20-40 μM (Sirotkin et al., 2010; J. Q. Wu & Pollard, 2005), and for c^* ~ 0.11 μM (Ti & Pollard, 2011) and δ ~ 2.7 nm, individual actin filaments are predicted to have a polymerization stalling force F_s smaller than 9 pN. However, *in vitro* measurements of the polymerization stalling force of a single filament are around 1 pN (Dmitrieff & Nedelec, 2015; Footer, Kerssemakers, Theriot, & Dogterom, 2007; D. R. Kovar & Pollard, 2004), due to the lower concentration of free actin used in these experiments. We expect actin polymerization force *in vivo* is closer to the lower estimate of ~1 pN than to the upper bound of 9 pN because only a fraction of actin in the cell is free to polymerize due to the abundance of actin-associated protein complexes and cytoplasmic actin oligomers in the cell (Chen & Pollard, 2013; Okreglak & Drubin, 2010).

The previous estimates assumed that actin polymerization applies a force on a surface that is perpendicular to the axis of the filament. If instead the filament has an angle θ with respect to the normal to the surface of the object, the force-velocity

relationship of actin polymerization becomes $V = cos\theta(V_p e^{(-F\delta cos\theta/k_B T)} - V_d)$ (**Figure 48A**) (Mogilner & Oster, 2003). The stalling force F_s is increased by a factor of $1/cos\theta$ at the expense of reduced velocity by a factor of $cos\theta$.

II. Force production from groups of filaments

In yeast cells during endocytosis, the membrane invagination speed is about 12 nm/s and the calculated force required to sustain an elongated tube is ~3000 pN (Dmitrieff & Nedelec, 2015). To achieve such a speed and force, assuming the force is equally shared among all the filaments, a population of more than 300 filaments would be needed, all nearly parallel to the membrane. If a more detailed actin population model is considered, where filaments are grouped into "working" filaments and "attached" filaments, and the spatial distribution of actin monomers is explicitly treated (Mogilner & Edelstein-Keshet, 2002; Mogilner & Oster, 2003), the required total number of filaments is even higher. This scenario is highly implausible for CME because the required number of working filaments is far higher than the estimated 8 growing filaments based on experimental data (Berro et al., 2010) and because Arp2/3-mediated branching of filaments will broaden the angular distribution. Ongoing modeling efforts will need to account for parameters unique to the endocytic site, such as the rates of nucleation, polymerization, and disassembly, as well as the specific geometries of filaments and the plasma membrane. However, many of these parameters remain to be experimentally measured in the context of CME.

III. Lever arm

An additional consideration of filament geometry is that the small forces generated by individual polymerizing filaments in a branched network could be amplified through a lever arm mechanism (**Figure 48B**). Dmitrieff and Nedelec (Dmitrieff & Nedelec, 2016) considered the geometry of a branched filament or otherwise membrane-anchored actin filament in a meshwork, with a long arm polymerizing against the membrane and a short arm acting as a pivot point against the membrane. They proposed that the force produced by polymerization of the long filament would be transmitted by the lever arm to the pivot point, producing an amplified force as a result of the length difference of the two filaments. Such a mechanism could enhance the force output of an actin network without requiring all filaments to be actively polymerizing, but experimental evidence is still needed to determine to what extent this effect might occur.

IV. The "push-pull" model

We have discussed how polymerization of individual actin filaments generates pushing force and how these forces can be amplified in an Arp2/3-branched actin meshwork. The two most potent Arp2/3 complex activators during CME are the C-terminal domain of WASp and myosin-I (Lee, Bezanilla, & Pollard, 2000; Sun et al., 2006). The intriguing question about endocytosis is precisely how actin polymerization generates forces that pull the plasma membrane towards the cytoplasm, since filaments' barbed ends are oriented towards the plasma membrane. A number of experimental and theoretical efforts have aimed to understand the geometry and dynamics of the actin meshwork in yeast CME.

Actin nucleation and polymerization appear to be localized to a ring-shaped region on the surface of the membrane surrounding the CCP (**Figure 48C**). This actin assembly profile produces forces that push against the plasma membrane and creates a retrograde flow of the actin meshwork towards the cytoplasm, which pulls the CCP via actin-binding proteins in the membrane coat.

The dynamic evolution of the membrane shape during initiation and tubular elongation has been simulated by minimizing the Helfrich bending energy of the membrane, assuming force balance between the pushing and pulling forces acting on the membrane. It is generally assumed that the membrane reaches steady state at each time step, because its relaxation times are on the millisecond time scale. Simulations by Carlsson and colleagues, which treated the actin meshwork as a continuous elastic material, were able to produce a pulling stress as large as 500 kPa on the CCP (Tweten et al., 2017). However, the result of this study implied that each growing actin filament must produce forces of 15 pN, which is significantly larger than the stalling force of individual filaments, as discussed above. Wang and Carlsson developed another model that coupled simplified actin dynamics with membrane deformation (X. Wang & Carlsson, 2017). In this model, actin dynamics consist of nucleation, branching and severing, with nucleation localized only in a ring-shaped region on the plasma membrane. Negative feedback of actin branching on the number of actin nucleators (WASp) resulted in an increased actin density with reduced nucleation. They estimated that the maximum pulling force generated by the actin meshwork was ~725 pN, which is still smaller than the required force to initiate invagination.

The push-pull model is supported by experimental observations that WASp and myosin-I are distributed in a ring-shaped region around the CCP base in budding yeast, while the HIP1R homologues (*S. cerevisiae* Sla2p and *S. pombe* End4p), which connect

actin filaments with the membrane, are concentrated inside the ring (Mund et al., 2017; Sochacki, Dickey, Strub, & Taraska, 2017). Ongoing experimental efforts will help determine how the actin machinery generates forces in CME, with novel geometries or previously-unobserved dynamics (such as enhanced rates of assembly or turnover). Given our current understanding, it seems that other non-polymerization-based mechanisms are required to produce the missing force.

V. The two-zone model

In fission yeast, both WASp and myosin-I are bound to the plasma membrane, but when the CCP elongates, myosin-I remains at the base of the tubule while WASp moves inward (Arasada & Pollard, 2011; Sirotkin et al., 2010). These observations led to the hypothesis that two independent actin meshworks could be created, one nucleated by myosin-I at the tubule base and one by WASp along the neck (**Figure 48C**). While actin filaments elongate, the growing meshworks expand and push against each other, and the WASp-nucleated meshwork transmits the forces to the CCP tip through its attachment via coat proteins, elongating the tubule. This idea is supported by *in vivo* experiments demonstrating that the presence of a single nucleator is not sufficient to elongate a CCP (Arasada & Pollard, 2011). Live-cell super-resolution imaging showed that two zones of actin are visible before vesicle scission, and the formation of two zones requires the presence of both Arp2/3 nucleators, WASp and myosin-I (R. Arasada, W. A. Sayyad, J. Berro, & T. D. Pollard, 2018). Recent mathematical modeling considering the actin meshworks as a visco-active fluid and using realistic parameters showed that a two-zone model may produce forces in the 1000 pN range (Boris M. Slepchenko, Masoud Nickaeen and Thomas Pollard, personal communication). However, fluorescence microscopy in budding yeast did not detect the inward motion of WASp

along the CCP neck (Mund et al., 2017; A. Picco et al., 2015). Further work will be required to determine whether the two-zone model is unique to fission yeast and to test whether the fusion of WASp to fluorescent proteins in budding yeast alters its dynamic localization.

VI. Crosslinking mechanism

The actin filaments at endocytic sites are highly crosslinked by fimbrin and deletion of fimbrin results in significant defects of endocytic internalization in yeast cells (M. Kaksonen et al., 2005; Kubler & Riezman, 1993; Skau et al., 2011). The role of fimbrin remains unclear but it has been proposed to rigidify the actin meshwork and allow force transmission (Kasza et al., 2010; Tharmann, Claessens, & Bausch, 2007; Zhu & Mogilner, 2012). Another promising hypothesis is that fimbrin crosslinkers store elastic energy that could be released to drive membrane deformation in the later stages of CME (Andrea Picco et al., 2018). Actin filaments at endocytic sites are shorter than 200 nm (Berro et al., 2010; Collins, Warrington, Taylor, & Svitkina, 2011), which is two orders of magnitude smaller than the persistence length of actin filaments (~10 μm). At this length scale, actin filaments behave as virtually unbendable rods, instead of semiflexible polymers as are usually assumed in models of actin filaments in cell motility, cytokinesis or acto-myosin contraction models. Thus, even though the filaments cannot bend, filament helicity and the high fimbrin density lead to highly strained crosslinkers that can store a large amount of elastic energy (**Figure 49A**). Indeed, simulations of crosslinked actin meshworks showed that the elastic energy stored in crosslinkers could account for up to 1/6 of the total energy cost of endocytosis if the crosslinkers' stiffness is high (Ma & Berro, 2018). They further showed that ordered detachment of crosslinkers could generate directed torque. Future theoretical work and simulations may determine

how this energy can be used in the context of endocytosis to enhance the forces generated by actin polymerization.

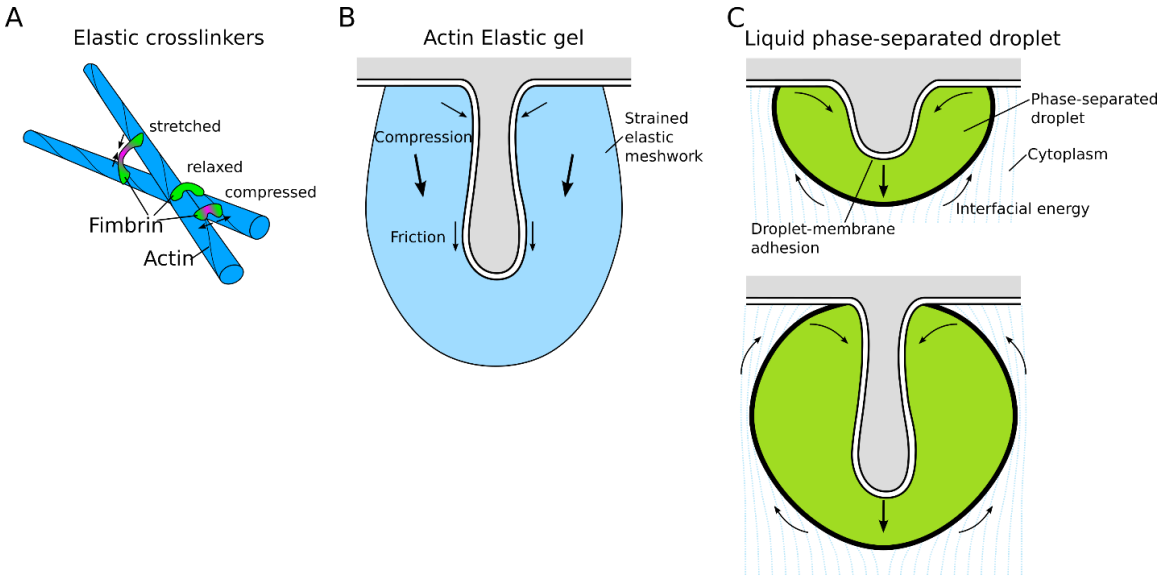

Figure 49. Higher-order force generation mechanisms. (A) Elastic crosslinkers can store energy. Due to the helical nature of actin filaments, most crosslinkers may be deformed from their optimal conformation, enabling the meshwork to convert chemical binding energy into elastic energy. (B) Models of actin meshwork as an elastic gel may reveal un-accounted-for forces of compression and friction or drag force on the membrane tubule surface. (C) Liquid phase separation mediated by disordered protein-protein interactions may exert force on the membrane surface because the interfacial energy causes the droplet to minimize its surface area for a given volume. Adhesion to the membrane surface pulls the CCP inward as the droplet grows and pushes to adopt a more spherical shape.

VII. The elastic gel model

The mechanical properties of actin meshworks have been extensively studied in the context of bacteria motility, such as *Listeria* and *Shigella*. *In vitro* reconstitution using cell extracts or purified proteins have been critical to compare the different mechanisms of force production of entangled actin meshworks nucleated by the Arp2/3 complex (Goldberg & Theriot, 1995; Loisel, Boujemaa, Pantaloni, & Carlier, 1999). In these experiments, micrometric hard (e.g. beads, rods) or deformable objects (e.g. lipid vesicles, oil droplets) were coated with an activator of the Arp2/3 complex and incubated in a solution of purified proteins or cell extract. After an initial phase where actin built up a shell around the coated object, an actin "comet tail" propelled the micron-size objects with speeds around 5 to 50 nm/s, producing forces around 100 to 1000 pN (Boukellal, Campas, Joanny, Prost, & Sykes, 2004; Giardini, Fletcher, & Theriot, 2003; Upadhyaya, Chabot, Andreeva, Samadani, & van Oudenaarden, 2003). Some of these experiments using deformable liposomes also demonstrated that friction between the actin meshwork and lipids occasionally created long tubules that eventually snapped into smaller vesicles (Giardini et al., 2003). Mathematical modeling and later experiments showed that the Brownian ratchet model was not sufficient to explain reconstituted motility (Bieling et al., 2016; Dayel et al., 2009). Better results were obtained by considering the actin meshwork as an elastic gel that builds up a circumferential tension and/or compressive forces orthogonal to the direction of movement, which are responsible for the observed teardrop shapes of lipid vesicles.

The set of proteins implicated in these motility experiments (actin, Arp2/3 complex, crosslinkers, capping proteins, etc.) is quite similar to the set of proteins required for endocytosis in yeast and therefore these elastic properties may contribute to endocytic invagination (**Figure 49B**). However, the dimensions of the endocytic actin

meshwork are 1-2 orders of magnitude smaller in space and 2-3 orders of magnitude shorter in time compared to the meshworks considered in these studies. It remains unclear if the results from the elastic gel model could be applied to scales relevant to CME, so future theoretical work should test if these unique geometrical constraints give rise to similar behaviors.

5. Myosin molecular motors

In addition to its nucleation-promoting activity (discussed above), myosin-I may generate force through its motor activity. In yeast, the activity of the motor domain of the monomeric type-I myosin (Myo3p and Myo5p in *S. cerevisiae*, Myo1p in *S. pombe*) is required for endocytosis (Basu, Munteanu, & Chang, 2014; Geli & Riezman, 1996; Sun et al., 2006). It is thought that myosin-I primarily contributes to elongation rather than scission of the endocytic vesicle (A. E. Carlsson & Bayly, 2014; Sun et al., 2006). However, it remains unclear whether myosin-Is are processive motors or force sensors and precisely how they contribute to endocytosis.

Myosin-Is exert their powerstroke toward the barbed end of actin filaments, producing force directed towards the pointed end. One hypothesis is that myosin-I pushes actin filaments away from the plasma membrane and helps CCP elongation (A. Picco et al., 2015; T. Zhang, Sknepnek, Bowick, & Schwarz, 2015) (**Figure 50A**). Since each myosin-I might produce up to ~2 pN of force (Greenberg & Ostap, 2013; Molloy, Burns, Kendrick-Jones, Tregear, & White, 1995), and up to ~300 myosin-I molecules are present at each endocytic site in yeast (Sirotkin et al., 2010), a generous upper bound of force produced by myosin-I motor activity is ~600 pN.

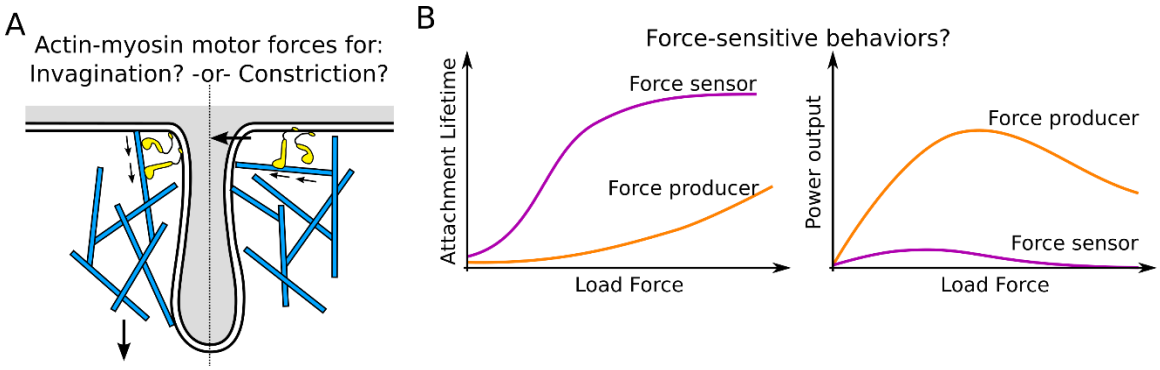

Figure 50. Myosin I force production and force sensing in endocytosis. (A) Depending on their relative orientation at the CCP base, myosin-I might exert force pushing the actin meshwork toward the cytoplasm (driving elongation) or compressing the meshwork towards the CCP center (driving constriction and scission). (B) Some myosin-I isoforms serve as force producers, increasing their power output under high load. Others act as force sensors, with their motor activity stalling under small load forces and remaining tightly bound under high forces. It is not known what type of behavior describes the myosin-I isoforms which are involved in CME.

Another hypothesis is that myosin-I motor activity increases the stress in the actin meshwork, turning the endocytic actin meshwork into an active elastic gel (F. Jülicher, Kruse, Prost, & Joanny, 2007). *In vitro* reconstitution of actomyosin networks with type-I or type-II myosins demonstrates that they can generate up to 1 MPa of tensile stress (Dasanayake & Carlsson, 2013; Dasanayake, Michalski, & Carlsson, 2011; Fujisaki, Albanesi, & Korn, 1985; Thoresen, Lenz, & Gardel, 2011). Alternatively, actomyosin contractility might contribute a compressive force on the membrane and pinch the membrane at scission, similarly to a contractile ring (A. E. Carlsson & Bayly, 2014). However, these ideas are speculative, as it is unclear if the actin filaments are arranged in a geometry that can be compressed (i.e. antiparallel) and myosin-I's biochemistry and mechanics might be sensitive to force. Future high-resolution imaging of actin and myosin at endocytic sites, with techniques such as cryo-electron tomography or single-molecule fluorescence, might reveal whether the geometry and motions within the endocytic actin meshwork are compatible with these hypotheses.

Generally, type-I myosin motors adjust their actin attachment lifetime, motility, power output, and duty ratio based on the direction and magnitude of force acting against their powerstroke (Greenberg & Ostap, 2013) (**Figure 50B**). Therefore, myosin-I may serve as a force-sensitive actin-membrane anchor. Little is known about the mechanical properties of yeast myosin-Is and their mammalian homolog, myosin-IE, which participates in endocytosis. In mammals, different myosin-I isoforms are sensitive to forces in different ways (**Figure 50B**), either tightening the actin-membrane connection or altering their force production under loads of a few pN, but it is unclear which of these behaviors the endocytic myosin-I exhibits. Single-molecule force measurements on endocytic myosin-Is are needed to distinguish between force-

sensitive or force-producing behavior and deepen our understanding of myosin-I's role in endocytosis.

6. Membrane-binding proteins and lipid-mediated mechanisms

Many other mechanisms contribute to membrane bending, elongation, and scission during CME by lowering the barriers to pit elongation and scission, while some directly produce forces and actively deform the membrane. Binding of the curved surface of a protein or oligomer of proteins to a membrane can cause the membrane to adopt the curvature of this protein scaffold if the membrane-binding energy exceeds the energetic cost of membrane bending (Jarsch, Daste, & Gallop, 2016; Kozlov et al., 2014; Zimmerberg & Kozlov, 2006). Membrane bending can also be achieved through steric crowding of large protein domains (Stachowiak et al., 2012), or through the wedge-like insertion of amphipathic helices or other motifs (McMahon & Boucrot, 2015). In addition to favoring increased membrane curvature and lowering the barrier for CME pit invagination, protein scaffolds also limit lipid diffusion and create frictional forces (Simunovic et al., 2017), and the dynamin scaffold can actively constrict to induce membrane scission (Daumke et al., 2014; A. Roux, Uyhazi, Frost, & De Camilli, 2006).

I. Membrane bending by clathrin

The clathrin cage that surrounds nascent endocytic vesicles is a polyhedral arrangement of triskelion subunits. Each triskelion is composed of three clathrin heavy chains and three clathrin light chains (Marko Kaksonen & Roux, 2018; Kirchhausen, Owen, & Harrison, 2014; B. M. Pearse, 1976). In yeast, clathrin appears to be important for regulating the vesicle's size but not the membrane curvature, suggesting

that clathrin is not strictly necessary for initial membrane bending or elongation (Avinoam, Schorb, Beese, Briggs, & Kaksonen, 2015; M. Kaksonen et al., 2005; Kukulski, Picco, Specht, Briggs, & Kaksonen, 2016). However, clathrin is sufficient to induce vesicle budding *in vitro* (Dannhauser & Ungewickell, 2012; Saleem et al., 2015). Polymerization into a clathrin cage may yield up to ~40 k_BT of energy per clathrin triskelion (den Otter & Briels, 2011; Nossal, 2001; Saleem et al., 2015), which, given that around 13 triskelia are assembled in fission yeast (Sirotkin et al., 2010), suggests that up to 500 k_BT of energy could be generated by clathrin cage assembly. This value is close to the required membrane bending energy so clathrin cage formation might contribute to membrane bending for low membrane tensions. However, the observation of flat clathrin lattices in cells suggests that the polymerization energy does not directly lead to membrane curvature without contributions of other membrane-deforming mechanisms (Avinoam et al., 2015; Bucher et al., 2018; Leyton-Puig et al., 2017). Thus, clathrin may contribute to - though not dominate - membrane bending *in vivo*.

II. Membrane bending by BAR domains

The BAR (Bin/Amphiphysin/Rvs) domains are a group of crescent-shaped membrane-binding proteins that can both sense and generate membrane curvature. Extensive studies *in vivo*, *in vitro*, and *in silico* have investigated the general mechanisms of BAR domains and their specific contributions to CME (C. Mim & Unger, 2012; Simunovic, Bassereau, & Voth, 2018; Simunovic, Voth, Callan-Jones, & Bassereau, 2015). At low protein concentrations, most BAR domains sense curvature by binding to membranes that display the curvature that matches their preferred curvature. At high protein concentrations, most BAR domains generate membrane curvature by

imposing a non-zero spontaneous curvature, typically around 15-40 nm radius (Frost, Unger, & De Camilli, 2009; Peter et al., 2004) (**Figure 51A**). In CME, several of the early membrane coat proteins contain moderately curved F-BAR domains (Fes-CIP4 homology BAR domain: Syp1/FCHo1-2, Bzz1/syndapin, Cdc15/Hof1/PSTPIP1-2), while several proteins involved in membrane scission contain more highly-curved N-BAR domains (N-terminal amphipathic helix BAR domain: Hob1-3/Rvs167-161/endophilin-amphiphysin) (C. Mim & Unger, 2012).

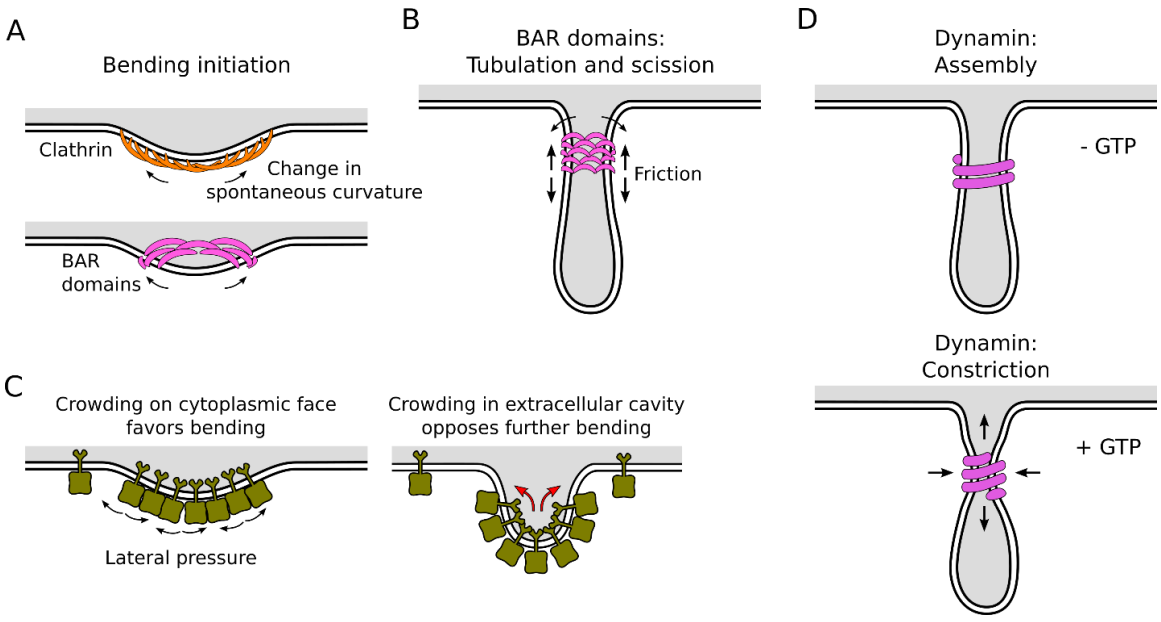

Figure 51. Membrane bending and scission during endocytosis. (A) Scaffolds of clathrin and BAR domain proteins can induce membrane bending by changing the spontaneous curvature of the membrane. (B) BAR domains stabilize the tubule neck but can also mediate scission by limiting lipid diffusion and creating friction forces as the tubule is pulled towards the cytoplasm. (C) Steric crowding of bulky domains favors membrane bending if there is an asymmetry of lateral pressure (left), however the extracellular domains of CCP cargo will also be crowded in the CCP lumen, generating force that opposes invagination (right). The net energy contribution to CME will be determined by the relative sizes and densities of the intracellular and extracellular domains. (D) Dynamin assembles at the membrane tubule neck. Binding of GTP induces the helical oligomer to undergo a conformational change driving constriction, reducing the radius and elongating along the tubule axis. GTP hydrolysis leads to both scission of the membrane neck and disassembly of the dynamin scaffold (not shown).

Calculations of typical BAR domain surfaces estimate the magnitude of binding energies is around 6 to 12 k_BT per protein (Zimmerberg & Kozlov, 2006). However, their ability to induce curvature depends on the membrane tension. *In vitro* experiments with the endophilin N-BAR domain show that for a low-tension membrane, tubulation occurs at a protein density of approximately 650 μm^{-2}, which is equivalent to 15 proteins on a patch of membrane the size of a CCP (Shi & Baumgart, 2015). At higher membrane tension (0.1 pN/nm), tubulation requires a density of 3,000 μm^{-2}, which is equivalent to about 70 proteins on a CCP, or about 10% of the membrane surface area (Shi & Baumgart, 2015). Importantly, tubulation was not observed at membrane tensions higher than 0.25 pN/nm (Shi & Baumgart, 2015).

These results suggest that BAR domains may be able to drive membrane bending in mammalian CME in some conditions, since membrane tension ranges from 0.003 to 0.3 pN/nm (Morris & Homann, 2001). However, BAR domains are likely not sufficient to drive membrane invagination in yeast since the turgor pressure adds a much higher barrier (**Table 11**). This argument is supported by correlative light and electron microscopy studies of yeast CME indicating that plasma membrane bending does not begin until the actin assembly phase (Kukulski et al., 2012).

III. Molecular Crowding

Contrary to the purified systems used *in vitro*, cell membranes are densely crowded with proteins. Membrane-associated proteins constitute around 2/3 of the mass of cellular membranes (Takamori et al., 2006; Wilhelm et al., 2014). Steric clashes of bulky membrane-associated proteins exert lateral pressure, favoring membrane curvature that relieves any asymmetry (Stachowiak et al., 2012) (**Figure 51C**). Crowding

can induce tubulation and scission of membranes *in vitro*, even with proteins containing cytoplasmic unstructured domains (Busch et al., 2015; Snead et al., 2017). However, extracellular proteins in the cavity of the developing CCP also exert steric forces, countering those produced by cytoplasmic proteins. Above a certain point, bulky cargoes are excluded from the nascent pit (DeGroot et al., 2018). The extreme case of maximal crowding at equal density on both faces of the membrane could double or triple the total energetic cost of forming a vesicle (Derganc & Copic, 2016). For crowding to have a major positive effect on CCP and vesicle formation, the cytoplasmic face would have to be extremely crowded and the extracellular face would have to be very sparse, but it is difficult to measure the local protein density in cells. Even if the specific force contributions are unclear, the fact that the cell membrane is extraordinarily crowded complicates the translation of results from theoretical models and reconstituted systems. Future modeling work should attempt to consider this factor, but further experimental characterization of cell membranes at endocytic sites will be needed to determine the true extent of crowding.

IV. Other membrane curvature-generating mechanisms

Other curvature-inducing protein domains in endocytosis include ENTH (epsin N-terminal homology: epsin/Ent1-2, Yap18/Yap1801-2/PICALM) and ANTH (AP180 N-terminal homology: Yap18/Yap1801-2/PICALM, Sla2/End4/Hip1-Hip1R) domains that form scaffolds on the plasma membrane (Kay, Yamabhai, Wendland, & Emr, 1999; Legendre-Guillemin, Wasiak, Hussain, Angers, & McPherson, 2004). N-BAR and ENTH domains further induce curvature by wedging their amphipathic helices into the bilayer surface (Drin & Antonny, 2010; Kozlov et al., 2014). This helix insertion adds to the membrane-bending forces and contributes to scission. Many of these curvature-

generating scaffolds also contain protein-interaction domains that enable other force production mechanisms – for example, Syp1/FCHo and Bzz1/Syndapin recruit WASp to localize actin nucleation (Arasada & Pollard, 2011).

V. Membrane scission by BAR domains

BAR domains play a different role in membrane scission. In fact, protein scaffolds stabilize the highly curved tube (**Figure 51B**). *In vitro* studies showed that the pulling force required to maintain a membrane tube from a liposome (around 20 to 50 pN depending on the tension) falls to near zero upon binding of an endophilin scaffold (Simunovic et al., 2016). However, if force is applied to rapidly extend the BAR-domain coated tubule, the protein scaffold acts as a barrier to lipid flow and creates friction on the membrane, leading to scission (Simunovic et al., 2017), whereas uncoated tubules do not undergo scission even at excessive pulling forces (Renard et al., 2015). Although the pulling speeds used in these experiments were an order of magnitude higher than the observed rate of tubule elongation in CME, this friction-mediated scission mechanism is likely a significant contributor to fission yeast CME and in clathrin- and dynamin-independent endocytosis in mammalian cells. Further experiments should aim to test these mechanisms *in vivo* where the membrane and protein scaffolds are much more complex and to dissect the interplay with other scission mechanisms such as dynamin.

VI. Membrane scission by dynamin

In mammals and many eukaryotes, scission of the membrane neck requires the GTPase dynamin. Dynamin assembles into a helical oligomeric scaffold around the neck

of the CCP at the late stages of CME (Hinshaw, 2000; A. Roux et al., 2006). Upon GTP binding the oligomer twists, which reduces the radius of curvature and extends the length of the scaffolded tube, and then, GTP hydrolysis triggers membrane scission and disassembly of the dynamin scaffold (**Figure 51D**). Precisely how GTP hydrolysis triggers membrane scission is debated but several plausible models have been proposed: instability at the boundary of the coated and uncoated membrane, collapse of the high-curvature tubule after the dynamin scaffold disassembles, or linear tension exerted by the extension of the tubule coat (Antonny et al., 2016).

Structural studies (Chappie et al., 2011; Faelber et al., 2011) and fluorescence imaging in mammalian cells (Cocucci, Gaudin, & Kirchhausen, 2014; Grassart et al., 2014) showed that fewer than two full turns of the helical oligomer (26 to 40 dynamin molecules) are sufficient to carry out scission *in vivo*. *In vitro* studies indicate that long dynamin scaffolds can generate very high torque, 700 to 1,000 pN*nm (Morlot et al., 2012), but it is unknown how much force is exerted by the smaller one- to two-turn helical oligomers that exist in cells for CME. The energy of GTP hydrolysis (if one GTP is hydrolyzed per dynamin molecule) yields a maximum of about 100 k_BT of mechanical energy from 15 molecules of dynamin, which is sufficient to overcome the barrier of the membrane shape transition for scission (Morlot et al., 2012).

Unexpectedly, no dynamin homologue is observed in fission yeast CME (Sirotkin et al., 2010). The budding yeast dynamin-like protein Vps1 has been reported to be involved in CME and its deletion causes defects in the timing of recruitment of several endocytic proteins (Smaczynska-de et al., 2010), but other studies report that Vps1 is only rarely recruited to CME sites and its deletion mimics (but does not enhance) the defect of deleting the amphiphysin homologue Rvs167 (Kishimoto et al., 2011a). These reports suggest that dynamin is not strictly required for membrane scission and instead

the BAR-domain proteins endophilin and amphiphysin (Hob1/3 in fission yeast, Rvs161/167 in budding yeast) drive membrane scission in yeast CME, as discussed above. However, it remains unclear how these and other mechanisms generate the very large mechanical forces supplied by dynamin in other organisms for membrane scission. The complex interplay of actin, BAR domain proteins, and dynamin for their recruitment, regulation, and mechanical contributions to scission are still not fully resolved but provide an exciting avenue for ongoing research (Antonny et al., 2016; Daumke et al., 2014).

VII. Membrane Line Tension

Different lipids may segregate to form distinct phases and generate an interfacial tension within the membrane. This interfacial tension, or line tension, destabilizes the membrane shape and could facilitate budding and scission of the vesicle (Frank Jülicher & Lipowsky, 1996; Wiese, Harbich, & Helfrich, 1992). Additionally, dynamin and BAR proteins could act as barriers to lipid flow on the membrane to facilitate phase separation of lipids into tube region and vesicle region (Daumke et al., 2014; J. Liu, Kaksonen, Drubin, & Oster, 2006; J. Liu, Sun, Drubin, & Oster, 2009). In model membrane systems, line tension generates forces on the order of 0.1-10 pN, constricting the tubule (Heinrich, Tian, Esposito, & Baumgart, 2010; A. Tian, Johnson, Wang, & Baumgart, 2007), but in complex systems with many species like the cell plasma membrane this value is likely to be significantly lower. Direct experimental observation of membrane phase separation during endocytosis *in vivo* is missing, and while it remains a technically challenging feat, such observations might be enabled by novel advances in lipid-specific fluorophores or super-resolution microscopy techniques. Even if it is physiologically relevant, it appears that line tension only has a minor role in producing the required force for CME.

7. Other putative mechanisms

VIII. Liquid phase separation

Phase-separated liquid droplets are regions with higher local concentrations of components within the structure compared to without. Droplets form when there are multivalent interactions between components, such as between proteins with modular protein-interaction domains, high charge densities, or intrinsically disordered regions (Banani, Lee, Hyman, & Rosen, 2017; L. P. Bergeron-Sandoval, Safaee, & Michnick, 2016). Recent work suggests that droplets may form at endocytic structures through interactions between intrinsically-disordered prion-like domains, which are found within several endocytic coat proteins (L.-P. Bergeron-Sandoval et al., 2017; Miao, Tipakornsaowapak, Zheng, Mu, & Lewellyn, 2018). Depending on the composition of the droplet, its surface tension might be large and the droplet will be viscoelastic (L. P. Bergeron-Sandoval et al., 2016). Such a droplet will exert force on the membrane surface because, in order to minimize its membrane and cytosolic interfacial energy, the droplet minimizes its surface area for a given volume (L.-P. Bergeron-Sandoval et al., 2017). Adhesion to the membrane pulls the CCP inward as the droplet grows and pushes to adopt a more spherical shape (**Figure 49C**). The droplet's interfacial energy is favorable up to an invagination depth of ~80 nm, close to the range that the CCP moves before scission (~100 nm) (Idrissi, Blasco, Espinal, & Geli, 2012; Kukulski et al., 2012), totaling ~1000 k_BT (L.-P. Bergeron-Sandoval et al., 2017). However, the interfacial energy minimum is reached at an invagination depth of ~40nm, which falls short of the expected invagination depth (L.-P. Bergeron-Sandoval et al., 2017). Furthermore, it remains unclear exactly what causes, disrupts, maintains, or

contributes to phase-separated droplet formation within endocytic structures and it is especially difficult to experimentally probe the dynamic stability of droplets in endocytosis, given that the process is out of equilibrium and completed within seconds. Additional experiments, perhaps on stalled endocytic patches, are needed to probe whether the endocytic proteins indeed behave as a viscoelastic, phase-separated droplet and to determine whether different stages of endocytosis have different mechanical properties.

IX. Local turgor pressure drop

Yeast cells maintain high concentrations of osmolytes such as glycerol, creating turgor pressure which pushes the membrane outward against the cell wall. Since the turgor pressure is proportional to the difference in concentrations of the solute between the inside and outside of the cell, the turgor pressure could be reduced if the membrane was permeable to that solute. It has been proposed that the glycerol concentration gradient could be locally equalized around individual sites of endocytosis and, thus, the turgor pressure locally reduced (Scher-Zagier & Carlsson, 2016). If an endocytic membrane patch of 45-nm diameter contained as many as 60 glycerol channels, the resulting glycerol transport could locally reduce the turgor pressure by up to 50% (Scher-Zagier & Carlsson, 2016). If the turgor pressure were reduced so drastically, much less than 3000 pN would be required for endocytosis. However, it is not clear whether glycerol channels do localize to endocytic sites, nor is it clear how the local opening of channels could be regulated throughout the stages of endocytosis. Even though the deletion of the glycerol transporter Fps1 causes a

failure of ~40% of endocytic events (S. Aghamohammadzadeh & Ayscough, 2009), it is unclear if those failures are due to a global increase of turgor pressure or a loss of local turgor pressure modulation. A 50% reduction in local turgor pressure is significant, as it would reduce the amount of force required for invagination by ~650 pN. However, there is little support for this model and convincing experimental evidence will be difficult to acquire.

Table 12. Summary of force production mechanisms in endocytosis.

Mechanism	Stage(s)	Proteins or lipids involved*	Force or energy contribution (pN or k_BT)**	References
Actin-based				
Push-Pull	Initiation, elongation, scission?	Actin, WASp, Myo1, etc. Membrane anchors (End4/Sla2, etc.)	100-700 pN	(Tweten et al., 2017)
Two-zones	Elongation, scission?	Actin, WASp, Myo1, etc. Membrane anchors (End4/Sla2, etc.)	~1000 pN	(Arasada & Pollard, 2011; R. Arasada et al., 2018) Slepchenko *et al*.***
Cross-linking	Elongation?, scission	Actin, Fimbrin	~ 800-8,000 k_BT	(Ma & Berro, 2018)
Elastic gel	Elongation, scission	Actin, Fimbrin	100-1000 pN	(Dayel et al., 2009; Giardini et al., 2003; Upadhyaya et al., 2003)
Myosins	Elongation, scission	Myosin-1e: Myo3/5 (*S.c.*), Myo1 (*S.p.*)	0 - 600 pN	(Greenberg & Ostap, 2013; T. Zhang et al., 2015)
Membrane-based				
Clathrin	Initiation	Clc1, Chc1	~500 k_BT	(den Otter & Briels, 2011; Saleem et al., 2015; Sirotkin et al., 2010)
BAR domain proteins	Initiation, elongation, scission	Syp1/FCHo1-2, Bzz1/syndapin, Cdc15/Hof1/PSTIPIP1-2 Hob1-3/Rvs167-161/endophilin-amphiphysin	20-50 pN for tube elongation, Lowers scission force to ~30 pN	(Simunovic et al., 2016; Simunovic et al., 2017)
Crowding	Initiation, elongation, scission	Any (Ent1/epsin, Yap18/Yap180/AP180)	-1000 to 1000 pN?	(Derganc & Copic, 2016; Snead et al., 2017; Stachowiak et al., 2012)
Dynamin	scission	Vps1(*S.c.*), none (*S.p.*)	~100 k_BT	(Morlot et al., 2012)
Line tension	scission	lipids	0.1-10 pN	(Heinrich et al., 2010; A. Tian et al., 2007)
Other putative mechanisms				
Local turgor pressure drop	Initiation, elongation	Fps1 or other channels?	~650 pN	(Scher-Zagier & Carlsson, 2016)
Phase-separated droplet	Initiation, elongation	Prion-like domains of Sla1/2, Ent1/2, Yap1801/2, etc.	~1200 k_BT	(L.-P. Bergeron-Sandoval et al., 2017)

* See Table 1 for listing of protein names in fission yeast, budding yeast, and mammals.
** Force production (pN) is listed for mechanisms where the direction and force output are clearly understood, or an energy amount (k_BT) is given when it is unclear how the energy is converted to mechanical force.
*** Boris M. Slepchenko, Masoud Nickaeen and Thomas Pollard.

8. Models of molecular force production: a concise and up-to-date summary

A wide variety of mechanisms are available to generate the forces needed to remodel the cell membrane to form endocytic vesicles (**Table 12**). While there are multiple mechanisms whose disruption can cause CME to fail, no single mechanism is solely responsible for generating the full magnitude of force required for CME in yeast. Several components add small or speculative amounts of force (BAR domains, clathrin, crowding, membrane line tension, liquid droplet, turgor pressure drop) but when combined in the context of the cell, they may make up a significant proportion of the overall required force for CME. The mechanisms that could contribute large amounts of force (actin polymerization, myosin, dynamin) have been extensively studied *in vitro*, but it remains unclear how the molecular organization leads to efficient and robust membrane remodeling in CME *in vivo*.

I. Connection to molecular assembly by protein-interaction domains

SH3 domains are thought to function as regulators of actin assembly during endocytosis, which relates them to force production through influencing actin polymerization (Sun et al., 2017). Yet, there may be a more substantial conceptual link between protein-interaction domains and mechanical force production during endocytosis.

The assembly of the endocytic machinery may operate according to at least two distinct conceptual frameworks: (1) molecules are biochemically and spatially connected in a coordinated temporal manner in order to internalize membrane or (2) molecules are spatiotemporally assembled in order to overcome mechanical barriers.

These ontologies are distinct because the latter implies feedback between biochemistry and mechanical work produced by the ensemble of molecules while the former, in the extreme, suggests that the cellular function may be limited by biochemistry, regardless of mechanical compensations. It is difficult to distinguish between these two endocytic ontologies; indeed, a remaining and interesting question is, is there coupling between biochemical assembly and mechanical force production?

SH3 domains are of particular interest in this question because the domain itself is thought to possess only protein-interaction functionality (Bhattacharyya et al., 2006; B. Mayer & Saksela, 2005; Ali Zarrinpar et al., 2003). Yet, SH3 domains may form liquid droplets *in vivo*, which may influence both actin polymerization (higher-order effect) and, in so forming a phase-separated viscoelastic structure, produce force (L.-P. Bergeron-Sandoval et al., 2017; Li et al., 2012). Therefore, the domain is itself offers a striking example how biochemical function is intertwined with mechanical force production, albeit possessing no structural or conformational ability beyond protein-protein binding. Yet, the broader question remains challenging to falsify experimentally. Even the question of how SH3 domains assembles endocytic proteins in a spatiotemporal manner remains a challenging and open question that especially lacks quantitative and experimental constraint (Xin et al., 2013).

To connect SH3 domains and force production in the future, one can perturb the mechanics during endocytosis by targeting one of the mechanisms that we have discussed here. For example, future experiments could include exposing cells to osmotic shock while tracking SH3 domain-containing proteins using quantitative microscopy approaches to interrogate the connection between SH3 domains, actin

assembly, and force production. If the mechanical perturbation does not change the assembly dynamics of SH3 domain-containing endocytic proteins, then SH3 domains may not be the direct conduit to translate mechanics to biochemistry or vice versa. Furthermore, if a range of osmotic shocks in SH3 domain deleted backgrounds show no difference to a range of osmotic shocks in WT backgrounds, then it is likely that SH3 domain-mediated assembly is uncoupled from mechanical feedback. In any case, future studies bridging SH3 domains and mechanical biology may provide a priority topic of study to interrogate biochemical and mechanical coupling during endocytosis.

II. Perspectives and future directions

Though it appears that enough total energy could be found across the various proposed mechanisms, no single model has successfully integrated the multiple plausible mechanisms to globally account for all of the energetic barriers to CME. Theoretical estimates sometimes assume the most generous conditions from a wide range of possible parameters or invoke speculative mechanisms to lower the energy requirements, which enables their favored mechanism to produce enough force for CME on its own. However, these assumptions and simplifications are seldomly validated experimentally. In addition, the contributions from the many minor force-producing mechanisms are often simplified or ignored, precluding a wholistic view of the force generating mechanisms at play during CME. Thus, the coordination across these mechanisms throughout the process of CME remains to be resolved.

Some of these open questions will be addressable by advances in modeling or experimental methods. Increasingly detailed simulations may reveal novel mechanisms

of force production such as higher-order and emergent properties of actin meshwork dynamics. Future theoretical work should attempt to consider complications such as the spatial or temporal differences in properties of the plasma membrane or the changes in activity of endocytic proteins due to protein post-translational modifications, for example. In addition, the magnitudes and directions of forces produced by individual protein modules likely change during the course of CME, but since these forces remain technically challenging to directly observe in cells it has been unclear whether and how to account for this behavior in theoretical models. Future simulations should attempt to address the changes in different dominant force production mechanisms at different stages of CME. For instance, at the early stage when the membrane is flat, the organization of actin filaments to generate forces toward the cytoplasm likely differs from the later organization of actin filaments at the time of scission, perhaps producing compressive forces by other mechanisms. These changes could be driven by membrane geometry or biochemical factors, and likely depend on complex crosstalk and feedback loops within the system.

Likewise, novel experimental approaches should aim to overcome the limitations that have prevented direct measurements of several valuable quantities and parameters, such as the amount of hydrolyzed ATP and GTP, the local membrane tension at sites of CME, and the molecular orientations and forces of actin filaments and myosin motors. Electron and super-resolution fluorescence microscopy may suggest previously unobserved architectures and dynamics of the actin and membrane-scaffold protein networks. Quantitative microscopy and new observations could revise the limits of known mechanisms. For example, if the actin meshwork turns over multiple times during CME, which has been proposed (Berro et al., 2010; Goode et al., 2015; M. Kaksonen et al., 2003) but not yet directly observed in physiological conditions, such an enhanced

filament polymerization rate would enable a greater amount of force than what has been calculated for the currently known number of filaments.

Even if no single mechanism is sufficient to fully generate the required forces, the cooperation of multiple mechanisms may provide a more robust solution for the cell to achieve successful CME in a variety of conditions. Fully understanding the complexity of CME and the synergy between multiple coexisting force production mechanisms remains challenging, but we are confident that ongoing experimental and theoretical work will continue to illuminate this vital cellular process.

B. Strains

Table 13. Strains constructed by genetic engineering or for use in studies described in this dissertation.

Strain	Genotype	Investigator
FY527	*ade6-M216 his3-D1 leu1-32 ura4-D18*	S. Forsburg
FY528	*ade6-M216 his3-D1 leu1-32 ura4-D18*	S. Forsburg
JB26	*capA-mEGFP-kanMX6*	Julien Berro
JB31	*capB-mEGFP-kanMX6 ade6-M216 his3-D1 leu1-32 ura4-D18*	Julien Berro
JB32	*capB-mEGFP-kanMX6 ade6-M210 his3-D1 leu1-32 ura4-D19*	Julien Berro
JB57	*fim1-mEGFP-NatMX6 ade6-M210 his3-D1 leu1-32 ura4-D18 leu1-32*	Julien Berro
JB115	*crn1GFP::kanMX6 for3D::kanMX6*	Julien Berro
JB134	*fim1-mEOS3.2-kanMX6 ade6-M216 his3-D1 leu1-32 ura4-D18*	Ronan Fernandez
JB142	*acp1-mEOS3.2-kanMX6 ade6-M216 his3-D1 leu1-32 ura4-D18*	Marianne Grafe
JB144	*myo1-mEOS3.2-kanMX6 ade6-M216 his3-D1 leu1-32 ura4-D18*	Marianne Grafe
JB145	*wsp1-mEOS3.2-kanMX6 ade6-M216 his3-D1 leu1-32 ura4-D18*	Marianne Grafe
JB155	*Arp3-mEGFP-KanMX6 pcp1-CDS_wsp1-NatMX6 ade6-M216 his3-D1 leu1-32 ura4-D18*	Ronan Fernandez
JB156	*hob1-mEGFP-kanMX6 ade6-M216 his3-D1 leu1-32 ura4-D18*	Ronan Fernandez
JB157	*hob3-mEGFP-kanMX6 ade6-M216 his3-D1 leu1-32 ura4-D18*	Ronan Fernandez
JB159	*crn1-mEGFP-kanMX6 ade6-M216 his3-D1 leu1-32 ura4-D18*	Ronan Fernandez
JB160	*vps1-mEGFP-kanMX6 ade6-M216 his3-D1 leu1-32 ura4-D18*	Ronan Fernandez
JB161	*cap1-mEGFP-kanMX6 ade6-M216 his3-D1 leu1-32 ura4-D18*	Ronan Fernandez
JB162	*abp1-mEGFP-kanMX6 ade6-M216 his3-D1 leu1-32 ura4-D18*	Ronan Fernandez
JB163	*vrp1-mEGFP-kanMX6 ade6-M216 his3-D1 leu1-32 ura4-D18*	Ronan Fernandez
JB164	*syj1-mEGFP-kanMX6 ade6-M216 his3-D1 leu1-32 ura4-D18*	Ronan Fernandez
JB165	*ent1-mEGFP-kanMX6 ade6-M216 his3-D1 leu1-32 ura4-D18*	Ronan Fernandez
JB166	*app1-mEGFP-kanMX6 ade6-M216 his3-D1 leu1-32 ura4-D18*	Ronan Fernandez
JB167	*bbc1-mEGFP-kanMX6 ade6-M216 his3-D1 leu1-32 ura4-D18*	Ronan Fernandez
JB168	*syp1-mEGFP-kanMX6 ade6-M216 his3-D1 leu1-32 ura4-D18*	Ronan Fernandez
JB171	*end4-mEGFP-kanMX6 ade6-M216 his3-D1 leu1-32 ura4-D18*	Ronan Fernandez
JB174	*wsp1Δ-kanMX6 ade6-M210 his3-D1 leu1-32 ura4-D18*	Ronan Fernandez
JB175	*myoΔ-kanMX6 ade6-M210 his3-D1 leu1-32 ura4-D18*	Ronan Fernandez
JB176	*fim1Δ-kanMX6 ade6-M210 his3-D1 leu1-32 ura4-D18*	Ronan Fernandez
JB198	*pil1-SNAP-kanMX6 ade6-M216 his3-D1 leu1-32 ura4-D18*	Ronan Fernandez
JB204	*pil1-mEGFP-kanMX6 ade6-M216 his3-D1 leu1-32 ura4-D18*	Ronan Fernandez
JB206	*ABD1:11aa:ABD2 ade6-M216 his3-D1 leu1-32 ura4-D18*	Ronan Fernandez
JB207	*ABD1:24aa:ABD2 ade6-M216 his3-D1 leu1-32 ura4-D18*	Ronan Fernandez
JB208	*ABD1:11aa:ABD2 acp1-mEGFP-KanMX6 ade6-M210 his3-D1 leu1-32 ura4-D18*	Ronan Fernandez
JB209	*ABD1:24aa:ABD2 acp1-mEGFP-KanMX6 ade6-M210 his3-D1 leu1-32 ura4-D18*	Ronan Fernandez
JB210	*ABD1:11aa:ABD2 fim1-mEGFP-KanMX6 ade6-M210 his3-D1 leu1-32 ura4-D18*	Ronan Fernandez
JB211	*ABD1:24aa:ABD2 fim1-mEGFP-KanMX6 ade6-M210 his3-D1 leu1-32 ura4-D18*	Ronan Fernandez

JB212	*ABD1:11aa:ABD2 end4-mEGFP-KanMX6 ade6-M216 his3-D1 leu1-32 ura4-D18*	Ronan Fernandez
JB213	*ABD1:24aa:ABD2 end4-mEGFP-KanMX6 ade6-M216 his3-D1 leu1-32 ura4-D18*	Ronan Fernandez
JB214	*mEGFP:myo1 ade6-M216 his3-D1 leu1-32 ura4-D18*	Ronan Fernandez
JB215	*mEGFP:mug137 ade6-M216 his3-D1 leu1-32 ura4-D18*	Ronan Fernandez
JB220	*ABD1:coiledcoil:ABD2 acp1-mEGFP-KanMX6 ade6-M210 his3-D1 leu1-32 ura4-D18*	Ronan Fernandez
JB225	*mEGFP-wsp1-KanMX6 ade6-M216 his3-D1 leu1-32 ura4-D18*	Neal Ravindra
JB226	*pil1-mCherry-NatMX6 ade6-M210 his3-D1 leu1-32 ura4-D18*	Neal Ravindra
JB227	*pil1-mCherry-3GS-SH3_bzz1-NatMX6 ade6-M210 his3-D1 leu1-32 ura4-D18*	Neal Ravindra
JB228	*pil1-mCherry-3GS-2SH3_bzz1-NatMX6 ade6-M210 his3-D1 leu1-32 ura4-D18*	Neal Ravindra
JB231	*mEGFP-fim1 ade6-M216 his3-D1 leu1-32 ura4-D18*	Ronan Fernandez
JB232	*mEGFP-myo1 ade6-M216 his3-D1 leu1-32 ura4-D18*	Ronan Fernandez
JB243	*fim1-GFP-KanMX6 pil1-mCherry-NatMX6 ade6-M210 his3-D1 leu1-32 ura4-D18*	Joel Lemiere
JB248	*Acp1-mEGFP-kanMX6 Pil1-mCherry-NatMX6*	Joel Lemiere
JB253	*ABD1:modified_coiledcoil_3leftCys_1extraright:ABD2 fim1-mEGFP-NatMX6 ade6-M210 his3-D1 leu1-32 ura4-D18*	Ronan Fernandez
JB254	*ABD1:modified_coiledcoil_3leftCys_1right:ABD2 fim1-mEGFP-NatMX6 ade6-M210 his3-D1 leu1-32 ura4-D18*	Ronan Fernandez
JB255	*ABD1:modified_coiledcoil_all_hydrophobic:ABD2 fim1-mEGFP-NatMX6 ade6-M210 his3-D1 leu1-32 ura4-D18*	Ronan Fernandez
JB256	*ABD1:modified_coiledcoil_3leftCys_1extraright:ABD2 acp1-mEGFP-KanMX6 ade6-M210 his3-D1 leu1-32 ura4-D18*	Ronan Fernandez
JB257	*ABD1:modified_coiledcoil_3leftCys_1right:ABD2 acp1-mEGFP-KanMX6 ade6-M210 his3-D1 leu1-32 ura4-D18*	Ronan Fernandez
JB258	*ABD1:modified_coiledcoil_all_hydrophobic:ABD2 acp1-mEGFP-KanMX6 ade6-M210 his3-D1 leu1-32 ura4-D18*	Ronan Fernandez
JB259	*ABD1:modified_coiledcoil_3leftCys_1extraright:ABD2 end4-mEGFP-KanMX6 ade6-M216 his3-D1 leu1-32 ura4-D18*	Ronan Fernandez
JB260	*ABD1:modified_coiledcoil_3leftCys_1right:ABD2 end4-mEGFP-KanMX6 ade6-M216 his3-D1 leu1-32 ura4-D18*	Ronan Fernandez
JB261	*ABD1:modified_coiledcoil_all_hydrophobic:ABD2 end4-mEGFP-KanMX6 ade6-M216 his3-D1 leu1-32 ura4-D18*	Ronan Fernandez
JB262	*41nmt1-mEGFP-actin-leu+ ΔPil1 ade6-M216 his3-D1 ura4-D19*	Joel Lemiere
JB263	*pil1-mEos3.2::kanMX6, ade6-M216, his3-D1, leu1-32, ura4-D18*	Neal Ravindra
JB264	*can1-mEos3.2::kanMX6, ade6-M216, his3-D1, leu1-32, ura4-D18*	Neal Ravindra
JB265		Neal Ravindra
JB266	*mEGFP-wsp1::kanMX6, pil1-mCherry::natMX6, ade6-M216, his3-D1, leu1-32, ura4-D18*	Neal Ravindra
JB267	*mEGFP-wsp1::kanMX6, pil1-mCherry-3GS-SH3_bzz1::natMX6, ade6-M216, his3-D1, leu1-32, ura4-D18*	Neal Ravindra
JB268	*syp1-mEGFP::kanMX6, pil1-mCherry::natMX6, ade6-M216, his3-D1, leu1-32, ura4-D18*	Neal Ravindra
JB272	*vrp1-mEGFP::kanMX6, pil1-mCherry::natMX6, ade6-M216, his3-D1, leu1-32, ura4-D18*	Neal Ravindra
JB273	*bbc1-mEGFP::kanMX6, pil1-mCherry::natMX6, ade6-M216, his3-D1, leu1-32, ura4-D18*	Neal Ravindra
JB274	*abp1-mEGFP::kanMX6, pil1-mCherry::natMX6, ade6-M216, his3-D1, leu1-32, ura4-D18*	Neal Ravindra
JB275	*fim1-mEGFP::kanMX6, pil1-mCherry::natMX6, ade6-M216, his3-D1, leu1-32, ura4-D18*	Neal Ravindra
JB276	*acp1-mEGFP::kanMX6, pil1-mCherry::natMX6, ade6-M216, his3-D1, leu1-32, ura4-D18*	Neal Ravindra

JB277	*cap1-mEGFP::kanMX6, pil1-mCherry::natMX6, ade6-M216, his3-D1, leu1-32, ura4-D18*	Neal Ravindra
JB278	*syp1-mEGFP::kanMX6, pil1-mCherry-3GS-SH3_bzz1::natMX6, ade6-M216, his3-D1, leu1-32, ura4-D18*	Neal Ravindra
JB279	*vrp1-mEGFP::kanMX6, pil1-mCherry-3GS-SH3_bzz1::natMX6, ade6-M216, his3-D1, leu1-32, ura4-D18*	Neal Ravindra
JB280	*bbc1-mEGFP::kanMX6, pil1-mCherry-3GS-SH3_bzz1::natMX6, ade6-M216, his3-D1, leu1-32, ura4-D18*	Neal Ravindra
JB281	*abp1-mEGFP::kanMX6, pil1-mCherry-3GS-SH3_bzz1::natMX6, ade6-M216, his3-D1, leu1-32, ura4-D18*	Neal Ravindra
JB282	*fim1-mEGFP::kanMX6, pil1-mCherry-3GS-SH3_bzz1::natMX6, ade6-M216, his3-D1, leu1-32, ura4-D18*	Neal Ravindra
JB283	*acp1-mEGFP::kanMX6, pil1-mCherry-3GS-SH3_bzz1::natMX6, ade6-M216, his3-D1, leu1-32, ura4-D18*	Neal Ravindra
JB284	*cap1-mEGFP::kanMX6, pil1-mCherry-3GS-SH3_bzz1::natMX6, ade6-M216, his3-D1, leu1-32, ura4-D18*	Neal Ravindra
JB285	*cap1-mEGFP::kanMX6, myo1-SH3Δ, ade6-M216, his3-D1, leu1-32, ura4-D18*	Neal Ravindra
JB286	*abp1-mEGFP::kanMX6, myo1-SH3Δ, ade6-M216, his3-D1, leu1-32, ura4-D18*	Neal Ravindra
JB287	*syp1-mEGFP::kanMX6, myo1-SH3Δ, ade6-M216, his3-D1, leu1-32, ura4-D18*	Neal Ravindra
JB288	*acp1-mEGFP::kanMX6, myo1-2xSH3_myo1, ade6-M216, his3-D1, leu1-32, ura4-D18*	Neal Ravindra
JB289	*pil1-mEGFP-Fex1 SPAC977.11Δ-NatMX6 SPBPB8B6.06cΔ-KanMX6 ade6-M216 his3-D1 leu1-32 ura4-D18*	Ronan Fernandez
JB290	*myo1-SH3Δ, ade6-M216, his3-D1, leu1-32, ura4-D18*	Neal Ravindra
JB291	*bbc1-mEGFP::kanMX6, myo1-SH3Δ, ade6-M216, his3-D1, leu1-32, ura4-D18*	Neal Ravindra
JB292	*crn1-mEGFP::kanMX6, myo1-SH3Δ, ade6-M216, his3-D1, leu1-32, ura4-D18*	Neal Ravindra
JB293	*end41-mEGFP::kanMX6, myo1-SH3Δ, ade6-M216, his3-D1, leu1-32, ura4-D18*	Neal Ravindra
JB294	*vrp1-mEGFP::kanMX6, myo1-SH3Δ, ade6-M216, his3-D1, leu1-32, ura4-D18*	Neal Ravindra
JB295	*acp1-mEGFP::kanMX6, myo1-SH3Δ, ade6-M216, his3-D1, leu1-32, ura4-D18*	Neal Ravindra
JB296	*app1-mEGFP::kanMX6, myo1-SH3Δ, ade6-M216, his3-D1, leu1-32, ura4-D18*	Neal Ravindra
JB297	*clc1-mEGFP::kanMX6, myo1-SH3Δ, ade6-M216, his3-D1, leu1-32, ura4-D18*	Neal Ravindra
JB298	*fim1-mEGFP::kanMX6, myo1-SH3Δ, ade6-M216, his3-D1, leu1-32, ura4-D18*	Neal Ravindra
JB299	*fex1Δ-NatMX6 fex2Δ ade6-M216 his3-D1 leu1-32 ura4-D18*	Neal Ravindra
JB300	*fex1Δ fex2Δ ade6-M216 his3-D1 leu1-32 ura4-D18*	Ronan Fernandez
JB308	*end4-mEGFP fex1Δ fex2Δ ade6-M216 his3-D1 leu1-32 ura4-D18*	Ronan Fernandez
JB309	*syp1-mEGFP fex1Δ fex2Δ ade6-M216 his3-D1 leu1-32 ura4-D18*	Ronan Fernandez
JB310	*crn1-mEGFP fex1Δ fex2Δ ade6-M216 his3-D1 leu1-32 ura4-D18*	Ronan Fernandez
JB311	*fim1-mEGFP fex1Δ fex2Δ ade6-M216 his3-D1 leu1-32 ura4-D18*	Ronan Fernandez
JB312	*acp1-mEGFP fex1Δ fex2Δ ade6-M216 his3-D1 leu1-32 ura4-D18*	Ronan Fernandez
JB313	*mEGFP-myo1 fex1Δ fex2Δ ade6-M216 his3-D1 leu1-32 ura4-D18*	Ronan Fernandez
JB314	*mEGFP-wsp1 fex1Δ fex2Δ ade6-M216 his3-D1 leu1-32 ura4-D18*	Ronan Fernandez
JB315	*pil1-mEGFP-KanMX6 fex1Δ fex2Δ ade6-M216 his3-D1 leu1-32 ura4-D18*	Ronan Fernandez
JB316	*fim1Δ::kanMX6, acp1-mEGFP, ade6-M210 his3-D1 leu1-32 ura4-D18*	Neal Ravindra
JB317	*pan1-mEGFP fex1Δ fex2Δ ade6-M216 his3-D1 leu1-32 ura4-D18*	Ronan Fernandez
JB323	*crn1-mEGFP abp1-SH3-2Δ fex1Δ fex2Δ ade6-M216 his3-D1 leu1-32 ura4-D18*	Neal Ravindra

JB324	*fim1-mEGFP abp1-SH3-2Δ fex1Δ fex2Δ ade6-M216 his3-D1 leu1-32 ura4-D18*	Neal Ravindra
JB325	*acp1-mEGFP abp1-SH3-2Δ fex1Δ fex2Δ ade6-M216 his3-D1 leu1-32 ura4-D18*	Neal Ravindra
JB326	*abp1-SH3-2Δ fex1Δ fex2Δ ade6-M216 his3-D1 leu1-32 ura4-D18*	Neal Ravindra
JB327	*bzz1-SH3-1Δ fim1-mEGFP fex1Δ fex2Δ ade6-M216 his3-D1 leu1-32 ura4-D18*	Neal Ravindra
JB328	*bbc1-SH3Δ fex1Δ fex2Δ ade6-M216 his3-D1 leu1-32 ura4-D18*	Neal Ravindra
JB392	*SPBC19C2.10-mEGFP fex1Δ fex2Δ ade6-M216 his3-D1 leu1-32 ura4-D18*	Ronan Fernandez
JB393	*SNAP-wsp1 fex1Δ fex2Δ ade6-M216 his3-D1 leu1-32 ura4-D18*	Mike Lacy
JB394	*abp1SH3-1Δ fex1Δ fex2Δ ade6-M216 his3-D1 leu1-32 ura4-D18*	Neal Ravindra
JB395	*abp1SH3-1Δ fex1Δ fex2Δ ade6-M210 his3-D1 leu1-32 ura4-D18*	Neal Ravindra
JB396	*abp1SH3-2Δ fex1Δ fex2Δ ade6-M216 his3-D1 leu1-32 ura4-D18*	Neal Ravindra
JB397	*bzz1SH3-2Δ fex1Δ fex2Δ ade6-M216 his3-D1 leu1-32 ura4-D18*	Neal Ravindra
JB398	*bzz1_SH3-2Δ fex1Δ fex2Δ ade6-M210 his3-D1 leu1-32 ura4-D18*	Neal Ravindra
JB399	*mug137SH3Δ fex1Δ fex2Δ ade6-M216 his3-D1 leu1-32 ura4-D18*	Neal Ravindra
JB400	*mug137SH3Δ fex1Δ fex2Δ ade6-M210 his3-D1 leu1-32 ura4-D18*	Neal Ravindra
JB401	*lsb1SH3Δ fex1Δ fex2Δ ade6-M216 his3-D1 leu1-32 ura4-D18*	Neal Ravindra
JB402	*lsb1SH3Δ fex1Δ fex2Δ ade6-M210 his3-D1 leu1-32 ura4-D18*	Neal Ravindra
JB403	*cdc15SH3->myo1SH3 fex1Δ fex2Δ ade6-M216 his3-D1 leu1-32 ura4-D18*	Neal Ravindra
JB404	*cdc15SH3->myo1SH3 fex1Δ fex2Δ ade6-M210 his3-D1 leu1-32 ura4-D18*	Neal Ravindra
JB405	*shd1SH3-3->myo1SH3 fex1Δ fex2Δ ade6-M216 his3-D1 leu1-32 ura4-D18*	Neal Ravindra
JB406	*shd1SH3-3->myo1SH3 fex1Δ fex2Δ ade6-M210 his3-D1 leu1-32 ura4-D18*	Neal Ravindra
JB407	*bbc1SH3->myo1SH3 fex1Δ fex2Δ ade6-M216 his3-D1 leu1-32 ura4-D18*	Neal Ravindra
JB408	*end4-Nterm:modified_coiledcoil_3leftCys_1extraright:end4-Cterm end4-mEGFP fex1Δ fex2Δ ade6-M216 his3-D1 leu1-32 ura4-D18*	Neal Ravindra
JB409	*end4-Nterm:modified_coiledcoil_3leftCys_1right:end4-Cterm end4-mEGFP fex1Δ fex2Δ ade6-M216 his3-D1 leu1-32 ura4-D18*	Neal Ravindra
JB410	*end4-Nterm:modified_coiledcoil_non-hydrophobic:end4-Cterm end4-mEGFP fex1Δ fex2Δ ade6-M216 his3-D1 leu1-32 ura4-D18*	Neal Ravindra
JB411	*cdc15SH3Δ fex1Δ fex2Δ ade6-M216 his3-D1 leu1-32 ura4-D18*	Neal Ravindra
JB412	*cdc15SH3Δ fex1Δ fex2Δ ade6-M210 his3-D1 leu1-32 ura4-D18*	Neal Ravindra
JB413	*shd1SH3-3Δ fex1Δ fex2Δ ade6-M210 his3-D1 leu1-32 ura4-D18*	Neal Ravindra
JB414	*shd1SH3-1-2->bzz1SH3-1-2 fim1-mEGFP fex1Δ fex2Δ ade6-M216 his3-D1 leu1-32 ura4-D18*	Neal Ravindra
JB415	*shd1SH3-1-2->bzz1SH3-1-2 fex1Δ fex2Δ ade6-M216 his3-D1 leu1-32 ura4-D18*	Neal Ravindra
JB416	*shd1SH3-1-2->bzz1SH3-1-2 fex1Δ fex2Δ ade6-M210 his3-D1 leu1-32 ura4-D18*	Neal Ravindra
JB417	*acp1-mEGFP cdc15SH3->myo1SH3 fex1Δ fex2Δ ade6-M216 his3-D1 leu1-32 ura4-D18*	Neal Ravindra
JB418	*acp1-mEGFP cdc15SH3->myo1SH3 fex1Δ fex2Δ ade6-M210 his3-D1 leu1-32 ura4-D18*	Neal Ravindra
JB419	*acp1-mEGFP shd1SH3-3->myo1SH3 fex1Δ fex2Δ ade6-M216 his3-D1 leu1-32 ura4-D18*	Neal Ravindra
JB420	*acp1-mEGFP shd1SH3-3->myo1SH3 fex1Δ fex2Δ ade6-M210 his3-D1 leu1-32 ura4-D18*	Neal Ravindra
JB421	*acp1-mEGFP bbc1SH3->myo1SH3 fex1Δ fex2Δ ade6-M216 his3-D1 leu1-32 ura4-D18*	Neal Ravindra

JB422	*SPBC19C2.10Δ acp1-mEGFP fex1Δ fex2Δ ade6-M216 his3-D1 leu1-32 ura4-D18*	Ronan Fernandez
JB423	*hob1-SH3Δ fex1Δ fex2Δ ade6-M210 his3-D1 leu1-32 ura4-D18*	Neal Ravindra
JB424	*mEGFP-myo1-SH3Δ fex1Δ fex2Δ ade6-M216 his3-D1 leu1-32 ura4-D18*	Neal Ravindra
JB425	*mEGFP-myo1-SH3Δ fex1Δ fex2Δ ade6-M210 his3-D1 leu1-32 ura4-D18*	Neal Ravindra
JB426	*shd1-SH3-3Δ fex1Δ fex2Δ ade6-M216 his3-D1 leu1-32 ura4-D18*	Neal Ravindra
JB427	*acp1-mEGFP lsb4-SH3Δ fex1Δ fex2Δ ade6-M216 his3-D1 leu1-32 ura4-D18*	Neal Ravindra
JB428	*acp1-mEGFP abp1-SH3-1Δ fex1Δ fex2Δ ade6-M216 his3-D1 leu1-32 ura4-D18*	Neal Ravindra
JB429	*acp1-mEGFP mug137-SH3Δ fex1Δ fex2Δ ade6-M216 his3-D1 leu1-32 ura4-D18*	Neal Ravindra
JB430	*acp1-mEGFP lsb1-SH3Δ fex1Δ fex2Δ ade6-M216 his3-D1 leu1-32 ura4-D18*	Neal Ravindra
JB431	*acp1-mEGFP shd1-SH3-3Δ fex1Δ fex2Δ ade6-M210 his3-D1 leu1-32 ura4-D18*	Neal Ravindra
JB432	*acp1-mEGFP shd1-SH3-1Δ-2Δ fex1Δ fex2Δ ade6-M210 his3-D1 leu1-32 ura4-D18*	Neal Ravindra
JB433	*acp1-mEGFP bzz1-SH3-2Δ fex1Δ fex2Δ ade6-M210 his3-D1 leu1-32 ura4-D18*	Neal Ravindra
JB434	*acp1-mEGFP cdc15-SH3Δ fex1Δ fex2Δ ade6-M216 his3-D1 leu1-32 ura4-D18*	Neal Ravindra
JB435	*acp1-mEGFP hob1-SH3Δ fex1Δ fex2Δ ade6-M210 his3-D1 leu1-32 ura4-D18*	Neal Ravindra
JB436	*acp1-mEGFP shd1-SH3-1Δ-2Δ fex1Δ fex2Δ ade6-M210 his3-D1 leu1-32 ura4-D18*	Neal Ravindra
JB437	*acp1-mEGFP abp1-SH3-2Δ fex1Δ fex2Δ ade6-M216 his3-D1 leu1-32 ura4-D18*	Neal Ravindra
JB438	*mEGFP-SPBC19C2.10 fex1Δ fex2Δ ade6-M216 his3-D1 leu1-32 ura4-D18*	Ronan Fernandez
JB439	*arp2E167A fex1Δ fex2Δ ade6-M216 his3-D1 leu1-32 ura4-D18*	Neal Ravindra
JB440	*arp3D198A fex1Δ fex2Δ ade6-M210 his3-D1 leu1-32 ura4-D18*	Neal Ravindra
JB441	*arp2E167A acp1-mEGFP fex1Δ fex2Δ ade6-M216 his3-D1 leu1-32 ura4-D18*	Neal Ravindra
JB442	*arp3E198A acp1-mEGFP fex1Δ fex2Δ ade6-M216 his3-D1 leu1-32 ura4-D18*	Neal Ravindra
JB443	*pil1Δ fex1Δ fex2Δ ade6-M216 his3-D1 leu1-32 ura4-D18*	Ronan Fernandez
JB444	*shd1_SH3-1Δ fex1Δ fex2Δ ade6-M216 his3-D1 leu1-32 ura4-D18*	Ronan Fernandez
JB445	*shd1_SH3-1Δ fex1Δ fex2Δ ade6-M210 his3-D1 leu1-32 ura4-D18*	Ronan Fernandez
JB329	*crn1-mEGFP bzz1-SH3-2Δ fex1Δ fex2Δ ade6-M216 his3-D1 leu1-32 ura4-D18*	Neal Ravindra
JB330	*fim1-mEGFP bzz1-SH3-1Δ-2Δ shd1-SH3-1-2(bzz1-SH3-1-2)-3Δ fex1Δ fex2Δ ade6-M216 his3-D1 leu1-32 ura4-D18*	Neal Ravindra
JB331	*acp1-mEGFP bzz1-SH3-2Δ fex1Δ fex2Δ ade6-M216 his3-D1 leu1-32 ura4-D18*	Neal Ravindra
JB332	*crn1-mEGFP bzz1-SH3-1-2Δ fex1Δ fex2Δ ade6-M216 his3-D1 leu1-32 ura4-D18*	Neal Ravindra
JB333	*fim1-mEGFP bzz1-SH3-1-2Δ fex1Δ fex2Δ ade6-M216 his3-D1 leu1-32 ura4-D18*	Neal Ravindra
JB334	*acp1-mEGFP bzz1-SH3-1-2Δ fex1Δ fex2Δ ade6-M216 his3-D1 leu1-32 ura4-D18*	Neal Ravindra
JB335	*bbc1-SH3Δ fex1Δ fex2Δ ade6-M210 his3-D1 leu1-32 ura4-D18*	Neal Ravindra
JB336	*fim1-mEGFP myo1-SH3Δ fex1Δ fex2Δ ade6-M216 his3-D1 leu1-32 ura4-D18*	Neal Ravindra
JB337	*bbc1-SH3Δ acp1-mEGFP fex1Δ fex2Δ ade6-M216 his3-D1 leu1-32 ura4-D18*	Neal Ravindra

JB340	*shd1-SH3-1Δ-2Δ-3Δ fim1-mEGFP fex1Δ fex2Δ ade6-M216 his3-D1 leu1-32 ura4-D18*	Neal Ravindra
JB341	*shd1-SH3-1Δ-2Δ-3Δ bzz1-SH3-1Δ-2Δ fim1-mEGFP fex1Δ fex2Δ ade6-M216 his3-D1 leu1-32 ura4-D18*	Neal Ravindra
JB342	*fim1-mEGFP shd1-SH3-1-2(bzz1-SH3-1-2) fex1Δ fex2Δ ade6-M216 his3-D1 leu1-32 ura4-D18*	Neal Ravindra
JB343	*shd1-SH3-1-2(bzz1-SH3-1-2) fex1Δ fex2Δ ade6-M216 his3-D1 leu1-32 ura4-D18*	Neal Ravindra
JB344	*bzz1-SH3-1Δ fex1Δ fex2Δ ade6-M210 his3-D1 leu1-32 ura4-D18*	Neal Ravindra
JB345	*bzz1-SH3-1Δ acp1-mEGFP fex1Δ fex2Δ ade6-M216 his3-D1 leu1-32 ura4-D18*	Neal Ravindra
JB349		Neal Ravindra
JB350	*shd1-SH3-1Δ-2Δ fex1Δ fex2Δ ade6-M216 his3-D1 leu1-32 ura4-D18*	Neal Ravindra
JB351	*shd1-SH3-1Δ-2Δ fex1Δ fex2Δ ade6-M210 his3-D1 leu1-32 ura4-D18*	Neal Ravindra
JB352	*shd1-SH3-1Δ-2Δ-3Δ fex1Δ fex2Δ ade6-M216 his3-D1 leu1-32 ura4-D18*	Neal Ravindra
JB353	*shd1-SH3-1Δ-2Δ-3Δ fex1Δ fex2Δ ade6-M210 his3-D1 leu1-32 ura4-D18*	Neal Ravindra
JB354	*shd1-SH3-1Δ-2Δ-3Δ acp1-mEGFP fex1Δ fex2Δ ade6-M216 his3-D1 leu1-32 ura4-D18*	Neal Ravindra
JB355	*fex1Δ fex2Δ ade6-M216 his3-D1 leu1-32 ura4-D18*	Ronan Fernandez
JB356	*KanMX6-Pmyo1-hs_MyoIEmotordomain_myo1 ade6-M216 his3-D1 leu1-32 ura4-D18*	Ronan Fernandez
JB357	*lsb4-SH3Δ fex1Δ fex2Δ ade6-M216 his3-D1 leu1-32 ura4-D18*	Neal Ravindra
JB358	*lsb4-SH3Δ fex1Δ fex2Δ ade6-M210 his3-D1 leu1-32 ura4-D18*	Neal Ravindra
JB361	*pil1-mEGFP-NatMX6 leu1-32 ura4-D18 his3-D1 ade6-M210*	Mike Lacy
JB362	*fex1Δ fex2Δ ade6-M210 his3-D1 leu1-32 ura4-D18*	Ronan Fernandez
JB363	*pil1-mEGFP-KanMX6 leu1-32 ura4-D18 his3-D1 ade6-M210*	Mike Lacy
JB365	*syp1-mEGFP fex1Δ fex2Δ ade6-M216 his3-D1 leu1-32 ura4-D18*	Ronan Fernandez
JB366	*acp1-mEGFP fex1Δ fex2Δ ade6-M216 his3-D1 leu1-32 ura4-D18*	Ronan Fernandez
JB367	*end4-mEGFP fex1Δ fex2Δ ade6-M216 his3-D1 leu1-32 ura4-D18*	Ronan Fernandez
JB368	*Pmyo1Δ fex1Δ fex2Δ ade6-M216 his3-D1 leu1-32 ura4-D18*	Ronan Fernandez
JB369	*mEGFP-myo1 fex1Δ fex2Δ ade6-M216 his3-D1 leu1-32 ura4-D18*	Ronan Fernandez
JB370	*mEGFP-fim1 fex1Δ fex2Δ ade6-M210 his3-D1 leu1-32 ura4-D18*	Ronan Fernandez
JB371	*mEGFP-myo1 fex1Δ fex2Δ ade6-M210 his3-D1 leu1-32 ura4-D18*	Ronan Fernandez
JB372	*mEGFP-fim1 fex1Δ fex2Δ ade6-M216 his3-D1 leu1-32 ura4-D18*	Ronan Fernandez
JB373	*end4-Nterm:modified_coiledcoil_3leftCys_1extraright:end4-Cterm acp1-mEGFP fex1Δ fex2Δ ade6-M216 his3-D1 leu1-32 ura4-D18*	Neal Ravindra
JB374	*end4-Nterm:modified_coiledcoil_3leftCys_1right:end4-Cterm acp1-mEGFP fex1Δ fex2Δ ade6-M216 his3-D1 leu1-32 ura4-D18*	Neal Ravindra
JB375	*end4-Nterm:modified_coiledcoil_non-hydrophobic:end4-Cterm acp1-mEGFP fex1Δ fex2Δ ade6-M216 his3-D1 leu1-32 ura4-D18*	Neal Ravindra
JB376		Neal Ravindra
JB377	*myo1-SH3Δ fex1Δ fex2Δ ade6-M216 his3-D1 leu1-32 ura4-D18*	Neal Ravindra
JB378	*myo1-SH3Δ fex1Δ fex2Δ ade6-M210 his3-D1 leu1-32 ura4-D18*	Neal Ravindra
JB379	*myo1-SH3Δ acp1-mEGFP fex1Δ fex2Δ ade6-M216 his3-D1 leu1-32 ura4-D18*	Neal Ravindra
JB380	*crn1-mEGFP fex1Δ fex2Δ ade6-M216 his3-D1 leu1-32 ura4-D18*	Ronan Fernandez
JB385	*mEGFP-wsp1 fex1Δ fex2Δ ade6-M216 his3-D1 leu1-32 ura4-D18*	Ronan Fernandez
JB386	*mEGFP-wsp1 fex1Δ fex2Δ ade6-M210 his3-D1 leu1-32 ura4-D18*	Ronan Fernandez
JB446	*abp1_SH3-1Δ fex1Δ fex2Δ ade6-M216 his3-D1 leu1-32 ura4-D18*	Ronan Fernandez
JB447	*abp1_SH3-1Δ fex1Δ fex2Δ ade6-M210 his3-D1 leu1-32 ura4-D18*	Ronan Fernandez

JB448	*lsb1_SH3Δ fex1Δ fex2Δ ade6-M216 his3-D1 leu1-32 ura4-D18*	Ronan Fernandez
JB449	*lsb1_SH3Δ fex1Δ fex2Δ ade6-M210 his3-D1 leu1-32 ura4-D18*	Ronan Fernandez
JB450	*shd1_SH3-1Δ acp1-mEGFP fex1Δ fex2Δ ade6-M216 his3-D1 leu1-32 ura4-D18*	Ronan Fernandez
JB451	*abp1_SH3-1Δ acp1-mEGFP fex1Δ fex2Δ ade6-M216 his3-D1 leu1-32 ura4-D18*	Ronan Fernandez
JB452	*lsb1_SH3Δ acp1-mEGFP fex1Δ fex2Δ ade6-M216 his3-D1 leu1-32 ura4-D18*	Ronan Fernandez
JB453	*myo1_W1143K fex1Δ fex2Δ ade6-M216 his3-D1 leu1-32 ura4-D18*	Ronan Fernandez
JB454	*myo1_W1143K fex1Δ fex2Δ ade6-M210 his3-D1 leu1-32 ura4-D18*	Ronan Fernandez
JB455	*shd1_SH3-2Δ fex1Δ fex2Δ ade6-M216 his3-D1 leu1-32 ura4-D18*	Ronan Fernandez
JB456	*shd1_SH3-2Δ fex1Δ fex2Δ ade6-M210 his3-D1 leu1-32 ura4-D18*	Ronan Fernandez
JB457	*shd1_SH3-2Δ acp1-mEGFP fex1Δ fex2Δ ade6-M216 his3-D1 leu1-32 ura4-D18*	Ronan Fernandez
JB458	*arp3E198A arp2E167A fex1Δ fex2Δ ade6-M216 his3-D1 leu1-32 ura4-D18*	Ronan Fernandez
JB459	*myo1_Scmyo3-SH3 fex1Δ fex2Δ ade6-M216 his3-D1 leu1-32 ura4-D18*	Ronan Fernandez
JB460	*myo1_Scmyo3-SH3 acp1-mEGFP fex1Δ fex2Δ ade6-M216 his3-D1 leu1-32 ura4-D18*	Ronan Fernandez
JB461	*myo1_Scmyo5-SH3 fex1Δ fex2Δ ade6-M216 his3-D1 leu1-32 ura4-D18*	Ronan Fernandez
JB462	*myo1_Scmyo5-SH3 acp1-mEGFP fex1Δ fex2Δ ade6-M216 his3-D1 leu1-32 ura4-D18*	Ronan Fernandez
JB464	*acp1-mEGFP arp3E198A arp2E167A fex1Δ fex2Δ ade6-M216 his3-D1 leu1-32 ura4-D18*	Ronan Fernandez
JB465	*lsb4-mEGFP fex1Δ fex2Δ ade6-M216 his3-D1 leu1-32 ura4-D18*	Ronan Fernandez
JB466	*shd1-mEGFP shd1-SH3-3Δ fex1Δ fex2Δ ade6-M216 his3-D1 leu1-32 ura4-D18*	Ronan Fernandez
JB467	*shd1-mEGFP shd1_SH3-2Δ fex1Δ fex2Δ ade6-M216 his3-D1 leu1-32 ura4-D18*	Ronan Fernandez
JB468	*shd1-mEGFP shd1_SH3-1Δ fex1Δ fex2Δ ade6-M216 his3-D1 leu1-32 ura4-D18*	Ronan Fernandez
JB469	*abp1-mEGFP fex1Δ fex2Δ ade6-M216 his3-D1 leu1-32 ura4-D18*	Ronan Fernandez
JB470	*abp1-mEGFP abp1_SH3-1Δ fex1Δ fex2Δ ade6-M216 his3-D1 leu1-32 ura4-D18*	Ronan Fernandez
JB471	*lsb1-mEGFP fex1Δ fex2Δ ade6-M216 his3-D1 leu1-32 ura4-D18*	Ronan Fernandez
JB472	*lsb1-mEGFP lsb1_SH3Δ fex1Δ fex2Δ ade6-M216 his3-D1 leu1-32 ura4-D18*	Ronan Fernandez
JB473	*myo1_W1143K mEGFP-myo1 fex1Δ fex2Δ ade6-M216 his3-D1 leu1-32 ura4-D18*	Ronan Fernandez
JB474	*hob1-mEGFP fex1Δ fex2Δ ade6-M210 his3-D1 leu1-32 ura4-D18*	Ronan Fernandez
JB475	*mEGFP-cdc15 fex1Δ fex2Δ ade6-M216 his3-D1 leu1-32 ura4-D18*	Ronan Fernandez
JB476	*mEGFP-cdc15 cdc15SH3Δ fex1Δ fex2Δ ade6-M216 his3-D1 leu1-32 ura4-D18*	Ronan Fernandez
JB477	*mEGFP-mug137 fex1Δ fex2Δ ade6-M216 his3-D1 leu1-32 ura4-D18*	Ronan Fernandez
JB478	*mEGFP-mug137 mug137SH3Δ fex1Δ fex2Δ ade6-M216 his3-D1 leu1-32 ura4-D18*	Ronan Fernandez
JB483	*fex1Δ fex2Δ adf1(K32A, S24A, R26A) acp1-SNAP ade6-M210 his3-D1 leu1-32 ura4-D18*	Mike Lacy
JB484	*lsb5-mEGFP fex1Δ fex2Δ ade6-M216 his3-D1 leu1-32 ura4-D18*	Ronan Fernandez
JB485	*fex1Δ fex2Δ adf1(K32A, S24A, R26A) acp1-mEGFP ade6-M210 his3-D1 leu1-32 ura4-D18*	Mike Lacy
JB486	*bbc1-mEGFP fex1Δ fex2Δ ade6-M216 his3-D1 leu1-32 ura4-D18*	Ronan Fernandez
JB487	*abp1-mEGFP abp1SH3-2Δ fex1Δ fex2Δ ade6-M216 his3-D1 leu1-32 ura4-D18*	Ronan Fernandez

JB488	*hob1-mEGFP hob1-SH3Δ fex1Δ fex2Δ ade6-M210 his3-D1 leu1-32 ura4-D18*	Ronan Fernandez
JB489	*bzz1-mEGFP bzz1_SH3-2Δ fex1Δ fex2Δ ade6-M210 his3-D1 leu1-32 ura4-D18*	Ronan Fernandez
JB490	*lsb4-mEGFP lsb4-SH3Δ fex1Δ fex2Δ ade6-M216 his3-D1 leu1-32 ura4-D18*	Ronan Fernandez
JB491	*bzz1-mEGFP bzz1-SH3-1Δ fex1Δ fex2Δ ade6-M210 his3-D1 leu1-32 ura4-D18*	Ronan Fernandez
JB497	*bbc1-mEGFP bbc1-SH3Δ fex1Δ fex2Δ ade6-M216 his3-D1 leu1-32 ura4-D18*	Ronan Fernandez
JB505	*bzz1-mEGFP fex1Δ fex2Δ ade6-M216 his3-D1 leu1-32 ura4-D18*	Ronan Fernandez
JB506	*acp1-mEGFP SNAP-fim1 fex1Δ fex2Δ ade6-M216 his3-D1 leu1-32 ura4-D18*	Ronan Fernandez
JB521	*modified_coiledcoil_3leftCys_1extraright-end4-mEGFP fex1Δ fex2Δ ade6-M216 his3-D1 leu1-32 ura4-D18*	Yuan Ren
JB528	*cdc15_SH3Δ::myo1_SH3 acp1-mEGFP fex1Δ fex2Δ ade6-M216 his3-D1 leu1-32 ura4-D18*	Ronan Fernandez
JB529	*cdc15_SH3Δ::bbc1_SH3 acp1-mEGFP fex1Δ fex2Δ ade6-M216 his3-D1 leu1-32 ura4-D18*	Ronan Fernandez
JB530	*bbc1_SH3Δ::myo1_SH3 acp1-mEGFP fex1Δ fex2Δ ade6-M216 his3-D1 leu1-32 ura4-D18*	Ronan Fernandez
JB531	*bbc1_SH3Δ::cdc15_SH3 acp1-mEGFP fex1Δ fex2Δ ade6-M216 his3-D1 leu1-32 ura4-D18*	Ronan Fernandez

C. Plasmids

Table 14. Plasmids used in these studies

Plasmid name	Insert of interest	Core Vector	Investigator
pJB4	pFA6a-mEGFP-Nat		Julien Berro
pJB45	pFA6a-mEGFP-kanMX6		Julien Berro
pJB53	pPAmCherry1-C1		Ronan Fernandez
pJB59	pFA6a-SNAP-KanMX6	pFA6a	Ronan Fernandez
pJB66	pFA6a-mEOS3.2-KanMX6	pFA6a	Ronan Fernandez
pJB109	pMZ374:target_pil1	pJB106	Ronan Fernandez
pJB110	pMZ374:target_fim1	pJB106	Ronan Fernandez
pJB111	pCRBlunt:ABD1-11aalinker-ABD2	pCRBlunt	Ronan Fernandez
pJB174	pJB106:targetFEX1&2	pJB106	Ronan Fernandez
pJB176	pJB166:target_fim1	pJB166	Ronan Fernandez
pJB180	pJB106:target_KanMX6	pJB106	Ronan Fernandez
pJB181	pJB166:target_NatMX6.3	pJB166	Ronan Fernandez
pJB182	pJB106:target_myo1_SH3	pJB106	Neal Ravindra
pJB187	pCRBlunt_Myo1_2SH3_a+b	pCRBlunt	Ronan Fernandez
pJB189	pCRBlunt:modified_dynein_stalk_3leftCys_1extrarightCys	pCRBlunt	Ronan Fernandez
pJB190	pCRBlunt:modified_dynein_stalk_3leftCys_1rightCys	pCRBlunt	Ronan Fernandez
pJB191	pCRBlunt:modified_dynein_stalk_all_hydrophobic	pCRBlunt	Ronan Fernandez
pJB206	pJB166:Target_KanMX6	pJB166	Ronan Fernandez
pJB207	pJET1.2blunt:PCR_NatMX6deletion	pJET1.2blunt	Ronan Fernandez
pJB208	pJB166:Target_NatMX6.2	pJB166	Ronan Fernandez
pJB209	pJB166:Target_KanMX6	pJB166	Ronan Fernandez
pJB210	pJET1.2blunt:Cas9_codon_optimized	pJET1.2blunt	Ronan Fernandez
pJB211	pJB106_Cas9_codon_optimized	pJB106	Ronan Fernandez
pJB212	pJB166_Cas9_codon_optimized	pJB166	Ronan Fernandez
pJB214	pJB106-Cas9+EcoRVsite	pJB106	Ronan Fernandez
pJB215	pJB166-Cas9+EcoRVsite	pJB166	Ronan Fernandez
pJB112	pCRBlunt:ABD1-24aalinker-ABD2	pCRBlunt	Ronan Fernandez
pJB113	pJB106-Ura6+KanMX6	pJB106	Ronan Fernandez
pJB123	pMZ374:gRNA_Ct_fim1		Ronan Fernandez
pJB124	pMZ374:gRNA_Ct_wsp1		Ronan Fernandez
pJB125	pMZ374:gRNA_Ct_myo1		Ronan Fernandez
pJB126	pMZ374:gRNA_Ct_SPBC19C2.10		Ronan Fernandez
pJB127	pMZ374:gRNA_Ct_SPBP8B7.26		Ronan Fernandez
pJB128	pMZ374:gRNA_Ct_mug137		Ronan Fernandez
pJB129	pMZ374:gRNA_Nt_fim1		Ronan Fernandez
pJB130	pMZ374:gRNA_Nt_wsp1		Ronan Fernandez
pJB131	pMZ374:gRNA_Nt_myo1		Ronan Fernandez
pJB132	pMZ374:gRNA_Nt_SPBC19C2.10		Ronan Fernandez

pJB133	pMZ374:gRNA_Nt_SPBP8B7.26		Ronan Fernandez
pJB134	pMZ374:gRNA_Nt_mug137		Ronan Fernandez
pJB140	pMZ374:gRNA_Ct_bzz1		Ronan Fernandez
pJB141	pMZ374:gRNA_Nt_cdc15		Ronan Fernandez
pJB142	pMZ374:gRNA_Nt_bzz1		Ronan Fernandez
pJB157	pJB106-Ura6+NatMX6		Ronan Fernandez
pJB158	pCRBlunt:ABD1-coiledcoil-ABD2	pCRBlunt	Ronan Fernandez
pJB160	pCRBlunt:PCRpil1Δ	pCRBlunt	Ronan Fernandez
pJB163	pCRBlunt:pil1-mEGFP+ext	pCRBlunt	Ronan Fernandez
pJB164	pFA6a-mCherry-3GS-SH3_bzz1-Nat	pJB28	Ronan Fernandez
pJB165	PFA6a-mCherry-3GS-2xSH3_bzz1-NatMX6	pJB28	Ronan Fernandez
pJB166	pJB106-Ura4+CDS_FEX1	pJB106	Ronan Fernandez
pJB167	pCRBlunt:pil1-mEGFP+BamHIext	pCRBlunt	Ronan Fernandez
pJB169	pJB162:CDS_pil1	pGEX6PI	Ronan Fernandez
pJB170	pJB162:CDS_pil1-mEGFP	pGEX6PI	Ronan Fernandez
pJB171	pJB106:gRNA_fim1	pJB106	Ronan Fernandez
pJB172	pJB166:target_pil1	pJB166	Ronan Fernandez
pJB218	pJET1.2:deletionSH3_1_abp1	pJET1.2	Ronan Fernandez
pJB219	pJET1.2:deletionSH3_1+2_abp1	pJET1.2	Ronan Fernandez
pJB223	pJET1.2_bzz1_SH3-1del	pJET1.2	Ronan Fernandez
pJB227	pJET1.2-shd1-SH3-1del-2del-3del		Neal Ravindra
pJB228	pJET1.2_hob1_SH3del	pJET1.2	Neal Ravindra
pJB229	pJET1.2_lsb4_SH3del	pJET1.2	Neal Ravindra
pJB230	pJET1.2_mug137_SH3del	pJET1.2	Neal Ravindra
pJB231	pJET1.2_myo1_SH3del	pJET1.2	Neal Ravindra
pJB232	pJET1.2_abp1_SH3-2del	pJET1.2	Neal Ravindra
pJB233	pJET1.2_bbc1_SH3del	pJET1.2	Neal Ravindra
pJB234	pJET1.2_bzz1_SH3-1del-2del	pJET1.2	Neal Ravindra
pJB235	pJET1.2_SPBC19C2.10_SH3del	pJET1.2	Neal Ravindra
pJB236	pJET1.2_PCR_SH3del_cdc15	pJET1.2	Ronan Fernandez
pJB237	pJET1.2_PCR_SH3del_lsb1	pJET1.2	Ronan Fernandez
pJB241	pJET1.2_end4_24aa	pJET1.2	Ronan Fernandez
pJB242	pJET1.2_KOD_fim1-mEGFP	pJET1.2	Ronan Fernandez
pJB243	pJET1.2_bzz1-SH3-2del	pJET1.2	Neal Ravindra
pJB246	pJB166:target_myo1_SH3	pJB166	Ronan Fernandez
pJB249	pJET1.2_myo1_W1143K		
pJB250	pJET1.2_shd1-SH3-1del	pJET1.2	Neal Ravindra
pJB251	pJET1.2_shd1-SH3-2del	pJET1.2	Neal Ravindra
pJB252	pJET1.2:Arp2_E167A	pJET1.2	Ronan Fernandez
pJB253	pJET1.2:Arp3_D198A	pJET1.2	Ronan Fernandez
pJB254	myo3->myo1		Neal Ravindra
pJB255	myo5->myo1		Neal Ravindra
pJB256	pJB166:target_bbc1-SH3	pJB166	Ronan Fernandez
pJB257	pJB166:target_shd1-SH3-3	pJB166	Ronan Fernandez
pJB258	pJET1.2_KODmEGFP-myo1	pJET1.2	Ronan Fernandez

pJB259	pET22b	pET22b	Ronan Fernandez
pJB260	pJET1.2blunt_CDSfim1+pET22bext	pJET1.2	Ronan Fernandez
pJB261	pET22b_CDSfim1	pET22b	Ronan Fernandez
pJB262	pET22b_CDSfim1(ABD1-24aalinker-ABD2	pET22b	Ronan Fernandez
pJB274	pJET1.2_KODlsb1-mEGFP+tailJB'1204	pJET1.2	Ronan Fernandez
pJB275	pJET1.2_cdc15SH3+ext	pJET1.2	Ronan Fernandez

D. Code and data availability

The datasets generated and analyzed for chapter II and VIII are available at git.yale.edu/ngr4 under the appropriate branch, organized by manuscript. All raw data is available on hard-drives in ISTC 214C, organized by acquisition date. Code to automatically track patches (Tinevez et al., 2017) was incorporated into PatchTrackingTools by Julien Berro (J. Berro & T. D. Pollard, 2014). Alignment of tracked endocytic patches is done using a temporal super-resolution method, authored by Julien Berro (J. Berro & T. D. Pollard, 2014). Parameter scan simulations were authored by NGR based off of a model encoded into a SimBiology MATLAB project environment by Julien Berro (Berro et al., 2010). Flow-control, execution, and post-processing of structural homology modeling algorithms was authored by NGR and based off code written by Andrej Sali and maintained by the Sali lab (Eswar et al., 2006; Fiser, Do, & Sali, 2000; Melo, Sanchez, & Sali, 2002; Sali & Blundell, 1993). All other software described in this dissertation was authored by NGR and is freely available for use under a MIT license at git.yale.edu/ngr4.

Acknowledgments

Whatever I am and have accomplished, I did with the unwavering support, help, and advice of my friends and family. I want to thank my parents, Bridget B. Ravindra and Baikadi A. Ravindra who supported me throughout my education, encouraged me, and helped me to believe in myself, regardless of ends and means.

I want to thank my sister, Tara R. Ravindra and her husband, Theodore D. Logan, who always welcomed me and frequently helped me think through what really matters and helped me to remember who I am and what I can be.

I want to thank my dear friends Lea Kiefer, Nandan G. Pandit, Garrett Debs, Martha Braun, and Curran Oi. They listened to me while I vented and struggled, they helped me to push through and accomplish my goals, tirelessly offering their advice, their time, and, always, by their presence, rejuvenating me. More frequently than they know, they revitalized me in the toughest moments of research and at those points in graduate school when I needed the most help. More frequently than we could realistically pursue in a lifetime, they enthusiastically brainstormed ideas, concepts, proposals, and scientific approaches with me and they taught me to love research and study.

I want to thank Antonio Delgado, my undergraduate academic advisor, who believed in me, often to a far greater extent than I, and steadfastly assured me that I was capable of contributing to scientific knowledge.

I want to thank those who showed me extraordinary generosity & patience in offering their advice and time while I was in graduate school, especially Tony Koleske, Karla Neugebauer, Enrique de la Cruz, Lynne Regan, Megan King, Jonathon Howard, Yong Xiong, Mark Solomon, Rui Ma, Mike Lacy, Ronan Fernandez, and Joel Lemiere.

I want to especially thank Ronan Fernandez, who offered me technical support throughout my studies and taught me molecular biology. Ronan always offered me a calm and fair perspective and his consistent lab hands always served as an excellent control when things were not working.

I want to thank Michael M. Lacy, who was always there for me, with advice, and who showed me how to be a good graduate student. He helped me to write concisely and tirelessly edited my work even when it was too dense for my own perusal.

I want to thank Rui Ma, who always listened to me and advised me when I had no one else to turn to. Mike and Rui were consistently there to counter isolation.

I want to thank my committee members, Lynne Regan, Jonathon Howard, and Megan King because, even though I did not always pose the simplest problems to resolve, they always found solutions to help me.

I want to thank Dr. Jeffrey Bender for encouraging me and helping to advance my career into new research projects with supportive mentors. I want to thank Katherine Woodford, Helen Beilinson, Fatima Mirza, Yasmin Zakiniaiez, Mike Lacy and all of the members of the Yale Journal of Biology & Medicine editorial board who have taught me professionalism and many lessons regarding management, leadership, and correspondence within the bastion of academic publishing.

I want to thank Dr. Nihar R. Desai and Dr. Tariq Ahmad for showing me how collaborative and inclusive research can be through supportive mentorship and enthusiastic leadership.

Finally, I want to thank Lea Kiefer and our feline family, Ori, Polli, and Jonny for their persistent and judgment-free love. Having a home and friends that always offer unconditional love continue to make it all worthwhile.

References

Adler, M., Mayo, A., Zhou, X., Franklin, R. A., Jacox, J. B., Medzhitov, R., & Alon, U. (2018). Endocytosis as a stabilizing mechanism for tissue homeostasis. *Proceedings of the National Academy of Sciences, 115*(8), E1926-E1935. doi:10.1073/pnas.1714377115

Aghamohammadzadeh, S., & Ayscough, K. R. (2009). Differential requirements for actin during yeast and mammalian endocytosis. *Nat Cell Biol, 11*(8), 1039-1042. doi:10.1038/ncb1918

Aghamohammadzadeh, S., Smaczynska-de Rooij, I. I., & Ayscough, K. R. (2014). An Abp1-dependent route of endocytosis functions when the classical endocytic pathway in yeast is inhibited. *PLoS One, 9*(7). doi:10.1371/journal.pone.0103311

Ago, T., Kitazono, T., Kuroda, J., Kumai, Y., Kamouchi, M., Ooboshi, H., . . . Iida, M. (2005). NAD(P)H oxidases in rat basilar arterial endothelial cells. *Stroke, 36*(5), 1040-1046. doi:10.1161/01.STR.0000163111.05825.0b

Akamatsu, M., Vasan, R., Serwas, D., Ferrin, M., Rangamani, P., & Drubin, D. G. (2019). doi:10.1101/678797

Ali, M., Chernova, T. A., Newnam, G. P., Yin, L., Shanks, J., Karpova, T. S., . . . Wilkinson, K. D. (2014). Stress-dependent Proteolytic Processing of the Actin Assembly Protein Lsb1 Modulates a Yeast Prion. *Journal of Biological Chemistry, 289*(40), 27625-27639. Retrieved from http://www.jbc.org/content/289/40/27625

Amaya, J., Ryan, V. H., & Fawzi, N. L. (2018). The SH3 domain of Fyn kinase interacts with and induces liquid-liquid phase separation of the low complexity domain of hnRNPA2. *Journal of Biological Chemistry*. doi:10.1074/jbc.RA118.005120

Anderson, B. L., Boldogh, I., Evangelista, M., Boone, C., Greene, L. A., & Pon, L. A. (1998). The Src homology domain 3 (SH3) of a yeast type I myosin, Myo5p, binds to verprolin and is required for targeting to sites of actin polarization. *The Journal of cell biology, 141*(6), 1357-1370. doi:10.1083/jcb.141.6.1357

Anderson, D., Koch, C., Grey, L., Ellis, C., Moran, M., & Pawson, T. (1990). Binding of SH2 domains of phospholipase C gamma 1, GAP, and Src to activated growth factor receptors. *Science, 250*(4983), 979-982. doi:10.1126/science.2173144

Antonny, B., Burd, C., De Camilli, P., Chen, E., Daumke, O., Faelber, K., . . . Schmid, S. (2016). Membrane fission by dynamin: what we know and what we need to know. *Embo j, 35*(21), 2270-2284. doi:10.15252/embj.201694613

Arasada, R., & Pollard, T. D. (2011). Distinct roles for F-BAR proteins Cdc15p and Bzz1p in actin polymerization at sites of endocytosis in fission yeast. *Current biology : CB, 21*(17), 1450-1459. doi:10.1016/j.cub.2011.07.046

Arasada, R., Sayyad, W. A., Berro, J., & Pollard, T. D. (2018). High-speed superresolution imaging of the proteins in fission yeast clathrin-mediated endocytic actin patches. *Mol Biol Cell, 29*(3), 295-303. doi:10.1091/mbc.E17-06-0415

Arasada, R., Sayyad, W. A., Berro, J., & Pollard, T. D. (2018). High-speed superresolution imaging of the proteins in fission yeast clathrin-mediated endocytic actin patches. *Molecular Biology of the Cell, 29*(3), 295-303. doi:10.1091/mbc.E17-06-0415

Avinoam, O., Schorb, M., Beese, C. J., Briggs, J. A., & Kaksonen, M. (2015). Endocytic sites mature by continuous bending and remodeling of the clathrin coat. *Science, 348*(6241), 1369-1372. doi:10.1126/science.aaa9555

Banani, S. F., Lee, H. O., Hyman, A. A., & Rosen, M. K. (2017). Biomolecular condensates: organizers of cellular biochemistry. *Nat Rev Mol Cell Biol, 18*(5), 285-298. doi:10.1038/nrm.2017.7

Banjade, S., & Rosen, M. K. (2014). Phase transitions of multivalent proteins can promote clustering of membrane receptors. *Elife*. Retrieved from elifesciences.org

Banjade, S., & Rosen, M. K. (2014). Phase transitions of multivalent proteins can promote clustering of membrane receptors. *Elife, 3*, e04123. doi:10.7554/eLife.04123

Barnett, P., Bottger, G., Klein, A. T., Tabak, H. F., & Distel, B. (2000). The peroxisomal membrane protein Pex13p shows a novel mode of SH3 interaction. *Embo j, 19*(23), 6382-6391. doi:10.1093/emboj/19.23.6382

Basu, R., Munteanu, E. L., & Chang, F. (2014). Role of turgor pressure in endocytosis in fission yeast. *Mol Biol Cell, 25*(5), 679-687. doi:10.1091/mbc.E13-10-0618

Bergeron-Sandoval, L.-P., Heris, H. K., Hendricks, A. G., Ehrlicher, A. J., Francois, P., Pappu, R. V., & Michnick, S. W. (2017). Endocytosis caused by liquid-liquid phase separation of proteins. *bioRxiv*. doi:10.1101/145664

Bergeron-Sandoval, L. P., Safaee, N., & Michnick, S. W. (2016). Mechanisms and Consequences of Macromolecular Phase Separation. *Cell, 165*(5), 1067-1079. doi:10.1016/j.cell.2016.05.026

Berro, J., & Pollard, T. D. (2014). Local and global analysis of endocytic patch dynamics in fission yeast using a new "temporal superresolution" realignment method. *Molecular Biology of the Cell, 25*(22), 3501-3514. doi:10.1091/mbc.E13-01-0004

Berro, J., & Pollard, T. D. (2014). Synergies between Aip1p and capping protein subunits (Acp1p and Acp2p) in clathrin-mediated endocytosis and cell polarization in fission yeast. *Molecular Biology of the Cell, 25*(22), 3515-3527. doi:10.1091/mbc.E13-01-0005

Berro, J., Sirotkin, V., & Pollard, T. D. (2010). Mathematical modeling of endocytic actin patch kinetics in fission yeast: disassembly requires release of actin filament fragments. *Molecular Biology of the Cell, 21*(16), 2905-2915. doi:10.1091/mbc.E10-12-0965

Bhattacharyya, R. P., Reményi, A., Yeh, B. J., & Lim, W. A. (2006). Domains, Motifs, and Scaffolds: The Role of Modular Interactions in the Evolution and Wiring of Cell Signaling Circuits. *Annu Rev Biochem, 75*(1), 655-680. doi:10.1146/annurev.biochem.75.103004.142710

Bieling, P., Li, T. D., Weichsel, J., McGorty, R., Jreij, P., Huang, B., . . . Mullins, R. D. (2016). Force Feedback Controls Motor Activity and Mechanical Properties of Self-Assembling Branched Actin Networks. *Cell, 164*(1-2), 115-127. doi:10.1016/j.cell.2015.11.057

Blanchoin, L., Boujemaa-Paterski, R., Sykes, C., & Plastino, J. (2014). Actin dynamics, architecture, and mechanics in cell motility. *Physiological reviews, 94*(1), 235-263. doi:10.1152/physrev.00018.2013

Boettner, D. R., Chi, R. J., & Lemmon, S. K. (2011). Lessons from yeast for clathrin-mediated endocytosis. *Nat Cell Biol, 14*(1), 2-10. doi:10.1038/ncb2403

Boukellal, H., Campas, O., Joanny, J. F., Prost, J., & Sykes, C. (2004). Soft Listeria: actin-based propulsion of liquid drops. *Phys Rev E Stat Nonlin Soft Matter Phys, 69*(6 Pt 1), 061906. doi:10.1103/PhysRevE.69.061906

Boulant, S., Kural, C., Zeeh, J. C., Ubelmann, F., & Kirchhausen, T. (2011). Actin dynamics counteract membrane tension during clathrin-mediated endocytosis. *Nat Cell Biol, 13*(9), 1124-1131. doi:10.1038/ncb2307

Bowles, N. E., Bowles, K. R., & Towbin, J. A. (2000). The "final common pathway" hypothesis and inherited cardiovascular disease. The role of cytoskeletal proteins in dilated cardiomyopathy. *Herz, 25*(3), 168-175. Retrieved from https://www.ncbi.nlm.nih.gov/pubmed/10904835

Brown, N. P., Leroy, C., & Sander, C. (1998). MView: a web-compatible database search or multiple alignment viewer. *Bioinformatics, 14*(4), 380-381. doi:10.1093/bioinformatics/14.4.380

Brugge, J. S., & Darrow, D. (1984). Analysis of the catalytic domain of phosphotransferase activity of two avian sarcoma virus-transforming proteins. *J Biol Chem, 259*(7), 4550-4557.

Bucher, D., Frey, F., Sochacki, K. A., Kummer, S., Bergeest, J. P., Godinez, W. J., . . . Boulant, S. (2018). Clathrin-adaptor ratio and membrane tension regulate the flat-to-curved transition of the clathrin coat during endocytosis. *Nat Commun, 9*(1), 1109. doi:10.1038/s41467-018-03533-0

Buday, L., & Downward, J. (1993). Epidermal growth factor regulates p21ras through the formation of a complex of receptor, Grb2 adapter protein, and Sos nucleotide exchange factor. *Cell, 73*(3), 611-620. doi:10.1016/0092-8674(93)90146-h

Burston, H. E., Maldonado-Báez, L., Davey, M., Montpetit, B., Schluter, C., Wendland, B., & Conibear, E. (2009). Regulators of yeast endocytosis identified by systematic quantitative analysis. *The Journal of cell biology, 185*(6), 1097. doi:10.1083/jcb.200811116

Busch, D. J., Houser, J. R., Hayden, C. C., Sherman, M. B., Lafer, E. M., & Stachowiak, J. C. (2015). Intrinsically disordered proteins drive membrane curvature. *Nat Commun, 6*, 7875. doi:10.1038/ncomms8875

Campillo, C., Sens, P., Koster, D., Pontani, L. L., Levy, D., Bassereau, P., . . . Sykes, C. (2013). Unexpected membrane dynamics unveiled by membrane nanotube extrusion. *Biophys J, 104*(6), 1248-1256. doi:10.1016/j.bpj.2013.01.051

Carbonell, P., Nussinov, R., & del Sol, A. (2009). Energetic determinants of protein binding specificity: Insights into protein interaction networks. *PROTEOMICS, 9*(7), 1744-1753. doi:10.1002/pmic.200800425

Carducci, M., Perfetto, L., Briganti, L., Paoluzi, S., Costa, S., Zerweck, J., . . . Cesareni, G. (2012). The protein interaction network mediated by human SH3 domains. *Biotechnology Advances, 30*(1), 4-15. doi:10.1016/j.biotechadv.2011.06.012

Carlsson, A. E. (2010). Actin dynamics: from nanoscale to microscale. *Annu Rev Biophys, 39*, 91-110. doi:10.1146/annurev.biophys.093008.131207

Carlsson, A. E. (2018). Membrane bending by actin polymerization. *Curr Opin Cell Biol, 50*, 1-7. doi:10.1016/j.ceb.2017.11.007

Carlsson, A. E., & Bayly, P. V. (2014). Force generation by endocytic actin patches in budding yeast. *Biophys J, 106*(8), 1596-1606. doi:10.1016/j.bpj.2014.02.035

Carnahan, R. H., & Gould, K. L. (2003). The PCH family protein, Cdc15p, recruits two F-actin nucleation pathways to coordinate cytokinetic actin ring formation in Schizosaccharomyces pombe. *Journal of Cell Biology, 162*(5), 851-862. doi:10.1083/jcb.200305012

Carpy, A., Krug, K., Graf, S., Koch, A., Popic, S., Hauf, S., & Macek, B. (2014). Absolute proteome and phosphoproteome dynamics during the cell cycle of Schizosaccharomyces pombe (Fission Yeast). *Mol Cell Proteomics, 13*(8), 1925-1936. doi:10.1074/mcp.M113.035824

Case, L. B., Zhang, X., Ditlev, J. A., & Rosen, M. K. (2019). Stoichiometry controls activity of phase-separated clusters of actin signaling proteins. *Science, 363*(6431), 1093-1097. doi:10.1126/science.aau6313

Chang, T.-J. J., Wang, W.-C. C., Hsiung, C. A., He, C.-T. T., Lin, M.-W. W., Sheu, W. H., . . . Group, S. (2016). Genetic Variation in the Human SORBS1 Gene is Associated With Blood Pressure Regulation and Age at Onset of Hypertension: A SAPPHIRe Cohort Study. *Medicine, 95*(10). doi:10.1097/MD.0000000000002970

Chappie, J. S., Mears, J. A., Fang, S., Leonard, M., Schmid, S. L., Milligan, R. A., . . . Dyda, F. (2011). A pseudoatomic model of the dynamin polymer identifies a hydrolysis-dependent powerstroke. *Cell, 147*(1), 209-222. doi:10.1016/j.cell.2011.09.003

Cheadle, C., Ivashchenko, Y., South, V., Searfoss, G. H., French, S., Howk, R., . . . Jaye, M. (1994). Identification of a Src SH3 domain binding motif by screening a random phage display library. *J Biol Chem, 269*(39), 24034-24039.

Chen, Q., & Pollard, T. D. (2013). Actin filament severing by cofilin dismantles actin patches and produces mother filaments for new patches. *Curr Biol, 23*(13), 1154-1162. doi:10.1016/j.cub.2013.05.005

Cheng, J., Grassart, A., & Drubin, D. G. (2012). Myosin 1E coordinates actin assembly and cargo trafficking during clathrin-mediated endocytosis. *Molecular Biology of the Cell, 23*(15), 2891-2904. doi:10.1091/mbc.E11-04-0383

Cicchetti, P., Mayer, B. J., Thiel, G., & Baltimore, D. (1992). Identification of a protein that binds to the SH3 region of Abl and is similar to Bcr and GAP-rho. *Science, 257*(5071), 803-806. doi:10.1126/science.1379745

Cocucci, E., Gaudin, R., & Kirchhausen, T. (2014). Dynamin recruitment and membrane scission at the neck of a clathrin-coated pit. *Mol Biol Cell, 25*(22), 3595-3609. doi:10.1091/mbc.E14-07-1240

Cohen, J. (1988). *Statistical power analysis for the behavioral sciences* (Second ed.): Lawrence Erlbaum Associates.

Collins, A., Warrington, A., Taylor, K. A., & Svitkina, T. (2011). Structural organization of the actin cytoskeleton at sites of clathrin-mediated endocytosis. *Curr Biol, 21*(14), 1167-1175. doi:10.1016/j.cub.2011.05.048

Crowther, R. A., Finch, J. T., & Pearse, B. M. F. (1976). On the structure of coated vesicles. *J Mol Biol, 103*, 785-798.

Dannhauser, P. N., & Ungewickell, E. J. (2012). Reconstitution of clathrin-coated bud and vesicle formation with minimal components. *Nat Cell Biol, 14*(6), 634-639. doi:10.1038/ncb2478

Dasanayake, N. L., & Carlsson, A. E. (2013). Stress generation by myosin minifilaments in actin bundles. *Phys Biol, 10*(3), 036006. doi:10.1088/1478-3975/10/3/036006

Dasanayake, N. L., Michalski, P. J., & Carlsson, A. E. (2011). General mechanism of actomyosin contractility. *Phys Rev Lett, 107*(11), 118101. doi:10.1103/PhysRevLett.107.118101

Daumke, O., Roux, A., & Haucke, V. (2014). BAR domain scaffolds in dynamin-mediated membrane fission. *Cell, 156*(5), 882-892. doi:10.1016/j.cell.2014.02.017

Dawson, J. C., Legg, J. A., & Machesky, L. M. (2006). Bar domain proteins: a role in tubulation, scission and actin assembly in clathrin-mediated endocytosis. *Trends Cell Biol, 16*(10), 493-498. doi:10.1016/j.tcb.2006.08.004

Dayel, M. J., Akin, O., Landeryou, M., Risca, V., Mogilner, A., & Mullins, R. D. (2009). In silico reconstitution of actin-based symmetry breaking and motility. *PLoS Biol, 7*(9), e1000201. doi:10.1371/journal.pbio.1000201

de Mendez, I., Homayounpour, N., & Leto, T. L. (1997). Specificity of p47phox SH3 domain interactions in NADPH oxidase assembly and activation. *Molecular and Cellular Biology, 17*(4), 2177-2185. Retrieved from https://www.ncbi.nlm.nih.gov/pubmed/9121467

DeGroot, A. C. M., Busch, D. J., Hayden, C. C., Mihelic, S. A., Alpar, A. T., Behar, M., & Stachowiak, J. C. (2018). Entropic Control of Receptor Recycling Using Engineered Ligands. *Biophys J, 114*(6), 1377-1388. doi:10.1016/j.bpj.2018.01.036

Demers, J. P., & Mittermaier, A. (2009). Binding mechanism of an SH3 domain studied by NMR and ITC. *J Am Chem Soc, 131*(12), 4355-4367. doi:10.1021/ja808255d

den Otter, W. K., & Briels, W. J. (2011). The generation of curved clathrin coats from flat plaques. *Traffic, 12*(10), 1407-1416. doi:10.1111/j.1600-0854.2011.01241.x

Derganc, J., & Copic, A. (2016). Membrane bending by protein crowding is affected by protein lateral confinement. *Biochim Biophys Acta, 1858*(6), 1152-1159. doi:10.1016/j.bbamem.2016.03.009

Desrochers, G., Cappadocia, L., Lussier-Price, M., Ton, A. T., Ayoubi, R., Serohijos, A., . . . Angers, A. (2017). Molecular basis of interactions between SH3 domain-containing proteins and the proline-rich region of the ubiquitin ligase Itch. *J Biol Chem, 292*(15), 6325-6338. doi:10.1074/jbc.M116.754440

Desrochers, G., Lussier-Price, M., Omichinski, J. G., & Angers, A. (2015). Multiple Src Homology 3 Binding to the Ubiquitin Ligase Itch Conserved Proline-Rich Region. *Biochemistry, 54*(50), 7345-7354. doi:10.1021/acs.biochem.5b01131

Dmitrieff, S., & Nedelec, F. (2015). Membrane Mechanics of Endocytosis in Cells with Turgor. *PLoS Comput Biol, 11*(10), e1004538. doi:10.1371/journal.pcbi.1004538

Dmitrieff, S., & Nedelec, F. (2016). Amplification of actin polymerization forces. *J Cell Biol, 212*(7), 763-766. doi:10.1083/jcb.201512019

Doherty, G. J., & McMahon, H. T. (2009). Mechanisms of endocytosis. *Annu Rev Biochem, 78*, 857-902. doi:10.1146/annurev.biochem.78.081307.110540

Downward, J., Yarden, Y., Mayes, E., Scrace, G., Totty, N., Stockwell, P., . . . Waterfield, M. D. (1984). Close similarity of epidermal growth factor receptor and v-erb-B oncogene protein sequences. *Nature, 307*(5951), 521-527.

Doyon, J. B., Zeitler, B., Cheng, J., Cheng, A. T., Cherone, J. M., Santiago, Y., . . . Drubin, D. G. (2011). Rapid and efficient clathrin-mediated endocytosis revealed in genome-edited mammalian cells. *Nat Cell Biol, 13*(3), 331-337. doi:10.1038/ncb2175

Drin, G., & Antonny, B. (2010). Amphipathic helices and membrane curvature. *FEBS Lett, 584*(9), 1840-1847. doi:10.1016/j.febslet.2009.10.022

East, D. A., & Mulvihill, D. P. (2011). Regulation and function of the fission yeast myosins. *J Cell Sci, 124*(9), 1383-1390. doi:10.1242/jcs.078527

Eckhart, W., Hutchinson, M. A., & Hunter, T. (1979). An activity phosphorylating tyrosine in polyoma T antigen immunoprecipitates. *Cell, 18*(4), 925-933.

El-Benna, J., Dang, P. M., Gougerot-Pocidalo, M. A., Marie, J. C., & Braut-Boucher, F. (2009). p47phox, the phagocyte NADPH oxidase/NOX2 organizer: structure, phosphorylation and implication in diseases. *Experimental & molecular medicine, 41*(4), 217-225. doi:10.3858/emm.2009.41.4.058

Erik, V., Matthias, S., Areti, G., Teja, A., Christiane, L., Victor Tapia, M., . . . Ben, D. (2015). Evolution of the SH3 Domain Specificity Landscape in Yeasts. *PLoS One, 10*(6). doi:10.1371/journal.pone.0129229

Esensten, J. H., Bluestone, J. A., & Lim, W. A. (2017). Engineering Therapeutic T Cells: From Synthetic Biology to Clinical Trials. In A. K. Abbas, J. C. Aster, & M. B. Feany (Eds.), *Annual Review of Pathology: Mechanisms of Disease, Vol 12* (Vol. 12, pp. 305-330).

Eswar, N., Webb, B., Marti-Renom, M. A., Madhusudhan, M. S., Eramian, D., Shen, M. Y., . . . Sali, A. (2006). Comparative protein structure modeling using Modeller.

Curr Protoc Bioinformatics, Chapter 5, Unit-5.6. doi:10.1002/0471250953.bi0506s15

Evangelista, M., Klebl, B. M., Tong, B. A., Leeuw, T., Leberer, E., Whiteway, M., . . . Boone, C. (2000). A role for myosin-I in actin assembly through interactions with Vrp1p, Bee1p, and the Arp2/3 complex. *Journal of Cell Biology, 148*(2), 353-362. doi:10.1083/jcb.148.2.353

Faelber, K., Posor, Y., Gao, S., Held, M., Roske, Y., Schulze, D., . . . Daumke, O. (2011). Crystal structure of nucleotide-free dynamin. *Nature, 477*(7366), 556-560. doi:10.1038/nature10369

Farrell, K. B., McDonald, S., Lamb, A. K., Worcester, C., Peersen, O. B., & Pietro, S. M. (2017). Novel function of a dynein light chain in actin assembly during clathrin-mediated endocytosis. *The Journal of cell biology, 216*(8), 2565-2580. doi:10.1083/jcb.201604123

Fazi, B., Cope, M., Douangamath, A., Ferracuti, S., Schirwitz, K., Zucconi, A., . . . Castagnoli, L. (2002). Unusual Binding Properties of the SH3 Domain of the Yeast Actin-binding Protein Abp1: structural and functional analysis. *Journal of Biological Chemistry, 277*(7), 5290-5298. doi:10.1074/jbc.M109848200

Feliciano, D., & Di Pietro, S. M. (2012). SLAC, a complex between Sla1 and Las17, regulates actin polymerization during clathrin-mediated endocytosis. *Molecular Biology of the Cell, 23*(21), 4256-4272. doi:10.1091/mbc.E11-12-1022

Feng, S., Chen, J. K., Yu, H., Simon, J. A., & Schreiber, S. L. (1994). Two binding orientations for peptides to the Src SH3 domain: development of a general model for SH3-ligand interactions. *Science, 266*(5188), 1241-1247. doi:10.1126/science.7526465

Feng, S., Kasahara, C., Rickles, R. J., & Schreiber, S. L. (1995). Specific interactions outside the proline-rich core of two classes of Src homology 3 ligands. *Proceedings of the National Academy of Sciences, 92*(26), 12408-12415. doi:10.1073/pnas.92.26.12408

Fernandez-Ballester, G., Blanes-Mira, C., & Serrano, L. (2004). The tryptophan switch: changing ligand-binding specificity from type I to type II in SH3 domains. *J Mol Biol, 335*(2), 619-629. doi:10.1016/j.jmb.2003.10.060

Fernandez, R., & Berro, J. (2016). Use of a fluoride channel as a new selection marker for fission yeast plasmids and application to fast genome editing with CRISPR/Cas9. *Yeast, 33*(10), 549-557. doi:10.1002/yea.3178

Field, M. C., Gabernet-Castello, C., & Dacks, J. B. (2007). Reconstructing the evolution of the endocytic system: insights from genomics and molecular cell biology. *Adv Exp Med Biol, 607*, 84-96. doi:10.1007/978-0-387-74021-8_7

Finn, R. D., Coggill, P., Eberhardt, R. Y., Eddy, S. R., Mistry, J., Mitchell, A. L., . . . Bateman, A. (2016). The Pfam protein families database: towards a more sustainable future. *Nucleic Acids Res, 44*(D1), D279-D285. doi:10.1093/nar/gkv1344

Fiser, A., Do, R. K., & Sali, A. (2000). Modeling of loops in protein structures. *Protein Sci, 9*(9), 1753-1773. doi:10.1110/ps.9.9.1753

Fletcher, D. A., & Mullins, D. (2010). Cell mechanics and the cytoskeleton. *Nature, 463*(7280), 485-492. doi:10.1038/nature08908

Footer, M. J., Kerssemakers, J. W., Theriot, J. A., & Dogterom, M. (2007). Direct measurement of force generation by actin filament polymerization using an optical trap. *Proc Natl Acad Sci U S A, 104*(7), 2181-2186. doi:10.1073/pnas.0607052104

Forsburg, S. L. (2003). Overview of Schizosaccharomyces pombe. *Curr Protoc Mol Biol, Chapter 13*, Unit 13.14. doi:10.1002/0471142727.mb1314s64

Francis, M. K., Holst, M. R., Vidal-Quadras, M., Henriksson, S., Santarella-Mellwig, R., Sandblad, L., & Lundmark, R. (2015). Endocytic membrane turnover at the leading edge is driven by a transient interaction between Cdc42 and GRAF1. *J Cell Sci, 128*(22), 4183-4195. doi:10.1242/jcs.174417

Freeman, N. L., Lila, T., Mintzer, K. A., Chen, Z., Pahk, A. J., Ren, R., . . . Field, J. (1996). A conserved proline-rich region of the Saccharomyces cerevisiae cyclase-associated protein binds SH3 domains and modulates cytoskeletal localization. *Molecular Cellular Biology, 16*(2), 548-556. doi:10.1128/MCB.16.2.548

Freund, C., Kühne, R., Yang, H., & Embo …, P.-S. (2002). Dynamic interaction of CD2 with the GYF and the SH3 domain of compartmentalized effector molecules. *The EMBO …*. Retrieved from http://emboj.embopress.org/content/21/22/5985.abstract

Friesen, H., Humphries, C., Ho, Y., Schub, O., Colwill, K., & Andrews, B. (2006). Characterization of the Yeast Amphiphysins Rvs161p and Rvs167p Reveals Roles for the Rvs Heterodimer In Vivo. *Molecular Biology of the Cell, 17*(3), 1306-1321. doi:10.1091/mbc.e05-06-0476

Frost, A., Unger, V. M., & De Camilli, P. (2009). The BAR domain superfamily: membrane-molding macromolecules. *Cell, 137*(2), 191-196. doi:10.1016/j.cell.2009.04.010

Fujisaki, H., Albanesi, J. P., & Korn, E. D. (1985). Experimental evidence for the contractile activities of Acanthamoeba myosins IA and IB. *J Biol Chem, 260*(20), 11183-11189.

Gaidarov, I., Santini, F., Warren, R. A., & Keen, J. H. (1999). Spatial control of coated-pit dynamics in living cells. *Nat Cell Biol, 1*(1), 1-7. doi:10.1038/8971

Gallego, O., Betts, M. J., Gvozdenovic-Jeremic, J., Maeda, K., Matetzki, C., Aguilar-Gurrieri, C., . . . Gavin, A.-C. C. (2010). A systematic screen for protein-lipid interactions in Saccharomyces cerevisiae. *Molecular Systems Biology, 6*, 430. doi:10.1038/msb.2010.87

Galletta, B. J., Chuang, D. Y., & Cooper, J. A. (2008). Distinct roles for Arp2/3 regulators in actin assembly and endocytosis. *PLoS Biol, 6*(1). doi:10.1371/journal.pbio.0060001

Geli, M. I., & Riezman, H. (1996). Role of type I myosins in receptor-mediated endocytosis in yeast. *Science, 272*(5261), 533-535.

Gerth, F., Japel, M., Sticht, J., Kuropka, B., Schmitt, X. J., Driller, J. H., . . . Freund, C. (2019). Exon Inclusion Modulates Conformational Plasticity and Autoinhibition of the Intersectin 1 SH3A Domain. *Structure*. doi:10.1016/j.str.2019.03.020

Giardini, P. A., Fletcher, D. A., & Theriot, J. A. (2003). Compression forces generated by actin comet tails on lipid vesicles. *Proc Natl Acad Sci U S A, 100*(11), 6493-6498. doi:10.1073/pnas.1031670100

Gibson, D. G., Young, L., Chuang, R.-Y., Venter, J. C., Hutchison Iii, C. A., & Smith, H. O. (2009). Enzymatic assembly of DNA molecules up to several hundred kilobases. *Nat Methods, 6*, 343. doi:10.1038/nmeth.1318

Giron-Perez, D. A., Piedra-Quintero, Z. L., & Santos-Argumedo, L. (2019). Class I myosins: Highly versatile proteins with specific functions in the immune system. *J Leukoc Biol, 105*(5), 973-981. doi:10.1002/JLB.1MR0918-350RRR

Goldberg, M. B., & Theriot, J. A. (1995). Shigella flexneri surface protein IcsA is sufficient to direct actin-based motility. *Proc Natl Acad Sci U S A, 92*(14), 6572-6576.

Goldenbogen, B., Giese, W., Hemmen, M., Uhlendorf, J., Herrmann, A., & Klipp, E. (2016). Dynamics of cell wall elasticity pattern shapes the cell during yeast mating morphogenesis. *Open Biol, 6*(9). doi:10.1098/rsob.160136

Goldenzweig, A., & Fleishman, S. J. (2018). Principles of Protein Stability and Their Application in Computational Design. *Annu Rev Biochem, 87*(1), 105-129. doi:10.1146/annurev-biochem-062917-012102

Goldstein, J. L., Anderson, R. G., & Brown, M. S. (1982). Receptor-mediated endocytosis and the cellular uptake of low density lipoprotein. *Ciba Found Symp*(92), 77-95.

Good, M. C., Zalatan, J. G., & Lim, W. A. (2011). Scaffold Proteins: Hubs for Controlling the Flow of Cellular Information. *Science, 332*(6030), 680. doi:10.1126/science.1198701

Goode, B. L., Eskin, J. A., & Wendland, B. (2015). Actin and endocytosis in budding yeast. *Genetics, 199*(2), 315-358. doi:10.1534/genetics.112.145540

Goode, B. L., Rodal, A. A., Barnes, G., & Drubin, D. G. (2001). Activation of the Arp2/3 complex by the actin filament binding protein Abp1p. *Journal of Cell Biology, 153*(3), 627-634. doi:10.1083/jcb.153.3.627

Gough, J., Karplus, K., Hughey, R., & Chothia, C. (2001). Assignment of homology to genome sequences using a library of hidden Markov models that represent all proteins of known structure11Edited by G. Von Heijne. *J Mol Biol, 313*(4), 903-919. doi:10.1006/jmbi.2001.5080

Grassart, A., Cheng, A. T., Hong, S. H., Zhang, F., Zenzer, N., Feng, Y., . . . Drubin, D. G. (2014). Actin and dynamin2 dynamics and interplay during clathrin-mediated endocytosis. *J Cell Biol, 205*(5), 721-735. doi:10.1083/jcb.201403041

Greenberg, M. J., & Ostap, E. M. (2013). Regulation and control of myosin-I by the motor and light chain-binding domains. *Trends Cell Biol, 23*(2), 81-89. doi:10.1016/j.tcb.2012.10.008

Haas, J., Roth, S., Arnold, K., Kiefer, F., Schmidt, T., Bordoli, L., & Schwede, T. (2013). The Protein Model Portal—a comprehensive resource for protein structure and model information. *Database, 2013*. doi:10.1093/database/bat031

Hagiwara, N., Kitazono, T., Kamouchi, M., Kuroda, J., Ago, T., Hata, J., . . . study, H. (2008). Polymorphism in the sorbin and SH3-domain-containing-1 (SORBS1) gene and the risk of brain infarction in the Japanese population: the Fukuoka Stroke Registry and the Hisayama study. *European journal of neurology, 15*(5), 481-486. doi:10.1111/j.1468-1331.2008.02105.x

Haling, J. R., Monkley, S. J., Critchley, D. R., & Petrich, B. G. (2011). Talin-dependent integrin activation is required for fibrin clot retraction by platelets. *Blood, 117*(5), 1719-1722. doi:10.1182/blood-2010-09-305433

Hammad, S. M., Barth, J. L., Knaak, C., & Argraves, W. S. (2000). Megalin acts in concert with cubilin to mediate endocytosis of high density lipoproteins. *J Biol Chem, 275*(16), 12003-12008. Retrieved from https://www.ncbi.nlm.nih.gov/pubmed/10766831

Hansen, D. F., Vallurupalli, P., Lundstrom, P., Neudecker, P., & Kay, L. E. (2008). Probing chemical shifts of invisible states of proteins with relaxation dispersion NMR spectroscopy: how well can we do? *J Am Chem Soc, 130*(8), 2667-2675. doi:10.1021/ja078337p

Harmon, T. S., Holehouse, A. S., Rosen, M. K., & Pappu, R. V. (2017). Intrinsically disordered linkers determine the interplay between phase separation and gelation in multivalent proteins. *Elife, 6*, e30294. doi:10.7554/eLife.30294

Hassinger, J. E., Oster, G., Drubin, D. G., & Rangamani, P. (2017). Design principles for robust vesiculation in clathrin-mediated endocytosis. *Proc Natl Acad Sci U S A, 114*(7), E1118-e1127. doi:10.1073/pnas.1617705114

Heim, J. B., Squirewell, E. J., Neu, A., Zocher, G., Sominidi-Damodaran, S., Wyles, S. P., . . . Meves, A. (2017). Myosin-1E interacts with FAK proline-rich region 1 to induce fibronectin-type matrix. *Proceedings of the National Academy of Sciences, 114*(15), 3933-3938. doi:10.1073/pnas.1614894114

Heinrich, M., Tian, A., Esposito, C., & Baumgart, T. (2010). Dynamic sorting of lipids and proteins in membrane tubes with a moving phase boundary. *Proc Natl Acad Sci U S A, 107*(16), 7208-7213. doi:10.1073/pnas.0913997107

Helfrich, W. (1973). Elastic properties of lipid bilayers: theory and possible experiments. *Zeitschrift für Naturforschung C, 28*(11-12), 693-703.

Henne, W. M., Kent, H. M., Ford, M. G. J., Hegde, B. G., Daumke, O., Butler, P. J. G., . . . McMahon, H. T. (2007). Structure and Analysis of FCHo2 F-BAR Domain: A Dimerizing and Membrane Recruitment Module that Effects Membrane Curvature. *Structure, 15*(7), 839-852. doi:10.1016/j.str.2007.05.002

Hernandez, D. A., Bennett, C. M., Dunina-Barkovskaya, L., Wedig, T., Capetanaki, Y., Herrmann, H., & Conover, G. M. (2016). Nebulette is a powerful cytolinker organizing desmin and actin in mouse hearts. *Molecular Biology of the Cell, 27*(24), 3869-3882. doi:10.1091/mbc.E16-04-0237

Herron, B. J., Rao, C., Liu, S., Laprade, L., Richardson, J. A., Olivieri, E., . . . Beier, D. R. (2005). A mutation in NFkB interacting protein 1 results in cardiomyopathy and abnormal skin development in wa3 mice. *Human molecular genetics, 14*(5), 667-677. doi:10.1093/hmg/ddi063

Hinshaw, J. E. (2000). Dynamin and its role in membrane fission. *Annu Rev Cell Dev Biol, 16*, 483-519. doi:10.1146/annurev.cellbio.16.1.483

Hinze, C., & Boucrot, E. (2018). Local actin polymerization during endocytic carrier formation. *Biochemical Society Transactions, 46*(3), 565-576. doi:10.1042/BST20170355

Hoffmann, S., Funke, S. A., Wiesehan, K., Moedder, S., Gluck, J. M., Feuerstein, S., . . . Willbold, D. (2010). Competitively selected protein ligands pay their increase in specificity by a decrease in affinity. *Mol Biosyst, 6*(1), 126-133. doi:10.1039/b910945e

Holland, D. O., Shapiro, B. H., Xue, P., & Johnson, M. E. (2017). Protein-protein binding selectivity and network topology constrain global and local properties of interface binding networks. *Sci Rep, 7*(1), 5631. doi:10.1038/s41598-017-05686-2

Holt, M. R., & Koffer, A. (2001). Cell motility: proline-rich proteins promote protrusions. *Trends Cell Biol, 11*(1), 38-46.

Horlbeck, M. A., Witkowsky, L. B., Guglielmi, B., Replogle, J. M., Gilbert, L. A., Villalta, J. E., . . . Weissman, J. S. (2016). Nucleosomes impede Cas9 access to DNA in vivo and in vitro. *Elife, 5*. doi:10.7554/eLife.12677

Howard, J. P., Hutton, J. L., Olson, J. M., & Payne, G. S. (2002). Sla1p serves as the targeting signal recognition factor for NPFX(1,2)D-mediated endocytosis. *J Cell Biol, 157*(2), 315-326. doi:10.1083/jcb.200110027

Hu, H., Columbus, J., Zhang, Y., Wu, D., Lian, L., Yang, S., . . . Herrero, J. J. (2004). A map of WW domain family interactions. *PROTEOMICS, 4*(3), 643-655. doi:10.1002/pmic.200300632

Huang, D., Sherman, B. T., & Lempicki, R. A. (2009). Systematic and integrative analysis of large gene lists using DAVID bioinformatics resources. *Nat Protoc, 4*(1), 44. doi:10.1038/nprot.2008.211

Huang, D. W., Sherman, B. T., & Lempicki, R. A. (2009). Bioinformatics enrichment tools: paths toward the comprehensive functional analysis of large gene lists. *Nucleic Acids Res, 37*(1), 1-13. doi:10.1093/nar/gkn923

Huckaba, T. M., Gay, A. C., Pantalena, L. F., Yang, H.-C., & Pon, L. A. (2004). Live cell imaging of the assembly, disassembly, and actin cable-dependent movement of endosomes and actin patches in the budding yeast, Saccharomyces cerevisiae. *The Journal of cell biology, 167*(3), 519-530. doi:10.1083/jcb.200404173

Hunter, T., & Sefton, B. M. (1980). Transforming gene product of Rous sarcoma virus phosphorylates tyrosine. *Proceedings of the National Academy of Sciences of the United States of America, 77*(3), 1311-1315. doi:10.1073/pnas.77.3.1311

Idrissi, F. Z., Blasco, A., Espinal, A., & Geli, M. I. (2012). Ultrastructural dynamics of proteins involved in endocytic budding. *Proc Natl Acad Sci U S A, 109*(39), E2587-2594. doi:10.1073/pnas.1202789109

Jacobs, J. Z., Ciccaglione, K. M., Tournier, V., & Zaratiegui, M. (2014). Implementation of the CRISPR-Cas9 system in fission yeast. *Nat Commun, 5*. doi:10.1038/ncomms6344

Jang, D. G., Sim, H. J., Song, E. K., Medina-Ruiz, S., Seo, J. K., & Park, T. J. (2015). A thioredoxin fold protein Sh3bgr regulates Enah and is necessary for proper sarcomere formation. *Developmental biology, 405*(1), 1-9. doi:10.1016/j.ydbio.2015.06.005

Jarsch, I. K., Daste, F., & Gallop, J. L. (2016). Membrane curvature in cell biology: An integration of molecular mechanisms. *J Cell Biol, 214*(4), 375-387. doi:10.1083/jcb.201604003

Jiménez, J. L., Guijarro, J. I., Orlova, E., Zurdo, J., Dobson, C. M., Sunde, M., & Saibil, H. R. (1999). Cryo-electron microscopy structure of an SH3 amyloid fibril and model of the molecular packing. *The EMBO Journal, 18*(4), 815-821. doi:10.1093/emboj/18.4.815

Jones, P., Binns, D., Chang, H. Y., Fraser, M., Li, W., McAnulla, C., . . . Hunter, S. (2014). InterProScan 5: genome-scale protein function classification. *Bioinformatics, 30*(9), 1236-1240. doi:10.1093/bioinformatics/btu031

Jülicher, F., Kruse, K., Prost, J., & Joanny, J. F. (2007). Active behavior of the Cytoskeleton. *Physics Reports, 449*(1-3), 3-28. doi:10.1016/j.physrep.2007.02.018

Jülicher, F., & Lipowsky, R. (1996). Shape transformations of vesicles with intramembrane domains. *Physical Review E, 53*(3), 2670-2683. doi:10.1103/PhysRevE.53.2670

Kaksonen, M., & Roux, A. (2018). Mechanisms of clathrin-mediated endocytosis. *Nature Reviews Molecular Cell Biology, 19*(5), 313-326. doi:10.1038/nrm.2017.132

Kaksonen, M., Sun, Y., & Drubin, D. G. (2003). A pathway for association of receptors, adaptors, and actin during endocytic internalization. *Cell, 115*, 475-487.

Kaksonen, M., Toret, C. P., & Drubin, D. G. (2005). A modular design for the clathrin- and actin-mediated endocytosis machinery. *Cell, 123*(2), 305-320. doi:10.1016/j.cell.2005.09.024

Karlsson, A. O., Sundell, G. N., Andersson, E., Ivarsson, Y., & Jemth, P. (2016). Improved affinity at the cost of decreased specificity: a recurring theme in PDZ-peptide interactions. *Scientific Reports, 6*(1), 34269. doi:10.1038/srep34269

Kasza, K. E., Broedersz, C. P., Koenderink, G. H., Lin, Y. C., Messner, W., Millman, E. A., . . . Weitz, D. A. (2010). Actin filament length tunes elasticity of flexibly cross-linked actin networks. *Biophys J, 99*(4), 1091-1100. doi:10.1016/j.bpj.2010.06.025

Kay, B. K. (2012). SH3 domains come of age. *FEBS Letters, 586*(17), 2606-2608. doi:10.1016/j.febslet.2012.05.025
Kay, B. K., Williamson, M. P., & Sudol, M. (2000). The importance of being proline: the interaction of proline-rich motifs in signaling proteins with their cognate domains. *Faseb j, 14*(2), 231-241.
Kay, B. K., Yamabhai, M., Wendland, B., & Emr, S. D. (1999). Identification of a novel domain shared by putative components of the endocytic and cytoskeletal machinery. *Protein Sci, 8*(2), 435-438. doi:10.1110/ps.8.2.435
Kazlauskas, A., Schmotz, C., Kesti, T., Hepojoki, J., Kleino, I., Kaneko, T., . . . Saksela, K. (2016). Large-scale screening of preferred interactions of human SH3 domains using native target proteins as affinity ligands. *Molecular & cellular proteomics : MCP*. doi:10.1074/mcp.M116.060483
Kelil, A., Levy, E. D., & Michnick, S. W. (2016). Evolution of domain-peptide interactions to coadapt specificity and affinity to functional diversity. *Proceedings of the National Academy of Sciences of the United States of America, 113*(27), E3862-E3871. doi:10.1073/pnas.1518469113
Kirchhausen, T., Owen, D., & Harrison, S. C. (2014). Molecular structure, function, and dynamics of clathrin-mediated membrane traffic. *Cold Spring Harb Perspect Biol, 6*(5), a016725. doi:10.1101/cshperspect.a016725
Kishimoto, T., Sun, Y., Buser, C., Liu, J., Michelot, A., & Drubin, D. G. (2011a). Determinants of endocytic membrane geometry, stability, and scission. *Proceedings of the National Academy of Sciences of the United States of America, 108*(44), E979-E988. doi:10.1073/pnas.1113413108
Kishimoto, T., Sun, Y., Buser, C., Liu, J., Michelot, A., & Drubin, D. G. (2011b). Determinants of endocytic membrane geometry, stability, and scission. *Proceedings of the National Academy of Sciences, 108*(44), E979-E988. doi:10.1073/pnas.1113413108
Kjaerulff, O., Brodin, L., & Jung, A. (2011). The structure and function of endophilin proteins. *Cell Biochem Biophys, 60*(3), 137-154. doi:10.1007/s12013-010-9137-5
Koster, G., Cacciuto, A., Derényi, I., Frenkel, D., & Dogterom, M. (2005). Force Barriers for Membrane Tube Formation. *Physical review letters, 94*(6), 068101. doi:10.1103/PhysRevLett.94.068101
Kostrub, C. F., Lei, E. P., & Enoch, T. (1998). Use of gap repair in fission yeast to obtain novel alleles of specific genes. *Nucleic Acids Res, 26*(20), 4783-4784. Retrieved from https://www.ncbi.nlm.nih.gov/pubmed/9753750
Kovar, D. R., & Pollard, T. D. (2004). Insertional assembly of actin filament barbed ends in association with formins produces piconewton forces. *Proc Natl Acad Sci U S A, 101*(41), 14725-14730. doi:10.1073/pnas.0405902101
Kovar, D. R., Wu, J.-Q., & Pollard, T. D. (2005). Profilin-mediated Competition between Capping Protein and Formin Cdc12p during Cytokinesis in Fission Yeast. *Molecular Biology of the Cell, 16*(5), 2313-2324. doi:10.1091/mbc.E04-09-0781
Kozlov, M. M., Campelo, F., Liska, N., Chernomordik, L. V., Marrink, S. J., & McMahon, H. T. (2014). Mechanisms shaping cell membranes. *Curr Opin Cell Biol, 29*, 53-60. doi:10.1016/j.ceb.2014.03.006
Kozlovsky, Y., & Kozlov, M. M. (2003). Membrane fission: model for intermediate structures. *Biophys J, 85*(1), 85-96. doi:10.1016/s0006-3495(03)74457-9
Krendel, M., Osterweil, E. K., & Mooseker, M. S. (2007). Myosin 1E interacts with synaptojanin-1 and dynamin and is involved in endocytosis. *FEBS Lett, 581*(4), 644-650. doi:10.1016/j.febslet.2007.01.021

Kubler, E., & Riezman, H. (1993). Actin and fimbrin are required for the internalization step of endocytosis in yeast. *Embo j, 12*(7), 2855-2862. Retrieved from https://www.ncbi.nlm.nih.gov/pubmed/8335001

Kukulski, W., Picco, A., Specht, T., Briggs, J. A., & Kaksonen, M. (2016). Clathrin modulates vesicle scission, but not invagination shape, in yeast endocytosis. *Elife, 5*. doi:10.7554/eLife.16036

Kukulski, W., Schorb, M., Kaksonen, M., & Briggs, J. A. (2012). Plasma membrane reshaping during endocytosis is revealed by time-resolved electron tomography. *Cell, 150*(3), 508-520. doi:10.1016/j.cell.2012.05.046

Kumar, V., Fricke, R., Bhar, D., Reddy-Alla, S., Krishnan, K. S., Bogdan, S., & Ramaswami, M. (2009). Syndapin promotes formation of a postsynaptic membrane system in Drosophila. *Mol Biol Cell, 20*(8), 2254-2264. doi:10.1091/mbc.E08-10-1072

Kurochkina, N., & Guha, U. (2013). SH3 domains: modules of protein-protein interactions. *Biophys Rev, 5*(1), 29-39. doi:10.1007/s12551-012-0081-z

Lacy, M. M., Baddeley, D., & Berro, J. (2019). Single-molecule turnover dynamics of actin and membrane coat proteins in clathrin-mediated endocytosis. *bioRxiv*, 617746. doi:10.1101/617746

Lacy, M. M., Ma, R., Ravindra, N. G., & Berro, J. (2018). Molecular mechanisms of force production in clathrin-mediated endocytosis. *FEBS Letters, 592*(21), 3586-3605. doi:10.1002/1873-3468.13192

Lavillette, D., Russell, S. J., & Cosset, F. L. (2001). Retargeting gene delivery using surface-engineered retroviral vector particles. *Curr Opin Biotechnol, 12*(5), 461-466.

Lechler, T., Shevchenko, A., Shevchenko, A., & Li, R. (2000). Direct involvement of yeast type I myosins in Cdc42-dependent actin polymerization. *Journal of Cell Biology, 148*(2), 363-374. doi:10.1083/jcb.148.2.363

Lee, W. L., Bezanilla, M., & Pollard, T. D. (2000). Fission yeast myosin-I, Myo1p, stimulates actin assembly by Arp2/3 complex and shares functions with WASp. *J Cell Biol, 151*(4), 789-800.

Legendre-Guillemin, V., Wasiak, S., Hussain, N. K., Angers, A., & McPherson, P. S. (2004). ENTH/ANTH proteins and clathrin-mediated membrane budding. *J Cell Sci, 117*(Pt 1), 9-18. doi:10.1242/jcs.00928

Lemière, J., & Berroa, J. (2018). Adaptation of actin dynamics and membrane tension control for yeast endocytosis. *bioRxiv*, 342030. doi:10.1101/342030

Lemos, B. R., Kaplan, A. C., Bae, J. E., Ferrazzoli, A. E., Kuo, J., Anand, R. P., . . . Haber, J. E. (2018). CRISPR/Cas9 cleavages in budding yeast reveal templated insertions and strand-specific insertion/deletion profiles. *Proceedings of the National Academy of Sciences, 115*(9), E2040-E2047. doi:10.1073/pnas.1716855115

Letunic, I., & Bork, P. (2018). 20 years of the SMART protein domain annotation resource. *Nucleic Acids Res, 46*(D1), D493-D496. doi:10.1093/nar/gkx922

Levinson, A. D., Courtneidge, S. A., & Bishop, J. M. (1981). Structural and functional domains of the Rous sarcoma virus transforming protein (pp60src). *Proceedings of the National Academy of Sciences of the United States of America, 78*(3), 1624-1628. doi:10.1073/pnas.78.3.1624

Leyton-Puig, D., Isogai, T., Argenzio, E., van den Broek, B., Klarenbeek, J., Janssen, H., . . . Innocenti, M. (2017). Flat clathrin lattices are dynamic actin-controlled hubs for clathrin-mediated endocytosis and signalling of specific receptors. *Nat Commun, 8*, 16068. doi:10.1038/ncomms16068

Li, P., Banjade, S., Cheng, H.-C. C., Kim, S., Chen, B., Guo, L., . . . Rosen, M. K. (2012). Phase transitions in the assembly of multivalent signalling proteins. *Nature*. Retrieved from http://dx.doi.org/10.1038/nature10879
Li, S. (2005). Specificity and versatility of SH3 and other proline-recognition domains: structural basis and implications for cellular signal transduction. *Biochemical Journal, 390*(3), 641-653. doi:10.1042/BJ20050411
Li, S. S. C. (2005). Specificity and versatility of SH3 and other proline-recognition domains: structural basis and implications for cellular signal transduction. *The Biochemical journal, 390*(Pt 3), 641-653. doi:10.1042/BJ20050411
Lim, C. S., Park, E. S., Kim, D. J., Song, Y. H., Eom, S. H., Chun, J. S., . . . Song, W. K. (2001). SPIN90 (SH3 protein interacting with Nck, 90 kDa), an adaptor protein that is developmentally regulated during cardiac myocyte differentiation. *J Biol Chem, 276*(16), 12871-12878. doi:10.1074/jbc.M009411200
Lim, W. A. (2002). The modular logic of signaling proteins: building allosteric switches from simple binding domains. *Curr Opin Struct Biol, 12*(1), 61-68.
Lim, W. A. (2010). Designing customized cell signalling circuits. *Nature Reviews Molecular Cell Biology, 11*, 393. doi:10.1038/nrm2904
https://www.nature.com/articles/nrm2904#supplementary-information
Lim, W. A., & June, C. H. (2017). The Principles of Engineering Immune Cells to Treat Cancer. *Cell, 168*(4), 724-740. doi:10.1016/j.cell.2017.01.016
Lim, W. A., Richards, F. M., & Fox, R. O. (1994). Structural determinants of peptide-binding orientation and of sequence specificity in SH3 domains. *Nature, 372*(6504), 375-379. doi:10.1038/372375a0
Liu, C.-Z., Li, X.-Y., Du, R.-H., Gao, M., Ma, M.-M., Li, F.-Y., . . . Guan, Y.-Y. (2016). Endophilin A2 Influences Volume-Regulated Chloride Current by Mediating ClC-3 Trafficking in Vascular Smooth Muscle Cells. *Circulation Journal, 80*(11), 2397-2406. doi:10.1253/circj.CJ-16-0793
Liu, J., Kaksonen, M., Drubin, D. G., & Oster, G. (2006). Endocytic vesicle scission by lipid phase boundary forces. *Proc Natl Acad Sci U S A, 103*(27), 10277-10282. doi:10.1073/pnas.0601045103
Liu, J., Sun, Y., Drubin, D. G., & Oster, G. F. (2009). The mechanochemistry of endocytosis. *PLoS Biol, 7*(9), e1000204. doi:10.1371/journal.pbio.1000204
Liu, Y. T., Sau, S., Ma, C. H., Kachroo, A. H., Rowley, P. A., Chang, K. M., . . . Jayaram, M. (2014). The partitioning and copy number control systems of the selfish yeast plasmid: an optimized molecular design for stable persistence in host cells. *Microbiol Spectr, 2*(5). doi:10.1128/microbiolspec.PLAS-0003-2013
Loisel, T. P., Boujemaa, R., Pantaloni, D., & Carlier, M. F. (1999). Reconstitution of actin-based motility of Listeria and Shigella using pure proteins. *Nature, 401*(6753), 613-616. doi:10.1038/44183
Lu, R., & Drubin, D. G. (2017). Selection and stabilization of endocytic sites by Ede1, a yeast functional homologue of human Eps15. *Molecular Biology of the Cell, 28*(5), 567-575. doi:10.1091/mbc.E16-06-0391
Ma, R., & Berro, J. (2018). Structural organization and energy storage in crosslinked actin assemblies. *PLoS Comput Biol, 14*(5), e1006150. doi:10.1371/journal.pcbi.1006150
MacArthur, M. W., & Thornton, J. M. (1991). Influence of proline residues on protein conformation. *J Mol Biol, 218*(2), 397-412. doi:10.1016/0022-2836(91)90721-h
MacQuarrie, C., Mangione, M., Carroll, R., James, M., Gould, K. L., & Sirotkin, V. (2018). Adaptor protein Bbc1 regulates localization of Wsp1 and Vrp1 during endocytic actin patch assembly. *bioRxiv*. doi:10.1101/389015

Madania, A., Dumoulin, P., Grava, S., Kitamoto, H., Schärer-Brodbeck, C., Soulard, A., . . . Drubin, D. (1999). The Saccharomyces cerevisiae Homologue of Human Wiskott–Aldrich Syndrome Protein Las17p Interacts with the Arp2/3 Complex. *Molecular Biology of the Cell, 10*(10), 3521-3538. doi:10.1091/mbc.10.10.3521

Mahadev, R. K., Di Pietro, S. M., Olson, J. M., Piao, H. L., Payne, G. S., & Overduin, M. (2007). Structure of Sla1p homology domain 1 and interaction with the NPFxD endocytic internalization motif. *The EMBO Journal, 26*(7), 1963-1971. doi:10.1038/sj.emboj.7601646

Manenschijn, H. E., Picco, A., Mund, M., Ries, J., & Kaksonen, M. (2018). Type-I myosins promote actin polymerization to drive membrane bending in endocytosis. *bioRxiv*, 490011. doi:10.1101/490011

Margolis, B., Rhee, S. G., Felder, S., Mervic, M., Lyall, R., Levitzki, A., . . . Schlessinger, J. (1989). EGF induces tyrosine phosphorylation of phospholipase C-II: A potential mechanism for EGF receptor signaling. *Cell, 57*(7), 1101-1107. doi:10.1016/0092-8674(89)90047-0

Mastrototaro, G., Liang, X., Li, X., Carullo, P., Piroddi, N., Tesi, C., . . . Bang, M.-L. L. (2015). Nebulette knockout mice have normal cardiac function, but show Z-line widening and up-regulation of cardiac stress markers. *Cardiovascular research, 107*(2), 216-225. doi:10.1093/cvr/cvv156

Maurer, M. E., & Cooper, J. A. (2006). The adaptor protein Dab2 sorts LDL receptors into coated pits independently of AP-2 and ARH. *J Cell Sci, 119*(Pt 20), 4235-4246. doi:10.1242/jcs.03217

Mayer, B., & Saksela, K. (2005). SH3 Domains. In G. Cesareni, M. Gimona, M. Sudol, & M. Yaffe (Eds.), *Modular protein domains*. Weinheim: WILEY-VCH Verlag GmbH & Co. KGaA.

Mayer, B. J. (2015). The discovery of modular binding domains: building blocks of cell signalling. *Nat Rev Mol Cell Biol, 16*(11), 691-698. doi:10.1038/nrm4068

Mayer, B. J., Hamaguchi, M., & Hanafusa, H. (1988). A novel viral oncogene with structural similarity to phospholipase C. *Nature, 332*(6161), 272-275. doi:10.1038/332272a0

Mayer, B. J., & Saksela, K. (2006). SH3 Domains. In G. Cesareni, M. Gimona, M. Sudol, & M. Yaffe (Eds.), *Modular protein domains* (pp. 37-58). Weinheim, Germany: Wiley-VCH.

McCall, P. M., Srivastava, S., Perry, S. L., Kovar, D. R., Gardel, M. L., & Tirrell, M. V. (2018). Partitioning and Enhanced Self-Assembly of Actin in Polypeptide Coacervates. *Biophys J, 114*(7), 1636-1645. doi:10.1016/j.bpj.2018.02.020

McMahon, H. T., & Boucrot, E. (2011). Molecular mechanism and physiological functions of clathrin-mediated endocytosis. *Nat Rev Mol Cell Biol, 12*(8), 517-533. doi:10.1038/nrm3151

McMahon, H. T., & Boucrot, E. (2015). Membrane curvature at a glance. *J Cell Sci, 128*(6), 1065-1070. doi:10.1242/jcs.114454

Melo, F., Sanchez, R., & Sali, A. (2002). Statistical potentials for fold assessment. *Protein Sci, 11*(2), 430-448. doi:10.1002/pro.110430

Meneses, E., & Mittermaier, A. (2014). Electrostatic interactions in the binding pathway of a transient protein complex studied by NMR and isothermal titration calorimetry. *J Biol Chem, 289*(40), 27911-27923. doi:10.1074/jbc.M114.553354

Merrifield, C. J., & Kaksonen, M. (2014). Endocytic accessory factors and regulation of clathrin-mediated endocytosis. *Cold Spring Harb Perspect Biol, 6*(11), a016733. doi:10.1101/cshperspect.a016733

Miao, Y., Tipakornsaowapak, T., Zheng, L., Mu, Y., & Lewellyn, E. (2018). Phospho-regulation of intrinsically disordered proteins for actin assembly and endocytosis. *FEBS J, 0*(ja). doi:10.1111/febs.14493

Mim, C., Cui, H., Gawronski-Salerno, Joseph A., Frost, A., Lyman, E., Voth, Gregory A., & Unger, Vinzenz M. (2012). Structural Basis of Membrane Bending by the N-BAR Protein Endophilin. *Cell, 149*(1), 137-145. doi:10.1016/j.cell.2012.01.048

Mim, C., & Unger, V. M. (2012). Membrane curvature and its generation by BAR proteins. *Trends Biochem Sci, 37*(12), 526-533. doi:10.1016/j.tibs.2012.09.001

Minc, N., Boudaoud, A., & Chang, F. (2009). Mechanical forces of fission yeast growth. *Curr Biol, 19*(13), 1096-1101. doi:10.1016/j.cub.2009.05.031

Moarefi, I., LaFevre-Bernt, M., Sicheri, F., Huse, M., Lee, C. H., Kuriyan, J., & Miller, W. T. (1997). Activation of the Src-family tyrosine kinase Hck by SH3 domain displacement. *Nature, 385*(6617), 650-653. doi:10.1038/385650a0

Mogilner, A., Allard, J., & Wollman, R. (2012). Cell polarity: quantitative modeling as a tool in cell biology. *Science, 336*(6078), 175-179. doi:10.1126/science.1216380

Mogilner, A., & Edelstein-Keshet, L. (2002). Regulation of actin dynamics in rapidly moving cells: a quantitative analysis. *Biophys J, 83*(3), 1237-1258. doi:10.1016/S0006-3495(02)73897-6

Mogilner, A., & Oster, G. (1996). Cell motility driven by actin polymerization. *Biophys J, 71*(6), 3030-3045. doi:10.1016/s0006-3495(96)79496-1

Mogilner, A., & Oster, G. (2003). Force generation by actin polymerization II: the elastic ratchet and tethered filaments. *Biophys J, 84*(3), 1591-1605. doi:10.1016/s0006-3495(03)74969-8

Molloy, J. E., Burns, J. E., Kendrick-Jones, J., Tregear, R. T., & White, D. C. (1995). Movement and force produced by a single myosin head. *Nature, 378*(6553), 209-212. doi:10.1038/378209a0

Mooren, O. L., Galletta, B. J., & Cooper, J. A. (2012). Roles for actin assembly in endocytosis. *Annu Rev Biochem, 81*, 661-686. doi:10.1146/annurev-biochem-060910-094416

Moran, M. F., Koch, C. A., Anderson, D., Ellis, C., England, L., Martin, G. S., & Pawson, T. (1990). Src homology region 2 domains direct protein-protein interactions in signal transduction. *Proceedings of the National Academy of Sciences of the United States of America, 87*(21), 8622-8626. doi:10.1073/pnas.87.21.8622

Moreira, K. E., Schuck, S., Schrul, B., Fröhlich, F., Moseley, J. B., Walther, T. C., & Walter, P. (2012). Seg1 controls eisosome assembly and shape. *The Journal of cell biology, 198*(3), 405-420. doi:10.1083/jcb.201202097

Moreno, S., Klar, A., & Nurse, P. (1991). Molecular genetic analysis of fission yeast Schizosaccharomyces pombe. *Methods Enzymology, 194*, 795-823.

Morlot, S., Galli, V., Klein, M., Chiaruttini, N., Manzi, J., Humbert, F., . . . Roux, A. (2012). Membrane shape at the edge of the dynamin helix sets location and duration of the fission reaction. *Cell, 151*(3), 619-629. doi:10.1016/j.cell.2012.09.017

Morris, C. E., & Homann, U. (2001). Cell surface area regulation and membrane tension. *J Membr Biol, 179*(2), 79-102.

Mulkearns, E. E., & Cooper, J. A. (2012). FCH domain only-2 organizes clathrin-coated structures and interacts with Disabled-2 for low-density lipoprotein receptor endocytosis. *Molecular Biology of the Cell, 23*(7), 1330-1342. doi:10.1091/mbc.E11-09-0812

Mullins, R. D., Stafford, W. F., & Pollard, T. D. (1997). Structure, Subunit Topology, and Actin-binding Activity of the Arp2/3 Complex from Acanthamoeba. *Journal of Cell Biology, 136*(2), 331-343. doi:10.1083/jcb.136.2.331

Mund, M., van der Beek, J. A., Deschamps, J., Dmitrieff, S., Monster, J. L., Picco, A., . . . Ries, J. (2017). Systematic analysis of the molecular architecture of endocytosis reveals a nanoscale actin nucleation template that drives efficient vesicle formation. *bioRxiv*. doi:10.1101/217836

Muro, S., Koval, M., & Muzykantov, V. (2004). Endothelial endocytic pathways: gates for vascular drug delivery. *Curr Vasc Pharmacol, 2*(3), 281-299.

Naito, Y., Hino, K., Bono, H., & Ui-Tei, K. (2015). CRISPRdirect: software for designing CRISPR/Cas guide RNA with reduced off-target sites. *Bioinformatics, 31*(7), 1120-1123. doi:10.1093/bioinformatics/btu743

Naito, Y., Hino, K., Bono, H., & Ui-Tei, K. (2015). CRISPRdirect: software for designing CRISPR/Cas guide RNA with reduced off-target sites. *Bioinformatics, 31*(7), 1120-1123. doi:10.1093/bioinformatics/btu743

Nash, P. D. (2012). Why modules matter. *FEBS Letters, 586*(17), 2572-2574. doi:10.1016/j.febslet.2012.04.049

Nguyen, J. T., & Lim, W. A. (1997). How Src exercises self-restraint. *Nat Struct Biol, 4*(4), 256-260.

Nguyen, J. T., Porter, M., Amoui, M., Miller, W. T., Zuckermann, R. N., & Lim, W. A. (2000). Improving SH3 domain ligand selectivity using a non-natural scaffold. *Chem Biol, 7*(7), 463-473.

Nguyen, J. T., Turck, C. W., Cohen, F. E., Zuckermann, R. N., & Lim, W. A. (1998). Exploiting the basis of proline recognition by SH3 and WW domains: design of N-substituted inhibitors. *Science, 282*(5396), 2088-2092.

Nishida, M., Nagata, K., Hachimori, Y., Horiuchi, M., Ogura, K., Mandiyan, V., . . . Inagaki, F. (2001). Novel recognition mode between Vav and Grb2 SH3 domains. *Embo j, 20*(12), 2995-3007. doi:10.1093/emboj/20.12.2995

Nossal, R. (2001). Energetics of clathrin basket assembly. *Traffic, 2*(2), 138-147.

Oh, Y., Schreiter, J., Nishihama, R., Wloka, C., Bi, E., & Chang, F. (2013). Targeting and functional mechanisms of the cytokinesis-related F-BAR protein Hof1 during the cell cycle. *Molecular Biology of the Cell, 24*(9), 1305-1320. doi:10.1091/mbc.e12-11-0804

Okreglak, V., & Drubin, D. G. (2007). Cofilin recruitment and function during actin-mediated endocytosis dictated by actin nucleotide state. *Journal of Cell Biology, 178*(7), 1251-1264. doi:10.1083/jcb.200703092

Okreglak, V., & Drubin, D. G. (2010). Loss of Aip1 reveals a role in maintaining the actin monomer pool and an in vivo oligomer assembly pathway. *The Journal of cell biology, 188*(6), 769-777. doi:10.1083/jcb.200909176

Padrick, S. B., Cheng, H.-C., Ismail, A. M., Panchal, S. C., Doolittle, L. K., Kim, S., . . . Rosen, M. K. (2008). Hierarchical Regulation of WASP/WAVE Proteins. *Molecular Cell, 32*(3), 426-438. doi:10.1016/j.molcel.2008.10.012

Parsell, D. A., & Sauer, R. T. (1989). The structural stability of a protein is an important determinant of its proteolytic susceptibility in Escherichia coli. *J Biol Chem, 264*(13), 7590-7595.

Pawson, T., & Nash, P. (2003). Assembly of cell regulatory systems through protein interaction domains. *Science, 300*(5618), 445-452. Retrieved from http://dx.doi.org/10.1126/science.1083653

Pawson, T., & Nash, P. (2010). Chapter 57 - Modular Protein Interaction Domains in Cellular Communication. In R. A. Bradshaw & E. A. Dennis (Eds.), *Handbook of Cell Signaling (Second Edition)* (pp. 399-411). San Diego: Academic Press.

Pearse, B. M. (1976). Clathrin: a unique protein associated with intracellular transfer of membrane by coated vesicles. *Proc Natl Acad Sci U S A, 73*(4), 1255-1259. Retrieved from https://www.ncbi.nlm.nih.gov/pubmed/1063406

Pearse, B. M. F. (1975). Coated vesicles from pig brain: purification and biochemical characterization. *J. Mol. Biol., 97*, 93-98.
Peskin, C. S., Odell, G. M., & Oster, G. F. (1993). Cellular motions and thermal fluctuations: the Brownian ratchet. *Biophys J, 65*(1), 316-324. doi:10.1016/s0006-3495(93)81035-x
Peter, B. J., Kent, H. M., Mills, I. G., Vallis, Y., Butler, P. J., Evans, P. R., & McMahon, H. T. (2004). BAR domains as sensors of membrane curvature: the amphiphysin BAR structure. *Science, 303*(5657), 495-499. doi:10.1126/science.1092586
Petrella, E. C., Machesky, L. M., Kaiser, D. A., & Pollard, T. D. (1996). Structural requirements and thermodynamics of the interaction of proline peptides with profilin. *Biochemistry, 35*(51), 16535-16543. doi:10.1021/bi961498d
Petrini, E., Baillet, V., Cridge, J., Hogan, C. J., Guillaume, C., Ke, H., . . . Varga-Weisz, P. (2015). A new phosphate-starvation response in fission yeast requires the endocytic function of myosin I. *J Cell Sci, 128*(20), 3707-3713. doi:10.1242/jcs.171314
Phillips, R., Kondev, J., & Theriot, J. (2009). *Physical biology of the cell*: Garland Science.
Picco, A., Kukulski, W., Manenschijn, H. E., Specht, T., Briggs, J. A. G., Kaksonen, M., & Lemmon, S. (2018). The contributions of the actin machinery to endocytic membrane bending and vesicle formation. *Molecular Biology of the Cell, 29*(11), 1346-1358. doi:10.1091/mbc.E17-11-0688
Picco, A., Mund, M., Ries, J., Nedelec, F., & Kaksonen, M. (2015). Visualizing the functional architecture of the endocytic machinery. *Elife, 4*. doi:10.7554/eLife.04535
Picco, A., Mund, M., Ries, J., Nédélec, F., & Kaksonen, M. (2015). Visualizing the functional architecture of the endocytic machinery. *Elife, 4*. doi:10.7554/eLife.04535
Pollard, T. D., Blanchoin, L., & Mullins, R. D. (2000). Molecular mechanisms controlling actin filament dynamics in nonmuscle cells. *Annu Rev Biophys Biomol Struct, 29*, 545-576. doi:10.1146/annurev.biophys.29.1.545
Pollard, T. D., & Borisy, G. G. (2003). Cellular motility driven by assembly and disassembly of actin filaments. *Cell, 112*(4), 453-465. Retrieved from https://www.sciencedirect.com/science/article/pii/S009286740300120X
Poon, B. Y., Ward, C. A., Cooper, C. B., Giles, W. R., Burns, A. R., & Kubes, P. (2001). alpha(4)-integrin mediates neutrophil-induced free radical injury to cardiac myocytes. *The Journal of cell biology, 152*(5), 857-866. Retrieved from https://www.ncbi.nlm.nih.gov/pubmed/11238444
Prokic, I., Cowling, B. S., & Laporte, J. (2014). Amphiphysin 2 (BIN1) in physiology and diseases. *Journal of molecular medicine (Berlin, Germany), 92*(5), 453-463. doi:10.1007/s00109-014-1138-1
Prudente, S., Morini, E., Larmon, J., Andreozzi, F., Di Pietro, N., Nigro, A., . . . Trischitta, V. (2011). The SH2B1 obesity locus is associated with myocardial infarction in diabetic patients and with NO synthase activity in endothelial cells. *Atherosclerosis, 219*(2), 667-672. doi:10.1016/j.atherosclerosis.2011.08.019
Purevjav, E., Varela, J., Morgado, M., Kearney, D. L., Li, H., Taylor, M. D., . . . Towbin, J. A. (2010). Nebulette mutations are associated with dilated cardiomyopathy and endocardial fibroelastosis. *Journal of the American College of Cardiology, 56*(18), 1493-1502. doi:10.1016/j.jacc.2010.05.045
Quintero-Monzon, O., Rodal, A. A., Strokopytov, B., Almo, S. C., & Goode, B. L. (2005). Structural and functional dissection of the Abp1 ADFH actin-binding domain

reveals versatile in vivo adapter functions. *Molecular Biology of the Cell, 16*(7), 3128-3139. doi:10.1091/mbc.e05-01-0059
Ram, R., & Blaxall, B. C. (2010). Nebulette mutations in cardiac remodeling: big effects from a small mechanosensor. *Journal of the American College of Cardiology, 56*(18), 1503-1505. doi:10.1016/j.jacc.2010.06.031
Rao, Y., Ma, Q., Vahedi-Faridi, A., Sundborger, A., Pechstein, A., Puchkov, D., . . . Haucke, V. (2010). Molecular basis for SH3 domain regulation of F-BAR-mediated membrane deformation. *Proc Natl Acad Sci U S A, 107*(18), 8213-8218. doi:10.1073/pnas.1003478107
Reider, A., Barker, S. L., Mishra, S. K., Im, Y. J., Maldonado-Báez, L., Hurley, J. H., . . . Wendland, B. (2009). Syp1 is a conserved endocytic adaptor that contains domains involved in cargo selection and membrane tubulation. *The EMBO Journal, 28*(20), 3103-3116. doi:10.1038/emboj.2009.248
Ren, G., Wang, J., Brinkworth, R., Winsor, B., Kobe, B., & Munn, A. L. (2005). Verprolin Cytokinesis Function Mediated by the Hof One Trap Domain. *Traffic, 6*(7), 575-593. doi:10.1111/j.1600-0854.2005.00300.x
Ren, R., Mayer, B. J., Cicchetti, P., & Baltimore, D. (1993). Identification of a ten-amino acid proline-rich SH3 binding site. *Science, 259*(5098), 1157-1161. doi:10.1126/science.8438166
Renard, H. F., Simunovic, M., Lemiere, J., Boucrot, E., Garcia-Castillo, M. D., Arumugam, S., . . . Johannes, L. (2015). Endophilin-A2 functions in membrane scission in clathrin-independent endocytosis. *Nature, 517*(7535), 493-496. doi:10.1038/nature14064
Rickles, R. J., Botfield, M. C., Weng, Z., Taylor, J. A., Green, O. M., Brugge, J. S., & Zoller, M. J. (1994). Identification of Src, Fyn, Lyn, PI3K and Abl SH3 domain ligands using phage display libraries. *Embo j, 13*(23), 5598-5604.
Robertson, A. S., Allwood, E. G., Smith, A. P., Gardiner, F. C., Costa, R., Winder, S. J., & Ayscough, K. R. (2009). The WASP homologue Las17 activates the novel actin-regulatory activity of Ysc84 to promote endocytosis in yeast. *Molecular Biology of the Cell, 20*(6), 1618-1628. doi:10.1091/mbc.E08-09-0982
Rodal, A. A., Manning, A. L., Goode, B. L., & Drubin, D. G. (2003). Negative Regulation of Yeast WASp by Two SH3 Domain-Containing Proteins. *Current Biology, 13*(12), 1000-1008. doi:10.1016/S0960-9822(03)00383-X
Roth, T. F., & Porter, K. R. (1964). Yolk Protein Uptake in the Oocyte of the Mosquito Aedes Aegypti. L. *J Cell Biol, 20*, 313-332. Retrieved from https://www.ncbi.nlm.nih.gov/pubmed/14126875
Rottner, K., Hanisch, J., & Campellone, K. G. (2010). WASH, WHAMM and JMY: regulation of Arp2/3 complex and beyond. *Trends Cell Biol, 20*(11), 650-661. doi:10.1016/j.tcb.2010.08.014
Roux, A. (2013). The physics of membrane tubes: soft templates for studying cellular membranes. *Soft Matter, 9*(29), 6726-6736. doi:10.1039/C3SM50514F
Roux, A., Uyhazi, K., Frost, A., & De Camilli, P. (2006). GTP-dependent twisting of dynamin implicates constriction and tension in membrane fission. *Nature, 441*(7092), 528-531. doi:10.1038/nature04718
Roybal, K. T., & Lim, W. A. (2017). Synthetic Immunology: Hacking Immune Cells to Expand Their Therapeutic Capabilities. In D. R. Littman & W. M. Yokoyama (Eds.), *Annual Review of Immunology, Vol 35* (Vol. 35, pp. 229-253).
Rozakis-Adcock, M., Fernley, R., Wade, J., Pawson, T., & Bowtell, D. (1993). The SH2 and SH3 domains of mammalian Grb2 couple the EGF receptor to the Ras activator mSos1. *Nature, 363*(6424), 83-85. doi:10.1038/363083a0

Ruan, X., Wülfing, C., & Murphy, R. F. (2017). Image-based spatiotemporal causality inference for protein signaling networks. *Bioinformatics, 33*(14), i217-i224. doi:10.1093/bioinformatics/btx258

Sadowski, I., Stone, J. C., & Pawson, T. (1986). A noncatalytic domain conserved among cytoplasmic protein-tyrosine kinases modifies the kinase function and transforming activity of Fujinami sarcoma virus P130gag-fps. *Molecular and Cellular Biology, 6*(12), 4396-4408. doi:10.1128/mcb.6.12.4396

Saksela, K., & Permi, P. (2012). SH3 domain ligand binding: What's the consensus and where's the specificity? *FEBS Letters, 586*(17), 2609-2614. doi:10.1016/j.febslet.2012.04.042

Saleem, M., Morlot, S., Hohendahl, A., Manzi, J., Lenz, M., & Roux, A. (2015). A balance between membrane elasticity and polymerization energy sets the shape of spherical clathrin coats. *Nat Commun, 6*, 6249. doi:10.1038/ncomms7249

Sali, A., & Blundell, T. L. (1993). Comparative protein modelling by satisfaction of spatial restraints. *J Mol Biol, 234*(3), 779-815. doi:10.1006/jmbi.1993.1626

Scher-Zagier, J. K., & Carlsson, A. E. (2016). Local Turgor Pressure Reduction via Channel Clustering. *Biophys J, 111*(12), 2747-2756. doi:10.1016/j.bpj.2016.10.040

Schmid, E. M., & McMahon, H. T. (2007). Integrating molecular and network biology to decode endocytosis. *Nature, 448*, 883-888. doi:10.1038/nature06031

Schmid, S. L. (2018). A nostalgic look back 40 years after the discovery of receptor-mediated endocytosis. *Molecular Biology of the Cell, 30*(1), 1-3. doi:10.1091/mbc.E18-06-0409

Schmid, S. L., Sorkin, A., & Zerial, M. (2014). Endocytosis: Past, Present, and Future. *Cold Spring Harbor perspectives in biology, 6*(12). doi:10.1101/cshperspect.a022509

Schultz, J., Milpetz, F., Bork, P., & Ponting, C. P. (1998). SMART, a simple modular architecture research tool: Identification of signaling domains. *Proceedings of the National Academy of Sciences, 95*(11), 5857-5864. doi:10.1073/pnas.95.11.5857

Sefton, B. M., & Hunter, T. (1986). From c-src to v-src, or the case of the missing C terminus. *Cancer Surv, 5*(2), 159-172.

Shaw, M. W. (1969). A glossary of genetics and cytogenetics. *American Journal of Human Genetics, 21*(5), 522-523. Retrieved from https://www.ncbi.nlm.nih.gov/pmc/articles/PMC1706565/

Sheng, M., & Sala, C. (2001). PDZ Domains and the Organization of Supramolecular Complexes. *Annual Review of Neuroscience, 24*(1), 1-29. doi:10.1146/annurev.neuro.24.1.1

Shi, Z., & Baumgart, T. (2015). Membrane tension and peripheral protein density mediate membrane shape transitions. *Nat Commun, 6*, 5974. doi:10.1038/ncomms6974

Shin, M., van Leeuwen, J., Boone, C., & Bretscher, A. (2018). Yeast Aim21/Tda2 both regulates free actin by reducing barbed end assembly and forms a complex with Cap1/Cap2 to balance actin assembly between patches and cables. *Molecular Biology of the Cell, 29*(8), 923-936. doi:10.1091/mbc.E17-10-0592

Sievers, F., Wilm, A., Dineen, D., Gibson, T. J., Karplus, K., Li, W., . . . Higgins, D. G. (2011). Fast, scalable generation of high-quality protein multiple sequence alignments using Clustal Omega. *Molecular Systems Biology, 7*(1). doi:10.1038/msb.2011.75

Sigrist, C. J. A., Cerutti, L., Hulo, N., Gattiker, A., Falquet, L., Pagni, M., . . . Bucher, P. (2002). PROSITE: a documented database using patterns and profiles as motif

descriptors. *Briefings in bioinformatics, 3*(3), 265-274. Retrieved from https://www.ncbi.nlm.nih.gov/pubmed/12230035
Simunovic, M., Bassereau, P., & Voth, G. A. (2018). Organizing membrane-curving proteins: the emerging dynamical picture. *Curr Opin Struct Biol, 51*, 99-105. doi:10.1016/j.sbi.2018.03.018
Simunovic, M., Evergren, E., Golushko, I., Prevost, C., Renard, H. F., Johannes, L., . . . Bassereau, P. (2016). How curvature-generating proteins build scaffolds on membrane nanotubes. *Proc Natl Acad Sci U S A, 113*(40), 11226-11231. doi:10.1073/pnas.1606943113
Simunovic, M., Manneville, J. B., Renard, H. F., Evergren, E., Raghunathan, K., Bhatia, D., . . . Callan-Jones, A. (2017). Friction Mediates Scission of Tubular Membranes Scaffolded by BAR Proteins. *Cell, 170*(1), 172-184 e111. doi:10.1016/j.cell.2017.05.047
Simunovic, M., Voth, G. A., Callan-Jones, A., & Bassereau, P. (2015). When Physics Takes Over: BAR Proteins and Membrane Curvature. *Trends Cell Biol, 25*(12), 780-792. doi:10.1016/j.tcb.2015.09.005
Sirotkin, V., Beltzner, C. C., Marchand, J. B., & Pollard, T. D. (2005). Interactions of WASp, myosin-I, and verprolin with Arp2/3 complex during actin patch assembly in fission yeast. *The Journal of cell biology, 170*(4), 637-648. doi:10.1083/jcb.200502053
Sirotkin, V., Berro, J., Macmillan, K., Zhao, L., & Pollard, T. D. (2010). Quantitative analysis of the mechanism of endocytic actin patch assembly and disassembly in fission yeast. *Molecular Biology of the Cell, 21*, 2894-2904. doi:10.1091/mbc.E10
Siton-Mendelson, O., & Bernheim-Groswasser, A. (2017). Functional Actin Networks under Construction: The Cooperative Action of Actin Nucleation and Elongation Factors. *Trends in Biochemical Sciences, 42*(6), 414-430. doi:10.1016/j.tibs.2017.03.002
Skår, J., Coveney, P. V., & Pawson, T. (2003). Organization of cell–regulatory systems through modular–protein–interaction domains. *Philosophical Transactions of the Royal Society of London. Series A: Mathematical, Physical and Engineering Sciences, 361*(1807), 1251-1262. doi:10.1098/rsta.2003.1197
Skau, C. T., Courson, D. S., Bestul, A. J., Winkelman, J. D., Rock, R. S., Sirotkin, V., & Kovar, D. R. (2011). Actin Filament Bundling by Fimbrin Is Important for Endocytosis, Cytokinesis, and Polarization in Fission Yeast. *Journal of Biological Chemistry, 286*(30), 26964-26977. doi:10.1074/jbc.M111.239004
Smaczynska-de, R., II, Allwood, E. G., Aghamohammadzadeh, S., Hettema, E. H., Goldberg, M. W., & Ayscough, K. R. (2010). A role for the dynamin-like protein Vps1 during endocytosis in yeast. *J Cell Sci, 123*(Pt 20), 3496-3506. doi:10.1242/jcs.070508
Smith, S. M., Baker, M., Halebian, M., & Smith, C. J. (2017). Weak Molecular Interactions in Clathrin-Mediated Endocytosis. *Front Mol Biosci, 4*, 72. doi:10.3389/fmolb.2017.00072
Snead, W. T., Hayden, C. C., Gadok, A. K., Zhao, C., Lafer, E. M., Rangamani, P., & Stachowiak, J. C. (2017). Membrane fission by protein crowding. *Proc Natl Acad Sci U S A, 114*(16), E3258-E3267. doi:10.1073/pnas.1616199114
Sochacki, K. A., Dickey, A. M., Strub, M. P., & Taraska, J. W. (2017). Endocytic proteins are partitioned at the edge of the clathrin lattice in mammalian cells. *Nat Cell Biol, 19*(4), 352-361. doi:10.1038/ncb3498
Soulard, A., Lechler, T., Spiridonov, V., Shevchenko, A., Shevchenko, A., Li, R., & Winsor, B. (2002). Saccharomyces cerevisiae Bzz1p is implicated with type I myosins in actin patch polarization and is able to recruit actin-polymerizing

machinery in vitro. *Molecular and Cellular Biology, 22*(22), 7889-7906. doi:10.1128/MCB.22.22.7889-7906.2002
Sparks, A. B., Rider, J. E., Hoffman, N. G., Fowlkes, D. M., Quillam, L. A., & Kay, B. K. (1996). Distinct ligand preferences of Src homology 3 domains from Src, Yes, Abl, Cortactin, p53bp2, PLCgamma, Crk, and Grb2. *Proc Natl Acad Sci U S A, 93*(4), 1540-1544. doi:10.1073/pnas.93.4.1540
Sparks, A. B., Rider, J. E., & Kay, B. K. (1998). Mapping the specificity of SH3 domains with phage-displayed random-peptide libraries. *Methods Mol Biol, 84*, 87-103. doi:10.1385/0-89603-488-7:87
Spiess, M., de Craene, J.-O. O., Michelot, A., Rinaldi, B., Huber, A., Drubin, D. G., . . . Friant, S. (2013). Lsb1 is a negative regulator of las17 dependent actin polymerization involved in endocytosis. *PLoS One, 8*(4). doi:10.1371/journal.pone.0061147
Stachowiak, J. C., Schmid, E. M., Ryan, C. J., Ann, H. S., Sasaki, D. Y., Sherman, M. B., . . . Hayden, C. C. (2012). Membrane bending by protein-protein crowding. *Nat Cell Biol, 14*(9), 944-949. doi:10.1038/ncb2561
Stahl, M. L., Ferenz, C. R., Kelleher, K. L., Kriz, R. W., & Knopf, J. L. (1988). Sequence similarity of phospholipase C with the non-catalytic region of src. *Nature, 332*(6161), 269-272. doi:10.1038/332269a0
Stamenova, S. D., French, M. E., He, Y., Francis, S. A., Kramer, Z. B., & Hicke, L. (2007). Ubiquitin binds to and regulates a subset of SH3 domains. *Molecular Cell, 25*(2), 273-284. doi:10.1016/j.molcel.2006.12.016
Stein, A., & Aloy, P. (2008). Contextual specificity in peptide-mediated protein interactions. *PLoS One, 3*(7). doi:10.1371/journal.pone.0002524
Sun, Y., Leong, N. T., Jiang, T., Tangara, A., Darzacq, X., & Drubin, D. G. (2017). Switch-like Arp2/3 activation upon WASP and WIP recruitment to an apparent threshold level by multivalent linker proteins in vivo. *Elife, 6*. doi:10.7554/elife.29140
Sun, Y., Martin, A. C., & Drubin, D. G. (2006). Endocytic Internalization in Budding Yeast Requires Coordinated Actin Nucleation and Myosin Motor Activity. *Developmental Cell, 11*(1), 33-46. doi:10.1016/j.devcel.2006.05.008
Szklarczyk, D., Morris, J. H., Cook, H., Kuhn, M., Wyder, S., Simonovic, M., . . . von Mering, C. (2017). The STRING database in 2017: quality-controlled protein-protein association networks, made broadly accessible. *Nucleic Acids Res, 45*(D1), D362-d368. doi:10.1093/nar/gkw937
Takamori, S., Holt, M., Stenius, K., Lemke, E. A., Gronborg, M., Riedel, D., . . . Jahn, R. (2006). Molecular anatomy of a trafficking organelle. *Cell, 127*(4), 831-846. doi:10.1016/j.cell.2006.10.030
Tan, P. K., Howard, J. P., & Payne, G. S. (1996). The sequence NPFXD defines a new class of endocytosis signal in Saccharomyces cerevisiae. *J Cell Biol, 135*(6 Pt 2), 1789-1800. doi:10.1083/jcb.135.6.1789
Tang, H. Y., Xu, J., & Cai, M. (2000). Pan1p, End3p, and S1a1p, three yeast proteins required for normal cortical actin cytoskeleton organization, associate with each other and play essential roles in cell wall morphogenesis. *Molecular and Cellular Biology, 20*(1), 12-25. doi:10.1128/MCB.20.1.12-25.2000
Taylor, M. J., Perrais, D., & Merrifield, C. J. (2011). A high precision survey of the molecular dynamics of mammalian clathrin-mediated endocytosis. *PLoS Biol, 9*(3). doi:10.1371/journal.pbio.1000604
Taylor, R. M., Lord, C. I., Riesselman, M. H., Gripentrog, J. M., Leto, T. L., McPhail, L. C., . . . Jesaitis, A. J. (2007). Characterization of surface structure and p47phox

SH3 domain-mediated conformational changes for human neutrophil flavocytochrome b. *Biochemistry, 46*(49), 14291-14304. doi:10.1021/bi701626p
Teyra, J., Huang, H., Jain, S., Guan, X., Dong, A., Liu, Y., . . . Sidhu, S. S. (2017). Comprehensive Analysis of the Human SH3 Domain Family Reveals a Wide Variety of Non-canonical Specificities. *Structure, 25*(10), 1598-1610.e1593. doi:10.1016/j.str.2017.07.017
Tharmann, R., Claessens, M. M., & Bausch, A. R. (2007). Viscoelasticity of isotropically cross-linked actin networks. *Phys Rev Lett, 98*(8), 088103. doi:10.1103/PhysRevLett.98.088103
Theriot, J. A., & Mitchison, T. J. (1991). Actin microfilament dynamics in locomoting cells. *Nature, 352*(6331), 126-131. doi:10.1038/352126a0
Thoresen, T., Lenz, M., & Gardel, M. L. (2011). Reconstitution of contractile actomyosin bundles. *Biophysical Journal, 100*(11), 2698-2705. doi:10.1016/j.bpj.2011.04.031
Ti, S. C., & Pollard, T. D. (2011). Purification of actin from fission yeast Schizosaccharomyces pombe and characterization of functional differences from muscle actin. *J Biol Chem, 286*(7), 5784-5792. doi:10.1074/jbc.M110.199794
Tian, A., Johnson, C., Wang, W., & Baumgart, T. (2007). Line tension at fluid membrane domain boundaries measured by micropipette aspiration. *Phys Rev Lett, 98*(20), 208102. doi:10.1103/PhysRevLett.98.208102
Tian, L., Chen, L., McClafferty, H., Sailer, C. A., Ruth, P., Knaus, H.-G. G., & Shipston, M. J. (2006). A noncanonical SH3 domain binding motif links BK channels to the actin cytoskeleton via the SH3 adapter cortactin. *FASEB journal : official publication of the Federation of American Societies for Experimental Biology, 20*(14), 2588-2590. doi:10.1096/fj.06-6152fje
Tinevez, J.-Y., Perry, N., Schindelin, J., Hoopes, G. M., Reynolds, G. D., Laplantine, E., . . . Eliceiri, K. W. (2017). TrackMate: An open and extensible platform for single-particle tracking. *Methods, 115*, 80-90. doi:10.1016/j.ymeth.2016.09.016
Tomas, A., Futter, C. E., & Eden, E. R. (2014). EGF receptor trafficking: consequences for signaling and cancer. *Trends Cell Biol, 24*(1), 26-34. doi:10.1016/j.tcb.2013.11.002
Tong, A. H., Drees, B., Nardelli, G., Bader, G. D., Brannetti, B., Castagnoli, L., . . . Cesareni, G. (2002). A combined experimental and computational strategy to define protein interaction networks for peptide recognition modules. *Science, 295*(5553), 321-324. doi:10.1126/science.1064987
Tonikian, R., Xin, X., Toret, C. P., Gfeller, D., & Landgraf, C. (2009). Bayesian modeling of the yeast SH3 domain interactome predicts spatiotemporal dynamics of endocytosis proteins. *PLoS Biol*. doi:10.1371/journal.pbio.1000218
Tossavainen, H., Aitio, O., Hellman, M., Saksela, K., & Permi, P. (2016). Structural Basis of the High Affinity Interaction between the Alphavirus Nonstructural Protein-3 (nsP3) and the SH3 Domain of Amphiphysin-2. *J Biol Chem, 291*(31), 16307-16317. doi:10.1074/jbc.m116.732412
Trahey, M., Wong, G., Halenbeck, R., Rubinfeld, B., Martin, G., Ladner, M., . . . et, a. (1988). Molecular cloning of two types of GAP complementary DNA from human placenta. *Science, 242*(4886), 1697-1700. doi:10.1126/science.3201259
Tsai, S. Q., & Joung, J. K. (2016). Defining and improving the genome-wide specificities of CRISPR-Cas9 nucleases. *Nat Rev Genet, 17*(5), 300-312. doi:10.1038/nrg.2016.28
Tsai, S. Q., Zheng, Z., Nguyen, N. T., Liebers, M., Topkar, V. V., Thapar, V., . . . Joung, J. K. (2015). GUIDE-seq enables genome-wide profiling of off-target cleavage by CRISPR-Cas nucleases. *Nat Biotechnol, 33*(2), 187-197. doi:10.1038/nbt.3117

Tweten, D. J., Bayly, P. V., & Carlsson, A. E. (2017). Actin growth profile in clathrin-mediated endocytosis. *Phys Rev E, 95*(5-1), 052414. doi:10.1103/PhysRevE.95.052414
Ullrich, A., Coussens, L., Hayflick, J. S., Dull, T. J., Gray, A., Tam, A. W., . . . Seeburg, P. H. (1984). Human epidermal growth factor receptor cDNA sequence and aberrant expression of the amplified gene in A431 epidermoid carcinoma cells. *Nature, 309*(5967), 418-425. doi:10.1038/309418a0
Upadhyaya, A., Chabot, J. R., Andreeva, A., Samadani, A., & van Oudenaarden, A. (2003). Probing polymerization forces by using actin-propelled lipid vesicles. *Proc Natl Acad Sci U S A, 100*(8), 4521-4526. doi:10.1073/pnas.0837027100
Urbanek, A. N., Chan, R., & Ayscough, K. R. (2015). Function and interactions of the Ysc84/SH3yl1 family of actin-and lipid-binding proteins. *Biochemical Society Transactions, 43*(1), 111-116. doi:10.1042/BST20140221
Verschueren, E., Spiess, M., Gkourtsa, A., Avula, T., Landgraf, C., Mancilla, V., . . . Distel, B. (2015). Evolution of the SH3 Domain Specificity Landscape in Yeasts. *PLoS One, 10*(6). doi:10.1371/journal.pone.0129229
Vilela, M., & Danuser, G. (2011). What's wrong with correlative experiments? *Nature Cell Biology, 13*, 1011. doi:10.1038/ncb2325
Walani, N., Torres, J., & Agrawal, A. (2015). Endocytic proteins drive vesicle growth via instability in high membrane tension environment. *Proc Natl Acad Sci U S A, 112*(12), E1423-1432. doi:10.1073/pnas.1418491112
Walther, T. C., Brickner, J. H., Aguilar, P. S., Bernales, S., Pantoja, C., & Walter, P. (2006). Eisosomes mark static sites of endocytosis. *Nature, 439*(7079), 998-1003. doi:10.1038/nature04472
Wang, D., Lehman, R. E., Donner, D. B., Matli, M. R., Warren, R. S., & Welton, M. L. (2002). Expression and endocytosis of VEGF and its receptors in human colonic vascular endothelial cells. *Am J Physiol Gastrointest Liver Physiol, 282*(6), G1088-1096. doi:10.1152/ajpgi.00250.2001
Wang, Q., Navarro, M. V., Peng, G., Molinelli, E., Goh, S. L., Judson, B. L., . . . Sondermann, H. (2009). Molecular mechanism of membrane constriction and tubulation mediated by the F-BAR protein Pacsin/Syndapin. *Proc Natl Acad Sci U S A, 106*(31), 12700-12705. doi:10.1073/pnas.0902974106
Wang, Q., & Ui-Tei, K. (2017). Computational Prediction of CRISPR/Cas9 Target Sites Reveals Potential Off-Target Risks in Human and Mouse. *Methods Mol Biol, 1630*, 43-53. doi:10.1007/978-1-4939-7128-2_4
Wang, X., & Carlsson, A. E. (2017). A master equation approach to actin polymerization applied to endocytosis in yeast. *PLoS Comput Biol, 13*(12), e1005901. doi:10.1371/journal.pcbi.1005901
Wang, X., Galletta, B. J., Cooper, J. A., & Carlsson, A. E. (2016). Actin-Regulator Feedback Interactions during Endocytosis. *Biophys J, 110*(6), 1430-1443. doi:10.1016/j.bpj.2016.02.018
Watanabe, S., Rost, B. R., Camacho-Perez, M., Davis, M. W., Sohl-Kielczynski, B., Rosenmund, C., & Jorgensen, E. M. (2013). Ultrafast endocytosis at mouse hippocampal synapses. *Nature, 504*(7479), 242-247. doi:10.1038/nature12809
Weinberg, J., & Drubin, D. G. (2012). Clathrin-mediated endocytosis in budding yeast. *Trends Cell Biol, 22*(1), 1-13. doi:10.1016/j.tcb.2011.09.001
Wiese, W., Harbich, W., & Helfrich, W. (1992). Budding of lipid bilayer vesicles and flat membranes. *Journal of Physics: Condensed Matter, 4*(7), 1647.
Wilhelm, B. G., Mandad, S., Truckenbrodt, S., Krohnert, K., Schafer, C., Rammner, B., . . . Rizzoli, S. O. (2014). Composition of isolated synaptic boutons reveals the

amounts of vesicle trafficking proteins. *Science, 344*(6187), 1023-1028. doi:10.1126/science.1252884
Willet, A. H., McDonald, N. A., Bohnert, K. A., Baird, M. A., Allen, J. R., Davidson, M. W., & Gould, K. L. (2015). The F-BAR Cdc15 promotes contractile ring formation through the direct recruitment of the formin Cdc12. *The Journal of cell biology, 208*(4), 391. doi:10.1083/jcb.201411097
Wood, V., Gwilliam, R., Rajandream, M. A. A., Lyne, M., Lyne, R., Stewart, A., . . . Gloux, S. (2002). The genome sequence of Schizosaccharomyces pombe. *Nature, 415*(6874), 871-880. doi:10.1038/nature724
Wood, V., Harris, M. A., McDowall, M. D., Rutherford, K., Vaughan, B. W., Staines, D. M., . . . Oliver, S. G. (2012). PomBase: a comprehensive online resource for fission yeast. *Nucleic Acids Res, 40*(D1), D695-D699. doi:10.1093/nar/gkr853
Wu, J. Q., & Pollard, T. D. (2005). Counting cytokinesis proteins globally and locally in fission yeast. *Science, 310*(5746), 310-314. doi:10.1126/science.1113230
Wu, X. S., Lee, S. H., Sheng, J., Zhang, Z., Zhao, W. D., Wang, D., . . . Wu, L. G. (2016). Actin Is Crucial for All Kinetically Distinguishable Forms of Endocytosis at Synapses. *Neuron, 92*(5), 1020-1035. doi:10.1016/j.neuron.2016.10.014
Xin, X., Gfeller, D., Cheng, J., Tonikian, R., Sun, L., Guo, A., . . . Bader, G. D. (2013). SH3 interactome conserves general function over specific form. *Molecular Systems Biology, 9*(1), 652. doi:10.1038/msb.2013.9
Xu, W., Harrison, S. C., & Eck, M. J. (1997). Three-dimensional structure of the tyrosine kinase c-Src. *Nature, 385*(6617), 595-602. doi:10.1038/385595a0
Yarrington, R. M., Verma, S., Schwartz, S., Trautman, J. K., & Carroll, D. (2018). Nucleosomes inhibit target cleavage by CRISPR-Cas9 in vivo. *Proc Natl Acad Sci, 115*(38), 9351-9358. doi:10.1073/pnas.1810062115
Yu, H., Chen, J. K., Feng, S., Dalgarno, D. C., Brauer, A. W., & Schreiber, S. L. (1994). Structural basis for the binding of proline-rich peptides to SH3 domains. *Cell, 76*(5), 933-945. doi:10.1016/0092-8674(94)90367-0
Yu, J. W., Mendrola, J. M., Audhya, A., Singh, S., Keleti, D., DeWald, D. B., . . . Lemmon, M. A. (2004). Genome-Wide Analysis of Membrane Targeting by S. cerevisiae Pleckstrin Homology Domains. *Molecular Cell, 13*(5), 677-688. doi:https://doi.org/10.1016/S1097-2765(04)00083-8
Zarrinpar, A., Bhattacharyya, R. P., & Lim, W. A. (2003). The structure and function of proline recognition domains. *Science Signaling, 2003*(179). doi:10.1126/stke.2003.179.re8
Zarrinpar, A., Park, S.-H. H., & Lim, W. A. (2003). Optimization of specificity in a cellular protein interaction network by negative selection. *Nature, 426*(6967), 676-680. doi:10.1038/nature02178
Zhang, T., Sknepnek, R., Bowick, M. J., & Schwarz, J. M. (2015). On the modeling of endocytosis in yeast. *Biophys J, 108*(3), 508-519. doi:10.1016/j.bpj.2014.11.3481
Zhang, X. H., Tee, L. Y., Wang, X. G., Huang, Q. S., & Yang, S. H. (2015). Off-target Effects in CRISPR/Cas9-mediated Genome Engineering. *Mol Ther Nucleic Acids, 4*, e264. doi:10.1038/mtna.2015.37
Zhao, H., Michelot, A., Koskela, E. V., Tkach, V., Stamou, D., David, D. G., & Lappalainen, P. (2013). Membrane-sculpting BAR domains generate stable lipid microdomains. *Cell Reports, 4*(6), 1213-1223. doi:10.1016/j.celrep.2013.08.024
Zhu, J., & Mogilner, A. (2012). Mesoscopic model of actin-based propulsion. *PLoS Comput Biol, 8*(11), e1002764. doi:10.1371/journal.pcbi.1002764
Zimmerberg, J., & Kozlov, M. M. (2006). How proteins produce cellular membrane curvature. *Nat Rev Mol Cell Biol, 7*(1), 9-19. doi:10.1038/nrm1784

From: Neal Ravindra
To: Cox, Katie; Neugebauer, Karla
Subject: Neal G. Ravindra, Final Thesis Submission
Date: Monday, August 26, 2019 3:02:13 PM
Attachments: Ravindra, Neal G. - MB&B Dept., December 2019.pdf

---

Hi Katie,

I have attached the final version of my thesis. My readers are:

1. Jonathon Howard (jonathon.howard@yale.edu)
2. Megan King (megan.king@yale.edu)
3. Bruce Goode (external reviewer, goode@brandeis.edu)

I submitted the unbound copy to the graduate school with all of the required forms.

Please let me know if there is anything else I can do at this time. And, especially, thanks for your patience with me--I know I haven't been the easiest student. I really appreciate it!

Best, Neal

--
Neal G. Ravindra, Ph.D. candidate in The Berro Lab
Molecular Biophysics & Biochemistry, Yale University